Catalysts for Sustainable Chemical Technologies

Di Iulio, Carlo

Award date:
2012

Awarding institution:
University of Bath

Catalysts for Sustainable Chemical Technologies

Carlo Di Iulio

A thesis submitted for the degree of Doctor of Philosophy

Department of Chemistry

University of Bath

October 2012

COPYRIGHT

Signed .....

Date .....

RESTRICTIONS

Abbreviations

AcOH	–	Acetic Acid
BDI	–	*β*-Diiminate
BnOH	–	Benzyl Alcohol
Btu	–	British Thermal Unit
CH_2Cl	–	Dichloromethane
$CHCl_3$	–	Chloroform
CH_3CN	–	Acetonitrile
DIP	–	Diisopropyl
DMF	–	Dimethylformamide
DMSO	–	Dimethylsulfoxide
D-LA	–	*D*-Lactide (R,R)
DSC	–	Differential Scanning Calorimetry
ESI-MS	–	Electron Spray Mass Spectrometry
GC-FID	–	Gas Chromatography Flame Ionisation Detection
GC-MS	–	Gas Chromatography Mass Spectrometry
GC-TCD	–	Gas Chromatography Thermal Conductivity Detection
GPC	–	Gel Permeation Chromatography
h, hrs	–	Hours
ICP-AES	–	Inductively Coupled Plasma-Atomic Emission Spectrometry
^{i}Bu	–	*iso*-butyl group
^{i}Pr	–	*iso*-propyl group
L-LA	–	*L*-lactide (S,S)
MAS	–	Magic Angle Spinning
MeOH	–	Methanol
meso-LA	–	*Meso*-lactide
mins	–	Minutes
NMR	–	Nuclear Magnetic Resonance
PLA	–	Polylactide
POSS®	–	Polyhedral Oligomeric Silsesquioxanes
rac-LA	–	Racemic-lactide
ROP	–	Ring Opening Polymerisation
s	–	Seconds
SEC	–	Size Exclusion Chromatography
^{t}Bu	–	tertiary-butyl group
THF	–	Tetrahydrofuran
VA	–	Veratryl Alcohol
XRD	–	X-ray Diffraction

Acknowledgements

Firstly I would like to thank Dr. Matthew Jones for his excellent supervision and mentorship. It was a challenge to develop a biochemist into a chemist but with his incredible support and guidance I like to think that we got there in the end.

I must express my gratitude to the ESPRC and Johnson Matthey who provided funding for this project through the centre for sustainable technologies (CSCT). I am grateful to Dr. John Lowe for his help with NMR spectroscopy, Dr. Mary Mahon for her support with X-Ray diffraction and Dr. Anneke Lubben for her assistance with Mass Spectrometry. Dr. Andrew Johnson is thanked for collaborative efforts contributing to Chapter Three, along with Mathew Middleton who contributed to the same chapter during his final year Natural Sciences project.

I also wish to thank all members of the Jones and Davidson research groups, past and present. In particular I would like to thank Dr. Catherine Frankis, Dr. Emma Whitelaw, Dr. Christine Cooper, Dr. Daniel Garcia Vivo and Kirsty Mokebo. They welcomed me with open arms into their lab and helped to make the first year of my PhD an outstanding one. I must express particular thanks to Emma for support during the ACS conference in Anaheim and for the epic road trip afterwards. Thanks also to Cathy for her honesty and always allowing me to speak freely and to Daniel for recently welcoming me into his home in Oviedo and teaching me the art of ‘escanciar’.

Thanks to Ben Jeffery, Chris Hawkins, Chris Ready, Lois Manton, Rhodri Owens, Stuart Hancock and Tom Forder for being great friends and always being willing to share their thoughts and ideas, not only about chemistry but about everything else too.

I express my gratitude to Dr. Gareth Lamb for our fishing trips, shared experiences, (many) beers and for him always being keen to discuss equity investments, much to the dismay of anyone else listening.

I must thank Dr. Justin O’Byrne, a man of unparalleled wit and humour who became a very close friend of mine over the final year of my PhD. I must thank him especially

for putting a roof over my head whilst I finished my time in the lab and for his many wise words which have helped me write this thesis.

I have been fortunate to call the aforementioned my colleagues over the past four years and hope that I can continue to call them my friends for many years to come.

Particular thanks must go to my close friends Neil Hopkins and Sam Fowler Holmes for always listening to my chemistry "chat" despite not being in the field, I look forward to standing alongside Neil as his best man very soon.

My family are immensely important to me and I must express my gratitude to them individually for making me the man that I am today. To Pops, whose enthusiasm for science and thirst for knowledge remains unmatched by anyone I have met so far in my life. I remain convinced my passion for science was triggered by an amazing fact he shared whilst I was sat on his knee, I can only guess which one. To Mam, for always giving everything she could and more to all of us. To Tino, for being an exceptional role model, always showing me the way and for bribing me into being good at school with £1 for each merit slip I brought home. To Angie, for always picking up the phone in the early hours of the morning and always getting me to school ontime, despite me hiding my shoes. To Marco, for always being available to chat whether it be over a round of golf, a beer, the phone, Skype or Steam. I grew up as his wingman and cannot express my gratitude enough for everything he has done for me over the years. To Gina, my older (but younger) sister and partner in crime, who has always made sure that my feet have remained firmly on the ground. To Tony, Nico and Ryan, my amazing nephews, for always making me smile.

Finally and most importantly, I would like to express my thanks to Gemma Tunbridge. We met on the first day of our undergraduate degrees in Bath eight years ago and we have been inseparable since. My time at university would've been infinitely more difficult without her endless patience and support, her vast knowledge of organic chemistry and her epic culinary skills. Our years together in Bath have been the best of my life and I know that we will share many more amazing years together in pastures new.

Abstract

Fossil fuels such as coal, oil and natural gas are, by the nature of their formation, a finite resource. Fossil fuel resources will eventually deplete or become uneconomical to use. If mankind is to maintain or improve its current quality of life over future generations, alternative means of producing usable energy and materials must be found. One feasible approach is bio-refining, which uses biomass to produce usable energy and materials from renewable sources. It has been stated that the main factor against the viability of a bio-refinery is the lack of available technology. The work described within this thesis aimed to enhance the technology in two areas within a potential bio-refinery; the depolymerisation of lignin to produce platform chemicals and the polymerisation of *rac*-lactide to produce bio-plastics.

Chapter 2 contains the synthesis of a range of novel zinc(II) and aluminium(III) heterogeneous silica tethered initiators for the ROP of *rac*-lactide were synthesised as well as their homogeneous silsesquioxane analogues. The heterogeneous complexes produced polylactide of reasonable molecular weight in a well controlled fashion, with Si-(L$^{\mathbf{H}}$O)Al showing a degree of stereocontrol (P_r = 0.32). ICP-AES analysis showed a reduction in the metal content of the polymer produced by heterogeneous initiators. A polymer synthesised by the heterogeneous Si-(L$^{\mathbf{tBu}}$O)Al complex contained 431 ppm Al compared to 2500 ppm Al when its homogeneous analogue, Al(L$^{\mathbf{tBu}}$O)Me$_2$, was used. A novel tetrametallic zinc(II) complex, Zn$_4$(L$^{\mathbf{H}}$O)$_4$(OMe)$_2$Me$_2$, was synthesised, demonstrating serendipitous oxygen insertion into the Zn-Me bond.

Chapter 3 involved the synthesis and characterisation of a range of novel zinc(II) complexes based on a *β*-ketoiminate ligand system with varying steric properties. These were also active for the synthesis of polylactide from *rac*-lactide but exhibited no stereocontrol. The complexes were active in the industrial preferred melt conditions.

Chapter 4 details analytical processes to assess the depolymerisation of lignin under oxidative conditions and a range of model lignin compounds were synthesised. Various approaches were utilised, based on heterogeneous and homogeneous catalysts.

The catalytical coupling of two –OH groups to form an ether moiety was observed in the presence of a Re(VII) complex and H_2O_2. A range of cobalt and vanadium complexes were synthesised and two solid state structures, CoSaL^{tBu}OO and V(L^{tBu}OO)O, were determined, these were screened for the depolymerisation of lignin and model compounds.

Contents

Chapter One

Introduction

1. Introduction

A recent report by the United Nations estimated that the world population has exceeded 7 billion and projections imply that it will reach 8 billion in 2024.[1] The annual energy demand of the global population was estimated to be 504×10^{15} Btu (British thermal units) in 2008 and is projected to increase by over 50 % to 769.8×10^{15} Btu in 2035.[2] The majority of the energy and material needs of the world population are currently met by the consumption of fossil fuel resources such as petroleum, coal and natural gas. These are termed fossil fuels as they are mainly formed by biogenic processes over periods of millions of years.

The timescale of the formation of fossil fuels means that they are a finite and non-renewable resource. The fundamental non-renewable nature of fossil fuel resources dictates that if consumption is to be maintained or increase then they will eventually be depleted. Mankind currently depends on these resources to provide the energy and materials for its current quality of life. If the quality of life of individuals across the globe is to be maintained or improved in future generations then the ever increasing global demand for energy and materials must be met by renewable and sustainable means.

The timescale upon which each fossil fuel will be depleted or become too costly to use is widely debated and in depth analysis is beyond the scope of this thesis. However, it is important to note that in recent times the price of fossil fuel resources, such as crude oil, have increased.[3] Figure 1.1 shows the average monthly spot price in dollars for a barrel of Brent Crude Oil over the past 15 years.[3] The data shows a significant increase in price since the start of the 21st century and despite dramatic short term shifts caused by external economic factors the trend appears to be continuing upwards.

Figure 1.1 – Average monthly spot price ($ per barrel) of European Brent Crude oil for the previous 15 years.[3]

The increase in the price of crude oil and other fossil fuels has brought issues of fossil fuel consumption to the front of global political debate. There has been a strong political desire across the world to reduce dependence on traditional fossil fuel feedstocks for the economic reasons discussed above along with environmental concerns of sustainability and greenhouse gas emissions. Political discussion has led to economic incentives and subsidies for the use of renewable materials as well as increased taxation for the use of fossil fuels.

Due to the geographical location of fossil fuels, the countries which currently consume the most resources often must import them from foreign nations. The reliance on the supply of resources such as crude oil from foreign nations has led to the issue of energy security. Energy security is related to concerns surrounding the supply of a crucial energy resource from a foreign nation. The supply of a resource can be vulnerable to natural disasters, political instability, cost, terrorist attacks and other factors. The issue of energy security has become a significant point of concern within importing nations who want to ensure the disruption of supply of feedstocks and materials will not have a significant detrimental effect on the country.

Due to the economic, environmental and security issues above there has been a large push for society to reduce its dependence on fossil fuel feedstocks and a plethora of potential alternatives have been proposed. This thesis is focused on one potential alternative; the exploitation of plant biomass as a renewable resource.

1.1. Plant Biomass

Plant biomass is the world's most abundant renewable material, the main constituents of which are hemicellulose (20-35 %), cellulose (30-50 %) and lignin (15-30 %). Hemicellulose describes a range of short chain polysaccharides which can be accessed relatively easily. One of the most promising uses for hemicellulose is as a feedstock for fermentation to produce bio-ethanol, which can be used as an alternative liquid fuel [4] or as a feedstock for the production other platform chemicals such as ethene and 1,3-butadiene.[5] Current commercial fermentation processes use yeasts (such as *Saccharomyces cerevisiae*) which convert the hemicellulose part of plant matter to ethanol, the feedstock is often pre-treated to convert the hemicellulosic fraction to monomeric sugars which are more easily accessible to yeast.[4,6-10] Brazil has a significant bio-ethanol program using sugarcane as a feedstock which they can grow in large amounts, in the year 2007 Brazil produced 16 billion litres of ethanol from plant feedstocks.[4]

The current commercial first generation bio-ethanol processes ferment easily accessible carbohydrates and do not utilise the lignocellulosic fractions of the feedstock. Second generation bio-ethanol processes are being developed, these processes use different microorganisms than traditional yeasts which can also feed on the cellulose within plants. Second generation processes, whilst utilising the cellulose within plants, will still produce lignin as a waste product.[11-13]

1.2. Bio-refinery Concept

If plant matter is to be used as an alternative to traditional chemical and energy sources it is important to unlock all the potential economic value that is contained within the feedstock. This has led to a proposed bio-refinery approach, which is comparable to a traditional petrochemical refinery but uses plant matter as a feedstock instead of crude oil.[14-16]

For the bio-refinery concept to be successful in the long term the most important factor is that it is economically viable. There must be a net gain in wealth for the processing of the feedstock after all costs are considered. There are obvious environmental benefits to using a feedstock which is renewable as opposed to depleting fossil fuel carbon sinks, but ultimately unless the process generates wealth then it will fail in the long term.

The petrochemical industry has evolved throughout the 20th century and modern refining processes are highly efficient. Bio-refining is a relatively new concept and the main barrier to commercial success has been identified as the lack of low cost processing technology.[17] Any commercially successful bio-refinery is likely to use a combination of biological, chemical and physical processes to fully utilise the plant feedstock. Significant research is still required into all processes and reactions that could potentially be used in a bio-refinery. As new technology is discovered and developed the costs of operating a bio-refinery will be reduced, if the price of crude oil and other fossil fuel resources continues to increase there will be a crossing point at which large scale bio-refineries will be economically viable.

The work described in this thesis is focused on two potential processes that could contribute to a commercial bio-refinery; the use of lignin as a feedstock to produce platform chemicals and the polymerisation of lactide to produce polylactide, a biorenewable plastic.

1.3. Lignin

1.3.1. Structure

Lignin describes a highly cross-linked 3-dimensional complex polymer with a large molecular mass (600-15000 kDa).[18,19] Lignin, unlike cellulose, contains a variety of different monomers and the relative composition of each monomer in the overall structure can vary depending on many factors, including growth conditions and the species of plant.[20] Due to the variable nature of the polymer it is difficult to characterise and its precise structure is still unknown. Hypothetical structures have been reported in the literature; one such structure is shown in Figure 1.2.[21]

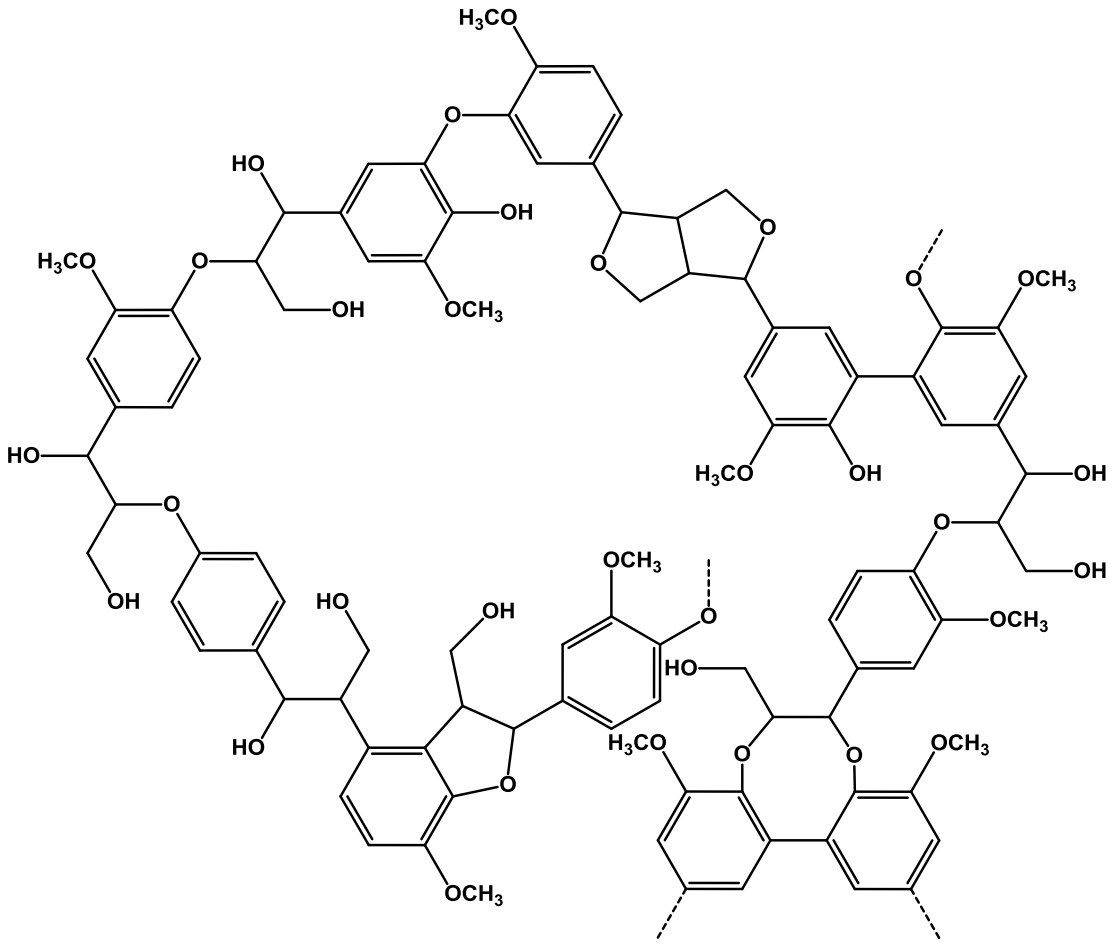

Figure 1.2 – A proposed hypothetical structure of lignin, adapted from *Weng et al.*[21]

Physiologically lignin adds strength to the plant, acts as a binder of cellulosic components and protects against microbial or fungal destruction of the cellulose fibres, in essence lignin adds bulk and rigidity to the plant.[22] Lignin is made up of many monomeric components which vary depending on the species of plant and growth

conditions. Three main monomers are broadly associated with lignin and are termed the monolignols, these are *p*-coumaryl alcohol, coniferyl alcohol and sinapyl alcohol (Figure 1.3).[6,8,19,23] Due to its polyphenolic nature, lignin offers the potential to be processed into a renewable source of aromatic functional material.

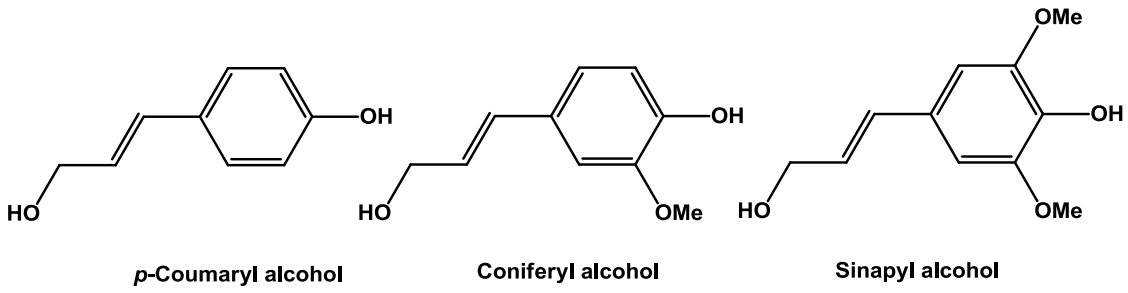

Figure 1.3 –The three main monomers associated with lignin, termed the monolignols.

The biosynthesis of lignin is not limited to these three monomers and dozens of phenolic monomers have been associated with lignin structure and biosynthesis. The composition of lignin will vary depending on species and growth conditions as the plant will vary the biosynthetic pathway to produce a lignin relative to its needs. The term 'lignin' therefore does not relate to a specific structure but a broad range of plant derived polyphenolic structures.[19,21,24,25]

1.3.2. Model Compounds

Due to the difficulties in the characterisation of the structure of lignin it is common practice for catalysts and processes to be demonstrated using model compounds. These compounds typically contain the characteristic ether bonds and functional alcohol groups associated with lignin. Over 100 lignin model compounds have been reported in the literature and are the subject of a section in a recent review by *Zekzeski et al*.[26] The reported compounds vary from simple monophenols to dimeric and oligomeric structures and offer the ability to mimic all of the functionality associated with lignin. With such a vast array of compounds reported selection of an appropriate compound for a given reaction is important. A model compound will be selected based on the linkages present in the compound, availability, ease of synthesis, cost and possible unfavourable side reactions. A selection of some of the model compounds selected for use in this thesis are shown in Figure 1.4.

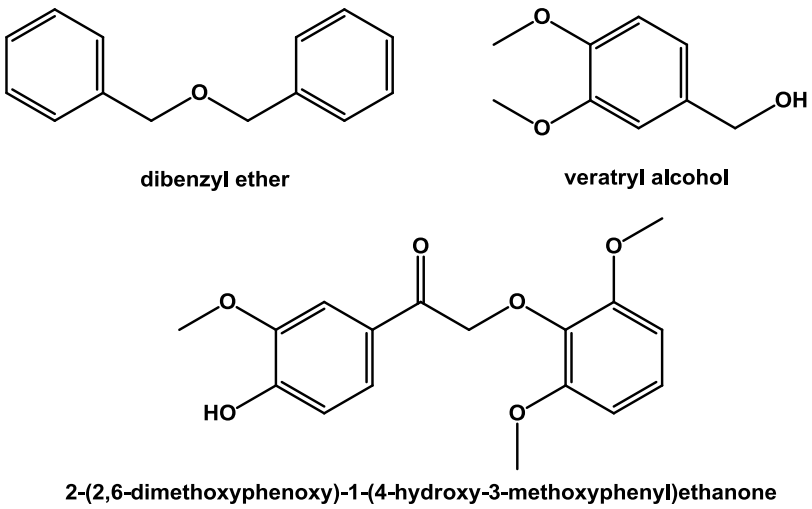

Figure 1.4 –A variety of the lignin model compounds used in this thesis.

Another beneficial aspect of model compounds is that they are often the degradation products of lignin. This allows the use of model compounds to be used to explore downstream processing steps to upgrade lignin feedstocks into useful products. An example is recent work by *Mialon et al* who upgraded vanillin, a major lignin product, into poly(dihydroferulic acid), a biorenewable PET alternative, in 3 reaction steps.[27]

1.3.3. Lignin as a Waste Product of the Kraft Process

The Kraft process is a chemical pulping process used to process wood feedstocks into purified pulps. The main commercial product of the Kraft process is purified cellulose fibers which are used to produce printing paper, 117 Mt of pulp was produced by the Kraft process in 2000.[28] In the Kraft process the wood feedstock is treated with sodium hydroxide and sodium sulphide at temperatures in excess of 170 °C; a combination of the alkalinity and heat of the process breaks the interactions between lignin and cellulose and solubilises the lignin. The purified cellulose fibres are used for paper manufacture and other commercial uses. The lignin can be recovered by neutralising the alkaline waste stream and current processes simply combust this material to produce heat energy.[29]

1.3.4. Current Technologies for Processing Lignin

Due to the complex and robust nature of lignin it is more difficult to exploit than other biopolymers such as cellulose. Lignin is already a significant side product of the paper industry and is likely to be a major product of any biorefinery that uses plant biomass as a feedstock. Current technologies for processing lignin into useful chemicals are

limited and the material is often simply combusted for heat energy. Significant value could be added to current and future processes if lignin could efficiently be broken down into commercially relevant single phenol units or other useful chemicals.

1.3.5. Catalysis

1.3.5.1. Hydrolysis

Various hydrolytic methods have been reported for the depolymerisation of lignin. Under hydrolytic conditions the lignin is generally reacted with hydrogen (added as H_2 or H^+) at high temperature and pressure with a catalyst, under these conditions the water is formed together with deoxygenated lignin products. The simplest methods use strong acids at high temperature without the addition of a catalyst, these processes are often used to pre-treat the lignin feedstock before further processing. The hydrolytic cleavage of lignin was reported as early as 1938 when *Harris et al* reported the reaction of lignin with hydrogen over a copper-chromium oxide catalyst.[30] Under these conditions full hydrogenation of the aromatic rings were reported to yield cyclohexanols and methanol. These early studies highlight the potential of hydrolytic cleavage of lignin to produce fuel-like products, however, greater value can be extracted from the lignin feedstock by controlled hydrolysis, where the aromatic content of the feedstock is retained and monomeric phenols are yielded. Early examples of controlled hydrolysis were reported by *Hibbert et al* in 1948 who reported the isolation of syringol (1,3-dimethoxy-2-hydroxybenzene) and guaiacol (2-methoxyphenol) components from maple wood lignin using a Raney Nickel catalyst at 173 °C with an initial pressure of 20.7 MPa of H_2 before heating.[31,32] *Pepper et al*, who contributed to the early work by *Hibbert et al*, later explored the hydrolysis of lignin using a variety of noble metal catalysts (Pd/C, Rh/C, Rh/Al_2O_3, Ru/C, Ru/Al_2O_3). In this work yields of up to 34 % of an ether extracted mixture mainly consisting of 4-propylguaiacol and dihydroconiferyl alcohol were obtained when using a Rh/C catalyst at 195 °C with an initial hydrogen pressure of 3.4 MPa (Figure 1.5). [33] They later reported the effect of H_2 pressure, catalyst loading and pH on the reaction.[34]

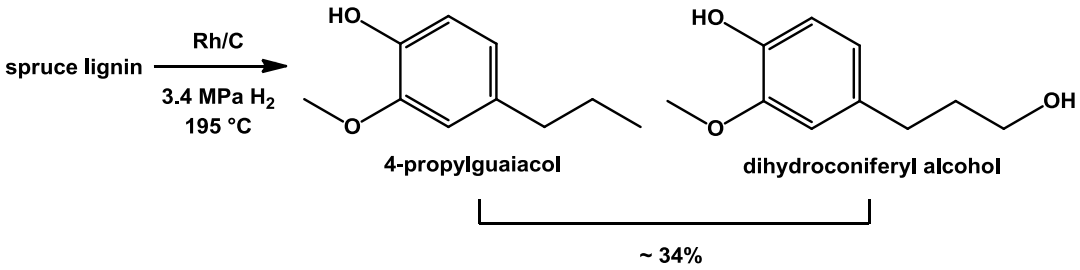

Figure 1.5 – Early work by *Pepper et al* reported the controlled hydrolysis of spruce lignin under relatively mild conditions over a Rh/C catalyst to yield a mixture containing mainly 4-propylguaiacol and dihydroconiferyl alcohol in an approximate yield of 34%.[33]

Since this early work the use of noble metal catalysts for the hydrolysis of lignin has been further explored. In 1992 *Meier et al* reported the decomposition of lignin over a Pd/C catalyst at 380 °C with an initial hydrogen pressure of 10 MPa to yield 80.6 wt% of an oil consisting mainly of monophenols.[35] More recently in 2008 *Dyson et al* reported the selective degradation of wood lignin by the use of noble metal catalysts.[36] In this work platinum, palladium, rhodium and ruthenium supported on carbon were all shown to catalyse the depolymerisation of lignin at temperatures ranging from 200-300 °C and an initial H_2 pressure of 4 MPa. Pt/C was shown to give the greatest yield of monomers and dimers (46.4 %wt) from lignin. When the monomer/dimer mixture was treated with a second processing step in which Pd/C was deployed the complete hydrolysis to alkanes and methanol was observed.[36]

Another system which has shown promise for the hydrodeoxygenation of lignin is the use of bimetallic catalysts containing molybdenum and another promoting metal centre (typically nickel or cobalt). These catalysts are commercially available and are typically used to remove nitrogen and sulphur from oil feedstocks. The activity of these catalysts has widely been assessed using model compounds and they have been shown to be capable of both the complete and partial hydrolysis of model compounds.[37-59] Fewer examples exist in which these catalysts have been applied to whole lignin and where reported they typically involve an initial processing step before treatment with a Ni-Mo or Co-Mo catalyst.[60-62] The extensive research into the transformation of model compounds and commercial availability of these catalysts make them good candidates for downstream processing of already depolymerised lignin into higher value products.

Hydrolytic cleavage of lignin uses relatively harsh reaction conditions with temperatures in excess of 200 °C and high pressures of H_2 but offers the potential to convert lignin into fuel products in a low number of steps. Controlled hydrolysis also offers the ability to tune a process to generate potentially useful monophenols from lignin.

1.3.5.2. Oxidation

A variety of oxidation catalysts have been reported for the depolymerisation of lignin. As opposed to hydrolytic conditions which remove functionality, oxidative reactions tend to form products with greater functionality which could potentially have uses as fine chemicals.

In 2000 *Herrmann et al* reported the cleavage of C=C bonds by a methyltrioxorhenium (ReO_3CH_3) (MTO) catalyst.[63] The proposed mechanism for this cleavage is shown in Figure 1.6. Inactivation of the MTO catalyst was observed after 1000-2000 cycles by formation of the perrhenate anion and other oxidised derivatives. The authors had previously reported a method to recover the perrhenate anion and transform it into catalytically active MTO in a one pot synthesis.[64]

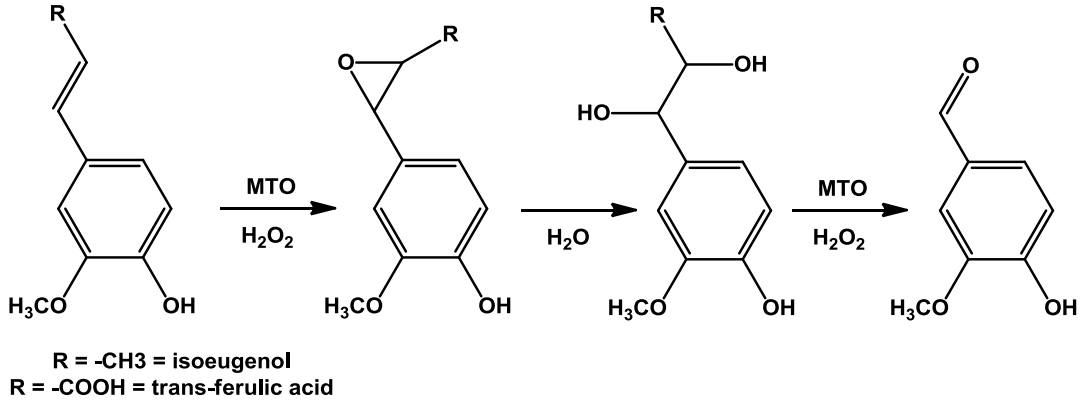

Figure 1.6 – Mechanism proposed by *Herrmann et al* for the reported cleavage of C=C bonds in isoeugenol and trans-ferulic acid in to form vanillin.[63]

Crestini et al later reported that when used in combination with H_2O_2, MTO was effective in the depolymerisation of a wide range of lignin model compounds as well as sugar cane lignin and red spruce kraft lignin.[65,66] In this work the oxidation of vanillyl and veratryl alcohol was reported to yield the corresponding acids, aldehydes and quinines in up to 49 % yield.

Another example of oxidative catalysts being used for the depolymerisation of lignin is the use of Co(salen) catalysts. The ability of Co(salen) to oxidise lignin are due to the ability to form cobalt-superoxo complexes and peroxo complexes upon reaction with oxygen.[67] *Drago et al* in 1985 reported the oxidation of isoeugenol to vanillin using a Co(salen) complex and gaseous oxygen (60 °C, 0.517 MPa).[68] *Bozell et al* demonstrated the oxidation of the phenolic groups of a variety of lignin model compounds to form benzoquinones at room temperature in low pressures of oxygen (0.345 MPa) with a variety of substituted Co(salen) catalysts.[67] The oxidation of veratryl alcohol to veratraldehyde using Co(salen) catalysts has been observed by a number of different research groups.[69-71] The activity of these complexes seem to be limited to the oxidation of OH groups or C=C bonds, making them promising catalysts for the upgrading of lignin feedstocks but unlikely candidates for the depolymerisation of lignin. It has been acknowledged that few studies exist in which the treatment of lignin feedstocks has been carried out with Co(salen) catalysts.[72]

More recently *Hanson et al* have reported the breakdown of lignin model compounds by vanadium(V) complexes.[73] The group reported a range of vanadium complexes based on previously reported dipicolinate vanadium(V) complexes[74] an example of which is shown in Figure 1.7. The catalytic breakdown of the lignin model compound 1-phenyl-2-phenoxy-ethanol was reported (Figure 1.8) under relatively mild conditions (air, 100 °C). The reactions proceeded to high conversion with good yields of phenol (77 %) and benzoic acid (81 %) as well as small amounts of other oxidised products.

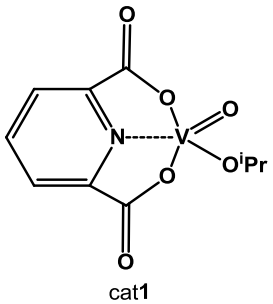

cat1

Figure 1.7 - Dipicolinate vanadium(V) complex originally reported by *Thorn et al* [74] were recently used in the breakdown of lignin model compounds.[73]

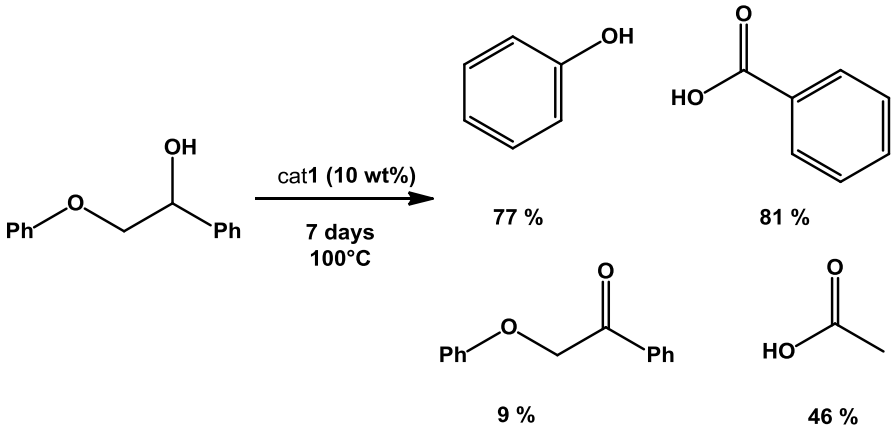

Figure 1.8 – Catalytic breakdown of the lignin model compound 1-phenyl-2-phenoxy-ethanol using a vanadium(V) complex.

Other examples of oxidative catalysts for lignin treatment include biomimetic metalloporphyrin catalysts, Fe-TAML (tetraamido macrocyclic ligand) catalysts and polyoxometalate catalysts which are summarised in a recent review article.[26]

1.3.5.3. Gasification

In a gasification process an organic feedstock is heated to a high temperature (typically 650 °C or greater) in the presence of oxygen and/or steam. As a result of the high temperature carbon monoxide is liberated from the organic feedstock and the product is a gaseous mixture of CO and H_2, known as syngas, as well as CO_2 and O_2. This technology has been derived from existing processes, which can be used to convert fossil fuels such as coal and natural gas into liquid fuels via Fischer-Tropsch catalysis.[75] This process has been widely studied, and to summarise simplistically; in the presence of a Fischer-Tropsch catalyst, such as cobalt, iron or ruthenium, the carbon monoxide in syngas is polymerised into longer chain alkanes. This occurs by the overall reaction shown in equation 1.1. It is important to note that side reactions occur to maintain this overall reaction.

$$(2n+1)\ H_2 + nCO \rightarrow C_nH_{(2n+2)} + nH_2O$$

Equation 1.1 – Overall equation for the Fischer-Tropsch conversion of CO to alkanes.

This process has long been thought of as a potential means of converting biomass into liquid fuels,[76,77] however, significant challenges remain. Some challenges for the gasification of biomass to become economically viable are the consistency of the feedstock, the removal of tar, removing catalyst poisons such as sulphur from the feedstock and the storage and transport of the syngas product.[78] In biomass gasification the ease of processing is largely dependent on the feedstock used which

means that potentially high-yield feedstocks could be developed.[79,80] Once an efficient process has been developed there are other applications of the syngas product, these include: conversion to chemical feedstocks, electricity generation and processing into traditional liquid fuels or ethanol.[78]

1.3.5.4. Pyrolysis

Pyrolysis is defined as the thermal decomposition of materials in the absence of oxygen. It is a rapid heating process in which the main product is oils. The products of pyrolysis are largely dependent on the process conditions and therefore the process can be tailored to specifically produce heat, chemicals or fuels depending on the requirements.[81] Fast pyrolysis is a process applied on a timescale of seconds and involves rapid heating (up to around 500 °C) of the biomass in purpose built reactors. Under these rapid heating conditions the biomass quickly decomposes into vapours with some char production. The hot vapours are rapidly cooled and condense to give a liquid bio-oil product in yields of up to 75 wt%. from dried biomass.[78] The pyrolysis of whole plant feedstocks is a complex area of active research and the focus of a recent review article by *Mohan et al*.[81] Pyrolysis processes have also been applied specifically to lignin. *Britt et al* studied the flash vacuum pyrolysis of a range of lignin model compounds and concluded that the depolymerisation reaction is dominated by free radical reactions.[82] *Kleinert et al* have developed a pyrolysis process of lignin in the presence of formic acid and ethanol at approximately 350 °C. The precise mechanism of the action of the formic acid has not been determined but the results reported show high yield of bio-oil (> 90 % as %wt. of starting material) and low levels of char (<5 %) and that the presence of formic acid is crucial to achieve these high yields.[18,83,84] The unfavourable repolymerisation of depolymerised products has been reported.[8,26] *Li et al* studied the repolymerisation of aspen wood during steam hydrolysis and found that the addition of 2-napthol suppressed the repolymerisation reaction. [85]

1.3.5.5. Supercritical Water

The use of water as a solvent is beneficial, not only for environmental and economical reasons, but as it also offers several advantages in the processing of lignin feedstocks. The use of water as a solvent eliminates any potential complications from using wet

feedstocks, which is often a problem when processing biomass, and allows easy separation of organic soluble products.[86]

The use of supercritical H_2O as a solvent for the depolymerisation of lignin has been studied. When temperature and pressure exceed the critical parameters of a substance, its state is described as supercritical. The critical temperature and pressure of water are 647 K and 22.1 MPa, respectively. Under these conditions the vapours and liquids combine to form a single phase, changing the chemical properties dramatically. When water becomes supercritical it is miscible with most liquid compounds and inorganic compounds such as salts become insoluble.[87,88] This provides an environment where organic compounds and oxygen are mixed in a single phase and so eliminates any rate limitation due to mass transfer. This property can be exploited to break ether linkages in lignin, however the small products tend to repolymerise leading to the formation of char.[26] Addition of phenol or *p*-cresol to the reaction mixture has been shown to reduce char formation. Lignin has been shown to degrade into 2-(4-hydroxy-benzyl)-4-methyl-phenol (BMP) (Figure 1.9) with yields of up to 80 % in a supercritical mixed solvent of water/p-cresol.[89-91]

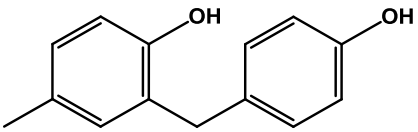

Figure 1.9 – Okuda et al reported 2-(4-Hydroxy-benzyl)-4-methyl-phenol (BMP) as a major product of lignin degradation in a supercritical mixed solvent of water and *p*-cresol. [90]

1.4. Lactic Acid & Polylactide

A biorefining process which can already be considered commercially successful is the large scale fermentation of corn starch and sugar beet to produce lactic acid. The commercial success of this process is due to the demand for polylactide (PLA) polymer which can be produced *via* several processing steps from lactic acid. The commercial manufacture of polylactide is performed by several companies worldwide; two notable producers are Natureworks and Purac. Natureworks market lactide monomers and polylactide products under their Ingeo® brand and have a current capacity of 140,000 tons per annum of PLA product at their main production facility in Blair, Nebraska.[92] Purac mainly market lactide monomers in their enantiomerically pure form but also produce PLA products and have recently opened a 75,000 ton production facility in Thailand.[93]

The demand for lactic acid is fuelled by the production of polylactide (PLA). The first commercial uses of PLA were medical applications which exploit the biocompatible nature of the polymer. Sutures and bone stents to be used *in vivo* are commonly manufactured from a copolymer of glycolide and lactide; poly(glycolic-co-lactic acid) (PLGA). In modern times advances in catalysis and the availability of low cost lactic acid has led to PLA being used as a commodity polymer.[92-94]

PLA can be produced by the polycondensation of lactic acid, however, the reaction proceeds *via* an equilibrium reaction limiting the molecular weight of the polymer. The equilibrium exists due to the presence of water; higher molecular weight polymer can be produced by the polymerisation of lactide which can be produced from the dehydration of two lactic acid units (Figure 1.10).

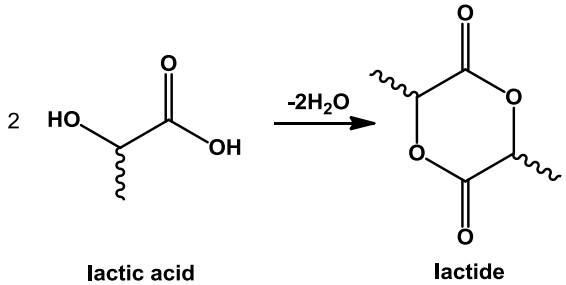

Figure 1.10 - Dehydration of lactic acid to form lactide

When produced on an industrial scale lactide is not produced by the direct condensation of two lactic acid units but is instead produced by the polymerisation of lactic acid to low density polylactide, followed by the depolymerisation to lactide monomers.[95,96]

The production and disposal of PLA lies within a renewable cycle.[97] Glucose is produced from the large scale fermentation of plant material which can be treated enzymatically to produce lactic acid. The lactic acid can be dehydrated and polymerised to produce useful polymer. After use the polymer can be recycled to low molecular weight oligomers by hydrolytic cleavage of the aliphatic backbone, these can then be easily recycled. PLA is classed as biodegradable as when given sufficient time in nature it will be broken down into carbon dioxide and water. The polymerisation of lactide to form PLA is not a trivial process and is widely achieved by the metal catalysed ring opening polymerisation of lactide which will be discussed at length later in section 1.5.5.

1.5. Ring Opening Polymerisation of Lactide

1.5.1. Coordination Insertion Mechanism

Although other mechanisms have been reported[98] the most common mechanism associated with the polymerisation of lactide is a coordination insertion mechanism (Scheme 1.1). This mechanism requires an initiator and metal based systems have been widely studied. The coordination-insertion mechanism was first formulated by *Dittrich et al* in 1971.[98,99]

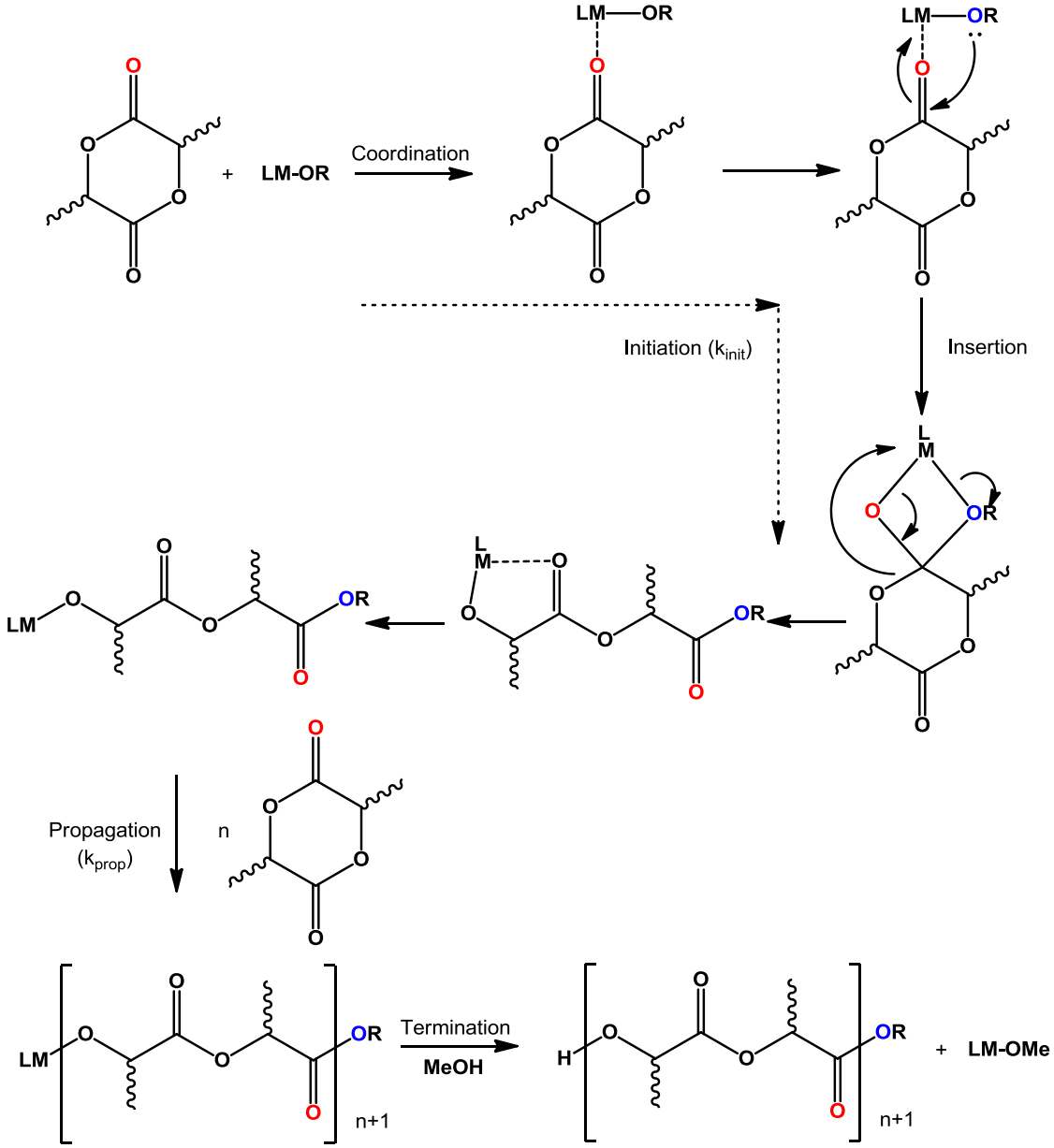

Scheme 1.1 – Coordination-insertion mechanism for the ROP of LA, adapted from[100].

The first step of the mechanism is the coordination of the carbonyl oxygen to the Lewis acidic metal centre (M). The coordination of the metal brings the carbonyl group of the monomer into close proximity of the nucleophilic initiating group (OR), allowing the insertion of the monomer into the M-OR bond via nucleophilic addition. The ring is then opened by the cleavage of the acyl-oxygen bond and propagation of the chain can occur by addition of LA monomers to the **LM** group. The polymerisation is terminated by the hydrolysis of the M-O bond, this can be achieved by the addition of MeOH leading to a LM-OMe species and a hydroxyl end group on the polymer chain. The end group at the other end of the chain is determined on the initiating group present in the metal-initiator (OR). Depending on the initiator the polymerisation of LA can often be described as living; this means that the degree of polymerisation is determined by the relative amount of monomer present in the reaction. The polymerisation will continue until the LA monomer has been used and the species will remain active unless terminated. If the reaction has not been terminated but all of the LA monomer has been consumed addition of further LA or another cyclic ester will continue the polymerisation process.

The metal initiated coordination insertion mechanism allows for control over the molecular weight of the polymer product provided certain conditions are met. The main factor is the relative rate of propagation (k_{prop}) compared to the rate of initiation (k_{init}). If $k_{init} > k_{prop}$ then all chains will quickly be initiated at the metal centre and chains will propagate simultaneously, leading to polymer chains of a similar molecular weight being produced. If $k_{prop} > k_{init}$ then chains will be initiated over a period of time whilst propagating at the same rate. Under these circumstances the chains initiated first will have a larger molecular weight than those initiated later which will result in a broad molecular weight distribution. The relative rates k_{prop} and k_{init} are mainly influenced by the metal centre (M), the initiating group (OR) and the ligand (L). Gel Permeation Chromatography (GPC), discussed later in section 1.5.4.2, can be used to characterise the molecular weight of the polymer as well as its polydispersity index (PDI) which is a measure of the distribution of molecular weights (M_w/M_n) in the polymer sample. Theoretical molecular weights can be predicted (equation 1.1) and compared to experimental values.

monomer:initiator ratio

M_n (calculated) = 144.13 x conversion (%) x 100 + (end groups)

RMM monomer

Equation 1.2 – Calculation of theoretical molecular weight for a 100:1 polymerisation of lactide

1.5.2. Transesterification

Another influence over the control of the polymerisation reaction is the extent of side reactions. The most significant side reaction in the ROP of LA is transesterification of the polymer chain. Transesterification occurs during propagation when the active metal reacts with an ester group from a polymer chain instead of a new monomer, this can happen within a polymer chain (intramolecular, Figure 1.11) or between two different polymer chains (intermolecular) (Figure 1.12).

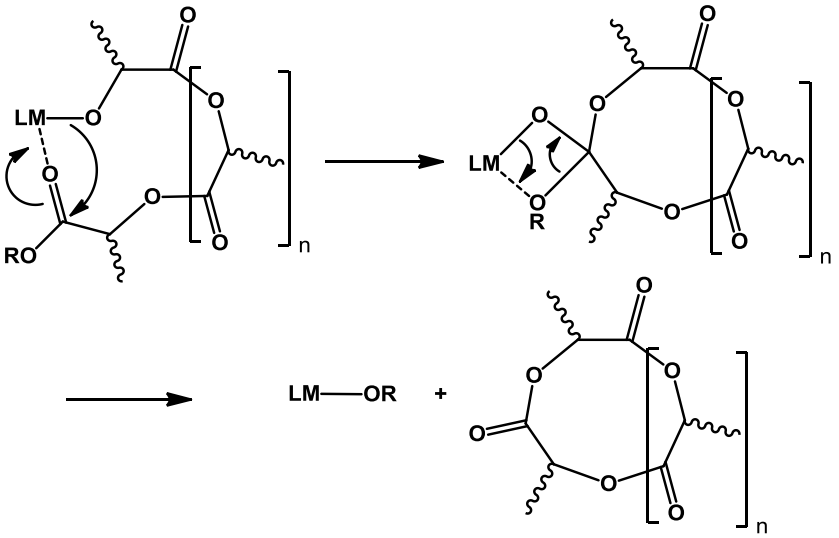

Figure 1.11 – Intramolecular transesterification in the polymerisation of lactide

The degree of both intramolecular and intermolecular transesterification reactions are highly dependent on reaction conditions, increasing with reaction time and temperature. The type of metal alkoxide initiator has also been shown to have a significant effect on transesterification and the following order has been observed: $Bu_2Sn(OR)_2 > Bu_3SnOR > Ti(OR)_4 > Zn(OR)_2 > Al(OR)_3$.[101] The stereochemistry of the polymer chain has also been linked to the extent of transesterification with isotactic PLA showing reduced levels when compared to atactic PLA. This effect has been attributed to the increased crystallinity of the isotactic polymer reducing the

degree of side reactions. The potential stereochemistries of PLA are further explored in section 1.53.

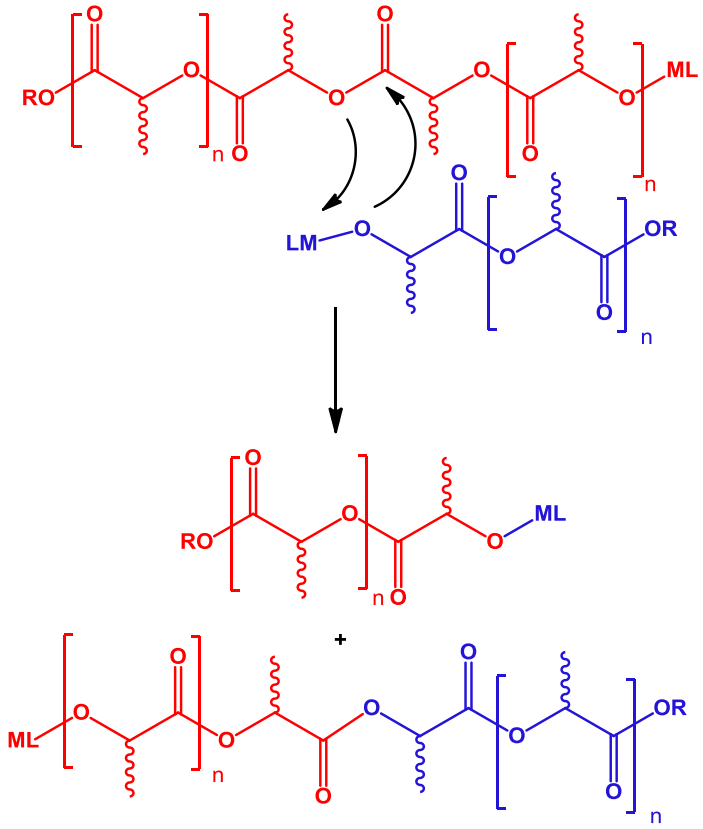

Figure 1.12 – Intermolecular transesterification in the polymerisation of lactide

Increased levels of transesterification will result in a broad molecular weight distribution and so higher PDI values will be observed in GPC analysis. The polymer can be further characterised by mass spectrometry, typically using Matrix Assisted Laser Desorption ionisation and Time of Flight detection (MALDI-TOF). MALDI-TOF can be used to assess the degree of transesterification in a polymer sample; if the polymer chains show no transesterification then the masses will be distributed by 144 mass units, the molecular weight of a single LA monomer. However, in the presence of transesterification a second distribution separated by 72 mass units will be observed due to the chain being transesterified at any carbonyl along the polymer chain. MALDI-TOF MS also allows determination of the end group of a polymer chain.

1.5.3. Polylactide Stereochemistry

The lactide monomer contains two stereocentres enabling three potential stereoforms of the cyclic ester, *L*-lactide (*L*-LA) (S,S), *D*-lactide (*D*-LA) (R,R) and *meso*-lactide (*meso*-LA) (S,R) (Figure 1.13).

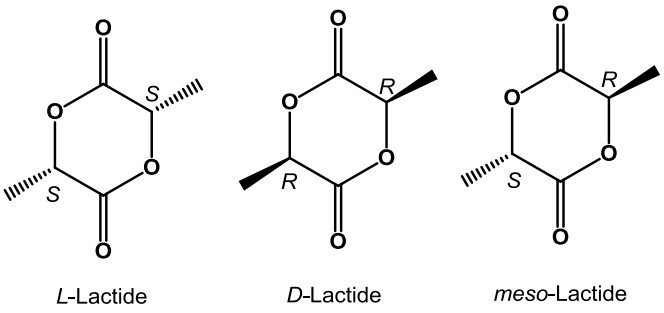

Figure 1.13 – Enantiomeric monomers of lactide

L-Lactide is the naturally occurring enantiomer and can be obtained in high purity from biological sources, the other forms are generally obtained by the racemisation of *L*-LA and other processing steps.[95] Polymerisation of pure *L*-LA or *D*-LA will lead to an isotactic polymer of PLLA or PDLA depending on which pure enantiomer was used as a starting material (Figure 1.14 top). Polymerisation of *meso*-LA can result in three polymer microstructures (Figure 1.14 middle), if a non-stereoselective initiator is used then an atactic polymer will be produced. If a stereoselective initiator is employed for the polymerisation of *meso*-LA then it can produce either heterotactic or syndiotactic polymer. The type of polymer produced depends on whether the initiator possesses selectivity for insertion of an identical stereocentre (heterotactic e.g. {–RRSS-}$_n$) or a different stereocentre (syndiotactic e.g. {–RSRS-}$_n$) to the end of the growing chain.

The polymerisation of a 50:50 mixture of *L*-LA and *D*-LA (*rac*-LA) will result in three general microstructures depending on the stereoselectivity of the initiator (Figure 1.14 bottom). A non-stereoselective initiator, such as the commercially popular tin(II) octanoate, shows no preference for the addition of either monomer to the end of the growing polymer chain and so will produce atactic PLA. Although atactic PLA is a polymer of randomly distributed *L*-LA and *D*-LA it is important to note that it still contains paired stereocentres (e.g. –RRSS-) due to the stereochemistry of the monomers. Stereoselective initiators can be selective for the addition of an identical or different monomer to the end of the growing chain. In the case of *rac*-LA if the initiator is selective to add an identical monomer then the result will be an isotactic polymer (e.g. {–RRRR-}$_n$), if it is selective to add a different monomer then a heterotactic polymer will be produced (e.g. {–RRSS-}$_n$). The composition and order of stereocentres in a polylactide polymer chain can have significant effects on the

physical properties of the polymer, for example isotactic PLA has a melting point of approximately 170 °C whereas stereoblock isotactic PLA has a melting point of approximately 230 °C.

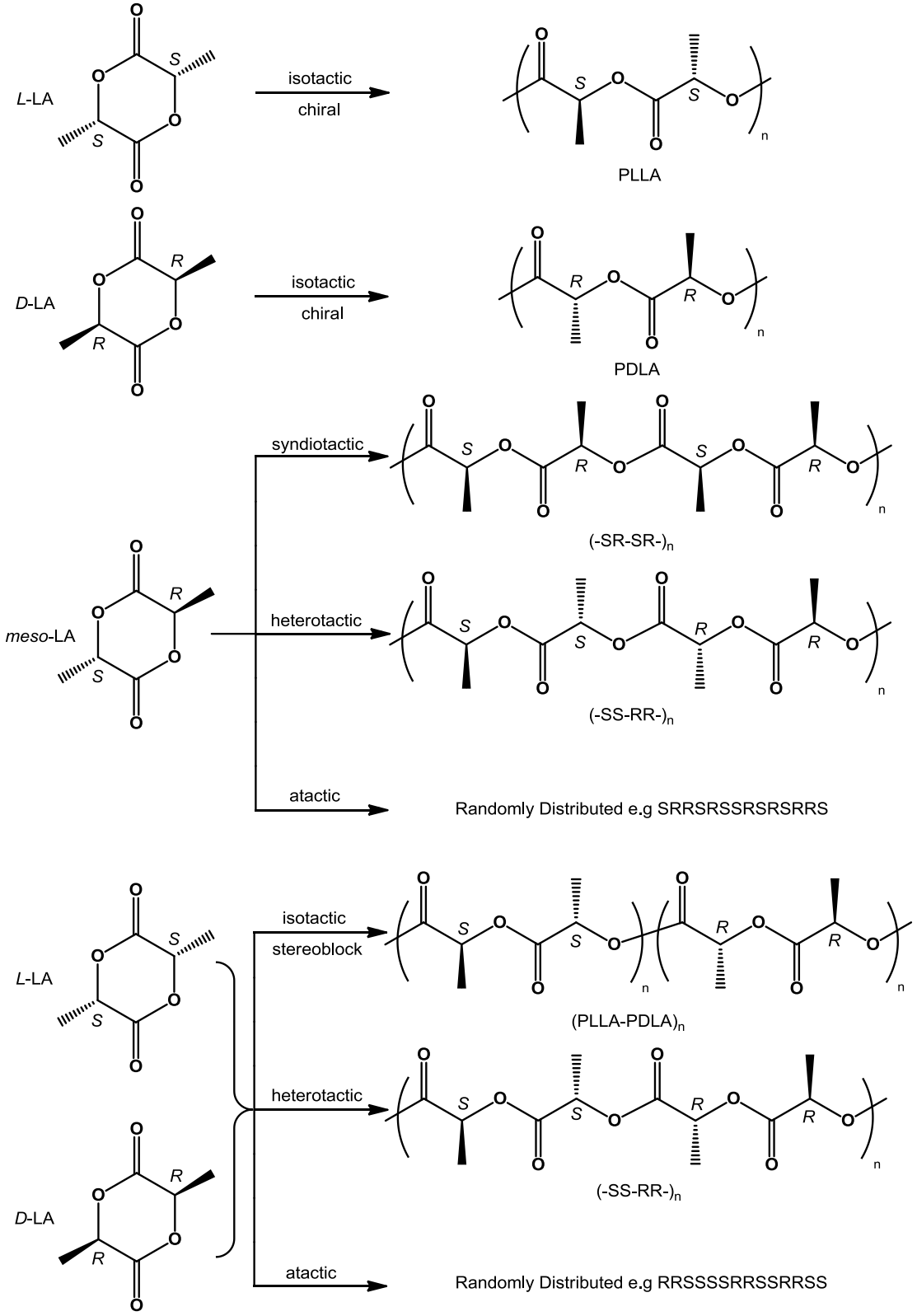

Figure 1.14 – Potential stereochemical polymers from enantiomeric lactide monomers.

1.5.4. Polylactide Polymer Characterisation Techniques

1.5.4.1. ^{1}H Homonuclear Decoupled NMR Spectroscopy

The composition and order of monomers in a PLA chain can be determined by analysis of the $^{13}C\{^{1}H\}$ or ^{1}H homonuclear decoupled NMR spectrum. The ^{1}H homonuclear decoupled method is preferred as it gives a greater signal to noise ratio and requires less time to obtain a spectrum. In this technique the intramolecular interaction of the methine groups is analysed to assess their relative enantiomeric abundance. The spectrum is decoupled in the methyl (~δ 1.62 ppm) region from the backbone of the polymer giving required the resolution in the methine region (~δ 5.20 ppm) to assess stereochemistry. The interactions observed in the methine region are influenced by the nature of the stereochemical tetrad in which a methine group resides. Sequential centres can be labelled relative to one another; two adjacent groups with the same stereochemistry are labelled *i* (*iso*) and those with different stereochemistry are labelled *s* (*syndio*) giving rise to eight possible tetrads.

Isotactic PLA synthesised from enantiomerically pure monomer will consist purely of the *iii* tetrad (Figure 1.15a top) and will have a single peak in the ^{1}H homonuclear decoupled NMR spectrum (Figure 1.15a bottom). Stereoblock isotactic PLA will predominantly contain the *iii* tetrad but will have a small number of *isi*, *iis* and *sii* tetrads from the point at which the blocks join (Figure 1.15b top) giving four peaks in the ^{1}H homonuclear decoupled NMR spectrum (Figure 1.15b bottom).

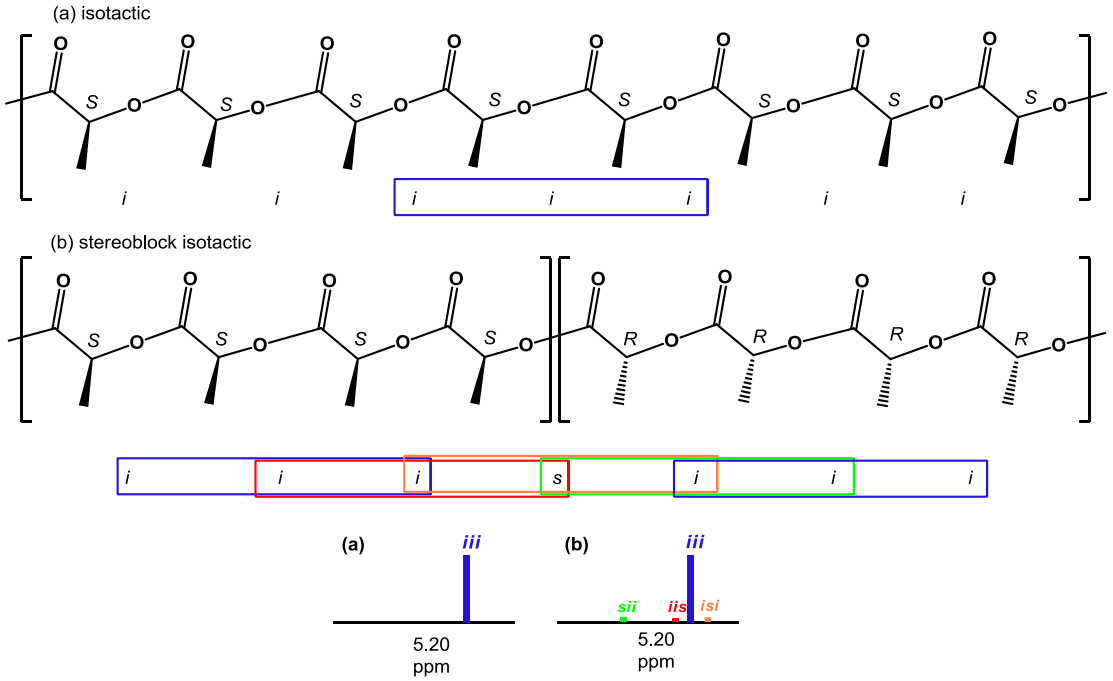

Figure 1.15 – Top: tetrad possibilities for isotactic polylactide bottom: schematic of ^{1}H homonuclear decoupled spectra for isotactic polylactide.

Heterotactic PLA synthesised from *rac*-LA consist of an equal amount of the *isi and sis* tetrad (Figure 1.16 top) giving two equal sized peaks in the ^{1}H homonuclear decoupled NMR spectrum (Figure 1.16 bottom).

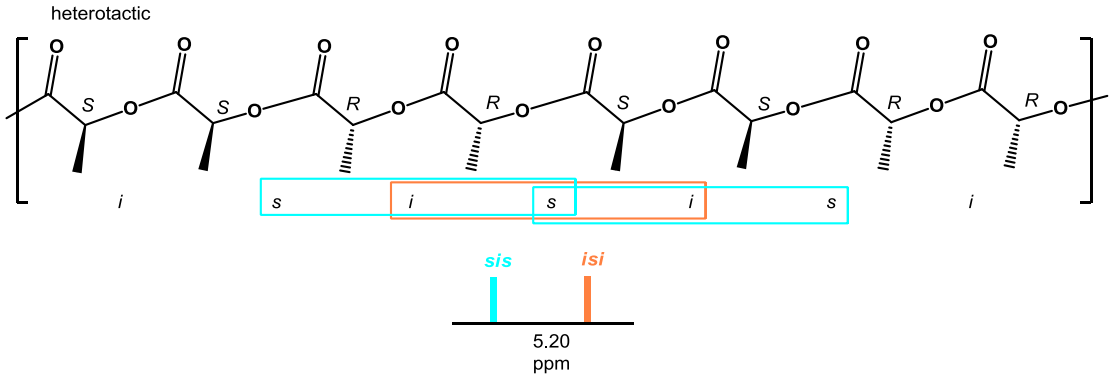

Figure 1.16 – Top: tetrad possibilities for heterotactic polylactide synthesised from *rac*-LA bottom: schematic of ^{1}H homonuclear decoupled spectra for heterotactic polylactide synthesised from *rac*-LA.

In atactic PLA synthesised from *rac*-LA the lactide units are distributed in a random order with no specificity. This gives rise to 5 tetrads; *sis*, *sii*, *iis*, *iii*, and *isi* (Figure 1.17 top). The tetrads will be present in the ratio of 1:1:1:3:2 (*sis*:*sii*:*iis*:*iii*:*isi*) giving peaks in the ^{1}H homonuclear decoupled NMR spectrum relative to this ratio (Figure 1.17 bottom).

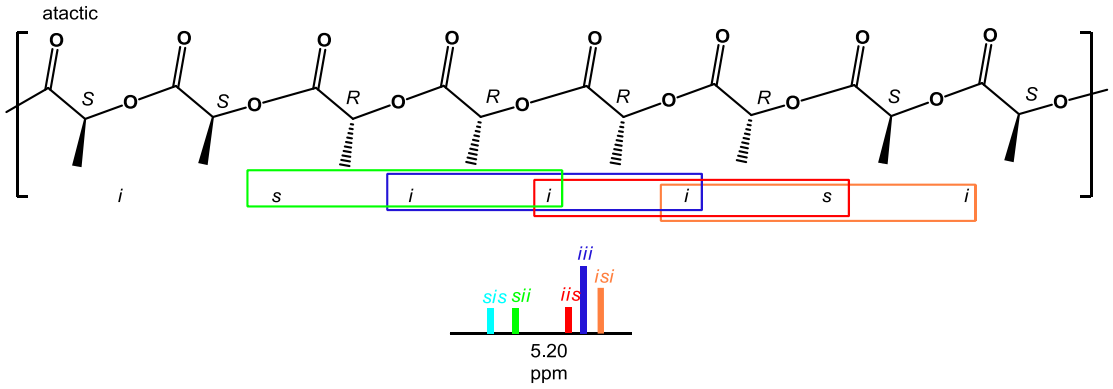

Figure 1.17 – Top: tetrad possibilities for atactic polylactide synthesised from *rac*-LA bottom: schematic of ^{1}H homonuclear decoupled spectra for atactic polylactide synthesised from *rac*-LA.

The ratio of tetrads in each polymer microstructure is dictated by Bernoullian statistics and the relative abundance of each tetrad can be predicted by the probabilities shown in Table 1.1. In the absence of side reactions the tetrads *sss*, *ssi* and *iss* do not occur in PLA synthesised from *rac*-LA.

	Probability	
tetrad	*rac*-LA	meso-LA
[iii]	$P_m^2 + P_rP_m/2$	0
[iis]	$P_rP_m/2$	0
[sii]	$P_rP_m/2$	0
[sis]	$P_r^2/2$	$(P_m^2 + P_rP_m)/2$
[sss]	0	$P_r^2 + P_rP_m/2$
[ssi]	0	$P_rP_m/2$
[iss]	0	$P_rP_m/2$
[isi]	$(P_r^2 + P_rP_m)/2$	$P_m^2/2$

Table 1.1 – Tetrad possibilities based on Bernoullian statistics.

It is often the case that a polymer sample is not entirely isotactic, heterotactic or atactic but will have an enrichment of one character. The probability of racemic enchainment (P_r) and *meso* enchainment (P_m) allow the quantification of the degree of tacticity within a polymer sample by ^{1}H homonuclear decoupled NMR spectroscopy. For the polymerisation of *rac*-LA the easiest way to quantify this is to relate (P_r) to the relative intensity of the peak given due to the [*sis*] tetrad. In PLA synthesised from *rac*-LA if $P_r = 1$ then there is a 100 % chance that the next monomer in the polymer chain will be racemic meaning that the polymer is heterotactic, conversely if $P_r = 0$ then there is zero chance that the next monomer is racemic and so the polymer will be isotactic. When $P_r = 0.5$ there is an equal chance that the next monomer is racemic or

meso and so the polymer is atactic. The degree of tacticity in a polymer sample can therefore be measured, if $P_r > 0.5$ then the polymer has a heterotactic bias and if $P_r < 0.5$ then the polymer has an isotactic bias.

The ROP of *meso*-LA will lead to a different set of stereochemical tetrads along the polymer chain, due to the intrinsic stereochemistry of the monomer. Atactic PLA produced from meso-LA will contain the five tetrads *sis*, *iss*, *ssi*, *sss* and *isi* (Figure 1.18a top). However, the experimental ^{1}H homonuclear decoupled NMR spectrum (Figure 1.18a bottom) often only contains two peaks, the *sis* peak and a single peak relating to the *iss/ssi*, *sss* and *isi* tetrads. This is due to a lack of resolution and the overlapping nature of the *iss*/*ssi* peaks. If a stereoselective initiator which selects for insertion of a different stereocentre to the growing chain is used in the polymerisation of *meso*-LA then syndiotactic PLA will be produced. Syndiotactic PLA will contain a single *sss* tetrad (Figure 1.18b top) giving rise to one peak in the ^{1}H homonuclear decoupled NMR spectrum (Figure 1.18b bottom). If a stereoselective initiator which selects for insertion of the same stereocentre to the growing chain is used in the polymerisation of *meso*-LA then heterotactic PLA will be produced. Heterotactic PLA produced from meso-LA will contain the same *isi* and *sis* tetrads seen in heterotactic PLA produced from *rac*-LA (Figure 1.18c top) with two peaks in the ^{1}H homonuclear decoupled NMR spectrum (Figure 1.18c bottom). To quantify the tacticity of a polymer synthesised *meso*-LA the [*sis*] tetrad can again be used to calculate a P_r value. In PLA synthesised from *meso*-LA if $P_r = 1$ then there is a 100 % chance that the next stereocentre added to the growing polymer chain will be racemic meaning that the polymer is syndiotactic, conversely if $P_r = 0$ then there is zero chance that the next stereocentre added is racemic and so the polymer will be isotactic. When $P_r = 0.5$ there is an equal chance that the next stereocentre is racemic or *meso* and so the polymer is atactic.

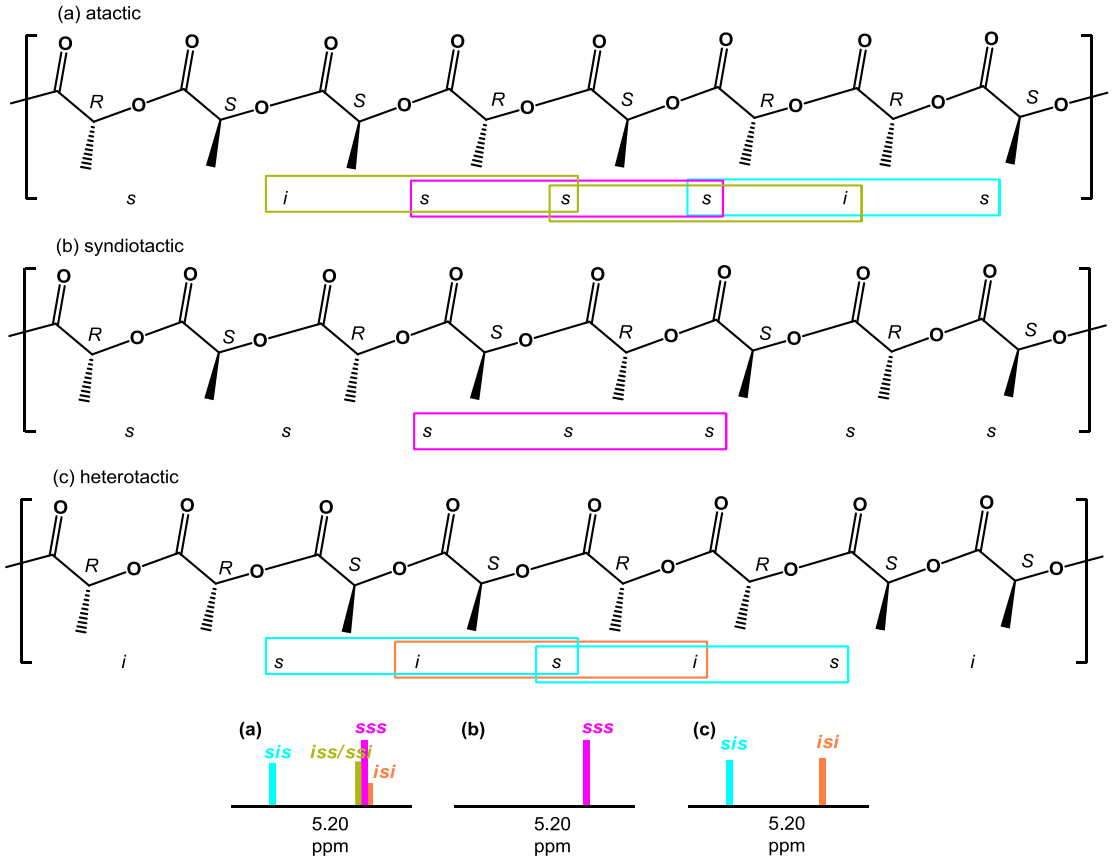

Figure 1.18 – Top: tetrad possibilities for polylactide synthesised from *meso*-LA bottom: schematic of ^{1}H homonuclear decoupled spectra for polylactide synthesised from *meso*-LA.

1.5.4.2. Gel Permeation Chromatography (GPC)

Gel permeation chromatography is a size exclusion chromatography (SEC) characterisation technique widely used to estimate the molecular weight of polymer samples. Size exclusion chromatography involves the use of a stationary phase of porous beads packed into a column. The porosity of the beads is controlled and different columns can be applied depending on the nature and molecular weight of the polymer sample to be analysed. The polymer is dissolved into the mobile phase and will interact with the beads; smaller molecules will enter into the pores and larger molecules will bypass them (Figure 1.19). The beads will have a porosity suited to a range of molecular weights; therefore the degree of interaction with the beads is inversely proportional to molecular weight with the smallest molecules having the longest elution time and *vice versa*. A standard sample of known molecular weight polymer can be characterised to produce a calibration curve for a column. A sample of unknown molecular weight can then be characterised and its molecular weight estimated by its elution time. It is important to note that the interaction with the stationary phase is not directly related to the molecular weight of the polymer sample

but is a function of its hydrodynamic radius; this must be accounted for when comparing polymers with differing hydrodynamic radii.

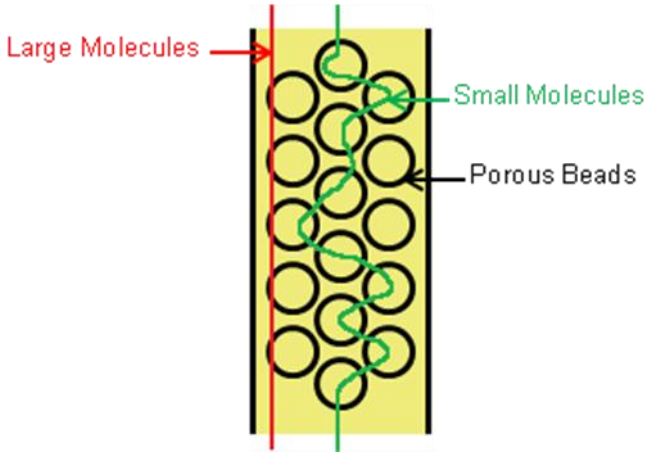

Figure 1.19 – Schematic diagram of size exclusion chromatography.

A variety of detectors are available to observe the eluted polymer, commonly used detectors include ultra-violet (UV), refractive index (RI), infrared (IR) and light angle scattering detectors. The detector gives a response that is proportional to the number of molecules eluted at any time and a distribution curve is obtained (Figure 1.20)

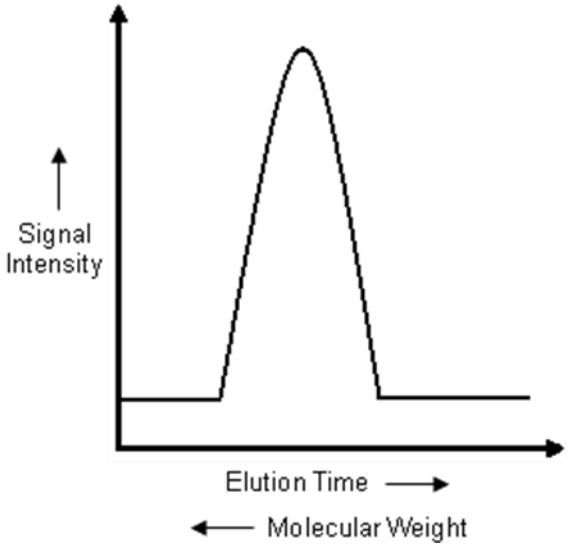

Figure 1.20 – Theoretical distribution curve of polymeric products measured by a GPC instrument

From this distribution curve the weight average molecular weight (M_w), number average molecular weight (M_n) and polydispersity index (PDI) can be calculated by equations 1.3, 1.4 and 1.5 respectively.

$$M_w = \sum W_i M_i \text{ where } W_i = N_i M_i / \sum N_i M_i$$

Equation 1.3: Calculation of M_w where N_i is the number of molecules of mass M_i

$$M_n = \sum M_i N_i / \sum N_i$$

Equation 1.4: Calculation of M_n where N_i is the number of molecules of mass M_i

$$PDI = M_w / M_n$$

Equation 1.5: Calculation of the polydispersity index (PDI) of a polymer sample

1.5.5. Metal Initiators for the ROP of lactide

As previously discussed the polymerisation of lactide requires a metal initiator. A wide variety of initiators has been studied.[102] The main qualities on which a reported initiator is judged are control of the polymerisation reaction, rate of reaction and stereocontrol. Other desirable characteristics are low cost, abundance, colour of polymer produced, robustness and low toxicity.

The current initiator most widely used in the commercial production of PLA is tin(II) bis(2-ethylhexanoate), also known as tin(II) octanoate ($SnOct_2$) (Figure 1.21). The popularity of this initiator is due to its low cost, ease of handling, solubility, robust and fast activity, ability to work under both solution and melt conditions and the colourless polymer produced.

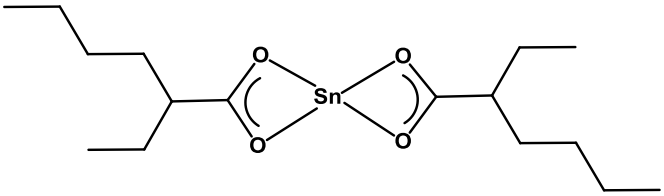

Figure 1.21 – Commercially used tin(II) bis(2-ethylhexanoate) ($SnOct_2$) initiator.

The mechanism of $SnOct_2$ for the ROP of lactide has been widely studied.[103-106] A consensus has been reached that the polymerisation proceeds by a coordination-insertion mechanism, at least when the polymer is carried out in the presence of an alcohol co-initiator and at temperatures <100 °C.[107] It seems that the initially reported poor control over molecular weight and end group analysis inconsistent with the ROP mechanism were caused by contaminants in the $SnOct_2$ such as water and octanoic acid. It is important to note that $SnOct_2$ offers no stereocontrol in the polymerisation of *rac*-lactide. The potential toxicity of tin in biological system also means that PLA produced by $SnOct_2$ may be unsuitable for biomedical applications.

1.5.5.1. Aluminium initiators

Aluminium complexes as simple as $Al(O^iPr)_3$ have been shown to be active for the ROP of lactide. However, these initiators have been shown to exhibit poor control over the polymerisation reaction and are less active than the commercially used $SnOct_2$ complex.[98] Ligand based aluminium systems have been examined extensively and have offered both controlled polymerisation and stereocontrol depending on the ligand and initiating group. Some highlights of the research into ligand based aluminium complexes for the ROP of lactide are presented below.

Pioneering work in this area was carried out by *Spassky et al* in the 1990s in which the controlled polymerisation of lactide with Al(salen) methoxide complexes was reported (Figure 1.22).[108,109] These complexes produced moderately isotactic PLA from *rac*-lactide in solution at 70 °C. PLA synthesised by the (R)–Binaphthyl complex (**2**) was reported to be chiral suggesting that the complex incorporated *D*-lactide preferentially into the chain.

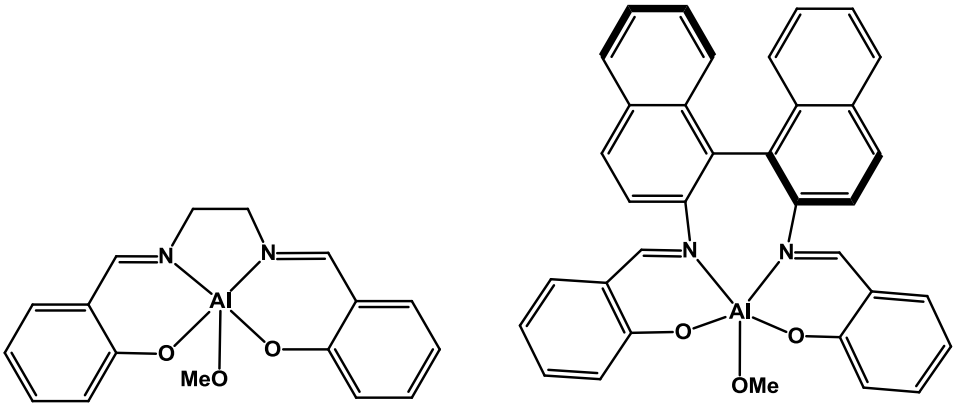

Figure 1.22 – Early Al(Salen) complexes synthesised by *Spassky et al* for the ROP of lactide.

This work was later developed by *Coates et al* who reported the synthesis of syndiotactic PLA from *meso*-LA using the (R)–binaphthyl complex (**2**) with enatioselectivity of 96 %.[110] The same group also synthesised a racemic mixture of the complex and found that when this was used as an initiator for *rac*-lactide polymerisation it produced isotactic stereoblock PLA.[111,112] These results were reinforced by *Baker et al* who reported similar enantioselectivity for the polymerisation of *rac*-lactide using a racemic mixture of a variant of the initiator (**2**) which contained an isopropoxide group in place of the methoxide.[113] The mechanism

of isotactic enrichment was thought to be a polymer chain transfer mechanism, in which each enantiomer of the initiator selectively polymerised one enantiomer but the growing chains exchanged between active metal centres.[111]

Feijen et al advanced the work in Al(salen) initiators when they reported an initiator based on the Jacobsen ligand, which is a commercially available and relatively inexpensive starting material (Figure 1.23, **3**, {R,R} variant).[114,115] This initiator showed controlled polymerisation of *rac*-lactide with isotactic enrichment under both solvent and industrially favoured solvent free conditions. Using a racemic mixture of **3** the group reported polymer with a P_m value of 0.88 under melt conditions (130 °C, solvent free) after 2 days. The enantiomeric selectivity was reported as being achieved *via* an enantiomorphic site controlled mechanism.[108,109]

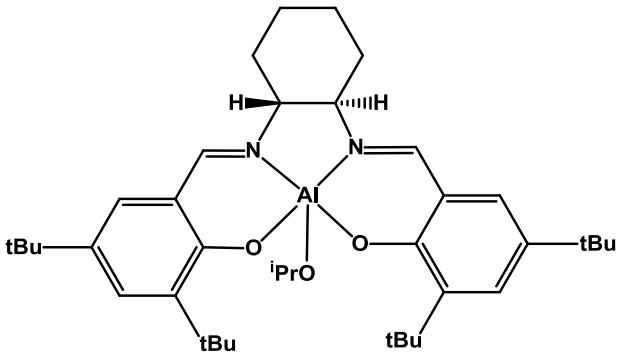

3

Figure 1.23 – An Al(salen)(R,R) complex reported by *Feijen et al* using Jacobsen Ligand.

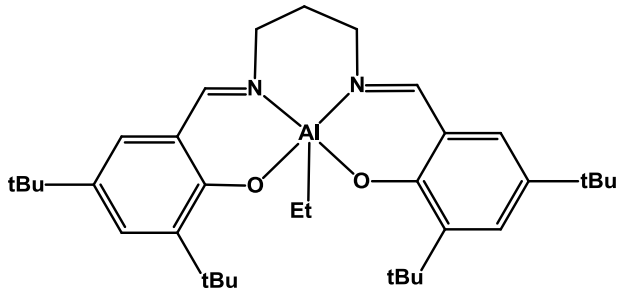

4

Figure 1.24 – An Al(salen) complex reported by *Nomura et al* which produces isotactically enriched PLA *via* a chain end control mechanism.

Later *Nomura et al* reported the production of isotactically-enriched PLA using an achiral catalyst (Figure 1.24, **4**).[116,117] In this case the enantiomeric selectivity is derived from a chain end control mechanism, where the stereochemistry of the end monomer of the growing chain influences the selectivity of the next monomer inserted. These initiators do not contain an internal alkoxide group and so a benzyl alcohol co-

initiator was added to the polymerisation reactions. A polymerisation initiated by **4** was reported to proceed to 95 % conversion over a 14 hour period producing an isotactically enriched polymer (P_m = 0.91) of good molecular weight (~ 22,400 Da, monomer:initiator ratio of 100:1) and a narrow polydispersity index (1.06).

Gibson et al studied a range of salan complexes for the ROP of lactide which showed "remarkable stereocontrol".[118] An interesting feature of these complexes is the ability to control the stereochemistry of the PLA chain produced by altering the R_1 and R_2 groups (Figure 1.25). When the complex containing R_1 = CH_2Ph and R_2 = H (**5**) is used in the polymerisation of lactide an isotactically enriched polymer (P_m = 0.79) is produced. However, when the complex containing R_1 = CH_2Ph and R_2 = Cl (**6**) is used a heterotactic polymer is produced (P_m = 0.04). This is indeed a remarkable result as the stereospecificity of the complex was transformed by the adjustment of the substituent R_2 group on the ligand. The author noted that all polymers produced using salan complexes were colourless, in contrast to polymer produced by most conjugated salen complexes.[118]

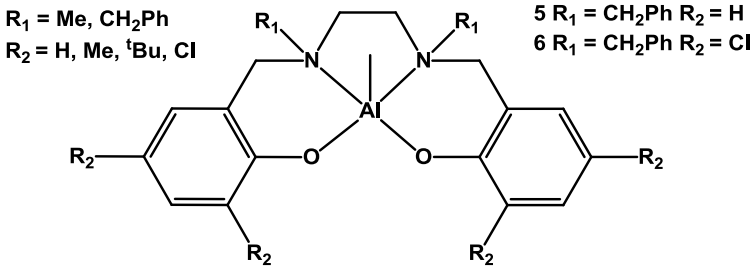

Figure 1.25 – A range of Al(salan) complexes reported by *Gibson et al* which produced both heterotactically and isotactically enriched PLA depending on the nature of R_1 and R_2.

More recently *Qian et al* synthesised a range of aluminium complexes by the complexation of reactive trialkylaluminium species with unsymmetrical substituted benzaminidate ligands (Figure 1.26).[119] All reported complexes were active for the ROP of *rac*-LA but differences were found in the activity of complexes depending on the electronic properties of the substituents on the phenyl ring. For example, when the group in the *ortho* position was F (**7**) the polymerisation reaction proceeded to 71 % conversion completion over a 72 hour period, however, when it was replaced with a methoxy group (**8**) the polymerisation only proceeded to 42 % over a 72 hour period (100:1 monomer:initiator ratio, toluene 70 °C).

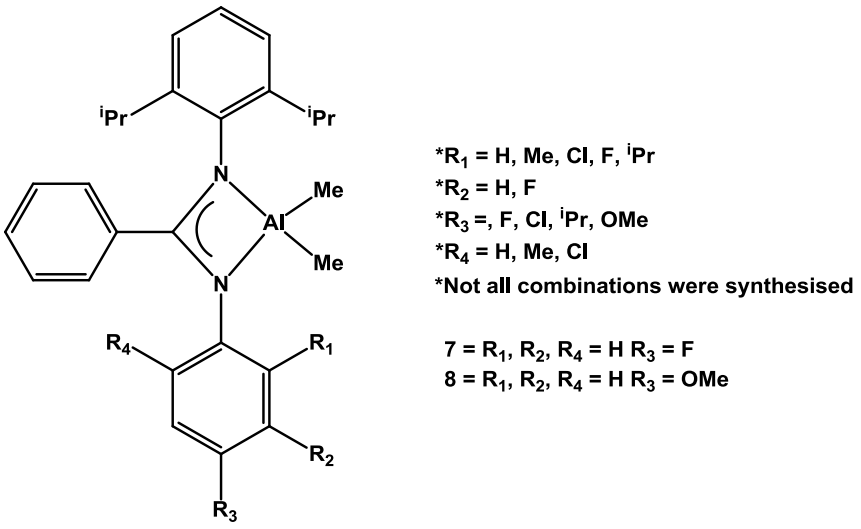

Figure 1.26 – A range of unsymmetrical *N*-substituted benzaminidate

In this work it was observed via ^{1}H NMR spectroscopy addition of an isopropanol co-initiator initiated the polymerisation *via* liberated $Me_2Al(O^iPr)$, $MeAl(O^iPr)_2$ or $Al(O^iPr)_3$. The complexes were shown to be active without the use of an alcohol initiator which was attributed to monomer insertion into the Al-N or Al-Me bond.[119]

1.5.5.2. Zinc initiators

Zinc offers strong potential as a metal for the ROP of lactide due to its high activity and low toxicity in humans.[97] When considering zinc complexes it is important to consider group two metal analogues as they are often bound by the same ligands. Early work on zinc initiators focused on relatively simple structures such as zinc lactate[120,121] amino acid salts[122] and halides.[123] Whilst many of these were found to be active initiators they suffered from a slow rate of reaction even at temperatures exceeding 130 °C. *Coates et al* pioneered the use of zinc complexes as initiators for the ROP of lactide with the development of initiators based on a *β*-diketiminate (BDI) ligand.[124,125] These complexes were highly active, for example an isopropoxide complex (Figure 1.27, **9**) was shown to polymerise *rac*-LA in a period of 20 minutes and *meso*-LA in a period of 4 hours at room temperature in CH_2Cl solution. These reactions also showed a strong degree of stereocontrol with the *rac*-LA (P_r = 0.94) producing heterotactically enriched polymer and the *meso*-LA producing syndiotactically enriched polymer (P_r = 0.76).

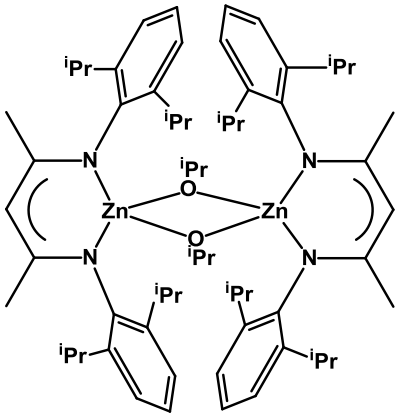

9

Figure 1.27 – Pioneering β-diketiminate (BDI) Zn complex reported by *Coates et al* which was highly active and produced polymer with heterotactic character (P_r = 0.90) from *rac*-LA.

The Mg(II) analogue of complex **9** was found to be more active than the Zn(II) catalyst, polymerising *rac*-LA to 97 % conversion in only 2 minutes at room temperature (100:1 monomer:initiator ratio, CH_2Cl solution). The increased activity was associated with the increased polarisation of the M-OR bond, however, the Mg(II) complex showed poor molecular weight control as well as no stereoselectivity.[117,118] *Chisholm et al* synthesised a range of closely related complexes as THF adducts as well as exploring further initiating groups.[126,127]

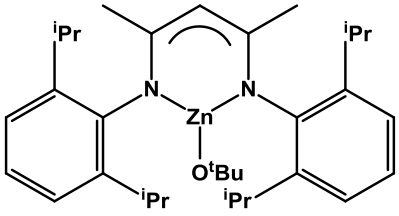

10

Figure 1.28 – Zn β-diketiminate (BDI) *tert*-butoxide complex reported by *Chisholm et al* which showed similar results to the previously reported BDI complex 5.

Complex **10** (Figure 1.28) showed similar rates and stereoselectivity as **9** with a 95 % conversion after 10 minutes in CH_2Cl. The same group later reported an analogous Ca(II) complex which was highly active for the polymerisation but offered no stereocontrol.[128] It was proposed that the lack of stereocontrol in the Ca(II) complex was due to a lack of bulk around the larger metal centre. This work was further developed by the synthesis of a range of complexes (Zn{II}, Mg{II}, Ca{II}) based on the tris(pyrazolyl)borate ligand system.[128-131] The calcium complex was found to be a highly active stereoselective initiator for the ROP of *rac*-LA producing

heterotactically enriched PLA (P_r = 0.90) in 1 minute at room temperature in CH_2Cl solution. Reactivity was reduced in the Mg(II) (1 h) and Zn(II) (6 days) complexes which was correlated to the polarity of the M-OR bond. [130]

Chisholm et al also developed Zn(II) complexes using Schiff base ligands and found them to be moderately active for the polymerisation of *rac*-lactide, although no stereoselectivity was observed.[132] *Williams et al* reported a zinc structure using a phenoxy diamine ligand (**11**, Figure 1.29) which polymerised *rac*-lactide to high conversion in less than 20 minutes at monomer:initiator ratios of up to 1500:1, although no stereoselectivity was observed, even at low temperatures. [133]

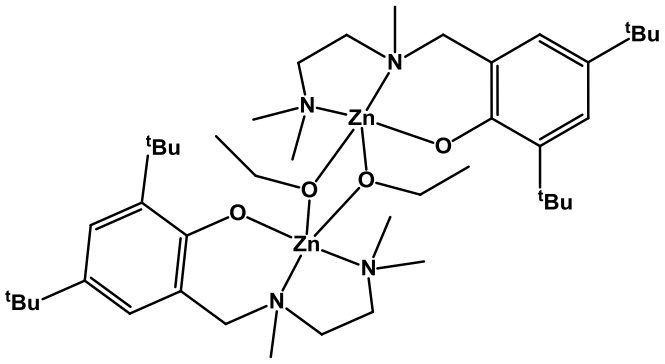

11

Figure 1.29 – Highly active Zn(II) complex synthesised using a phenoxy diamine ligand.

The work described within this thesis is focused on the development of zinc(II) and aluminium(III) initiators, however, many initiators using other metals have been shown to be active for the ROP of *rac*-lactide. For example, *Davidson et al* reported the synthesis of heterotactically enriched PLA under solvent free conditions using zirconium(IV) and hafnium(IV) complexes.[134] The complexes were synthesised by reacting the corresponding isopropoxide to a previously reported bulky amine *tris*(phenolate) ligand (Figure 1.30).[135] The hafnium complex produced heterotactically enriched PLA (P_r = 0.88) with high conversion (95 %) after 30 minutes using a monomer:initiator ratio of 300:1 under solvent free conditions (130 °C). The zirconium initiator showed higher activity, with 78 % conversion after only 6 minutes under the same conditions (P_r = 0.96). A titanium complex also showed activity but showed no stereocontrol. It was suggested that the hererotactic control offered by these complexes could be due either to a chain end transfer

mechanism due to the bulk of the ligand or inversion of axial chirality during chain propagation.

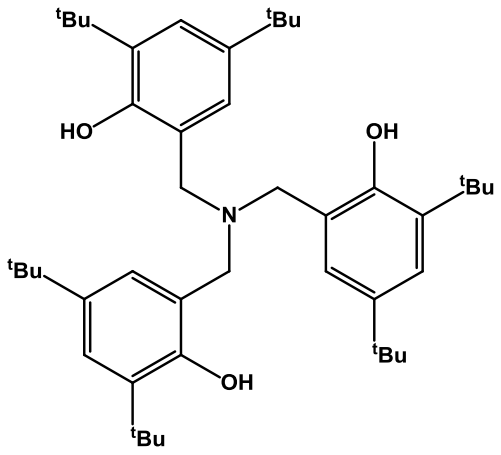

Figure 1.30 – Amine *tris*(phenolate) ligand used by *Davidson et al* to produce Zr and Hf initiators for the ROP of *rac*-lactide. The initiators produced polymer with significant heterotactic bias (P_r = 0.96 Zr, 0.88 Hf).[134,135]

A review of initiators not based on zinc(II) or aluminium(III) is beyond the scope of this thesis, however many are detailed in a recent review article[97] as well as two recent theses submitted to the University of Bath.[100,136]

1.6. Project Aims

The aim of the work described in this thesis was to explore new technology which could contribute to the processes contained within a potential bio-refinery. The work was focused in two areas, the depolymerisation of lignin and the polymerisation of lactide to produce PLA.

The depolymerisation of lignin is a complicated area of research and many potential processes and catalysts have been reported. Research in this area can be restricted depending on the availability of suitable reactor vessels and analytical equipment. The aim of this work was to further explore the mild oxidative catalytic depolymerisation of lignin and lignin model compounds in the hope of discovering a novel catalyst with promising activity.

The second area of research was in the area of the polymerisation of lactide to produce PLA. This is a widely studied reaction and many initiators have been reported to date each with their own positive and negative properties. The main aim of the work in this project was to explore novel zinc(II) and aluminium(III) initiators for the polymerisation of PLA. Another significant aim was to explore the synthesis of heterogeneous catalysts and their analogues which could potentially offer advantages in downstream processing of the PLA product.

Chapter Two

Zinc (II) and Aluminium (III) Silsesquioxane Complexes for the ROP of rac-lactide

2. Zinc (II) and Aluminium (III) Silsesquioxane Complexes for the ROP of rac-lactide

2.1. Introduction

2.1.1. Silsesquioxanes

Silsesquioxane is the general name applied to a range of organic siloxane species with the empirical formula $(RSiO_{1.5})_n$. The R group is typically a hydrogen atom or alkyl group, the presence of which can allow solubility in organic solvents. The backbone of silicon bound to three oxygen atoms is chemically comparable to the bulk structure of amorphous silica, which is widely used as a heterogeneous support for catalysis.[137-141] The chemistry of silsesquioxanes is similar to that of silica with the benefit of solubility in organic solvents; therefore silsesquioxanes have been used as soluble models of heterogeneous silica catalysts. The work described in this chapter is focused on cubic incompletely condensed silsesquioxanes as models for heterogeneous silica catalysts, however the work in this area is by no means limited to these species and a vast array of syntheses and applications exist which are beyond the scope of this work but are the subject of two major reviews in the area.[142,143]

2.1.2. Synthesis of Incompletely Condensed Silsesquioxanes

The synthesis of a corner removed trisilanol silsesquioxane species was first discovered by *Brown et al* in 1965.[144] In this work it was discovered that if a solution of cyclohexyltrichlorosilane in acetone was treated with an excess of H_2O and refluxed for 24 hours then crystals of the silsesquioxane product formed over a period of months (Figure 2.1).

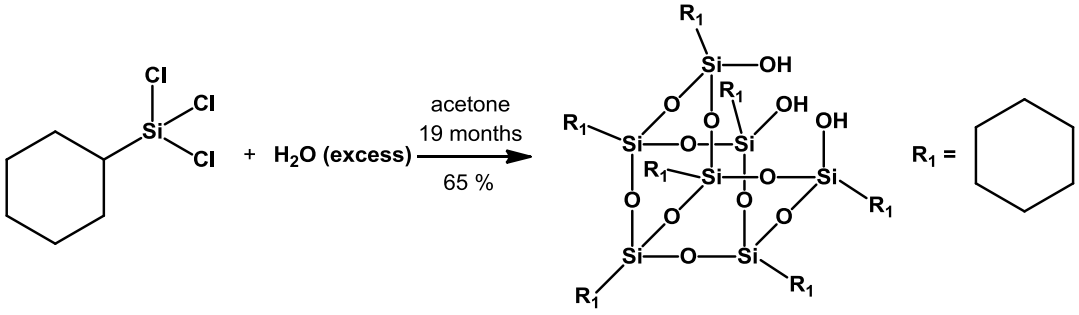

Figure 2.1 - First synthesis of an incompletely condensed silsesquioxane, discovered by *Brown et al* in 1965.[144]

This synthesis was revisited by *Feher et al* in 1989 who noted that repeated attempts to shorten the reaction time had been unsuccessful but reported a 70 % yield of the trisilanol cyclohexylsilsesquioxane over 36 months on a 3.0 mol scale.[145]

Lichtenhan et al developed a synthesis of isobutyl and ethyl silsesquioxanes, this involves the dropwise addition of trimethoxysilane to lithium hydroxide and water in a mix of acetone/MeOH (88 %/12 %) at reflux (Figure 2.2). After 2 hours mixture is then acidified, filtered and washed with CH_3CN to give the trisilanol silsesquioxane in 94 % yield. A patent was granted in 2005 and the materials are commercially available from Hybrid Plastics in the United States who market them as Polyhedral Oligomeric Silsesquioxanes (POSS®).[146]

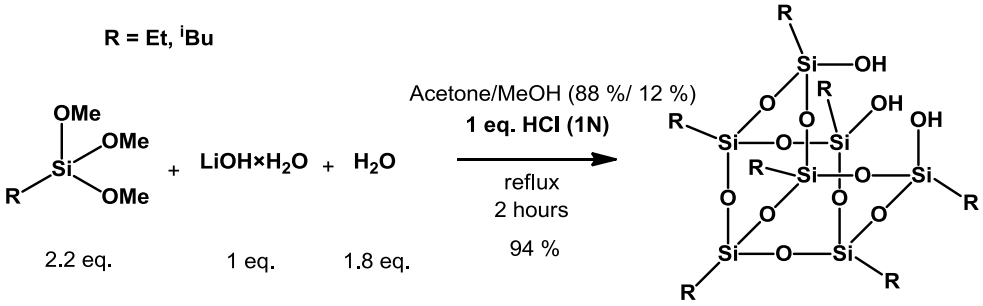

Figure 2.2 – Patented synthesis of ethyl and isobutyl trisilanol silsesquioxanes.[146]

2.1.3. Silica as a Heterogeneous Support

Amorphous silica is widely used as a support for the immobilisation of a metal centre to form a solid heterogeneous catalyst. Silica is made up of a network of saturated tetrahedral SiO_2 units with a largely unsaturated surface of silanol sites. Four different surface sites mainly exist which are termed isolated (SiO_3OH), geminal ($SiO_2(OH)_2$), vicinal (SiO_3OH, with H bonding) and saturated (SiO_4) (Figure 2.3).

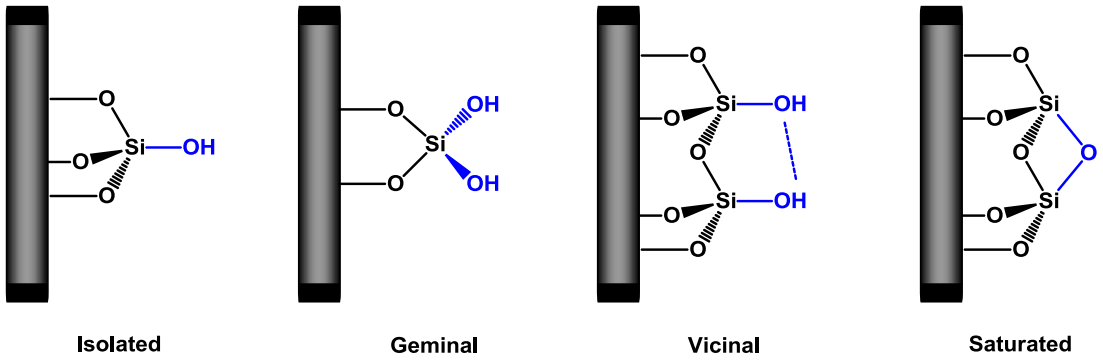

Figure 2.3 – Chemical environment of surface sites in silica.

The surface hydroxyl groups allow reactivity and therefore the anchoring of a metal centre or organic moiety. The reactive surface hydroxyl groups combined with a relatively large surface area make silica an ideal support for the immobilisation of metal centres for catalysis. When a metal centre is bound to the surface the stability, selectivity and activity of the catalyst will be affected by the nature of the silanol site that it is bound to. Due to the insoluble nature of silica characterisation is limited to solid state bulk methods which are not sensitive enough to provide detail of the surface silanol sites and their interactions with the metal centre. It is therefore difficult to fully characterise the mechanisms of catalysis of silica supported metal catalysts, hence there is a need for soluble metal systems to model the activity.[147]

2.1.4. Incompletely Condensed Silsesquioxanes

Incompletely condensed silsesquioxanes can be used to replicate the co-ordination environment of surface silanol sites. The isolated, geminal, vicinal and saturated sites at a silica surface can each be mimicked by a corresponding silsesquioxane (Figure 2.4).

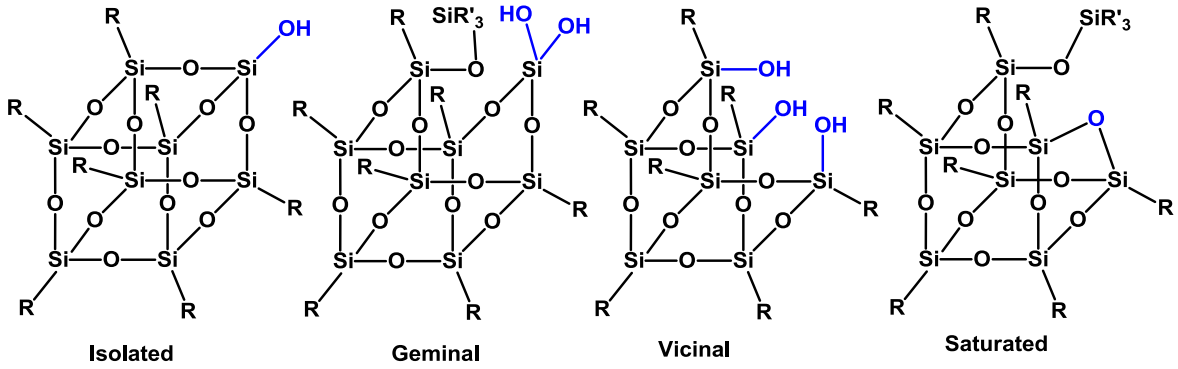

Figure 2.4 – Incompletely condensed silsesquioxanes as models of surface silanol sites

The benefit to this approach is that when reacted with a metal centre the resultant complex is often soluble in organic solvents. The complex can be used as a catalyst to mimic the heterogeneous silica loaded equivalent but can also be characterised by methods such as NMR spectroscopy and X-ray diffraction. The use of these analytical techniques and other methods allows deeper probing into the mechanism of a catalytic reaction and can provide insight into the effect of the various surface silica chemistries on the metal centres involved.

The method of using an incompletely condensed silsesquioxane as a ligand for a metal complex was first developed in 1986 by *Feher et al* who reported a crystallographically characterised complex of $[R_7Si_7O_{12}]ZrX$ (where R= C_6H_{11} and X= C_5Me_5).[148] This pioneering work led to incompletely condensed silsesquioxanes being widely adopted as a model for silica catalysis and the same group contributed many structures based on a vast array of elements bound to silsesquioxanes including aluminium(III), antimony(III), boron(III), chromium(VI), gallium(III), germanium(IV), molybdenum(III, VI), titanium (IV), phosphorus(III), tin(IV) and vanadium(V).[145,149-160]

Ducheateau et al have prepared zinc(II) alkylsilsesquioxane complexes as model catalysts for the copolymerization of cyclohexene oxide and CO_2 for the production of polycarbonates.[161] The same group have also reported zirconium(IV) based silsesquioxanes as model complexes for alkene polymerisation[162,163] and a range of aluminium(III), boron(III), gallium(III), and tin(II) complexes.[164-167]

An example where the homogenous silsesquioxane model has been shown to closely represent the heterogeneous silica equivalent is in the use of titanium silsesquioxane complexes of type $[R_7Si_7O_{12}]TiX$ (where R= C_5H_9, C_6H_{11}; X= alkyl, alkoxide, amido, cyclopentadienyl) as olefin epoxidation catalysts (Figure 2.5). These catalysts have shown to be strong models of titanium surface sites found in heterogeneous TS-1 and MCM-41 catalysts.[142,168-173]

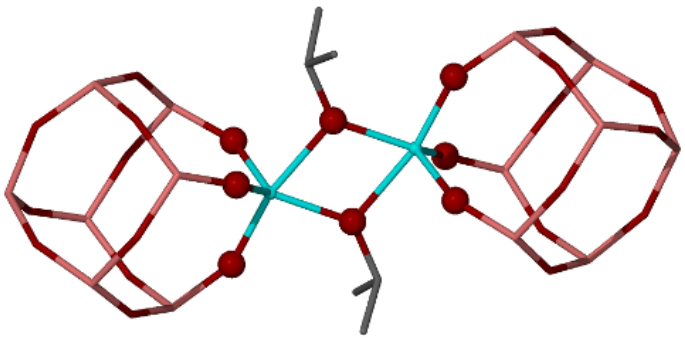

Figure 2.5 – A silsesquioxane complex of R_7Si_7TiX (R = ^iBu, X = ^iPr). Ti = cyan, O = red, C = grey, Si = pink.

Previous work by *Jones et al* focused on a range of titanium(IV), aluminum(III), and zinc(II) systems as models for heterogeneous lactide polymerisation initiators.[174-176] In this work both the heterogeneous silica loaded catalysts and the homogeneous model

silsesquioxanes were synthesised. Both homogenous and heterogeneous systems were found to be active for the polymerisation of *rac*-lactide with the homogeneous silsesquioxane systems being more active.

2.1.5. Tethered Silica Ligands

Another approach to produce heterogeneous catalysts tethered to silica involves the progressive construction of organic ligands onto the surface. In this approach instead of reacting the surface silanol sites directly with a metal centre an organic moiety is used to tether a ligand to the surface of the silica followed by the complexation of a metal centre to the ligand. This technique allows the creation of co-ordination environments far beyond simple silanol groups and gives scope to complex a wide variety of metal centres. This technique is widely exploited in the literature and a classic example of this technique is to first react the silica with $(MeO)_3Si(CH_2)_3NH_2$ and then use the tethered amine functionality to further develop the ligand (Figure 2.6).[138-141]

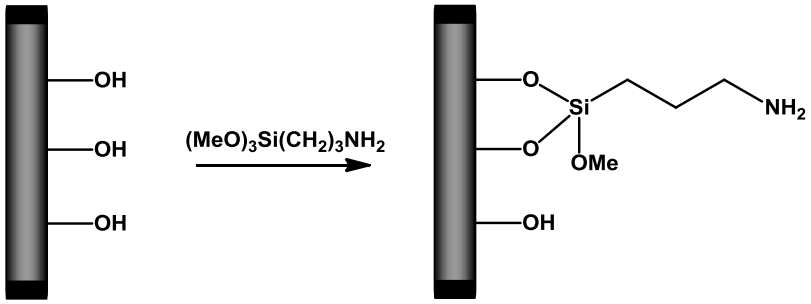

Figure 2.6 – Synthesis of a silica tethered amine which can be used as a precursor to other ligands.

The amine functionality can be exploited to synthesise a wide array of ligands. This method is widely used; a recent example by *Karimi et al* used this system to produce a reusable and thermally stable Pd (II) catalyst for the oxidation of alcohols using molecular oxygen from air (Figure 2.7).[137]

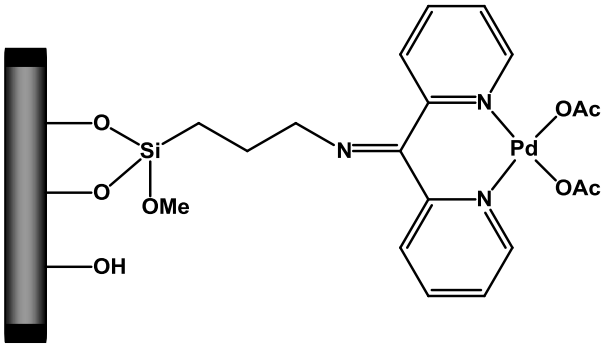

Figure 2.7 – A recent example of a Pd(II) catalyst on silica synthesised by *Karimi et al* using the amine tethering method.[137]

2.1.6. Silsesquioxanes as Models for Tethered Silica Catalysts

Despite the wide use of incompletely condensed silsesquioxanes as models for silica catalysts very few examples exist where incompletely condensed silsesquioxanes have been used as soluble models for tethered catalysts. One example of this work has been reported by *Maschmeyer et al* who have reported a tethered system in which they synthesised silsesquioxanes as models for osmium(IV) and rhodium(II) catalysts.[139,177] The rhodium(II) system was tested for the hydroformylation of alkenes and the crystal structure of a tethered rhodium complex synthesised from a diphenylphosphine tethered silsesquioxane was reported (Figure 2.8). *Duchateau et al* have also reported a tethered zirconocene complex for olefin polymerisation.[162]

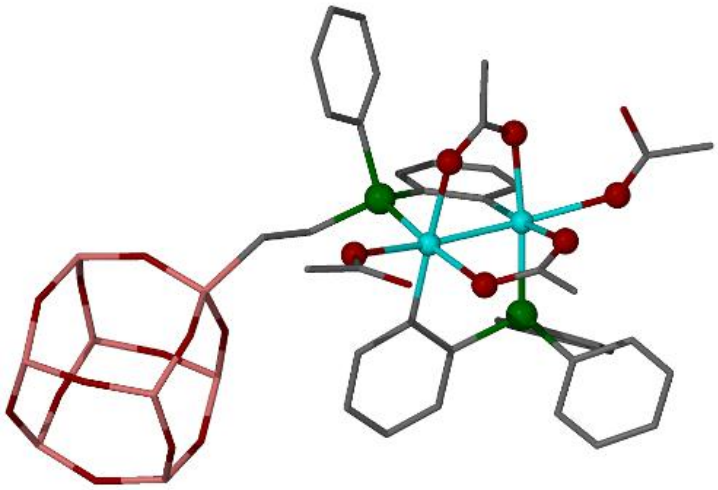

Figure 2.8 – Tethered diphenylphosphine Rh(II) silsesquioxane complex reported by *Maschmeyer et al.* Rh = cyan, P = green, O = red, C = grey, Si = pink.

The work described in this chapter represents a selection of the first crystallographically characterised examples of a tethered silsesquioxane complex and is the first example of a crystallographically characterised complex that uses the common *n*-propyl system.[178]

2.2. Silsesquioxane Ligand Synthesis

The series of silsesquioxane ligands discussed here on in are given the notation $\mathbf{L^{R}}$OH and were accessed *via* a 2 step synthesis. The first step involved the silylation of the hydroxyl groups to complete the cube structure and give the pendent amine functionality (L-NH_2). This was achieved by stirring the incompletely condensed silsesquioxane starting material with one equivalent of (3-aminopropyl)trimethoxysilane over a period of 24 hours (Scheme 2.1). This was performed under the same reaction conditions as similar silylation reactions used in the functionalisation of silica.[137-141]

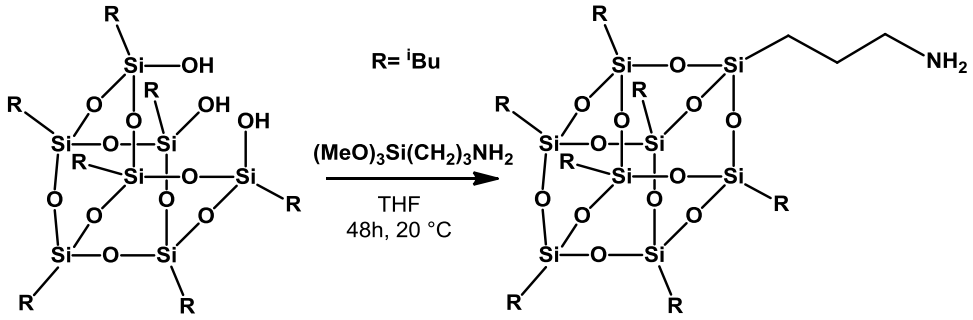

Scheme 2.1 – Reaction of (1,3,5,7,9,11,14-heptaisobutyltricyclo[7.3.3.15,11]-heptasiloxane-endo-3,7,14-triol) with $(MeO)_3Si(CH_2)NH_2$.

The second step of the synthesis was an imine condensation reaction between the previously synthesised amine, L-NH_2 and an appropriate salicylaldehyde derivative (Scheme 2.2). This was a relatively straightforward synthesis in which the two reagents were stirred together over a period of 24 hours to give the desired product in good yield (71-77 %).

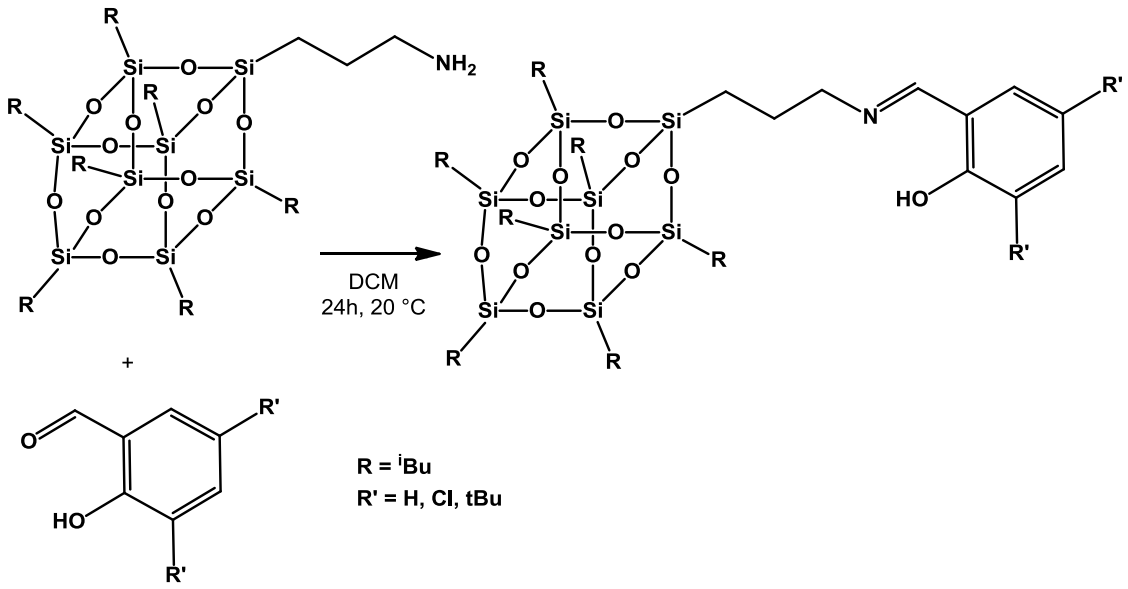

Scheme 2.2 – Synthesis of $L^{H}OH$, $L^{tBu}OH$ and $L^{Cl}OH$.

Three substituted ligands were synthesised which possess different steric and electronic properties depending on the groups *ortho* and *para* to the hydroxyl. These groups were hydrogen atoms ($L^{H}OH$), *tert*-butyl groups ($L^{tBu}OH$) and chlorine atoms ($L^{Cl}OH$). The ^{1}H NMR spectrum (Figure 2.9) of $L^{H}OH$ shows resonances at 0.84 ppm (CH_2), 1.08 ppm (CH_3) and 2.07 ppm (CH) due to the *iso*-butyl groups from the silsesquioxane cage. The other resonances in the spectrum relate to the tethered ligand and can be used to verify the success of the tethering process, for example the triplet at 3.21 ppm relates to the CH_2 group adjacent to the imine moiety in $L^{H}OH$, this can be compared to the CH_2 in the L-NH_2 starting material which has a shift of 2.57 ppm. This along with the appearance of an imine resonance at 7.76 ppm and aromatic resonances relating to the phenoxy ring of the ligand demonstrate the successful synthesis of the tethered silsesquioxane. The ^{1}H NMR spectra for $L^{tBu}OH$ and $L^{Cl}OH$ are comparable to the presented spectra for $L^{H}OH$ with expected differences related to the presence of the corresponding functional groups.

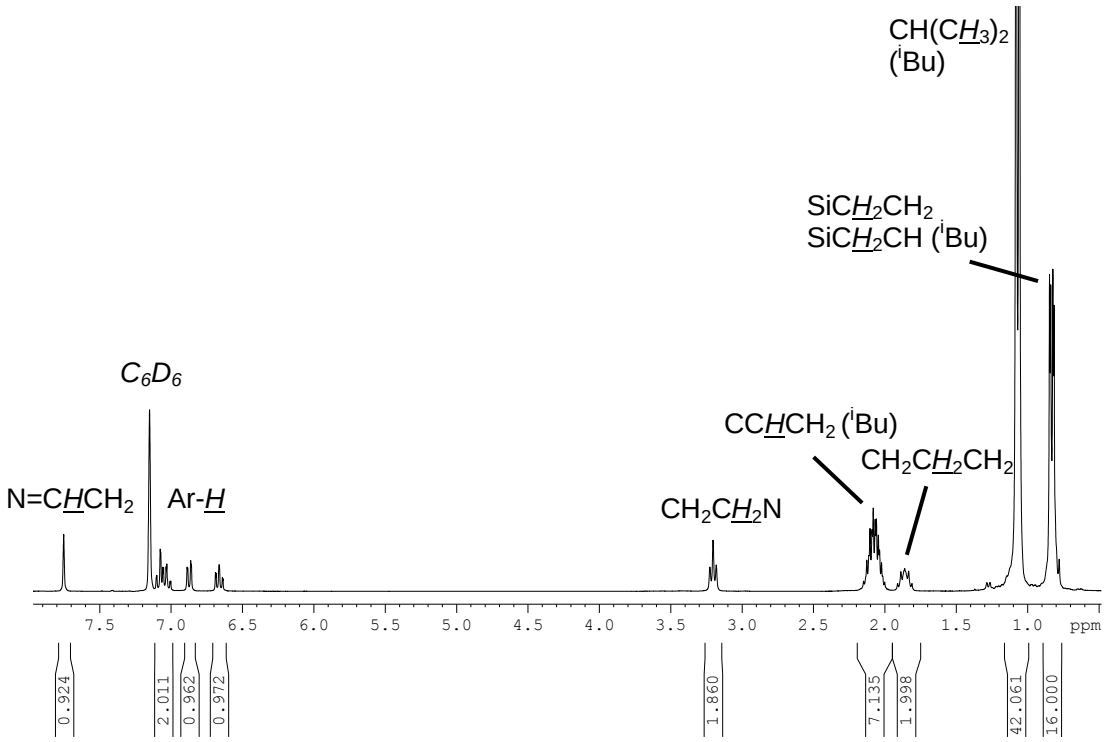

Figure 2.9 – Annotated ^{1}H NMR spectrum of L^{H}OH.

A HR ESI-MS spectrum of L^{H}OH is presented in Figure 2.10b along with a theoretical spectrum in Figure 2.10a. The observed value of the main peak 978.3445 amu is within experimental error (2 ppm) when compared to the theoretical value 978.3465 amu. The experimental spectrum shows relative abundances and an isotope pattern consistent with the theoretical spectrum for $C_{38}H_{75}O_{13}Si_8N + H^+$.

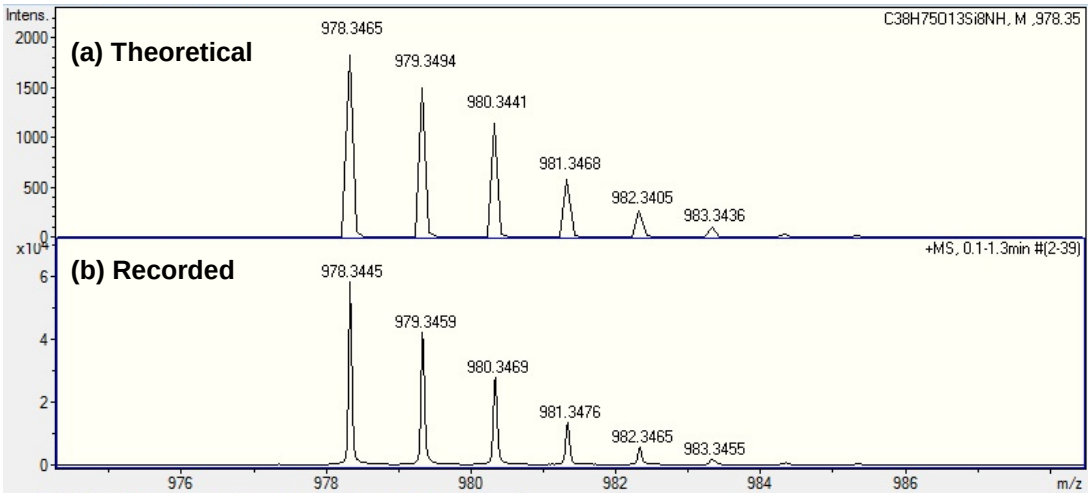

Figure 2.10 – (a) Theoretical HR ESI-MS spectrum of L^{H}OH and (b) recorded experimental spectrum of L^{H}OH.

All ligands were characterised by ^{1}H, $^{13}C\{^{1}H\}$, $^{29}Si\{^{1}H\}$ NMR spectroscopy and high resolution ESI-MS providing data consistent with the structures presented in Scheme 2.2. To the best of the knowledge of the author these ligands have not been previously reported in the literature.

2.3. Homogeneous Zinc(II) Silsesquioxane Complexes

Ligands $L^{H}OH$, $L^{tBu}OH$ and $L^{Cl}OH$ were reacted with $ZnMe_2$ and $ZnEt_2$ in a 1:1 or 2:1 ratio. These reactions yielded either monometallic species or tetrametallic zinc(II) complexes depending on the nature of the starting material and ratio of reagents added (Scheme 2.3).

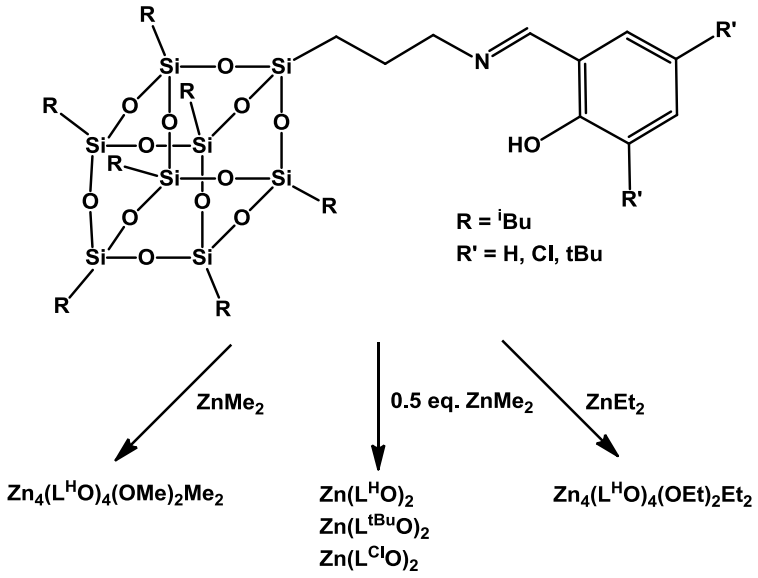

Scheme 2.3 – Complexation of $L^{H}OH$, $L^{tBu}OH$ and $L^{Cl}OH$ to zinc(II).

The monometallic species $Zn(L^{H}O)_2$ was the expected product based on analogous Schiff base species prepared by Darensbourg, Chisholm and others.[176,179-183] However, the $Zn_4(L^{H}O)_4(OMe)_2Me_2$ species observed upon reaction of $L^{H}OH$ with a stoichiometric amount of $ZnMe_2$ was not similarly predicted.

The molecular structure of $Zn_4(L^{H}O)_4(OMe)_2Me_2$ (Figure 2.11 top) consists of a central $Zn_4O_6C_2$ core (Figure 2.11 bottom), which can be described as an inversion-related, corner-removed face shared cube with two distinct zinc(II) centres. Zn(1) is bound to two imine nitrogen atoms, two phenoxides, and the μ_3-methoxide in a pseudo-octahedral environment with the Zn(1)-N(1)-O(1) angle being 162.96(18)°

and the O(2)-Zn(1)-O(1) angle being 77.93(15)°. The Zn(2) is bound to a methyl group, μ_3-methoxide, and two phenoxides in a pseudo-tetrahedral environment with the C(1)-Zn(2)-O(3) angle being 126.1(3)º and the O(2)-Zn(2)-O(3) angle being 96.10(17)º. The Zn(1)-O(1) length of 2.117(4) Å and the Zn(1)-O(2) distance of 2.091(4) Å are in agreement with literature precedent (Figure 2.12), as are the Zn(2)-O(1) and Zn(2)-C(1) distance of 2.021(4) Å and 1.957(7) Å respectively.[184] Selected bond lengths and bond angles are shown and compared to literature values in Tables 2.1 and 2.2.

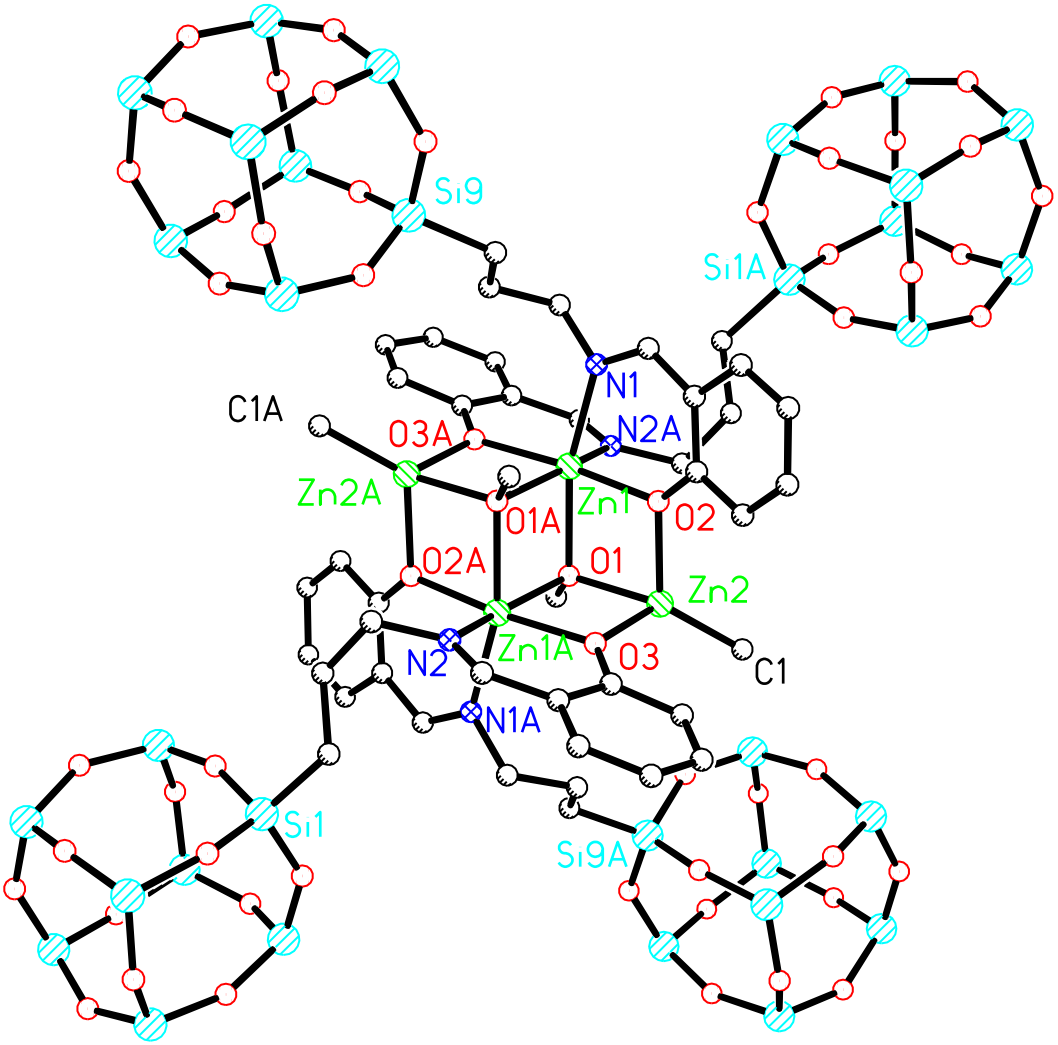

Figure 2.11 Top: Crystal structure of $Zn_4(L^HO)_4(OMe)_2Me_2$, isobutyl groups have been removed for clarity as some showed significant disorder.
Bottom: $Zn_4O_6C_2$ core from $Zn_4(L^HO)_4(OMe)_2Me_2$

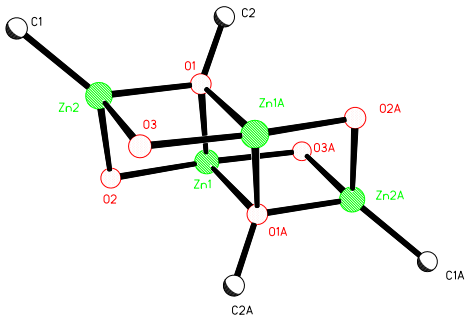

		$Zn_4(L^HO)_4(OMe)_2Me_2$	*Lewinski et al* [184]
Zn(1)	N(1)	2.127(5)	2.194(2)
Zn(1)	O(1)	2.117(4)	2.141(1)
Zn(1)	O(2)	2.091(4)	2.082(1)
Zn(2)	C(1)	1.957(7)	1.986(3)
Zn(2)	O(1)	2.021(4)	2.094(1)
Zn(2)	O(2)	2.033(4)	2.025(1)
Zn(2)	O(3)	2.028(4)	1.987(1)

Table 2.1 – Selected bond lengths from $Zn_4(L^HO)_4(OMe)_2Me_2$ compared to a similar complex reported by *Lewinski et al*.[184]

			$Zn_4(L^HO)_4(OMe)_2Me_2$	*Lewinski et al* [184]
O(3)	Zn(2)	C(1)	126.1(3)	121.36(9)
O(3)	Zn(2)	O(2)	96.10(17)	99.80(5)
O(1)	Zn(1)	N(1)	162.96(18)	151.20(6)
O(2)	Zn(1)	O(1)	77.93(15)	83.27(5)

Table 2.2 - Selected bond angles from $Zn_4(L^HO)_4(OMe)_2Me_2$ compared to a similar complex reported by *Lewinski et al*.[184]

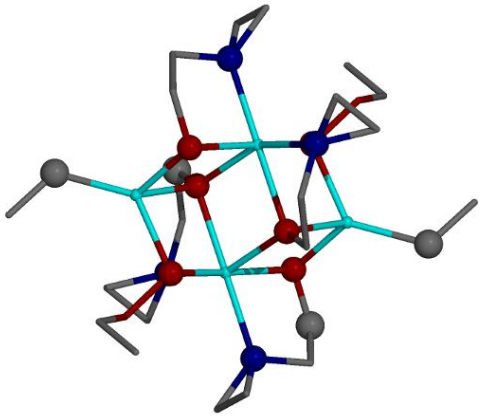

Figure 2.12 Crystal structure of a structurally analogous complex reported by *Lewinski et al*.[184] Zn = cyan, N = blue, O = red, C = grey

The XRD data collected for the $Zn_4(L^HO)_4(OMe)_2Me_2$ complex showed significant disorder but with considerable effort the structure was unambiguously determined. The main problem was disorder in the isobutyl groups attached to the silsesquioxane cube. To solve this atoms were left anisotropic or isotropic on merit and idealised C-C distance restraints were included as appropriate to assist convergence in the region of the of the isobutyl groups.

^1H, $^{13}C\{^1H\}$, $^{29}Si\{^1H\}$ solution NMR spectrum confirmed that the solid state structure of $Zn_4(L^HO)_4(OMe)_2Me_2$ is maintained in solution at 298 K. The ^1H NMR spectrum (Figure 2.13 top) in C_6D_6 shows a 6H resonance at 0.14 ppm for the Zn-Me group and a 6H resonance at 3.30 ppm for the Zn-OMe. The CH_2 group adjacent to the imine

produces a resonance at 3.21 ppm in the $L^{H}OH$ starting material, however in the $Zn_4(L^{H}O)_4(OMe)_2Me_2$ complex the resonance for this group is split across two resonances at 3.50 ppm (4H) and 3.73 ppm (4H). The splitting of this CH_2 resonance is caused by the presence of two different chemical environments in the tethered moiety, one is caused by N(1)-CH_2 and the other by N(2)-CH_2. The $^{29}Si\{^{1}H\}$ NMR has four resonances at - 67.5 ppm, - 67.5 ppm, - 67.4 ppm and - 67.3 ppm in a 1:3:1:3 ratio (Figure 2.13 bottom).

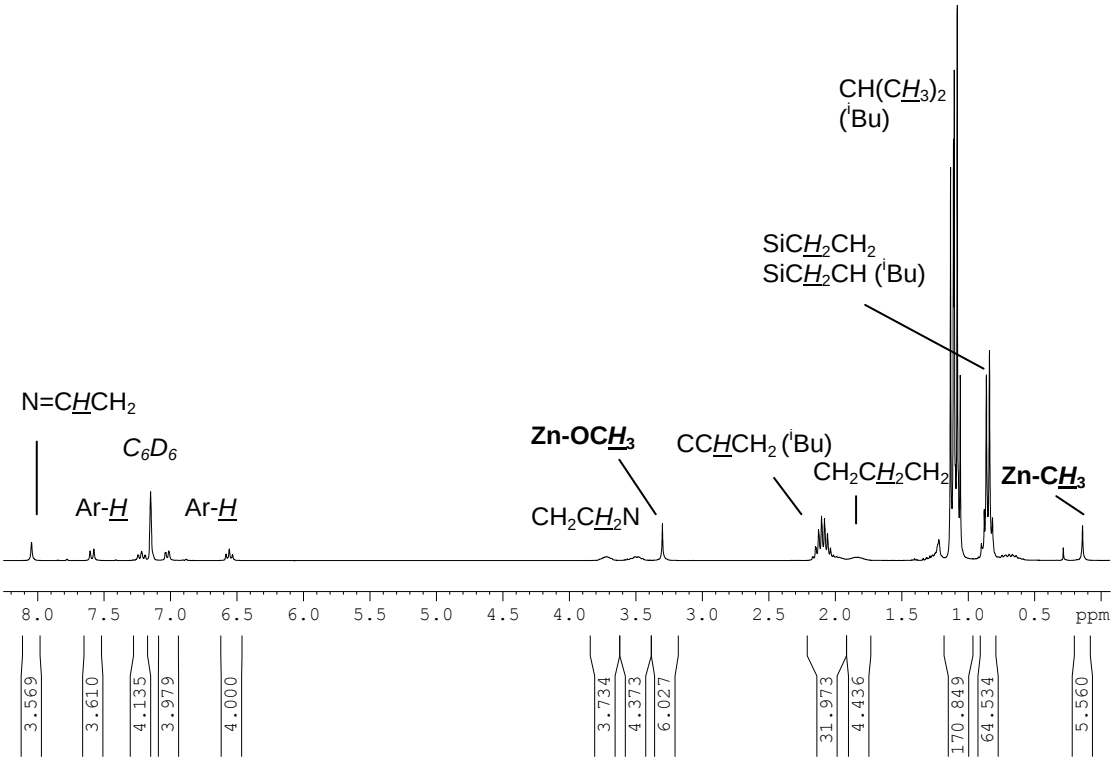

Figure 2.13 - Top: Annotated ^{1}H NMR spectrum of $Zn_4(L^{H}O)_4(OMe)_2Me_2$ showing the presence of Zn-OMe and Zn-Me species. Bottom: $^{29}Si\{^{1}H\}$ NMR Spectrum of $Zn_4(L^{H}O)_4(OMe)_2Me_2$ showing 1:3:1:3 ratio.

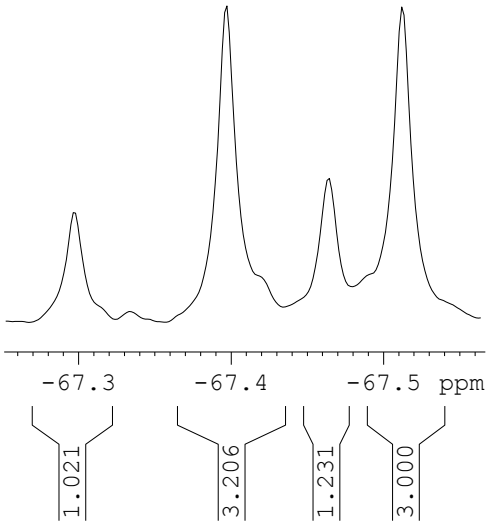

The formation of alkoxide species from the reaction between a zinc alkyl and dioxygen has previously been described by *Lewinski et al.*[184] This reaction has further been investigated and other examples can now be found in the literature.[185-191] The mechanism proposed first involves the dissociation of a ligand from the Zn centre, followed by the attack of dioxygen to form a radical pair. The proposed mechanism describes the formation of a peroxide species observed at low reaction temperatures. (Figure 2.14) The Zn-O-R species is formed from the breaking of the O-O peroxide bond and subsequent radical steps.

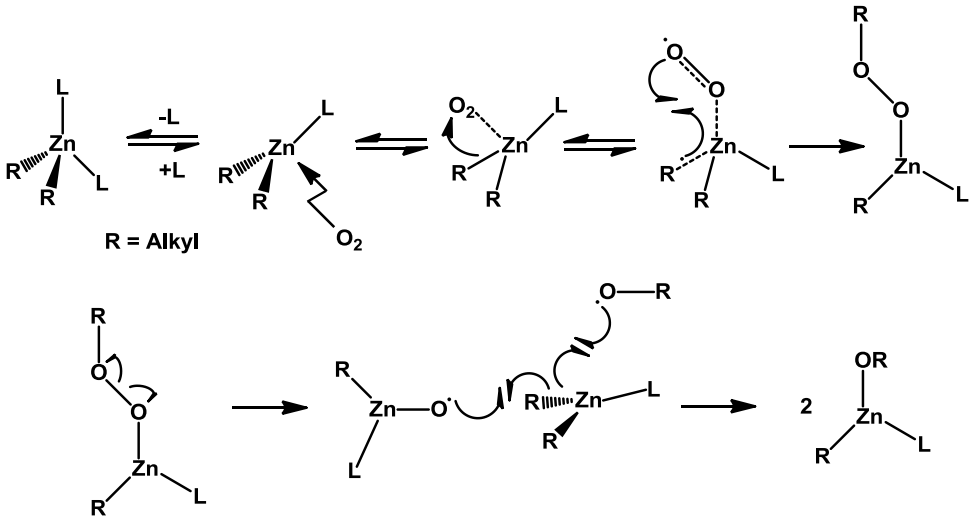

Figure 2.14 – Proposed mechanism for peroxide formation in Zn-Alkyl bonds [184,187] and formation of Zn-O-R species.

It was strongly believed that a similar reaction had occurred in the formation of $Zn_4(L^HO)_4(OMe)_2Me_2$, however, since methanol had been used for solvent washes in the synthesis of L^HOH it was important to rule out the insertion of small amounts of contaminated methanol as a possible source of the Zn-OMe species. L^HOH was reacted with 1 equivalent of $ZnEt_2$ to yield $Zn_4(L^HO)_4(OEt)_2Et_2$ which was crystallographically characterised (Figure 2.15). The formation of the $Zn_4(L^HO)_4(OEt)_2Et_2$ complex demonstrates that the zinc(II) alkoxy species is formed from the zinc(II) alkyl starting material; this is proved by the presence of the ethyl and ethoxy moieties in $Zn_4(L^HO)_4(OEt)_2Et_2$.

The structure of $Zn_4(L^HO)_4(OEt)_2Et_2$ (Figure 2.15) is similar to the previously discussed $Zn_4(L^HO)_4(OMe)_2Me_2$ with two distinct zinc(II) centres. Zn(1) is bound to two imine nitrogen atoms, two phenoxides, and the μ_3-ethoxide in a pseudo-octahedral environment with the Zn(1)-N(1)-O(1) angle being 164.72(17)° and the

O(2)-Zn(1)-O(1) angle being 79.40(15)°. The Zn(2) is bound to a ethyl group, μ_3-ethoxide, and two phenoxides in a pseudo-tetrahedral environment with the C(1)-Zn(2)-O(3) angle being 121.5(2)º and the O(2)-Zn(2)-O(3) angle being 97.60(16)º. The Zn(1)-O(1) length of 2.162(4) Å and the Zn(1)-O(2) distance of 2.039(4) Å are in agreement with $Zn_4(L^{H}O)_4(OMe)_2Me_2$ and literature precedent, as are the Zn(2)-O(1) and Zn(2)-C(1) distance of 2.026(4) Å and 1.989(6) Å respectively. Selected bond lengths (Table 2.3) and angles (Table 2.4) are shown and compared to $Zn_4(L^{H}O)_4(OMe)_2Me_2$ and a previously reported structure from the literature. Despite several attempts it proved difficult to isolate a significant quantity of the $Zn_4(L^{H}O)_4(OEt)_2Et_2$ complex and so no further characterisation or catalytic data could be collected.

The XRD data collected for the $Zn_4(L^{H}O)_4(OEt)_2Et_2$ complex showed significant disorder but with considerable effort the structure was unambiguously determined. There were two main areas of disorder in the structure, the isobutyl groups attached to the silsesquioxane cubes and one of the silsesquioxane cubes itself. To solve this carbon atoms of disordered isobutyl groups were treated isotropically as the electron density associated with these regions in the electron density map was partially smeared. A number of C-C, Si…C and C…C restraints were necessitated, in order to stabilize the refinement. One silsesquioxane cube (Si{9} to Si{23}) and associated isobutyl groups were modelled over two positions in a 55:45 ratio and several isobutyl groups were modelled with different ratios.

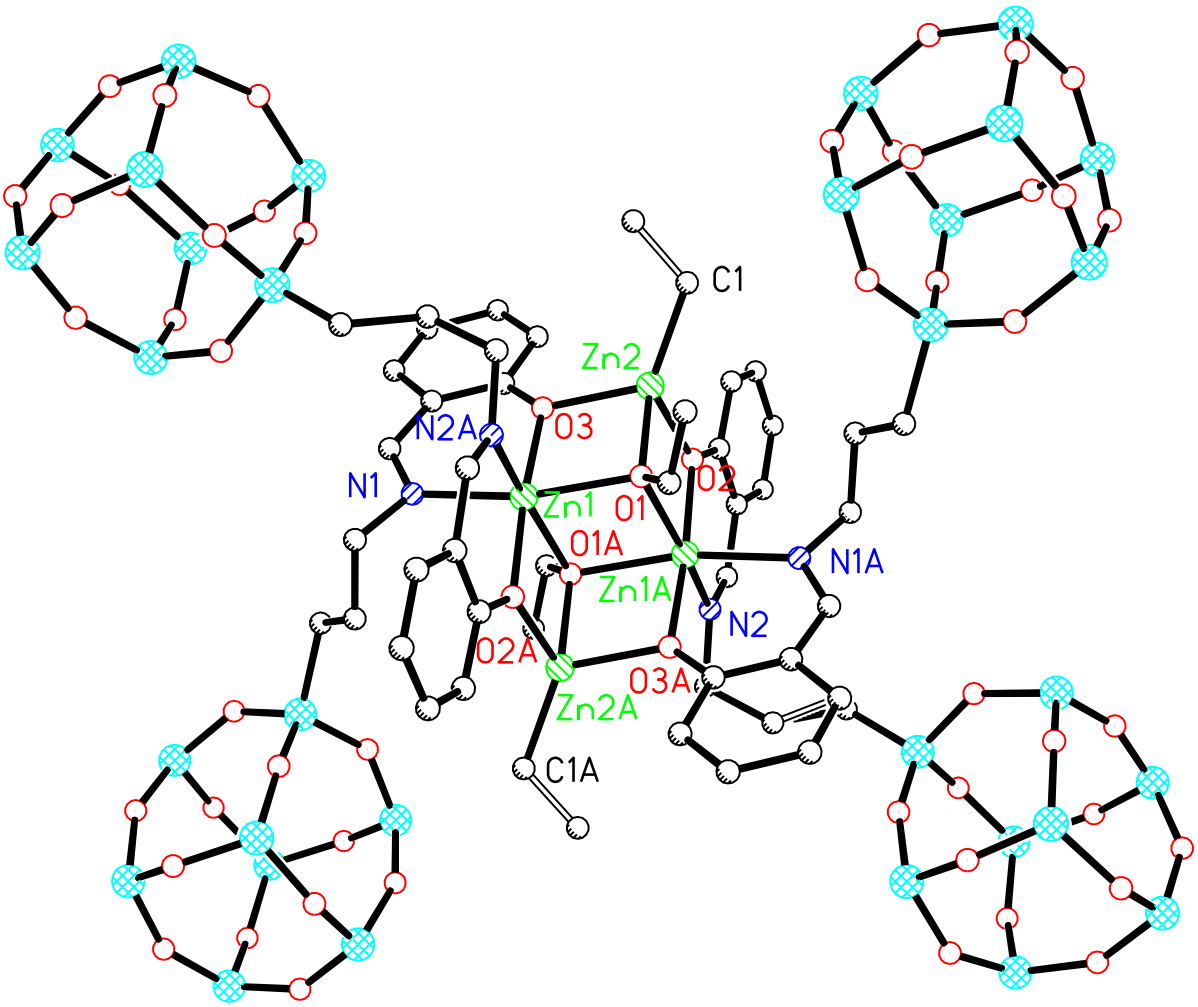

Figure 2.15 – Crystal structure of $Zn_4(L^HO)_4(OEt)_2Et_2$, isobutyl groups showed significant disorder and have been removed for clarity. One silsesquioxane cube was modelled across two sites in a 55:45 ratio.

		$Zn_4(L^HO)_4(OEt)_2Et_2$	$Zn_4(L^HO)_4(OMe)_2Me_2$	*Lewinski et al* [184]
Zn(1)	N(1)	2.149(6)	2.127(5)	2.194(2)
Zn(1)	O(1)	2.162(4)	2.117(4)	2.141(1)
Zn(1)	O(2)	2.039(4)	2.091(4)	2.082(1)
Zn(2)	C(1)	1.989(6)	1.957(7)	1.986(3)
Zn(2)	O(1)	2.026(4)	2.021(4)	2.094(1)
Zn(2)	O(2)	2.038(4)	2.033(4)	2.025(1)
Zn(2)	O(3)	2.038(4)	2.028(4)	1.987(1)

Table 2.3 – Selected bond lengths from $Zn_4(L^HO)_4(OEt)_2Et_2$ compared to $Zn_4(L^HO)_4(OMe)_2Me_2$ and a similar complex reported by *Lewinski et al*.[184]

			$Zn_4(L^HO)_4(OEt)_2Et_2$	$Zn_4(L^HO)_4(OMe)_2Me_2$	*Lewinski et al* [184]
O(3)	Zn(2)	C(1)	121.5(2)	126.1(3)	121.36(9)
O(3)	Zn(2)	O(2)	97.60(16)	96.10(17)	99.80(5)
O(1)	Zn(1)	N(1)	164.72(17)	162.96(18)	151.20(6)
O(1)	Zn(1)	O(1)	79.40(15)	77.93(15)	83.27(5)

Table 2.4 - Selected bond angles from $Zn_4(L^HO)_4(OEt)_2Et_2$ compared compared to $Zn_4(L^HO)_4(OMe)_2Me_2$ and a similar complex reported by *Lewinski et al.*[184]

When L^HOH was reacted with 0.5 equivalent of $ZnMe_2$ the expected monometallic structure $Zn(L^HOH)_2$ was observed in good yield (Figure 2.16). The structure shows a central zinc(II) atom, Zn(1), bound to two imine nitrogen atoms and two phenoxides from two (L^HOH) ligands in a pseudo-tetrahedral environment with a Zn(1)-O(1)-N(1) bond angle of 95.63(14)º and a Zn(1)-O(2)-N(1) bond angle of 114.52(15)º.

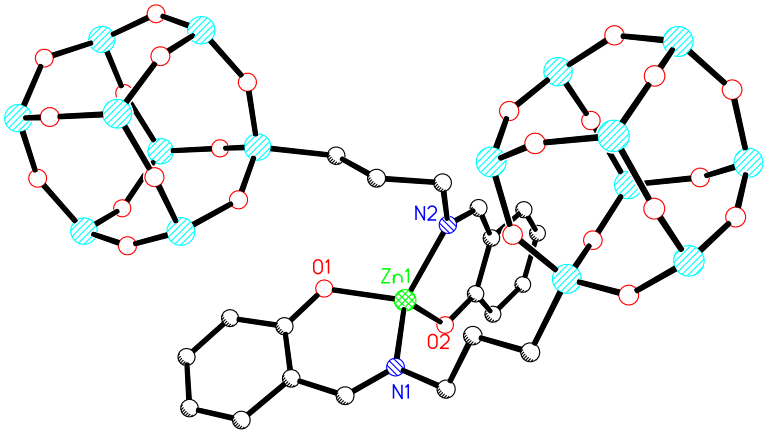

Figure 2.16 – Crystal structure of $Zn(L^HO)_2$

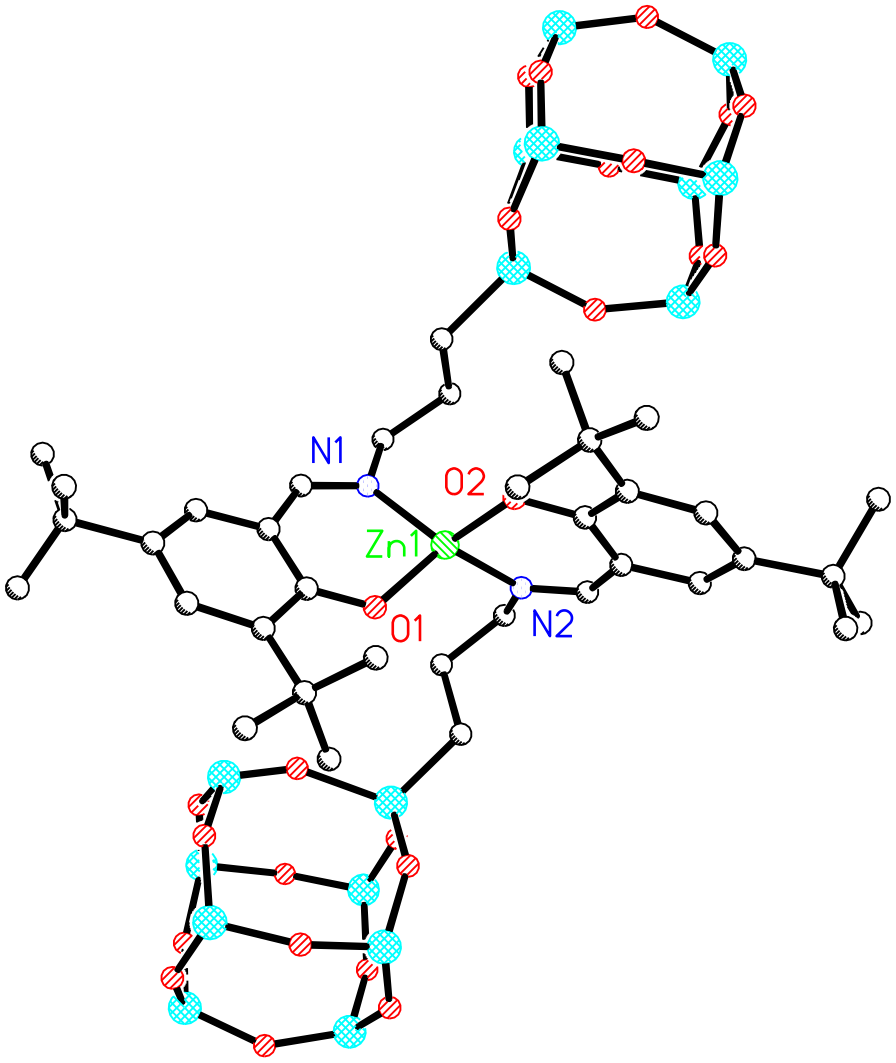

Figure 2.17 – Crystal structure of Zn($L^{tBu}O$)$_2$

Reaction of di-*tert*-butyl substituted ligand $L^{tBu}OH$ with varying equivalents of $ZnMe_2$ always yielded the Zn($L^{tBu}O$)$_2$ complex (Figure 2.17). The solid state structure of Zn($L^{tBu}O$)$_2$ shows a central zinc(II) atom, Zn(1), bound to two imine nitrogen atoms and two phenoxides from two $L^{tBu}OH$ ligands. The Zn(1) centre is in a pseudo-tetrahedral environment with a Zn(1)-O(1)-N(1) bond angle of 94.9(2)º and a Zn(1)-O(2)-N(1) bond angle of 120.4(2)º. Selected bond lengths (Table 2.5) and angles (Table 2.6) from Zn($L^{H}O$)$_2$ and Zn($L^{tBu}O$)$_2$ have been compared to a similar complex previously reported by *Benisvy et al*.[181]

The Zn(1)-O(1) and Zn(1)-O(2) bond lengths in the $Zn(L^{H}O)_2$ structures are 1.922(3) Å and 1.914(4) Å and show similar values to the $Zn(L^{tBu}O)_2$ structure. However the Zn-O bond lengths in the $Zn_4(L^{H}O)_4(OMe)_2Me_2$ and $Zn_4(L^{H}O)_4(OEt)_2Et_2$ structures are significantly longer at 2.117(4) Å and 2.162(4) Å respectively. The increase in bond lengths in the tetrametallic structures can be attributed to the bound oxygen being bridged between two zinc centres. In contrast to this the oxygen atoms in the monometallic structures are terminal and bound only to the phenyl ring of the ligand and a single metal centre.

		$Zn(L^{H}O)_2$	$Zn(L^{tBu}O)_2$	*Benisvy et al* [181]
Zn(1)	O(1)	1.922(3)	1.921 (6)	1.919(2)
Zn(1)	O(2)	1.914(4)	1.913 (4)	1.919(2)
Zn(1)	N(1)	1.996(4)	1.986 (6)	1.979(2)
Zn(1)	N(2)	2.011(3)	1.986 (7)	1.979(2)

Table 2.5 – Selected bond lengths from $Zn(L^{H}O)_2$ and $Zn(L^{tBu}O)_2$ compared to a similar complex previously reported in the literature.[181]

			$Zn(L^{H}O)_2$	$Zn(L^{tBu}O)_2$	*Benisvy et al* [181]
Zn(1)	O(1)	N(1)	95.63(14)	94.9 (2)	93.92(6)
Zn(1)	O(2)	N(1)	114.52(15)	120.4 (2)	115.66(6)
Zn(1)	N(1)	N(2)	129.13(14)	116.8 (2)	121.85(9)

Table 2.6 - Selected bond angles from $Zn(L^{H}O)_2$ and $Zn(L^{tBu}O)_2$ compared to a similar complex previously reported in the literature.[181]

$L^{Cl}OH$ was also reacted with $ZnMe_2$ in various ratios and always yielded the $Zn(L^{Cl}O)_2$ complex. Unfortunately, no crystals of the $Zn(L^{Cl}O)_2$ complex that were suitable for X-ray diffraction were obtained but other characterisation data was consistent with the proposed structure $Zn(L^{Cl}O)_2$. All complexes were characterised by ^{1}H, $^{13}C\{^{1}H\}$, $^{29}Si\{^{1}H\}$ NMR Spectroscopy and HR ESI-MS which showed data consistent with the solid state structures. The ^{1}H NMR spectrum of $Zn(L^{H}O)_2$ is presented (Figure 2.18 top) along with the ESI-MS spectrum (Figure 2.18 bottom). The ^{1}H NMR spectrum shows a similar spectrum to that of the free ligand $L^{H}OH$ and shows no splitting of the $C\underline{H}_2$-N resonance as seen in the $Zn_4(L^{H}O)_4(OMe)_2Me_2$ spectrum. This is consistent with the solid state structure as the two ligands appear to be in the same chemical environment. Despite the spectrum being very similar to that of the free ligand $L^{H}OH$ (Figure 2.9) slight changes in the chemical shift of all resonances as well as the disappearance of the OH resonance at 13.58 show the successful binding of Zn(II).

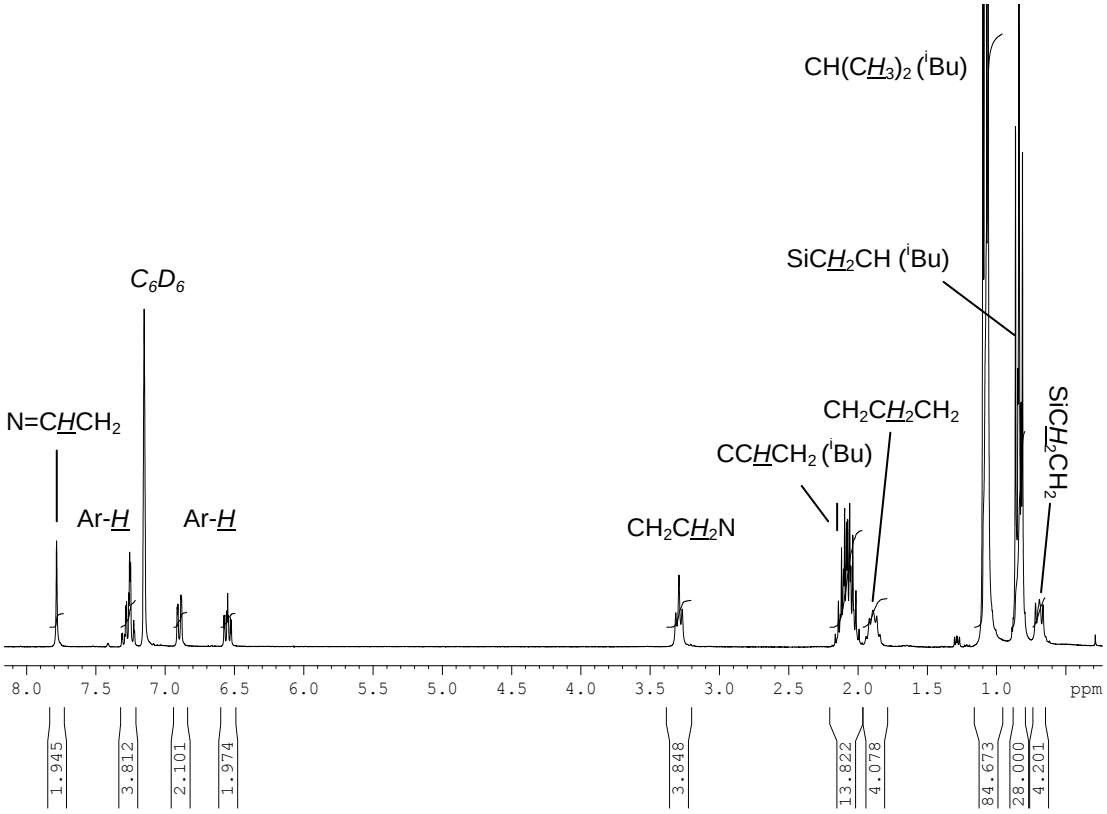

Figure 2.18 top: Annotated ^{1}H NMR Spectrum of Zn($L^{H}O$)$_2$ bottom: (a) Theoretical HR ESI-MS Spectrum of Zn($L^{H}O$)$_2$ (b) Recorded HR ESI-MS Spectrum of Zn($L^{H}O$)$_2$

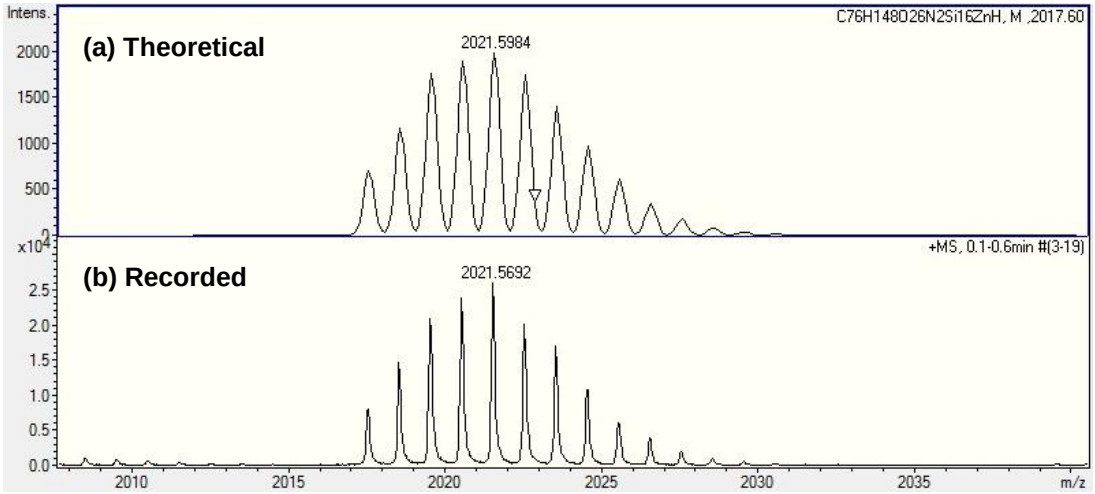

2.4. Heterogeneous Zinc(II) Complexes

As previously discussed in section 2.1, the immobilisation of metals for catalysis is common place, however, the heterogenenisation of catalysts for the ROP of cyclic esters has only recently been demonstrated.[192-194] In the current commercial synthesis of polylactide as a commodity polymer the homogenous catalyst is not separated from the polymer product resulting in any metal from the catalyst being present in the polymer. The use of heterogeneous catalysts in the polymerisation reaction potentially offers the ability to easily separate the metal catalyst from the polymer product. The presence of metal residues in the polymer can impact polymer performance, particularly for biological applications; there is therefore a drive to lower the metal content of the polymer product.[175,178]

Several groups have demonstrated the use of heterogeneous initiators for the production of polyesters.[195-197] The majority of these examples have involved reacting a support with a simple metal-alkoxide. For example, *Hamaide et al* developed silica based yttrium complexes for the polymerization of ε-caprolactone.[198,199] Whilst these methods have produced interesting results, with this approach they are limited by the surface chemistry of the support which does not allow the steric or electronic environment around the metal centre to be altered. Further examples include those by *CW Jones et al* who immobilised Coates' Zn-β-diiminate initiators to SBA-15 for the ROP of lactide.[141,200] Other groups have used polystyrene as a support, for example Bu_2SnCl_2 has been heterogenised onto polystyrene beads and used as a recyclable catalyst for the ROP of ε-caprolactone.[193,201] Presented in this section are a range of tethered silica ligands which have been complexed to zinc(II) and aluminium(III) and used for the melt polymerisation of *rac*-lactide. These complexes act as a direct comparison to the homogeneous silsesquioxane complexes reported in section 2.3.

2.4.1. Silica Tethering

The first step in the tethering process was the reaction of the surface silanol groups of the silica with $(MeO)_3Si(CH_2)_3NH_2$ to give a tether with amine functionality ($Si\text{-}NH_2$). In this preparation a loading of 1 mmol of organic ligand per gram of silica was targeted. This reaction was conducted by simply stirring a slurry of the silica with the

desired amount of $(MeO)_3Si(CH_2)_3NH_2$ (1 mmol g^{-1} silica) at 298 K for 24 hours and gave the tethered amine product in high yield (90 %) (Scheme 2.4).

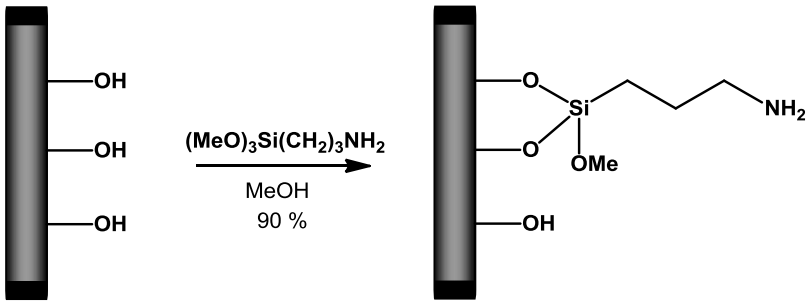

Scheme 2.4 – Synthesis of Si-NH_2.

The second step was an imine condensation reaction of the silica tethered amine with the appropriate salicylaldehyde derivative. This was a relatively straightforward synthesis in which a slurry of the tethered amine product was stirred together with a solution of the appropriate aldehyde (1 mmol g^{-1} silica) in MeOH over a period of 24 hours to give the desired product in high (85-90 %) yield (Scheme 2.5).

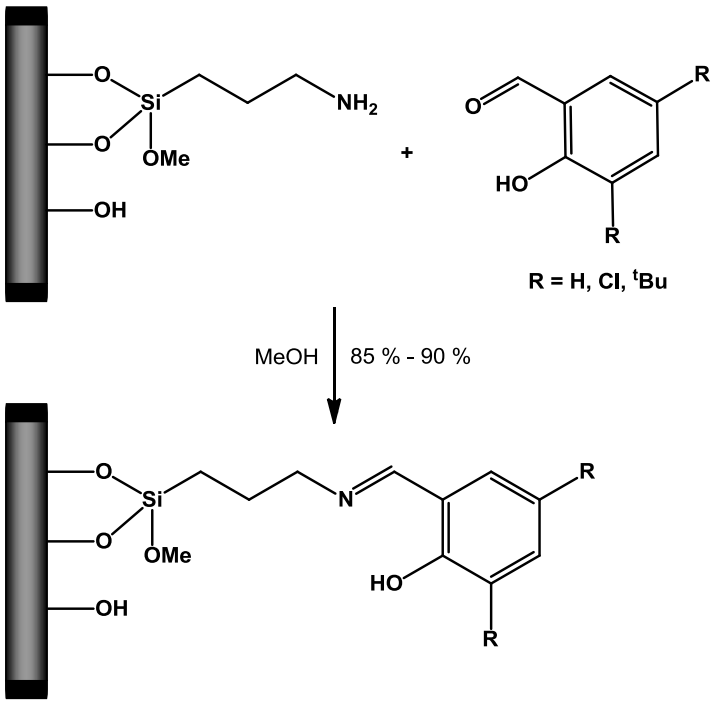

Scheme 2.5 – Synthesis of Si-L^{H}OH, Si-L^{tBu}OH and Si-L^{Cl}OH.

The tethered silica ligands are referred to as Si-L^{H}OH, Si-L^{tBu}OH, Si-L^{Cl}OH depending on the functionality of the two groups in the *ortho* and *para* positions relative to the hydroxyl group of the phenoxy moiety. The ligands were characterised by solid state $^{13}C\{^{1}H\}$ NMR spectroscopy (Figure 2.19).

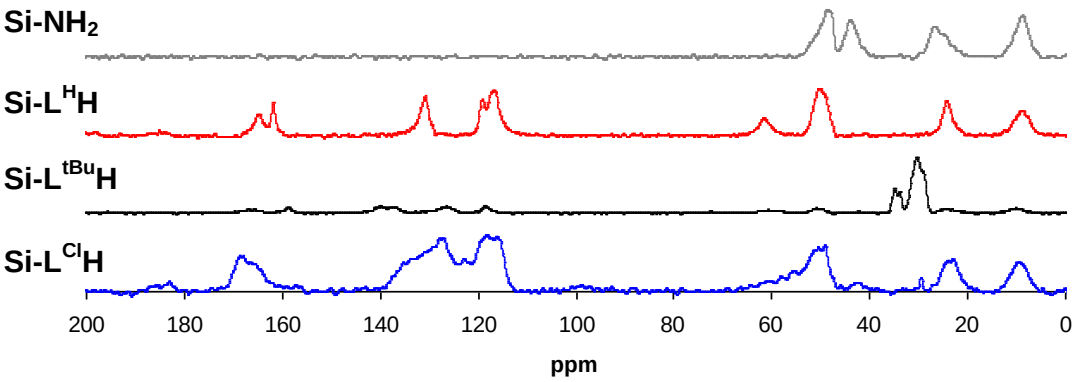

Figure 2.19 - Solid state $^{13}C\{^{1}H\}$ mAS NMR spectra for the Si-NH_2, Si-L^{H}OH, Si-L^{tBu}OH and Si-L^{Cl}OH ligands.

The solid state $^{13}C\{^{1}H\}$ MAS NMR spectrum of Si-NH_2 shows four broad resonances between 5 and 50 ppm which correspond to the three CH_2 carbon atoms from the propyl tether and one carbon atom from the Si-methoxy group. The spectra from the Si-L^{H}OH and Si-L^{Cl}OH ligands have resonances between 10 and 60 ppm relating to the same four carbon atoms as the Si-NH_2 spectrum, with a shift in the resonance seen at 45 ppm in the Si-NH_2 to ~60 ppm in the imine structures. This shift is most likely due to the $\underline{C}H_2$-NH_2 species caused by the NH_2 changing from amine to an imine. There are also extra resonances between 110 and 200 ppm relating to the additional aromatic carbon atoms in the imine structures. The Si-L^{tBu}OH spectrum has similar resonances to the Si-L^{H}OH and Si-L^{Cl}OH ligands but has two extra distinct resonances at 30-35 ppm which are a result of the CH and CH_3 carbon atoms from the *tert*-butyl groups. The Si-L^{Cl}OH spectrum shows significant broadening of resonances when compared to the other structures, which is potentially related to the quadrupolar nature of chlorine.

2.4.2. Metalation with Zinc(II)

The tethered silica ligands (Si-L^{H}OH, Si-L^{tBu}OH, Si-L^{Cl}OH) were thoroughly dried by heating to 130 °C for 5 hours under strong vacuum and then reacted with 1 equivalent of $ZnMe_2$ (1 mmol g^{-1} silica) under Schlenk line conditions. $ZnMe_2$ was also complexed to untethered dried amorphous silica (Si-OH) under the same conditions to provide an untethered comparison (Si-Zn) (Scheme 2.6).

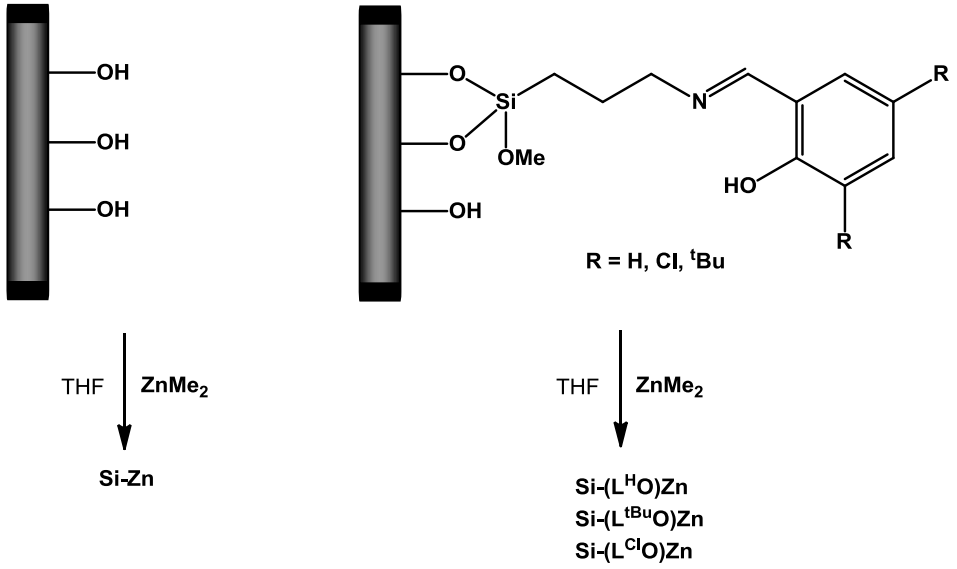

Scheme 2.6 – Complexation of Zinc(II) to silica and Si-L^{H}OH, Si-L^{tBu}OH, Si-L^{Cl}OH.

The complexes, referred to as Si-(L$^{\mathbf{H}}$O)Zn, Si-(L$^{\mathbf{tBu}}$O)Zn, Si-(L$^{\mathbf{Cl}}$O)Zn and Si-Zn, were all characterised by CHN elemental analysis and ICP-AES for zinc content (Table 2.7) and compared to theoretical values (Table 2.8). Si-(L$^{\mathbf{H}}$O)Zn was also analysed by $^{13}C\{^{1}H\}$ solid state NMR spectroscopy (Figure 2.20) and X-ray photoelectron spectroscopy (XPS) (Figure 2.21, Table 2.9). The solid state $^{13}C\{^{1}H\}$ CP/MAS NMR spectrum shows a similar trace to the Si-(L$^{\mathbf{H}}$O)Zn ligand with slight changes in the shape of some peaks (e.g ~120ppm) attributed to the binding of zinc.

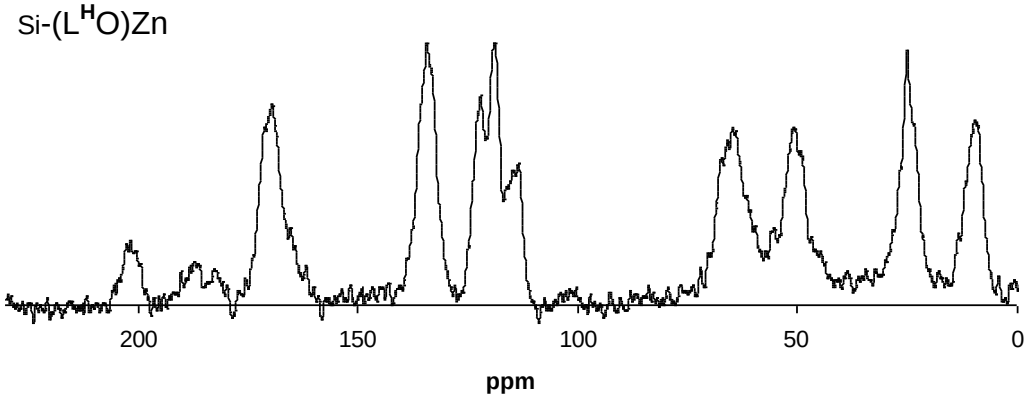

Figure 2.20 - Solid state $^{13}C\{^{1}H\}$ NMR spectra of Si-(L^{H}O)Zn.

Complex	C (%)	H (%)	N (%)	Zn (%)
Si-Zn	1.60	1.01	0.00	6.58
Si-(L^{H}O)Zn	9.97	1.45	1.11	7.03
Si-(L^{tBu}O)Zn	14.40	2.33	1.07	7.01
Si-(L^{Cl}O)Zn	9.48	1.30	1.06	6.97

Table 2.7 – Carbon, nitrogen, hydrogen and zinc content for heterogeneous zinc complexes as determined CHN elemental analysis and ICP-AES.

Complex	C (%)	H (%)	N (%)	Zn (%)
Si-(L^{H}O)Zn	11.8	1.59	1.06	6.14
Si-(L^{tBu}O)Zn	17.6	2.58	0.98	6.14
Si-(L^{Cl}O)Zn	11.2	1.37	1.01	6.14

Table 2.8 – Theoretical carbon, nitrogen, hydrogen and zinc content for heterogeneous zinc complexes.

The elemental analysis data (Table 2.7) is consistent with estimated values (Table 2.8) based on a sequential loading of 1 mmol g^{-1} of ligand and zinc. This demonstrates the successful tethering and subsequent complexation of zinc to produce a range of novel tethered heterogeneous zinc complexes. The theoretical values were calculated based on a 1 mmol g^{-1} loading of ligand onto the silica surface.

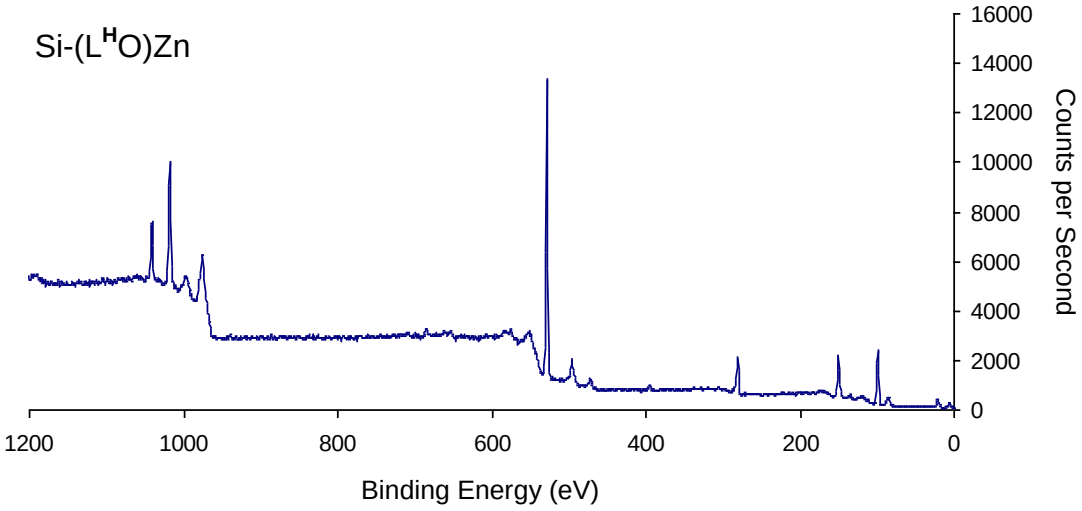

Figure 2.21 – XPS spectrum of Si-(L^{H}O)Zn.

Element	Si	N	C	Zn	O
Atom Abundance (%)	28.01	1.47	16.93	3.64	49.95
Binding Energy (eV)	103.1	399.5	284.7	1045.2	532.3

Table 2.9 – XPS data showing relative abundance and corresponding binding energies (eV) for Si, N, C, Zn, O in Si-(L^{H}O)Zn.

The XPS spectrum confirms the presence of Zn(II) at the surface of the catalyst as well as the presence of the organic ligand. It is important to note the relative abundances in XPS are only at the surface and not representative of the overall abundance in the material.

2.5. Zinc(II) Complexes for the ROP of *rac*-lactide.

2.5.1. Homogeneous Zinc Complexes

The homogenous complexes $Zn_4(L^{H}O)_4(OMe)_2Me_2$, $Zn(L^{H}O)_2$, $Zn(L^{tBu}O)_2$ and $Zn(L^{Cl}O)_2$ were tested for the ROP of *rac*-lactide. The $Zn_4(L^{H}O)_4(OMe)_2Me_2$ complex contains an intramolecular alkoxide due to the serendipitous oxygen insertion discussed in section 2.3 which could potentially act as an initiating group for the ROP of lactide. All complexes were tested under solvent free conditions without the addition of a co-initiator. The $Zn(L^{H}O)_2$, $Zn(L^{tBu}O)_2$ and $Zn(L^{Cl}O)_2$ complexes do not possess an alkoxy initiator group and were all found to be inactive for the polymerisation of *rac*-lactide. However, the $Zn_4(L^{H}O)_4(OMe)_2Me_2$ complex was active both under solvent free conditions at 403 K and in toluene at 298 K (Table 2.10).

Initiator	Conversion (%)	M_n	M_w	PDI	P_r
$Zn_4(L^{H}O)_4(OMe)_2Me_2$ [a]	70	40050	70400	1.76	0.56
$Zn_4(L^{H}O)_4(OMe)_2Me_2$ [b]	96	206000	293950	1.42	0.59

Table 2.10 –The complex $Zn_4(L^{H}O)_4OMe_2Me_2$ was tested for the ROP of *rac*-lactide under both solvent free conditions at 403 K and in toluene at 298 K. *[a] polymerisation carried out with a 300:1 monomer:initiator ratio at 403 K for 10 minutes under solvent free conditions. [b] polymerisation carried out with a 300:1 monomer:initiator ratio at 298 K for 96 hours in toluene.*

$Zn_4(L^{H}O)_4(OMe)_2Me_2$ successfully polymerised rac-LA to produce PLA. The observed molecular weights are higher than theoretical values (*ca*. 43250), this could be due to slow initiation of the polymer chains ($k_{int}<k_{prop}$) or transesterification. The polymers isolated showed slight heterotactic bias when analysed by ^1H homonuclear decoupled NMR spectroscopy.

2.5.2. Heterogeneous Zinc Complexes

The heterogeneous complexes Si-Zn, Si-($L^{H}O$)Zn, Si-($L^{tBu}O$)Zn and Si-($L^{Cl}O$)Zn were tested for the ROP of *rac*-lactide under solvent free conditions for 24 hours at 403 K (Table 2.11). The complexes were all active for the polymerisation without the addition of a co-initiator and produced high molecular weight atactic PLA, hence P_r ~0.5 in all cases. The tethered complexes Si-($L^{H}O$)Zn, Si-($L^{tBu}O$)Zn and Si-($L^{Cl}O$)Zn reacted to higher conversion and produced polymer of significantly higher molecular weight than the untethered complex Si-Zn. This demonstrates that the presence of the organic tether has a positive effect on the reactivity of the initiator.

Initiator	Conversion (%)	M_n	M_w	PDI
Si-Zn	40	18550	27200	1.47
Si-L^{H}H-Zn	55	54200	83050	1.53
Si-L^{tBu}H-Zn	60	81800	131550	1.61
Si-L^{Cl}H-Zn	73	77150	122200	1.58

Table 2.11 –The complex $Zn_4(L^{H}H)_4OMe_2Me_2$ was tested for the ROP of *rac*-lactide under both solvent free conditions at 403 K and in toluene at 298 K.

2.6. Homogeneous Aluminium(III) Silsesquioxane Complexes

Ligands L^{H}OH, L^{tBu}OH and L^{Cl}OH were reacted with $AlMe_3$ in a 1:1 and 2:1 ratio. From analysis of the ^{1}H NMR spectrum of the reaction mixture of ligands L^{H}OH and L^{Cl}OH with $AlMe_3$ in a 1:1 ratio two species were observed. One series of resonances was due to Al(L$^{(H/Cl)}$O)$_2$Me and other set due to Al(L$^{(H/Cl)}$O)Me$_2$ respectively; unfortunately attempts to purify these mixtures proved fruitless. Fortunately, if the reaction were repeated with 2 equivalents of ligand per metal centre pure complexes of the form Al(L$^{(H/Cl)}$O)$_2$Me were isolated. For example, in the ^{1}H NMR spectrum of Al(L^{H}O)$_2$Me a 2H-imine resonance was present at 7.68 ppm and a 3H resonance was also observed at 0.42 ppm corresponding to an Al-CH_3 and consequently a resonance at 2.0 ppm was present in the ^{13}C{^{1}H} NMR spectrum. When L^{tBu}OH was reacted with $AlMe_3$ it exclusively formed the Al(L^{tBu}O)Me$_2$ complex even when an excess of L^{tBu}OH was added. The difference in reactivity of the L^{tBu}OH complex is attributed to the steric bulk of the *tert*-butyl groups preventing the binding of a second ligand to the metal (Scheme 2.8).

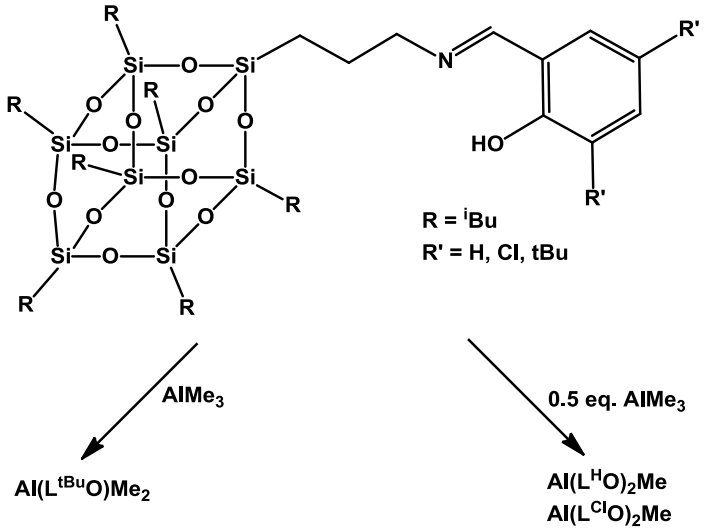

Scheme 2.7 - Complexation of $L^{H}OH$, $L^{tBu}OH$ and $L^{Cl}OH$ to aluminium(III).

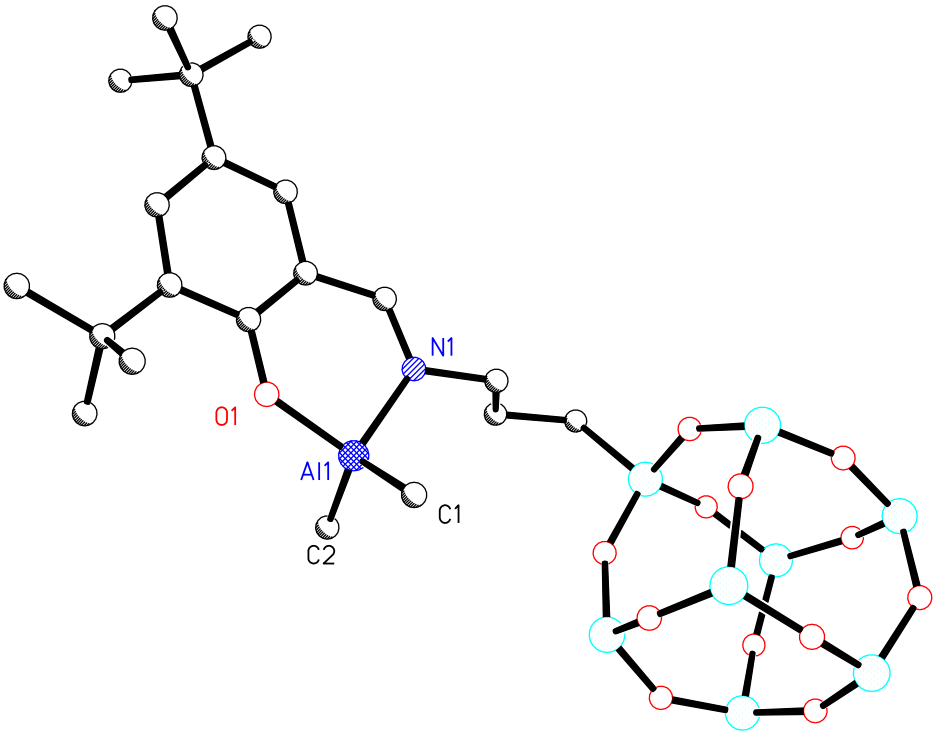

Figure 2.22 – Crystal structure of $Al(L^{tBu}O)Me_2$.

		$Al(L^{tBu}O)Me_2$	*Dagorne et al* [202]
Al(1)	O(1)	1.774 (4)	1.762 (1)
Al(1)	C(1)	1.954 (6)	1.964 (2)
Al(1)	C(2)	1.965 (6)	1.953 (2)
Al(1)	N(1)	1.951 (5)	2.011(1)

Table 2.12 – Selected bond lengths from $Al(L^{tBu}O)Me_2$ compared to a similar complex previously reported in the literature. [202]

			Al(L^{tBu}O)Me_2	*Dagorne et al* [202]
Al(1)	O(1)	N(1)	95.02 (18)	94.61 (6)
Al(1)	O(1)	C(1)	111.7 (2)	112.19 (8)
Al(1)	C(1)	C(2)	120.8 (3)	115.99 (9)

Table 2.13 - Selected bond angles from Al(L^{tBu}H)Me_2 compared to a similar complex previously reported in the literature. [202]

Single crystal XRD data was collected for Al(L^{tBu}O)Me_2 (Figure 2.22), however, despite considerable effort it proved impossible to grow crystals of Al(L^{H}O)$_2$Me and Al(L^{Cl}O)$_2$Me suitable for XRD analysis. The crystal structure of Al(L^{tBu}O)Me_2 shows an aluminium centre bound to one $L^{tBu}O^-$ ligand. The aluminium centre is in a pseudo-tetrahedral environment with an Al(1)-O(1)-N(1) bond angle of 95.02(18)º, a Al(1)-C(1)-C(2) bond angle of 120.8(3)º and is bound to the phenoxide and imine nitrogen from the ligand as well as two methyl groups which are retained from the $AlMe_3$ starting material. The Al(1)-O(1) 1.774 Å bond length is consistent with previously reported structures and selected bond lengths and angles from a similar structure are reported in Tables 2.12 and 2.13 respectively.[202] All complexes were characterised by ^{1}H, ^{13}C{^{1}H}, ^{29}Si{^{1}H} NMR spectroscopy and elemental analysis.

2.7. Silica Tethered Aluminium(III) Complexes

The tethered silica ligands (Si-L^{H}OH, Si-L^{tBu}OH and Si-L^{Cl}OH) were thoroughly dried by heating to 130°C for 5 hours under strong vacuum and then reacted with 1 equivalent of $AlMe_3$ (1 mmol g^{-1} silica) under air sensitive conditions. $AlMe_3$ was also complexed to untethered dried amorphous silica (Si-OH) under the same conditions to provide a comparison (Si-Al) (Scheme 2.8).

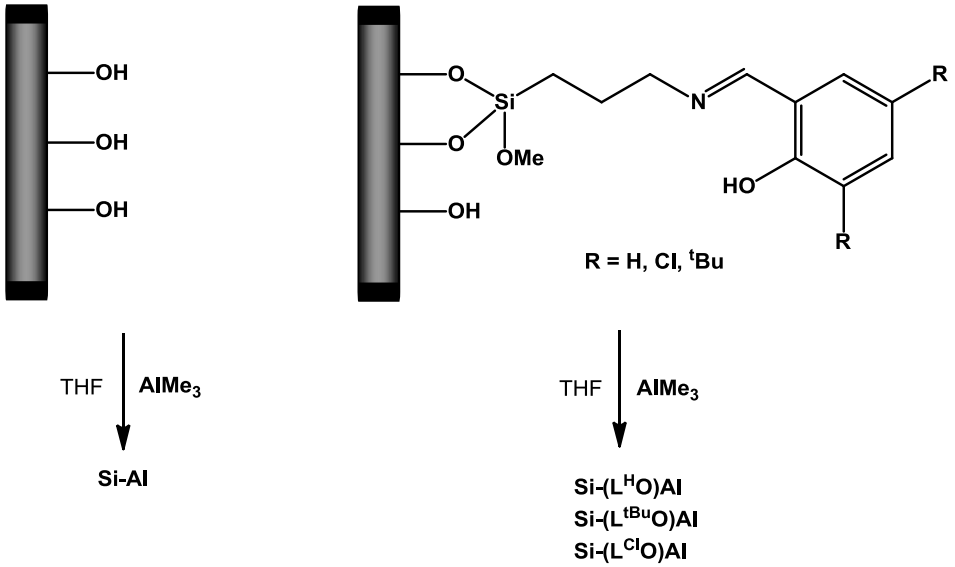

Scheme 2.8 - Complexation of aluminium(III) to silica and Si-L^{H}OH, Si-L^{tBu}OH, Si-L^{Cl}OH.

The complexes, referred to here on in as Si-Al, Si-(L^{H}O)Al, Si-(L^{tBu}O)Al and Si-(L^{Cl}O)Al were all characterised by $^{13}C\{^{1}H\}$ and $^{27}Al\{^{1}H\}$ MAS solid state NMR spectroscopy (Figure 2.23). The complexes were also characterised by CHN elemental analysis and ICP-AES for aluminium content (Table 2.14) and compared to theoretical values based on the sequential tethering of 1 mmol g^{-1} ligand and aluminium (Table 2.15).

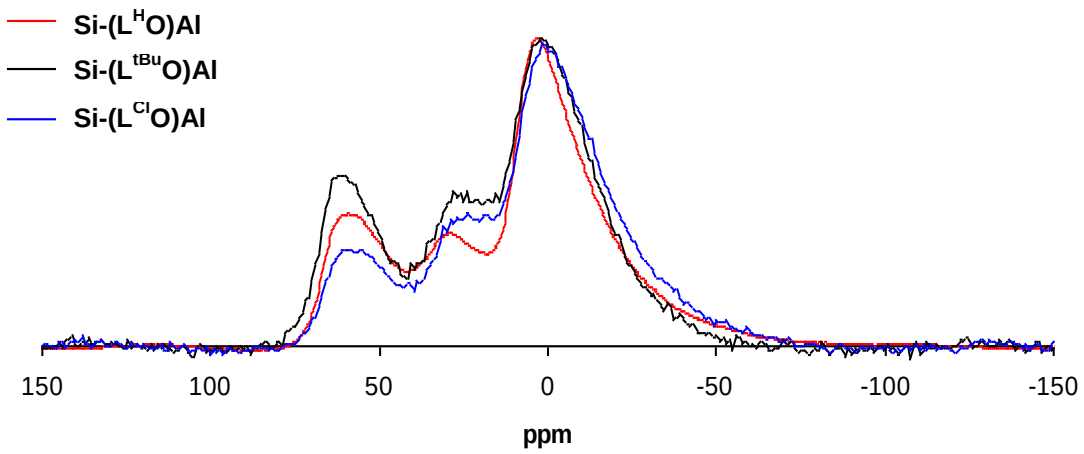

Figure 2.23 – Top: ^{27}Al Solid state NMR of Si-L^{H}H-Al (red), Si-L^{tBu}H-Al (black), Si-L^{Cl}H-Al (blue) Bottom: ^{13}C Solid state NMR of Si-L^{H}H-Al (red), Si-L^{tBu}H-Al (black), Si-L^{Cl}H-Al (blue)

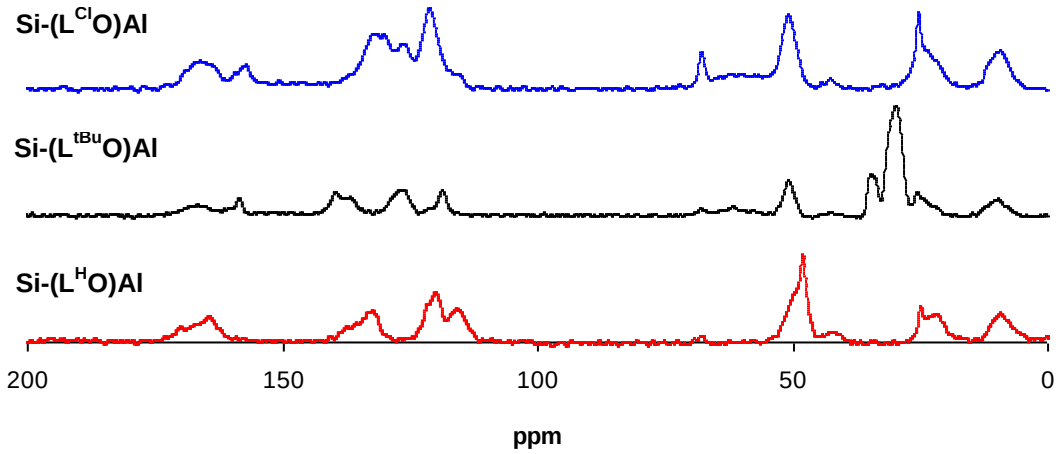

Complex	C (%)	H (%)	N (%)	Al (%)
Si-Al	4.82	1.54	0.02	2.92
Si-(L^{H}O)Al	11.9	1.85	1.18	2.75
Si-(L^{tBu}O)Al	16.9	2.72	1.16	1.43
Si-(L^{Cl}O)Al	12.2	1.63	1.14	2.03

Table 2.14 – Carbon, nitrogen, hydrogen and zinc content for heterogeneous zinc complexes as determined CHN elemental analysis and ICP-AES.

Complex	C (%)	H (%)	N (%)	Al (%)
Si-(L^{H}O)Al	12.2	1.64	1.09	2.63
Si-(L^{tBu}O)Al	18.1	2.65	1.00	2.63
Si-(L^{Cl}O)Al	11.5	1.41	1.04	2.63

Table 2.15 – Theoretical carbon, nitrogen, hydrogen and zinc content for heterogeneous aluminium complexes.

The CHN elemental analysis and ICP-AES analysis for aluminium are consistent with theoretical values. The solid state $^{13}C\{^{1}H\}$ MAS NMR spectra are consistent with the successful binding of Al to the organic tether when compared to their relative ligand spectra (Figure 2.19) and the Si-($L^{H}O$)Al spectrum is similar to the Si-($L^{H}O$)Zn spectrum reported in Figure 2.20. The solid state $^{27}Al\{^{1}H\}$ MAS spectra confirm the presence of aluminium in the heterogeneous complexes and show the aluminium to be present in its 4, 5 and 6 coordinate forms. The characterisation data is consistent with estimated values expected for the successful surface tethering and subsequent complexation with $AlMe_3$.

2.8. Aluminium(III) Complexes for the ROP of *rac*-lactide.

2.8.1. Homogeneous Aluminium Complexes

The $Al(L^{H}O)_2Me$, $Al(L^{Cl}O)_2Me$ and $Al(L^{tBu}O)Me_2$ complexes were all tested for the ring opening polymerisation of *rac*-lactide with a benzyl alcohol co-initiator. As previously discussed the presence of an alkoxide group close to the metal centre is required for the initiation of the polymerisation. The benzyl alcohol reacts with the Al-methyl groups to generate the required alkoxide *in situ* and initiate the polymer chain. The polymerisations were conducted with 1 g of lactide monomer at 353 K in toluene with a 100:1 ratio of monomer to initiator and 1 equivalent of BnOH per Al-Me and the results are presented in Table 2.16.

Initiator	Time	Conversion (%)	M_n	M_w	PDI	P_r
$Al(L^{H}O)_2Me$	24h	99+	13850	18800	1.36	0.41
$Al(L^{tBu}O)Me_2$	24h	99+	12500	14500	1.16	0.46
$Al(L^{Cl}O)_2Me$	24h	99+	13000	16000	1.23	0.44

Table 2.16 – Polymerisation data for homogeneous aluminium silsesquioxane complexes used for the ROP of *rac*-lactide.

The $Al(L^{H}O)_2Me$, $Al(L^{Cl}O)_2Me$ and $Al(L^{tBu}O)Me_2$ complexes all showed activity for the ROP of *rac*-lactide. The polymerisations reacted to high conversion and gave polymer products with molecular weights that relate closely to theoretical values for the growth of one polymer chain per Al-Me group. Analysis of the polymers via MALDI-ToF MS indicated that the end group were -OCH_2Ph and -H as expected from a coordination insertion mechanism. Furthermore, the repeat unit was 72 g mol^{-1}, which is indicative of a degree of transesterification occurring. A ^{1}H NMR spectrum of the polymer produced by $Al(L^{H}O)_2Me$ is presented (Figure 2.24, top) , along with

the methine region of the homonuclear decoupled ^{1}H NMR spectrum (Figure 2.24, bottom) and a GPC chromatograph in Figure 2.25.

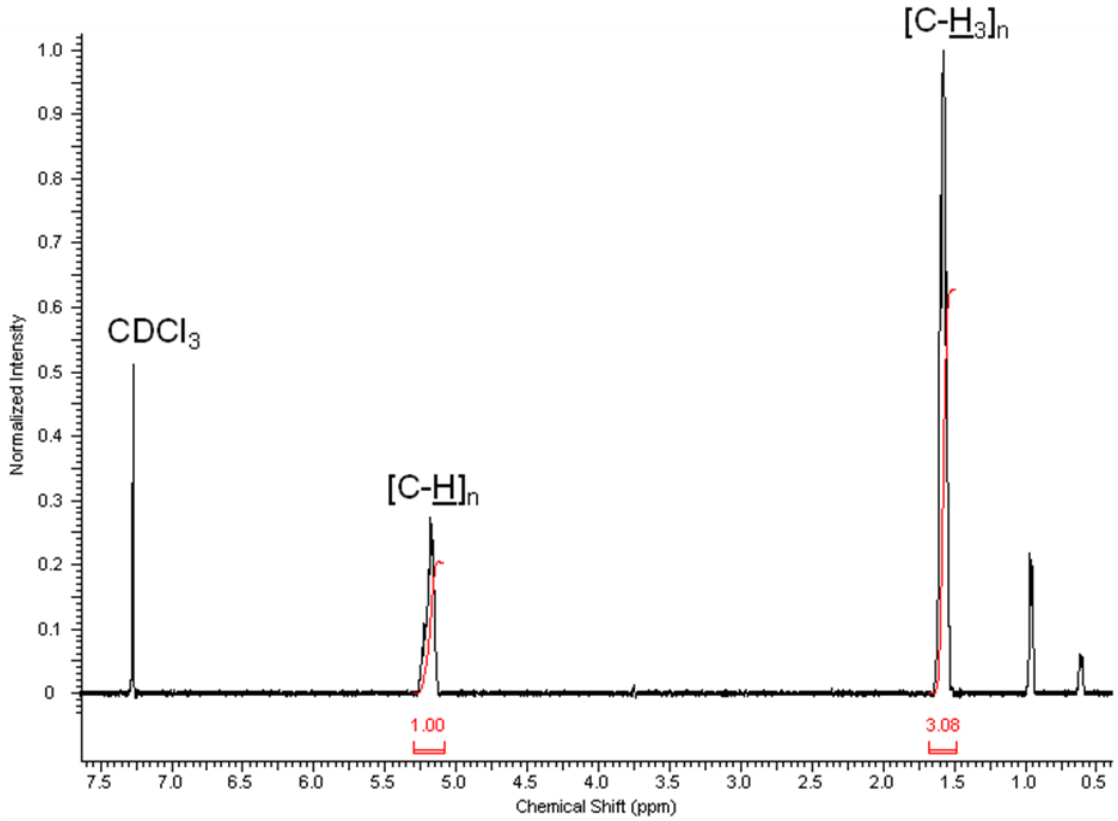

Figure 2.24 – Top: Annotated ^{1}H NMR spectrum of polylactide produced by Al(L^{H}O)$_2$Me. Bottom: Integrated methine region of the homonuclear decoupled ^{1}H NMR spectrum of polylactide produced by Al(L^{H}O)$_2$Me.

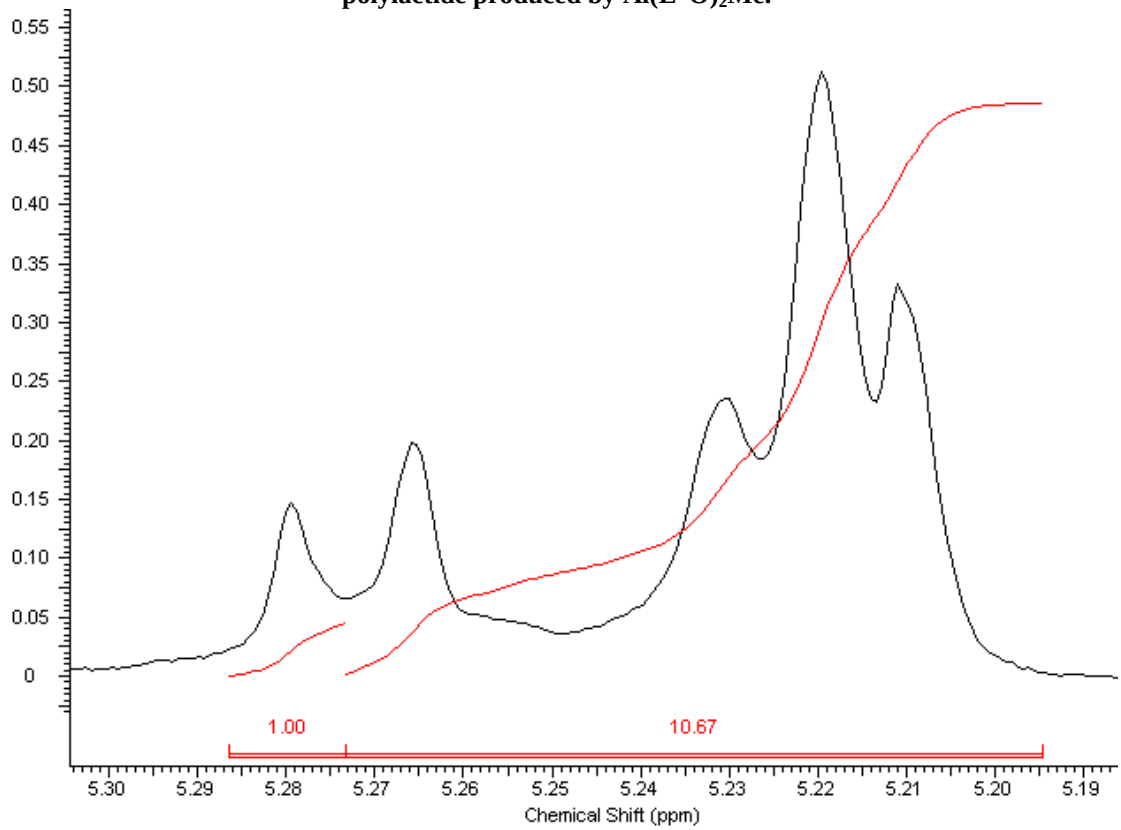

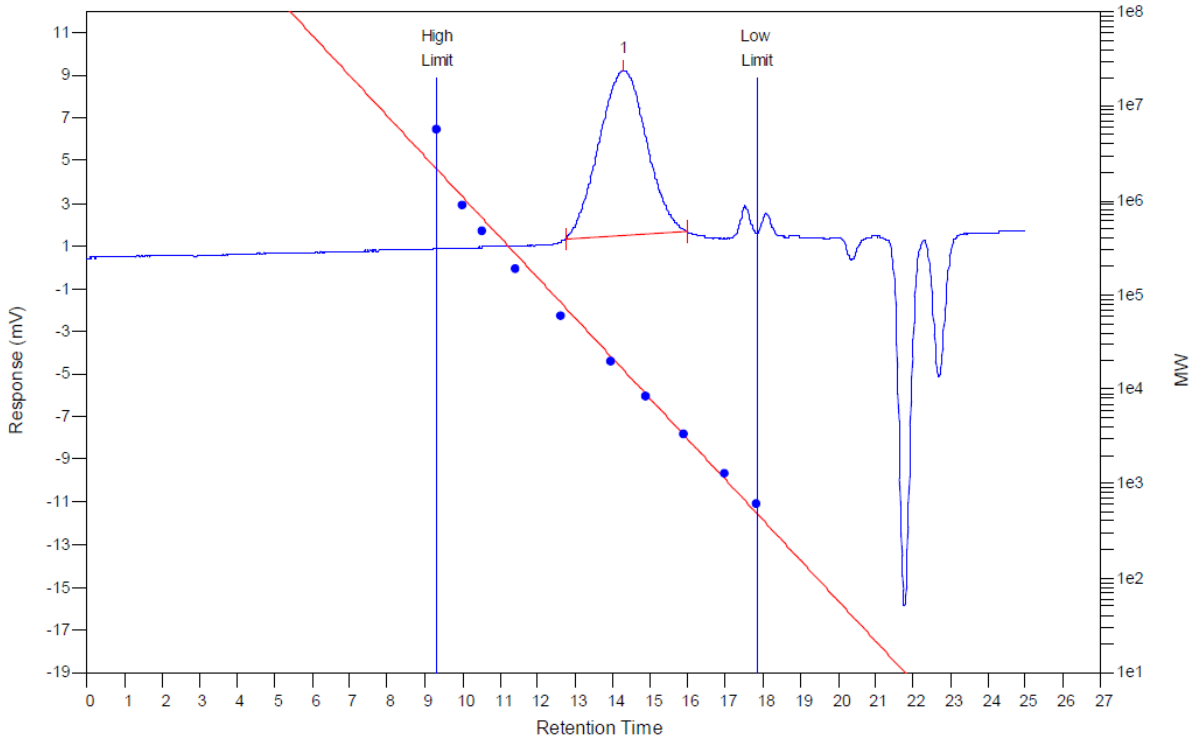

Figure 2.25 – GPC chromatograph of polylactide produced by Al(L^{H}O)$_2$Me.

2.8.2. Heterogeneous Aluminium Complexes

The tethered silica complexes Si-(L^{H}O)Al, Si-(L^{tBu}O)Al and Si-(L^{Cl}O)Al were tested for the ROP of *rac*-lactide alongside the untethered silica loaded aluminium complex Si-Al. The polymerisations were carried out with 1 g of lactide monomer at 353 K in toluene with a 100:1 ratio of monomer to initiator and 1 equivalent of a benzyl alcohol co-initiator and the results are presented in Table 2.17.

Catalyst	Time	Conversion (%)	M_n	M_w	PDI	P_r
Si-Al	24h	17	*	*	*	*
Si-(L^{H}O)Al	24h	61	5400	6000	1.11	0.32
Si-(L^{tBu}O)Al	24h	96	10450	11600	1.11	0.55
Si-(L^{Cl}O)Al	24h	47	3200	3600	1.12	0.41
Si-(L^{H}O)Al	72h	97	8100	9650	1.19	0.53
Si-(L^{tBu}O)Al	72h	97	8400	12800	1.52	0.52
Si-(L^{Cl}O)Al	72h	64	4200	4600	1.09	0.43

Table 2.17 – Heterogeneous silica tethered aluminium(III) complexes were used for the polymerisation of *rac*-lactide ****polymer not isolated in sufficient quantity for analysis.***

The untethered system Si-Al was unsuccessful as an initiator with low conversion and produced no polymer that could be isolated for analysis. The tethered systems were successful and produced polymers of reasonable molecular weight. The molecular weights are lower than expected values for 100 equivalents of monomer which could

possibly be due to termination by unreacted OH groups on the silica surface. Si-(L^{H}O)Al catalyst produced a polymer with moderate isotactic bias over a reaction time of 24 hours with a P_r value of 0.32, although this bias was lost when the polymerisation continued to completion over 72 hours. The loss of tacticity at high conversion is possibly due to transesterification or epimerisation caused by the presence of additional acidic SiOH sites on the surface of the heterogeneous catalyst. Further polymerisation data was gathered in the absence of a co-initiator and is presented in Table 2.18.

Catalyst	Time	Conversion (%)	M_n	M_w	PDI	P_r
Si-Al	24h	8	22250	27450	1.23	0.53
Si-(L^{H}O)Al	24h	26	20150	22550	1.12	0.50
Si-(L^{tBu}O)Al	24h	24	47250	52650	1.11	0.38
Si-(L^{Cl}O)Al	24h	11	33400	75700	2.27	0.44

Table 2.18 – Heterogeneous silica tethered aluminium(III) complexes were used for the polymerisation of *rac*-lactide in the absence of a co-initiator.

Unlike the zinc complexes reported in section 2.5.2, the aluminium complexes Si-Al, Si-(L^{H}O)Al, Si-(L^{tBu}O)Al and Si-(L^{Cl}O)Al proved poor initiators for the ROP of lactide in the absence of a co-initiator. These silica tethered complexes represent some of the very few examples of heterogeneous initiators for the polymerisation of *rac*-lactide and is the first heterogeneous system to offer any stereoselectivity in the polymerisation.

As previously discussed in section 2.4 there is a demand for polymer product with low metal content, however, it remains a challenge to produce metal free polymer through homogeneous processes. In homogeneous processes the initiator is not separated from the polymer product after the polymerisation reaction and so any metal catalyst remains in the polymer product. In this work, the heterogeneous initiators were removed by filtration after the polymerisation reaction and the polymer product produced by the homogeneous catalyst Al(L^{tBu}O)Me$_2$ and the heterogeneous catalyst Si-(L^{tBu}O)Al under the same polymerisation conditions (100:1, 353 K, 1 eq BnOH, 24 hours) were analysed for aluminium content by ICP-AES to provide a direct comparison between the homogeneous and heterogeneous systems (Table 2.19).

Initiator	Conversion (%)	M_n	M_w	PDI	P_r	Al Content (ppm)
Al(L^{tBu}O)Me_2	99+	12500	14500	1.16	0.46	2500
Si-(L^{tBu}O)Al	96	10450	11600	1.11	0.55	431

Table 2.19 – Comparison of polymer produced by a homogeneous and heterogeneous initiator showing lower metal content in the polymer produced *via* a heterogeneous reaction.

Analysis of the final polymer from Si-(L^{tBu}O)Al showed there to be 431 ppm of aluminium after workup, whilst the PLA produced from the analogous homogeneous initiator, Al(L^{tBu}O)Me_2, contained 2500 ppm, indicating a significant reduction in metal content. However, the quantity of aluminium in the polymer produced by the heterogeneous system is higher than expected. This may be due to leaching or removal and solubilisation of the aluminium ions during the termination and work-up steps. The significant improvement offered by Si-(L^{tBu}O)Al is an interesting result and a good platform for further work to explore and optimise this system.

2.9. Future Work

The *n*-propyl tethered silsesquioxane ligand system described within this chapter represents a novel approach for the study of tethered silica catalysts. The amine tethered silsesquioxane (L-NH_2) could be used to access a wide range of ligands that mimic their heterogeneous silica loaded analogues. It is well known that group 4 metals centres are active for the polymerisation of *rac*-lactide. Although used for zinc(II) and aluminium(III) in this work, this ligand set could also be used for novel group 4 systems.

Polymerisation of *rac*-lactide by heterogeneous catalysts has not been widely studied. The work described in this chapter highlights some potential benefits of using a heterogeneous catalyst and demonstrates reduced metal content in the polymer product. There is a wide scope for further work in this area, which includes but is not limited to: further exploring the metal content of polymers for homogeneous and heterogeneous initiators, recyclability of heterogeneous catalysts, continuous flow polymerisations and development of novel heterogeneous catalysts with varying metal centres.

2.10. Summary

Within this chapter the synthesis of a series of silica ligands with varying organic tethers was described, along with their silsesquioxane analogues. Reaction of these ligands with zinc(II) and aluminium(III) alkyl species generated a variety of novel complexes. All complexes were thoroughly characterised and their potential use as initiators for the controlled ROP of *rac*-lactide was examined.

The tethered heterogeneous zinc(II) complexes were found to be active for the ROP of *rac*-lactide and produced polymer of significantly higher molecular weight than the untethered Si-Zn complex. Upon reaction with $ZnMe_2$ and $ZnEt_2$ the tethered silsesquioxane $L^{H}OH$ unexpectedly formed a tetrametallic species $Zn_4(L^{H}O)_4(OX)_2X_2$ (X = Me, Et) with two distinct Zn co-ordination environments. The $Zn_4(L^{H}O)_4(OMe)_2Me_2$ complex was found to be active for the ROP of *rac*-lactide without the addition of a co-initiator under solvent free conditions.

The tethered heterogeneous aluminium systems all reacted to good conversion and produced polymer of high molecular weight. The untethered Si-Al system reacted to low conversion (10 %) over 24 hours and no polymer could be isolated from the reaction, this demonstrated the necessity of the organic tether for successful metal binding and catalysis.

The Si-($L^{H}O$)Al appeared to exhibit some degree of stereocontrol producing a moderately isotactic polymer (P_r: 0.32). The homogeneous silsesquioxane complexes $Al(L^{H}O)_2Me$, $Al(L^{Cl}O)_2Me$ and $Al(L^{tBu}O)Me_2$ were all active for the ROP of *rac*-lactide and appear to exhibit a slight isotactic bias (Pr: 0.41-0.46).

Finally, heterogeneous and homogeneous polymers were compared for aluminium content by ICP-AES. The polymer produced by heterogeneous polymerisation showed a fivefold reduction in aluminium content when compared with its homogeneous counterpart.

Chapter Three

β-ketoiminate based Zinc(II) complexes and their application for the ROP of rac-lactide.

3. *β*-ketoiminate based Zinc(II) complexes and their application for the ROP of *rac*-lactide.

3.1. Introduction

As discussed in section 1.5.5.2 *Coates et al* demonstrated the stereocontrolled ROP of *rac*-lactide using a range of zinc(II) complexes using a *β*-Diiminate (BDI) ligand system.[124,125] An example of a highly active and stereoselective zinc(II) BDI complex is shown in Figure 3.1.

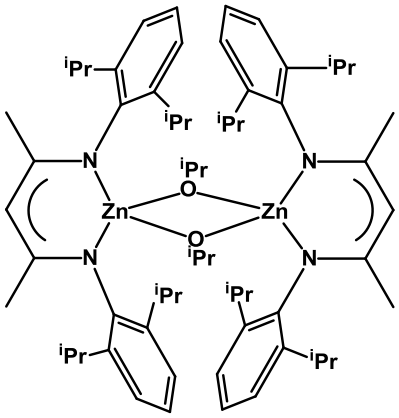

Figure 3.1 – Pioneering β-diketiminate (BDI) Zn complex reported by *Coates et al* which was highly active and produced polymer with heterotactic character (P_r = 0.90) from *rac*-LA.

This ligand system has been further explored using *β*-ketoiminate zinc(II) systems which contain a single imine and retain a carbonyl from the acetyl acetone backbone. These *β*-ketoiminate zinc(II) systems have also been tested for the ROP of *rac*-lactide and a variety of structures have been reported which have shown activity for the polymerisation reaction.[203-205] The work described in this chapter further explores the steric properties of different *β*-ketoiminate zinc(II) complexes. A range of different ligands were synthesised which were used to explore the effect of varying steric groups along both the backbone of the ligand and the iminate phenyl ring. The proposed ligands are shown in Figure 3.2 and any that were successfully synthesised were complexed to zinc(II) and tested for the ROP of *rac*-lactide.

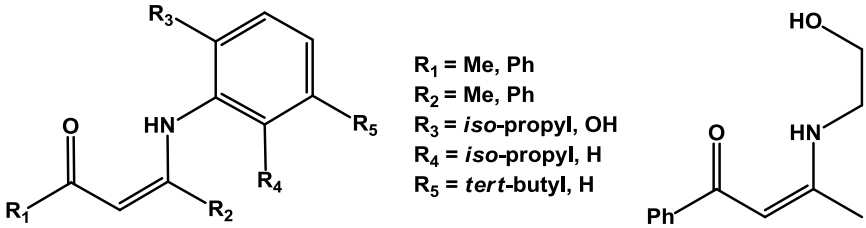

Figure 3.2 – *β*-ketoiminate ligands.

3.2. Ligand Preparation

A range of β-ketoiminate ligands were synthesised *via* a single step from commercially available starting materials. The ligands were synthesised by a single imine condensation reaction between a range of acetylacetone (acac) based starting materials (Figure 3.3) and 1 equivalent of a range of selected amines. The resulting ligands are named R_1R_2 X based on the aryl functionality (R_1R_2) of the acac type starting material and the functionality of the amine (X). All ligands were characterised by ^{1}H and $^{13}C\{^{1}H\}$ NMR spectroscopy and HR-MS. Single crystal X-ray diffraction data was collected for ligands PhMe PhDIP, PhPh PhOH and PhPh Ph^{tBu}OH.

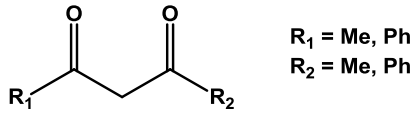

Figure 3.3 – Acetylacetone based starting materials.

3.2.1. Acetylacetone Based (MeMe) Ligands

Acetylacetone was reacted with 1 equivalent of 2-aminophenol and 2,6-diisopropylaniline to yield the corresponding substituted imine ligands MeMe PhOH and MeMe PhDIP (DIP = Diisopropyl) (Scheme 3.1) in good yields. An annotated ^{1}H NMR spectrum for MeMe PhOH is presented in Figure 3.4. The ^{1}H NMR spectrum shows 3H resonances at 1.75 ppm and 2.00 ppm relating to the methyl groups, a total of 4H resonances relating to the aromatic protons (6.80 – 7.21 ppm), a 1H resonance at 5.21 ppm relating to C=CH and a 1H resonance at 11.71 ppm relating to the secondary amine. The presence of the 1H C=CH resonance and the secondary amine resonance demonstrates that the double bond has migrated to sit in conjugation with the carbonyl as an alkene and therefore there is no resonance present in the ^{1}H NMR relating to the imine.

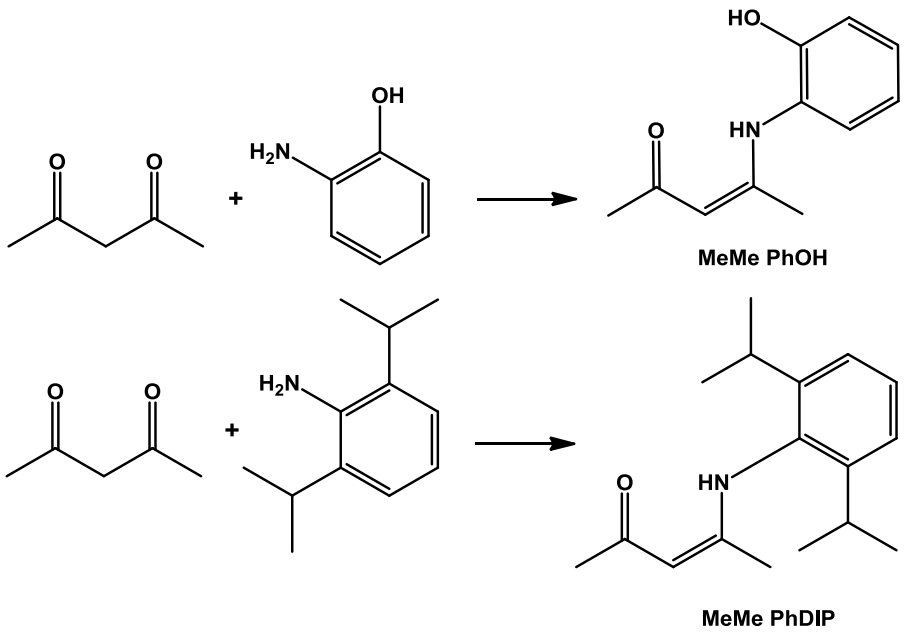

Scheme 3.1 – Synthesis of ligands MeMe PhOH and MeMe PhDIP.

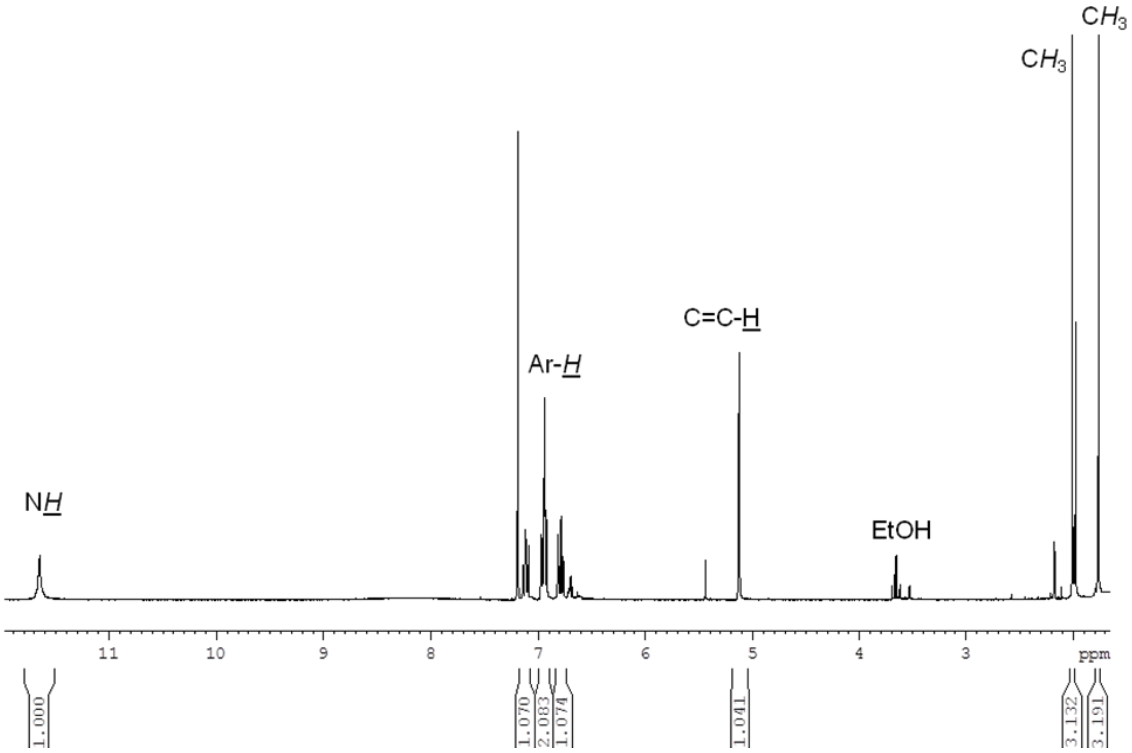

Figure 3.4 – Annotated ^{1}H NMR spectrum of MeMe PhOH

3.2.2. Benzoyl Acetone Based (PhMe) Ligands

Benzoyl acetone was reacted with 1 equivalent of 2-aminophenol, 2,6-diisopropylaniline and 2-aminoethanol to yield the corresponding substituted *β*-ketoiminate ligands in moderate yields (52 – 68 %) (Scheme 3.2).

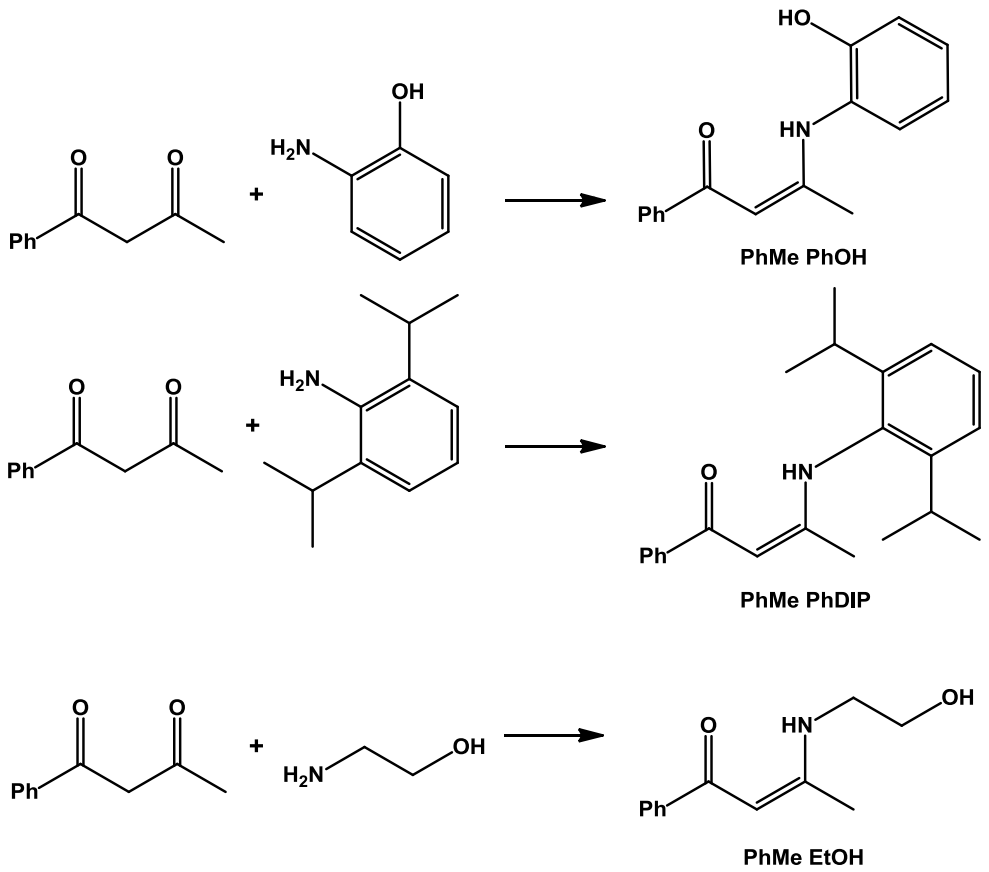

Scheme 3.2 – Synthesis of ligands PhMe PhOH and PhMe PhDIP and PhMe EtOH

Crystals of PhMe PhDIP suitable for analysis by single crystal X-ray diffraction were obtained and the structure is presented in Figure 3.5. The structure shows the presence of the N(1)-H(1) and C(8)-H(8) bonds confirming that the ligand rests as an alkene rather than an imine in the solid state. The C(7)-O(1), C(7)-C(8) and C(8)-C(9) bond lengths are 1.2592(16) Å, 1.4185(18) Å and 1.3862(18) Å respectively which highlights the conjugated nature of the system. An annotated ^{1}H NMR spectrum of PhMe PhDIP is shown in Figure 3.6. The presence of the 1H N-H (12.57 ppm) and 1H C=C-H (5.86 ppm) resonances confirm that the solid state structure is maintained in solution. Characterisation data obtained for PhMe PhOH and PhMe EtOH confirmed the structures reported in Scheme 3.2 above.

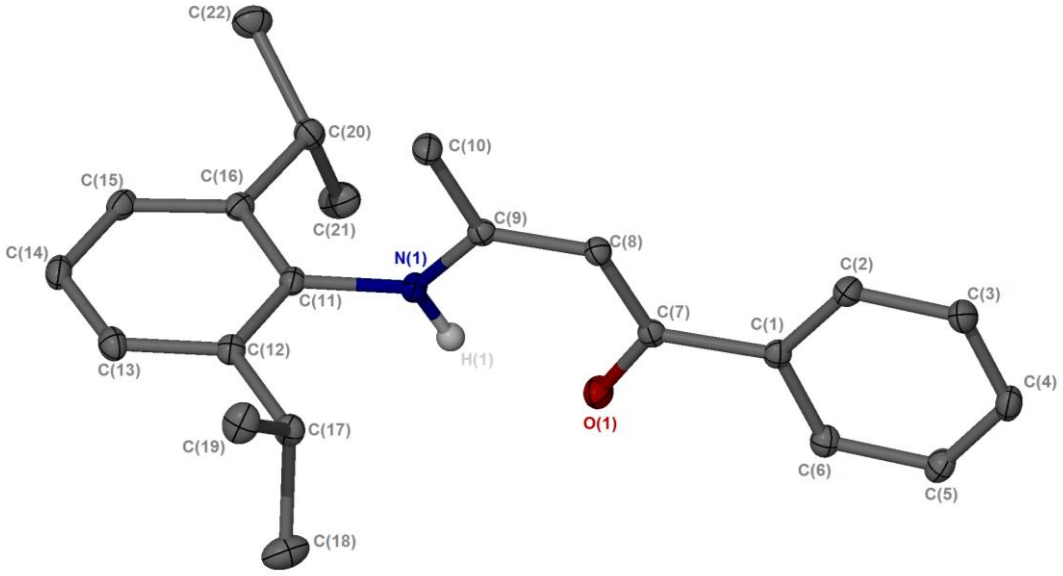

Figure 3.5 – Single crystal XRD structure of PhMe PhDIP, ellipsoids are shown at the 30% probability level.

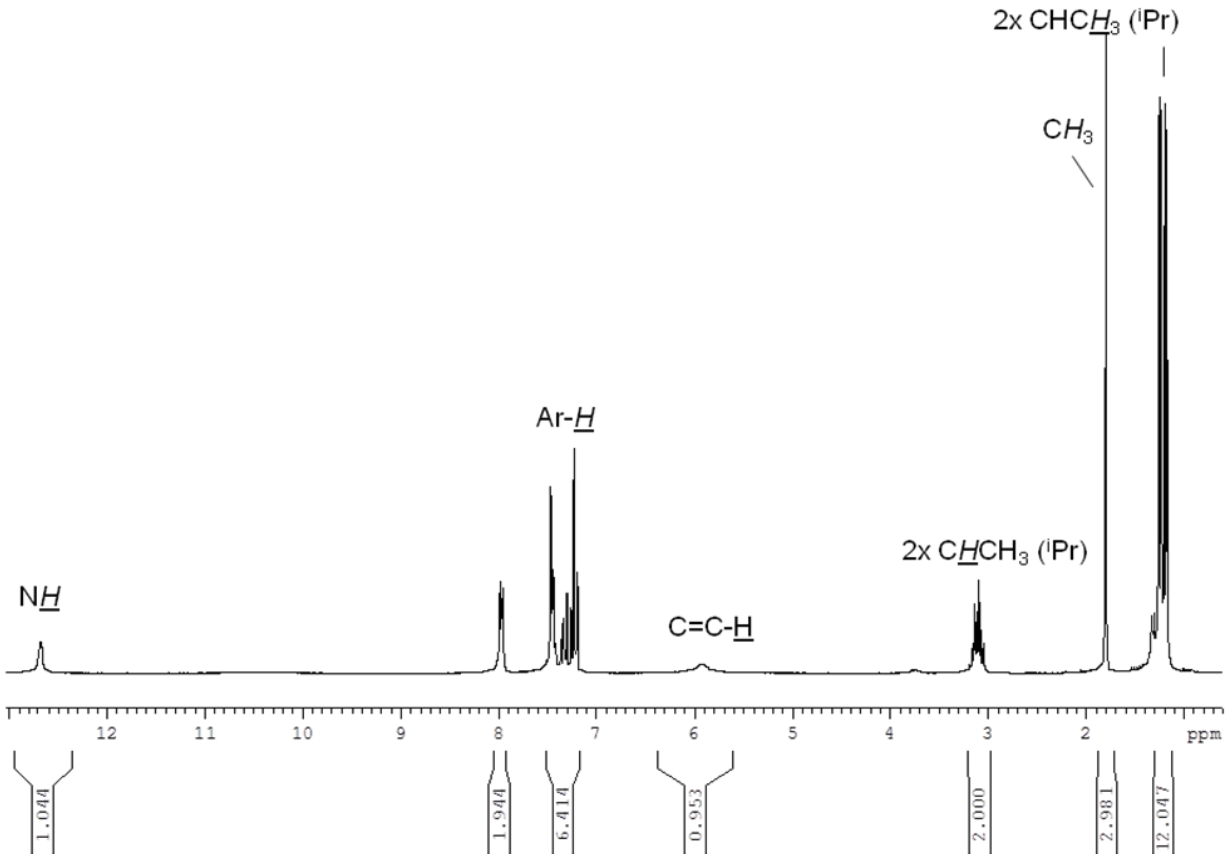

Figure 3.6 – Annotated ^{1}H NMR spectrum of PhMe PhDIP

3.2.3. 1,3-diphenylpropane-1,3-dione Based (PhPh) Ligands

1,3-diphenylpropane-1,3-dione was reacted with 1 equivalent of 2-aminophenol and 2-amino-4-(*tert*-butyl)phenol to yield the corresponding substituted imine ligands in low yields (13 % and 32 %) respectively (Scheme 3.3). The low yields were due to the formation of unknown by-products leading to the need for purification, pure products were obtained by repeated recrystallisation from MeOH or flash chromatography.

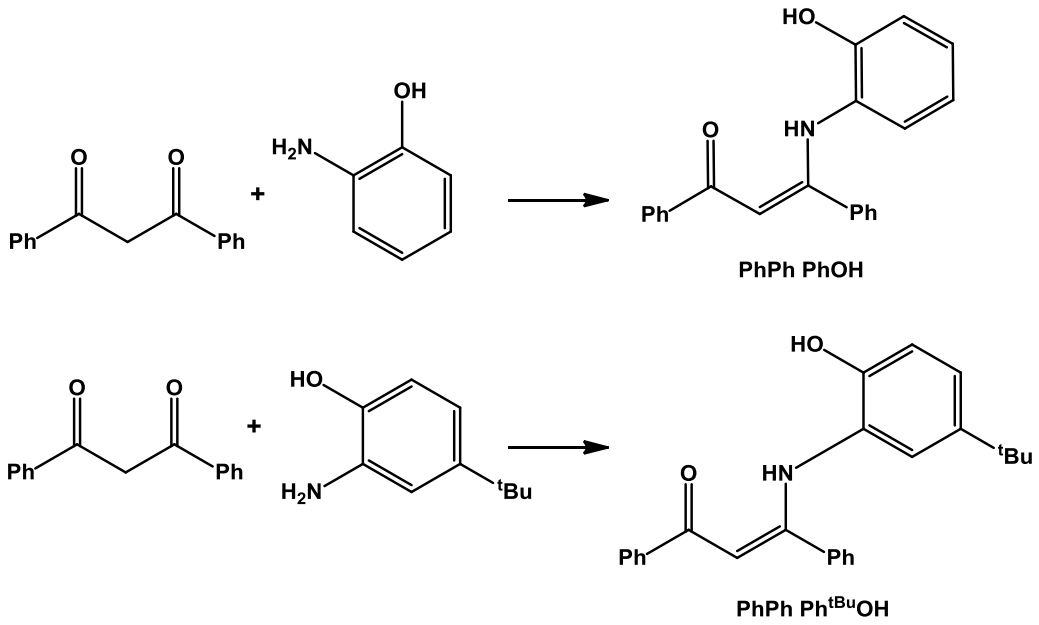

Scheme 3.3 – Synthesis of ligands PhPh PhOH and PhPh Ph^{tBu}OH.

Crystals of PhMe PhOH suitable for analysis by single crystal X-ray diffraction were obtained. The observed structure of PhMe PhOH is presented in Figure 3.7. The structure is comparible to the previously discussed PhDIP structure with respect to the presence of the alkene and contains similar C=C-H and C=O bond lengths. A single crystal X-ray diffraction structure of PhPh Ph^{tBu}OH was also obtained and is presented in Figure 3.8. A search of the Cambridge Crystallographic Data Centre (CCDC) revealed that these ligands have not previously been reported. An annotated ^{1}H NMR spectrum of PhPh Ph^{tBu}OH is also presented in Figure 3.9.

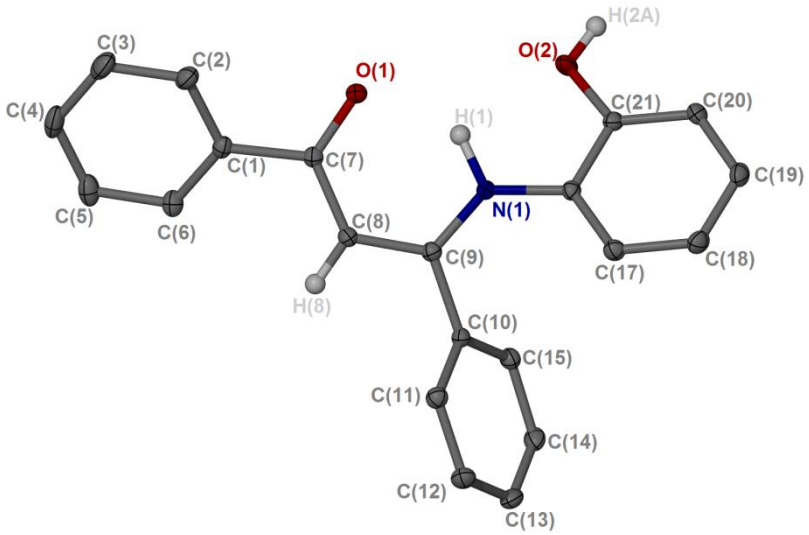

Figure 3.7 – Single crystal XRD structure of PhPh PhOH, ellipsoids are shown at the 30% probability level.

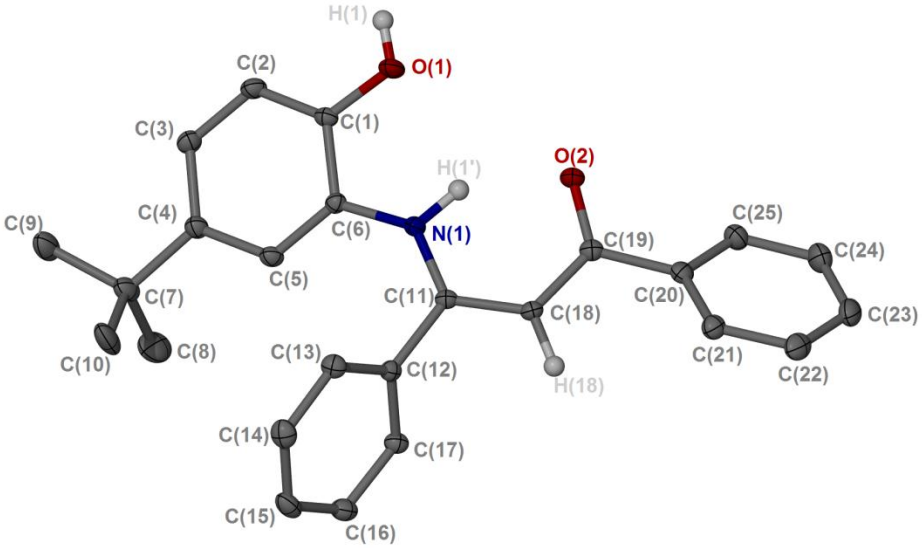

Figure 3.8 – Single crystal XRD structure of PhMe Ph^{tBu}OH, ellipsoids are shown at the 30% probability level.

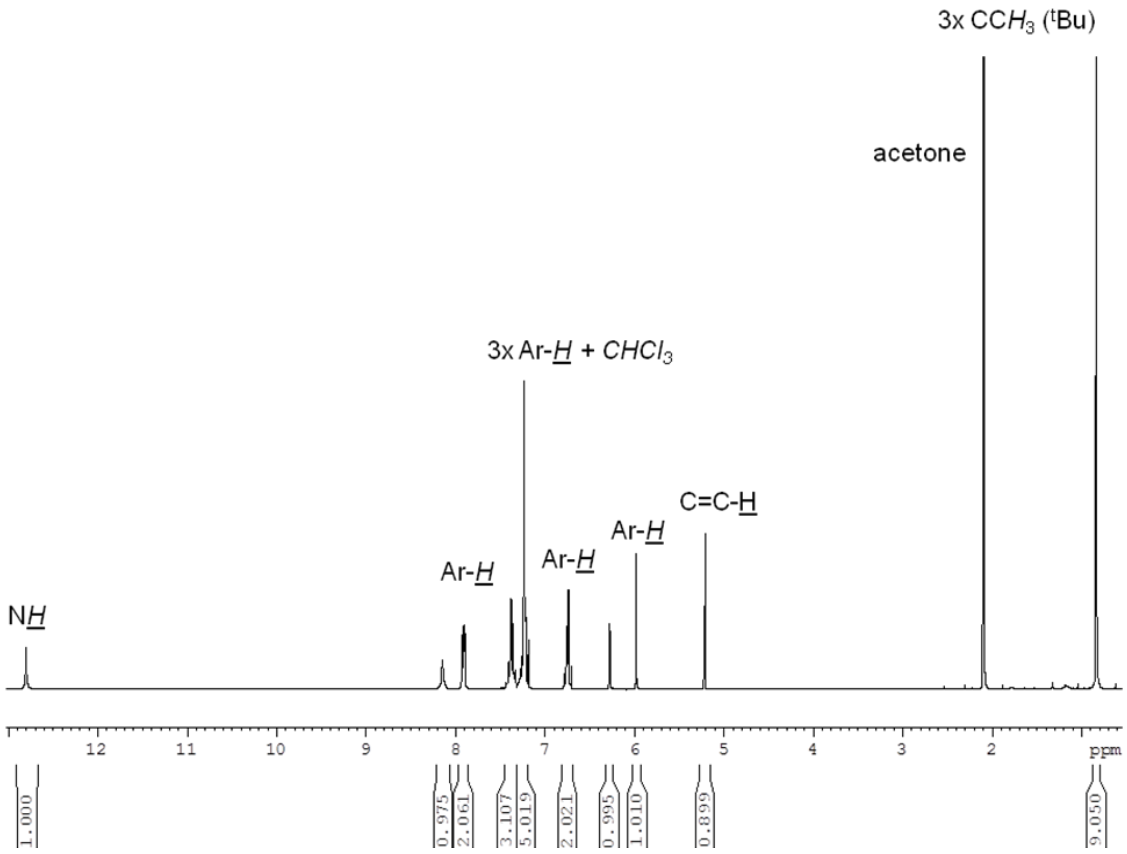

Figure 3.9 – Annotated ^{1}H NMR spectrum of PhPh Ph^{tBu}OH

The ^{1}H NMR and ^{13}C{^{1}H} spectra are consistent with the solid state structure reported in Figure 3.6. The spectrum shows a 9H resonance at 0.82 ppm relating to the methyl protons of the *tert*-butyl group, a 1H resonance at 6.02 relating to the C=C-H, 13H resonances between 6.30 and 7.90 ppm relating to the aromatic protons and a 1H resonance at 12.78 ppm relating to the secondary amine. There is also a broad resonance at 8.12 which is presumed to be related to the alcohol group.

All of the reported MeMe, PhMe and PhPh ligands were reacted to form zinc(II) complexes which were characterised and tested for the ROP of *rac*-lactide.

3.3. Zinc(II) Complexes

3.3.1. Acetylacetone Based (MeMe) Zinc(II) Complexes

The ligands MeMe PhOH and MeMe PhDIP were reacted with 1 equivalent of $ZnMe_2$ to yield the complexes (MeMe $PhO)_2Zn$ and (MeMe PhDIP)ZnMe (Scheme 3.4). The complexes were analysed by ^1H and $^{13}C\{^1H\}$ NMR spectroscopy and were consistent with the proposed structures of (MeMe $PhO)_2Zn$ and (MeMe PhDIP)ZnMe. Crystals suitable for X-ray diffraction were obtained for (MeMe PhDIP)ZnMe and the solid state structure is presented in Figure 3.10 along with an annotated ^1H NMR spectrum in Figure 3.11.

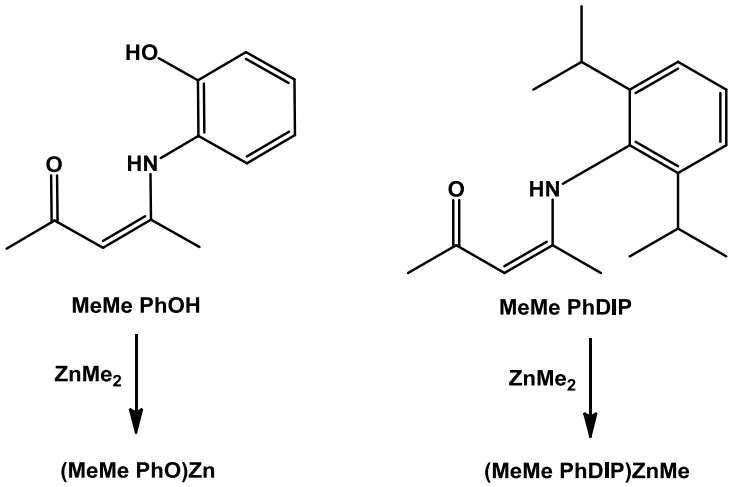

Scheme 3.4 – Complexation of ligands MeMe PhOH and MeMe PhDIP with $ZnMe_2$

The solid state structure of (MeMe PhDIP)ZnMe shows a zinc(II) metal centre co-ordinated to the ligand via the oxygen and nitrogen. The solid state structure is dimeric with the carbonyl moiety bridging the two metal centres. The Zn(1)-O(1) bond length is 2.0240(9) Å, the Zn(1)-N(1) bond length is 2.0291(11) Å and the Zn(1)-C(101) bond length is 1.9613(15) Å. The Zn(II) centre is in a pseudo-tetrahedral environment with the Zn(1)-N(1)-O(1) bond angle being 90.87(4) ° and the C(101)-Zn(1)-O(1) bond angle being 124.93(6) °. The bond angles and lengths are consistent with literature precedent.[203]

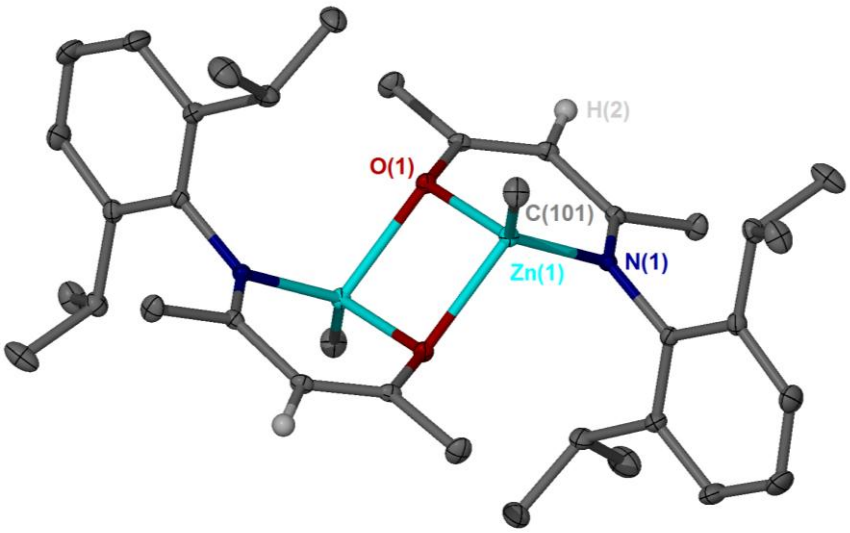

Figure 3.10 – Single crystal XRD structure of (MeMe PhDIP)ZnMe.
Hydrogen atoms have been removed for clarity with the exception of H(2), ellipsoids are shown at the 30% probability level.

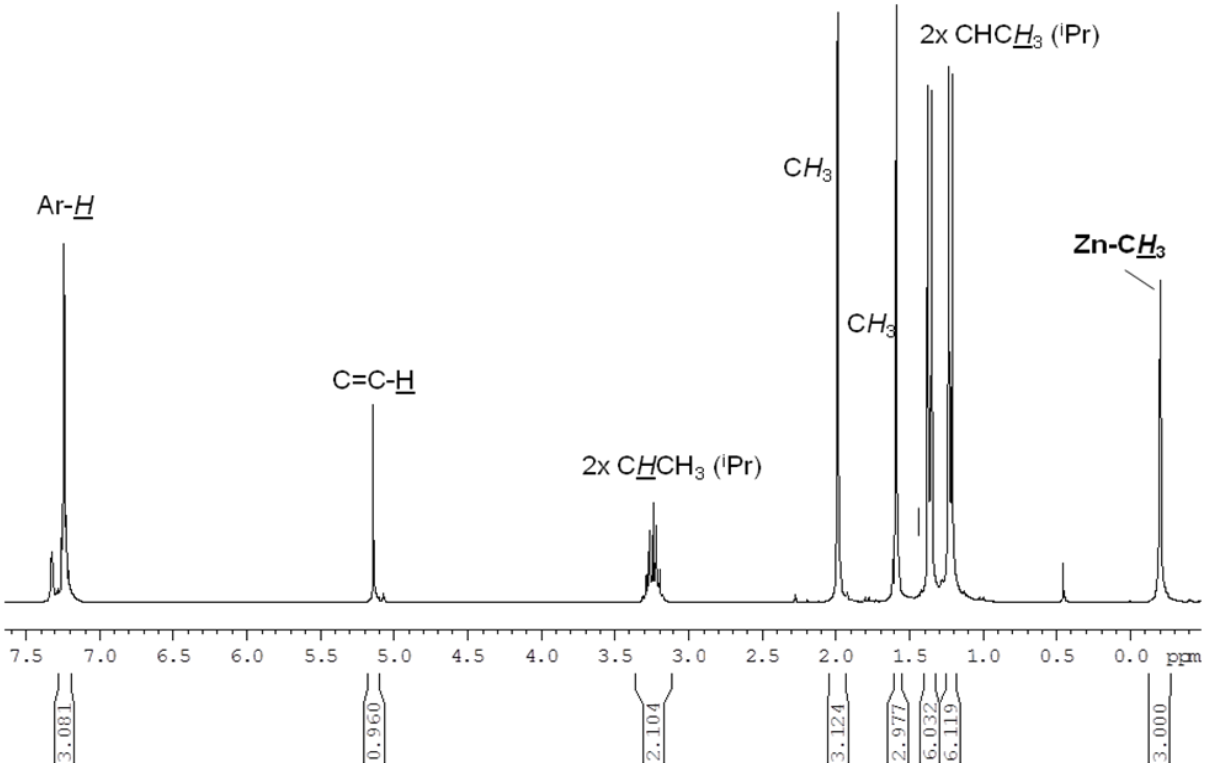

Figure 3.11 – Annotated ^{1}H NMR spectrum of (MeMe PhDIP)ZnMe

The ^{1}H NMR spectrum shows that the solid state structure is maintained in solution. The spectrum shows a 3H resonance relating to the preserved Zn-Me group (-0.20 ppm), 6x3H resonances between 1.21 and 1.99 ppm relating to the methyl protons from the aryl *iso*-propyl groups and the acetyl acetone backbone, a 2H resonance at

3.23 ppm relating to the two CH protons from the *iso*-propyl groups, a 1H resonance at 5.13 relating the alkene C-H and a 3H resonance at 7.20 relating to the aromatic protons from the ligand.

3.3.2. Benzoyl Acetone Based (PhMe) Zinc(II) Complexes

The ligands PhMe PhOH and PhMe EtOH were reacted with 1 equivalent of $ZnMe_2$. The ligand PhMe PhDIP was reacted with 1 eq. and 0.5 eq. of $ZnMe_2$. (Scheme 3.5)

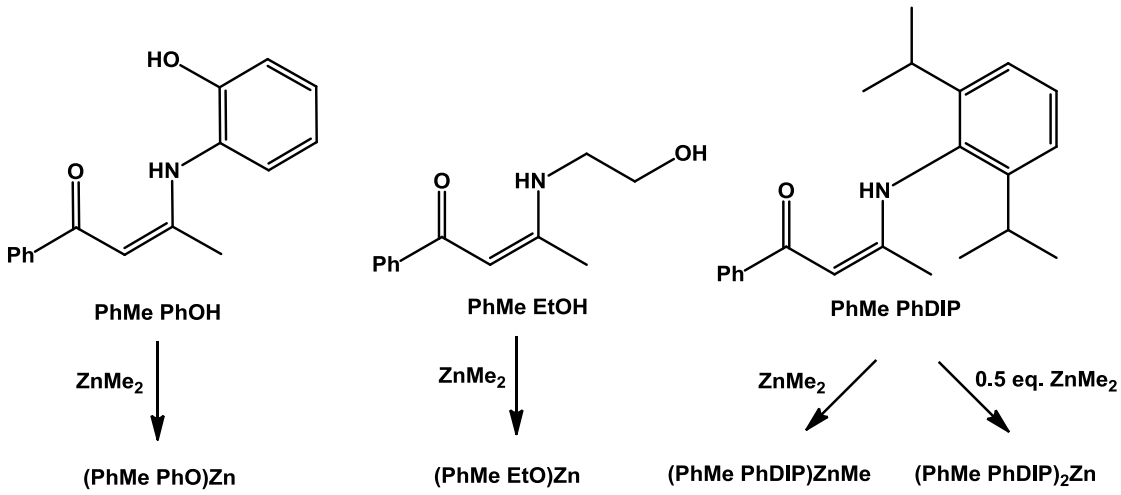

Scheme 3.5 – Complexation of ligands PhMe PhOH, PhMe EtOH and PhMe PhDIP with $ZnMe_2$

Crystals of the (PhMe PhO)Zn complex co-ordinated with DMSO were obtained upon the addition of a few drops of DMSO and were suitable for X-ray diffraction analysis. The solid state structure of the (PhMe PhO)Zn DMSO complex is presented in Figure 3.12. The solid state structure shows a dimeric complex of (PhMe PhO)$_2$Zn$_2${(CH$_3$)$_2$SO}$_2$, with the phenoxide moieties {O(2) and O(4)} bridging the two zinc centres. The zinc(II) centres are in a pseudo-trigonal bipyramidal environment with a Zn(1)-O(1)-O(2) bond angle of 168.67(11) °, a Zn(1)-O(2)-O(5) bond angle of 90.01(12) ° and a Zn(1)-O(5)-N(1) bond angle of 111.23(13) °. The complex contains a Zn(1)-O(1) bond length of 1.986(3) Å and a Zn(1)-N(1) bond length of 2.031(3) Å which are analogous to the (MeMe PhDIP)ZnMe complex discussed in section 3.3.1. The (PhMe PhO)Zn complex was insoluble in all available deuterated solvents other than d_6-DMSO. ^{1}H and ^{13}C{^{1}H} NMR spectra were obtained in d_6-DMSO, showing the (PhMe PhO)Zn DMSO complex. When the complex was not exposed to DMSO CHN analysis gave results consistent with the species (PhMe PhO)Zn.

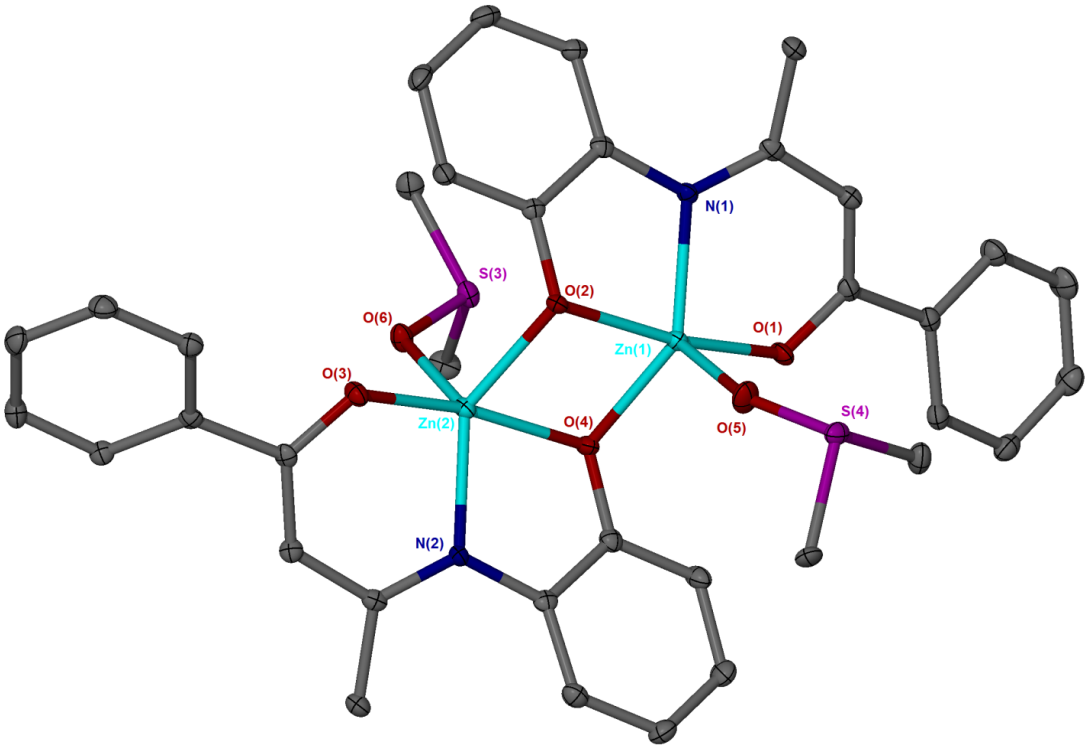

Figure 3.12 – Single crystal XRD structure of a (PhMe PhO)Zn dimer co-ordinated to DMSO. One molecule of DMSO is disordered over two positions in a 75:25 ratio. All hydrogen atoms have been removed for clarity, ellipsoids are shown at the 30% probability level.

The ligand PhMe EtOH was reacted with 1 equivalent of $ZnMe_2$ to yield the (PhMe EtO)Zn complex. Crystals suitable for analysis by X-ray diffraction were obtained and the structure is presented in Figure 3.13. In the solid state the structure was observed as a tetrametallic species containing 4 equivalent zinc centres and 4 ligands. The Zn centres are in a pseudo-trigonal bypyramidal environment with a O(1)-Zn(1)-O(2) of 168.39(7) °, a O(1)-Zn(1)-N(1) bond angle of 94.35(7) ° and a N(1)-Zn(1)-O(2) bond angle of 121.99(7) °. The Zn(1)-O(1) observed bond length was 1.9650(17) Å, Zn(1)-N(1) bond length was 1.9952(18) Å and the Zn(1)-O(2) bond length was 2.0096(16) Å. Solution state NMR data, as expected, shows the absence of amine, alcohol and Zn-alkyl resonances. NMR spectroscopic data also shows that the ethyl backbone is locked in position as observed by diastereotopic splitting patterns in the complex.

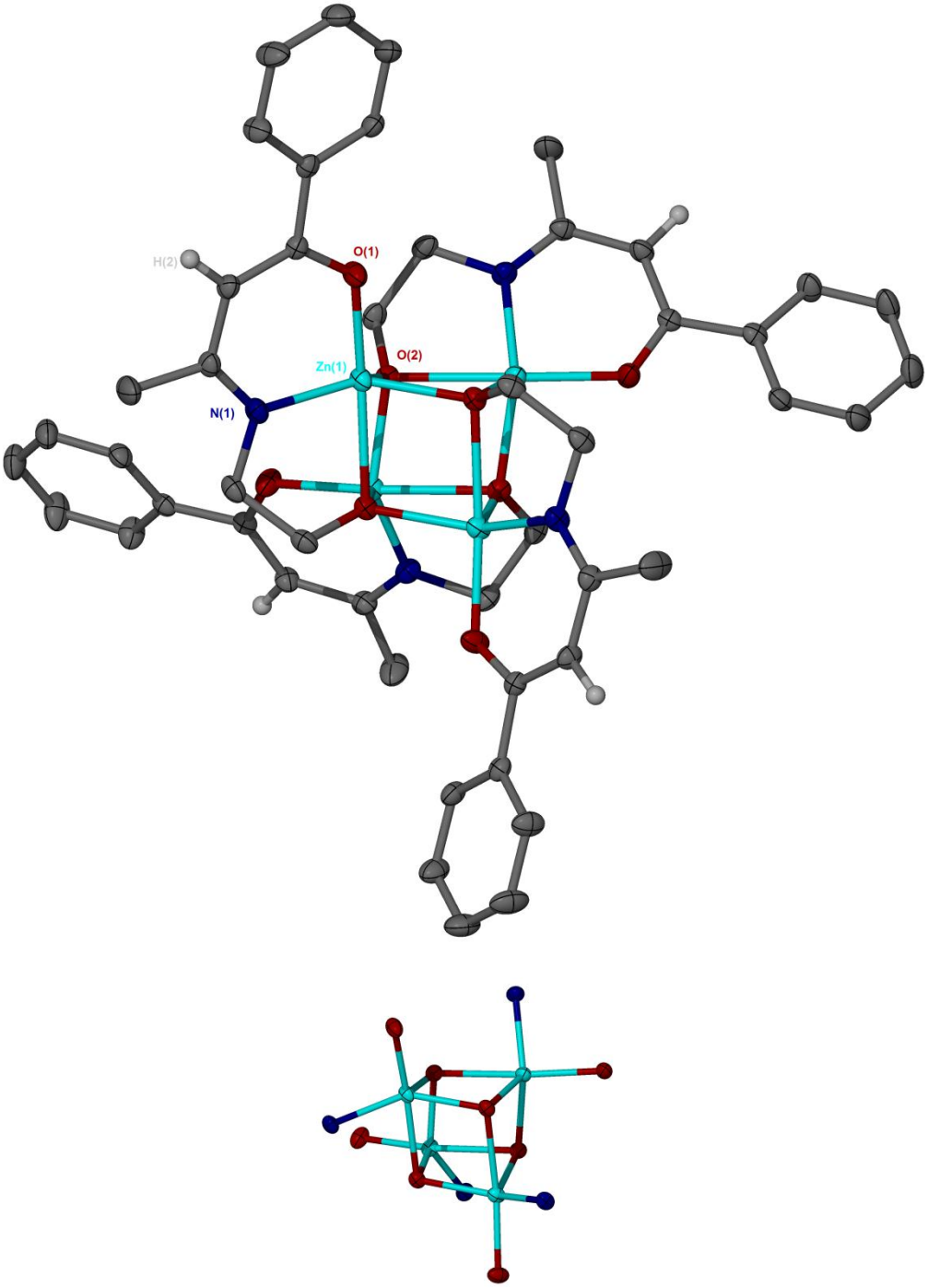

Figure 3.13 – Top: single crystal XRD structure of the (PhMe EtO)Zn complex. Bottom: $Zn_4O_8N_4$ Core of (PhMe EtO)Zn, ellipsoids are shown at the 30% probability level.

The PhMe PhDIP ligand was reacted with both 1 and 0.5 equivalents of $ZnMe_2$ to yield (PhMe PhDIP)ZnMe and $(PhMe\ PhDIP)_2Zn$ complexes respectively. Crystals suitable for analysis by X-ray diffraction were obtained for both complexes and the solid state structures are presented in Figures 3.14 and 3.15 respectively. (PhMe PhDIP)ZnMe contains a dimeric Zn centre with the carbonyl {O(1)} bridging between the two centres, whereas $(PhMe\ PhDIP)_2Zn$, as expected, is monomeric in the solid state. The Zn metal centre is in a pseudo-tetrahedral environment in both complexes. Selected bond lengths and angles from both the PhMe DIP derived structures are presented in Tables 3.1 and 3.2 along with those from the (MeMe PhDIP)ZnMe structure reported in section 3.3.1 for comparison. All complexes were characterised by ^{1}H NMR spectroscopy, $^{13}C(^{1}H)$ NMR spectroscopy and CHN elemental analysis. A ^{1}H NMR spectrum of (PhMe PhDIP)ZnMe is presented in Figure 3.16.

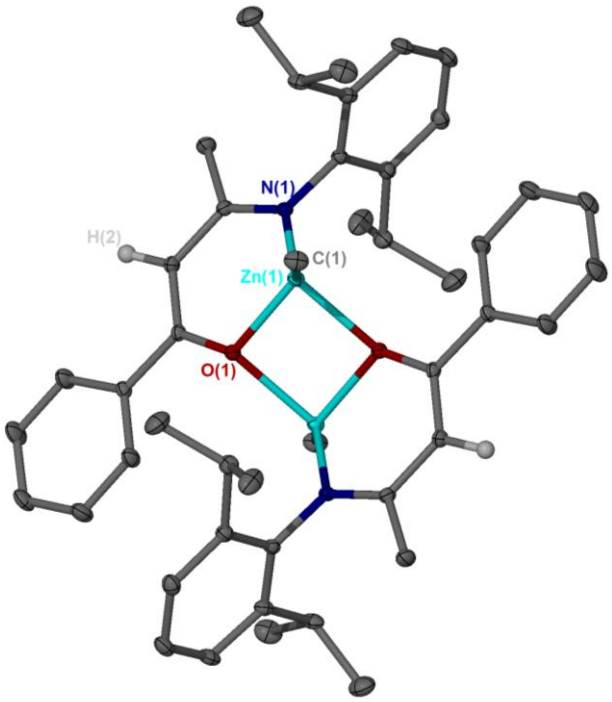

Figure 3.14 – Single crystal XRD structure of the (PhMe PhDIP)ZnMe complex. Hydrogen atoms have been removed for clarity with the exception of H(2), ellipsoids are shown at the 30% probability level.

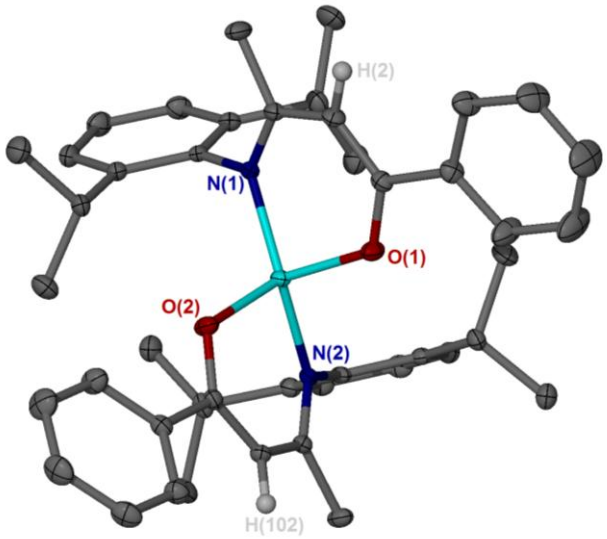

Figure 3.15 – Single crystal XRD structure of the (PhMe PhDIP)$_2$Zn. Hydrogen atoms have been removed for clarity with the exception of H(2) and H(102), ellipsoids are shown at the 30% probability level.

Bond	(MeMe PhDIP)ZnMe	(PhMe PhDIP)ZnMe	(PhMe PhDIP)$_2$Zn
Zn(1)-O(1)	2.0240(9) Å	2.0346(9) Å	1.955(2) Å
Zn(1)-N(1)	2.0291(11) Å	2.0429(11) Å	1.963(2) Å
Zn(1)-C(1)	1.9613(15) Å	1.9657(14) Å	N/A*

Table 3.1 – Selected bond lengths from XMe PhDIP Zn complexes (X = Me, Ph).
**** N/A as no Zn-C bond present in structure.***

Bond	(MeMe PhDIP)ZnMe	(PhMe PhDIP)ZnMe	(PhMe PhDIP)$_2$Zn
O(2)-Zn(1)-O(1)	82.81(4)*	82.54(4)*	104.58(10)
C(1)-Zn(1)-O(1)	124.93(6)	125.18(5)	N/A[ǂ]
O(1)-Zn(1)-N(1)	90.87(4)	90.11(4)	97.31(9)
O(2)-Zn(1)-N(1)	101.35(4)*	104.95(4)*	112.05(9)

Table 3.2 – Selected bond angles from XMe PhDIP Zn complexes (X = Me, Ph).
****O(2) is equivalent {O(1)'} in (MeMe PhDIP)ZnMe and (PhMe PhDIP)ZnMe.***
[ǂ] N/A as no Zn-C bond present in structure.

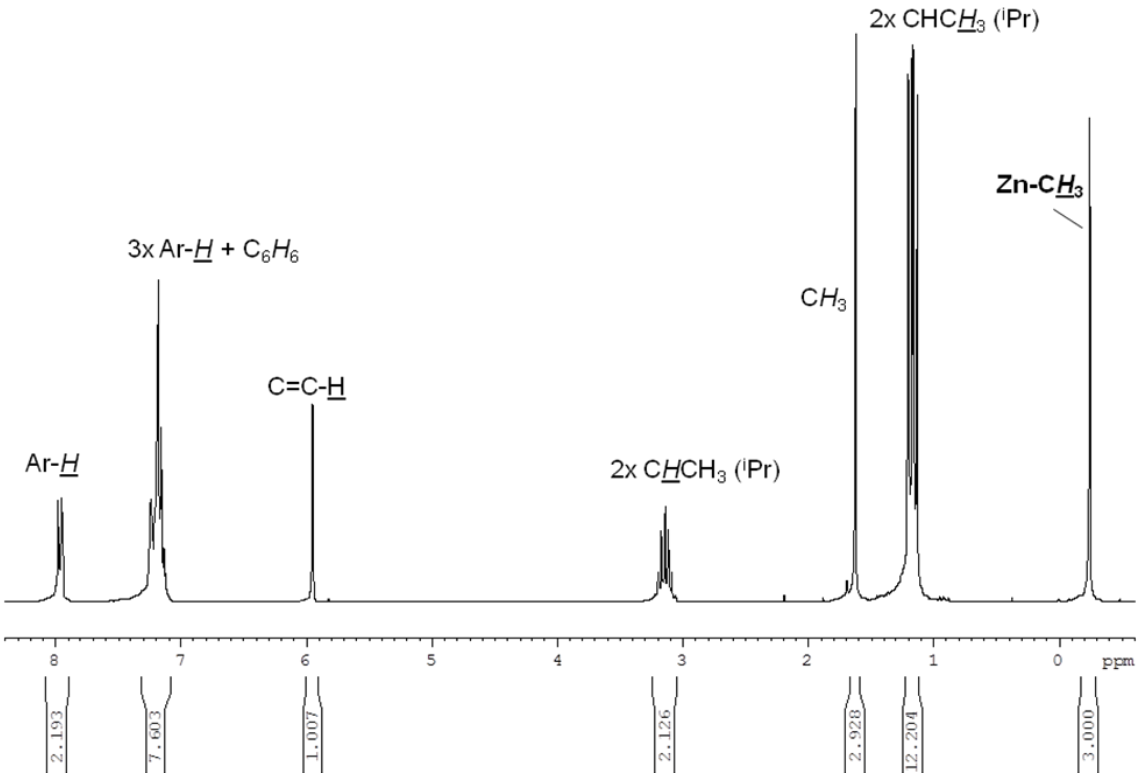

Figure 3.16 – Annotated ^{1}H NMR spectrum of (PhMe PhDIP)ZnMe complex.

The ^{1}H NMR spectrum of (PhMe PhDIP)ZnMe shows that the solid state structure is maintained in solution. The spectrum shows a 3H resonance relating to the preserved Zn-Me group (-0.25 ppm), 5x3H resonances between 1.16 and 1.62 ppm due to the methyl protons from the aryl *iso*-propyl groups and the PhMe backbone, a 2H resonance at 3.14 ppm corresponding to the two CH protons from the *iso*-propyl groups, a 1H resonance at 5.94 due to the alkene C-H, a 6H resonance at 7.17 ppm and a 2H resonance at 7.95 ppm relating to the aromatic protons from the ligand.

3.3.3. 1,3-diphenylpropane-1,3-dione Based (PhPh) Zinc(II) Complexes

The ligands PhPh PhOH and PhPh Ph^{tBu}OH were reacted with 1 equivalent of $ZnMe_2$ to yield the complexes (PhPh PhO)Zn and (PhPh Ph^{tBu}O)Zn (Scheme 3.6). Both complexes were recrystallised from DMSO to give crystals suitable for analysis by X-Ray diffraction. The solid state structure of (PhPh PhO)Zn is presented in Figure 3.17 and the solid state structure of (PhPh Ph^{tBu}O)Zn is presented in Figure 3.18. Both complexes show a Zn(II) metal centre in a seesaw configuration coordinated to the oxygen and nitrogen from the corresponding ligand in a 1:1 ratio. Selected bond lengths and angles from both complexes are presented in Table 3.3 and 3.4

respectively. Both complexes were characterised by ^{1}H NMR spectroscopy, ^{13}C(^{1}H) NMR spectroscopy and CHN elemental analysis. A ^{1}H NMR spectrum of (PhPh Ph^{tBu}O)ZnMe is presented in Figure 3.19.

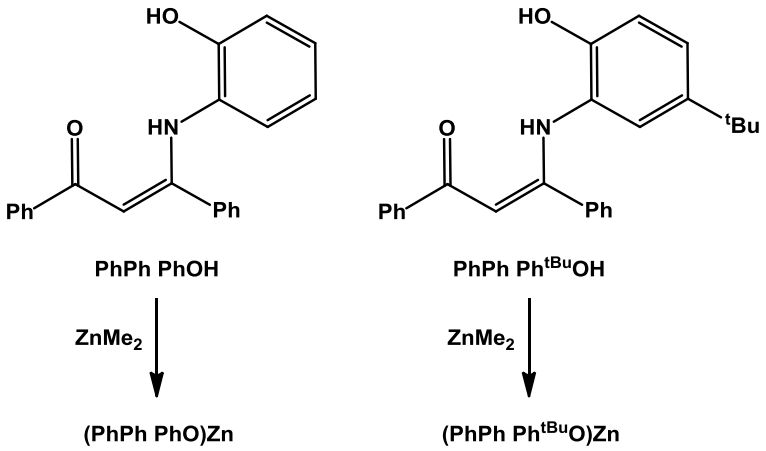

Scheme 3.6 – Complexation of ligands PhPh PhOH and PhPh Ph^{tBu}OH with ZnMe$_2$.

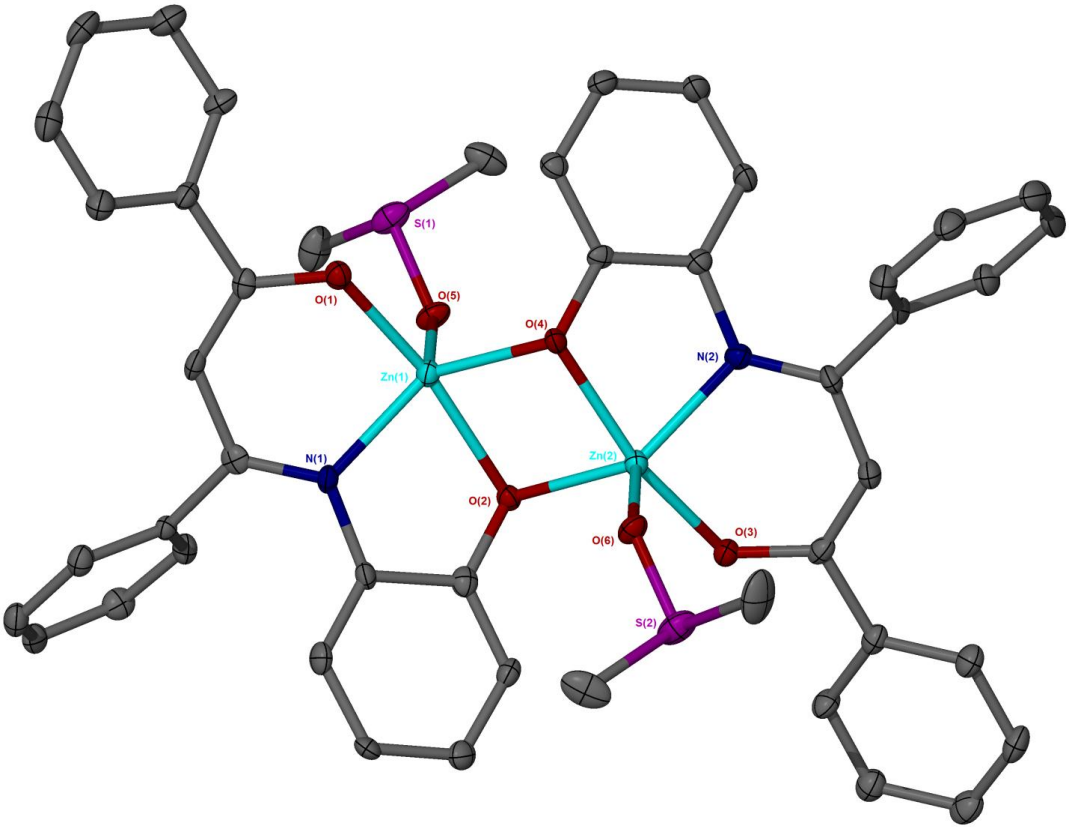

Figure 3.17 – Single crystal XRD structure of the (PhPh PhO)$_2$Zn DMSO complex. Hydrogen atoms have been removed for clarity. ellipsoids are shown at the 30% probability level.

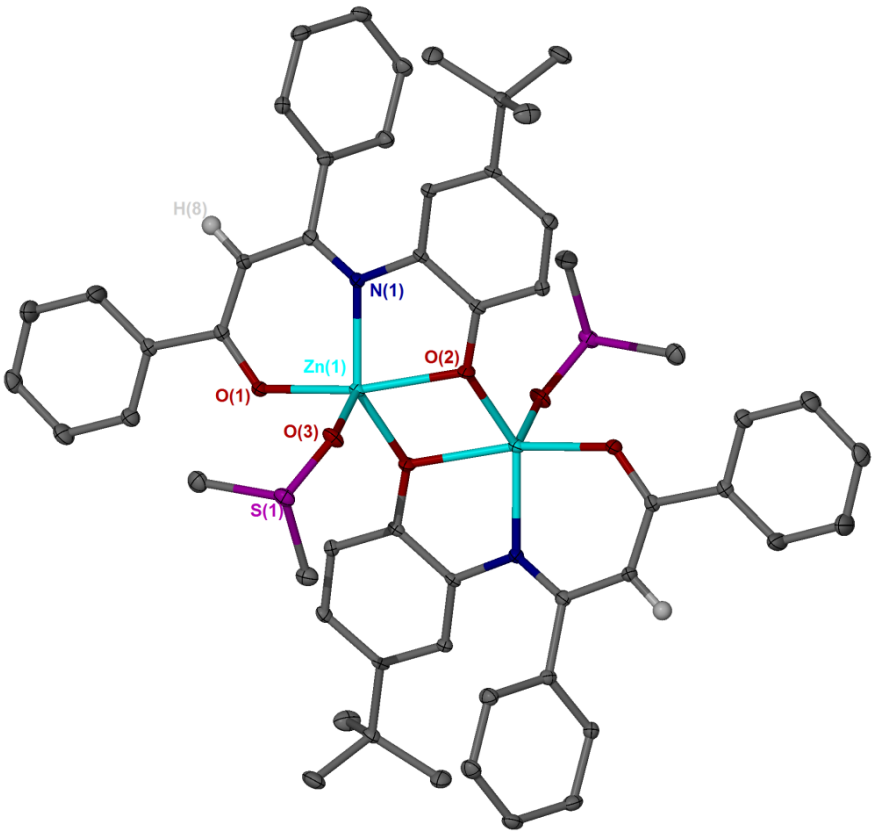

Figure 3.18 – Single crystal XRD structure of the (PhPh Ph^{tBu}O)Zn DMSO complex. Hydrogen atoms have been removed for clarity with the exception of H(8), ellipsoids are shown at the 30% probability level.

Bond	(PhPh PhO)Zn	(PhPh Ph^{tBu}O)$_2$Zn
Zn(1)-O(1)	2.021(5)	1.9931(15)
Zn(1)-N(1)	2.002(6)	2.0515(17)
Zn(1)-O(5)	2.007(5)	2.0545(16)*

Table 3.3 – Selected bond lengths from (PhPh PhtBuO)Zn and (PhPh PhO)Zn complexes
**** Refers to corresponding bond in (PhPh Ph^{tBu}O)Zn.***

Bond	(PhPh PhO)Zn	(PhPh Ph^{tBu}O)Zn
O(1)-Zn(1)-N(1)	91.3(2)	92.50(6)
O(4)-Zn(1)-N(1)	137.5(2)	138.95(7)*
O(1)-Zn(1)-O(2)	169.1(2)	163.39(6)
O(1)-Zn(1)-O(4)	102.9(2)	101.24(6)*
O(1)-Zn(1)-O(5)	99.1(2)	100.07(7)*

Table 3.4 – Selected bond angles from (PhPh PhtBuO)Zn and (PhPh PhO)Zn complexes
**** Refers to corresponding angle in (PhPh Ph^{tBu}O)Zn.***

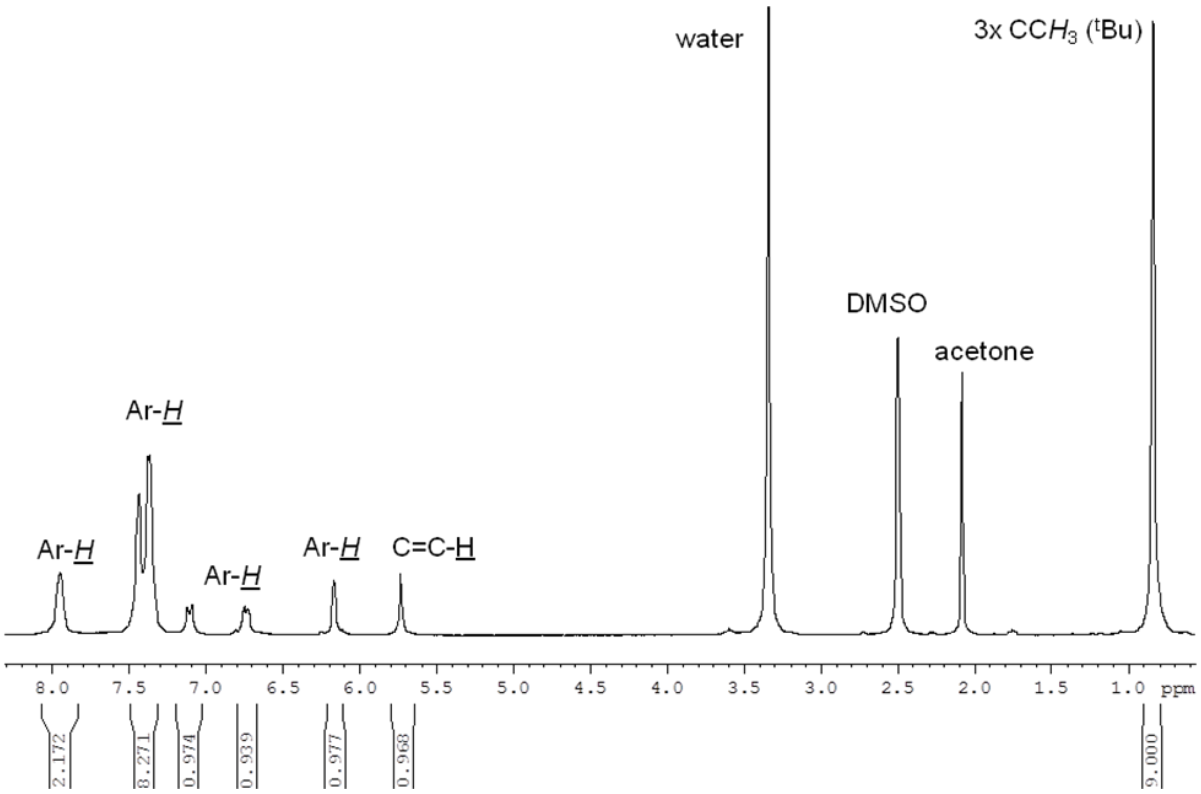

Figure 3.19 – Annotated ^{1}H NMR spectrum of (PhPh Ph^{tBu}O)Zn complex.

The ^{1}H NMR spectrum of (PhPh Ph^{tBu}O)ZnMe shows that the solid state structure is maintained in d_6-DMSO solution. The spectrum shows a 9H resonance relating to the methyl protons from the *tert*-butyl group (0.89 ppm), a 1H resonance at 5.79 ppm corresponding to the alkene C-H and resonances between 6.22 and 8.00 ppm due to the aromatic protons. CHN analysis for both complexes suggest that in absence of DMSO the complexes reside in a 1:1 ratio of ligand:Zn.

3.4. Zn(II) Complexes Polymerisation of *rac*-lactide

All of the Zn(II) complexes reported in sections 3.3.1, 3.3.2 and 3.3.3 were tested for the ring opening polymerisation of *rac*-lactide. Complexes with a Zn-Me species were tested in solution with a benzyl alcohol co-initiator to generate a Zn-OCH_2Ph initiator in situ. Complexes without the Zn-alkyl species were tested under solvent free polymerisation conditions without the addition of a co-initiator. Solvent free polymerisations were conducted with 2 g of lactide monomer at 403.15 K in toluene with a 1000:1 ratio of monomer to initiator for a period of 24 hours or until a solid product was observed. Solution polymerisations were conducted with 1.44 g of monomer in 10 ml of toluene at 333 K with 1 equivalent of BnOH per Zn-Me. For solution polymerisations a 100:1 ratio of monomer to initiator was used and reactions were tested over 1 hour and 24 hour periods. A ^{1}H NMR homonuclear decoupled spectrum of the polymer produced by (PhMe PhO)Zn is presented in Figure 3.20, along with a GPC chromatograph in Figure 3.21.

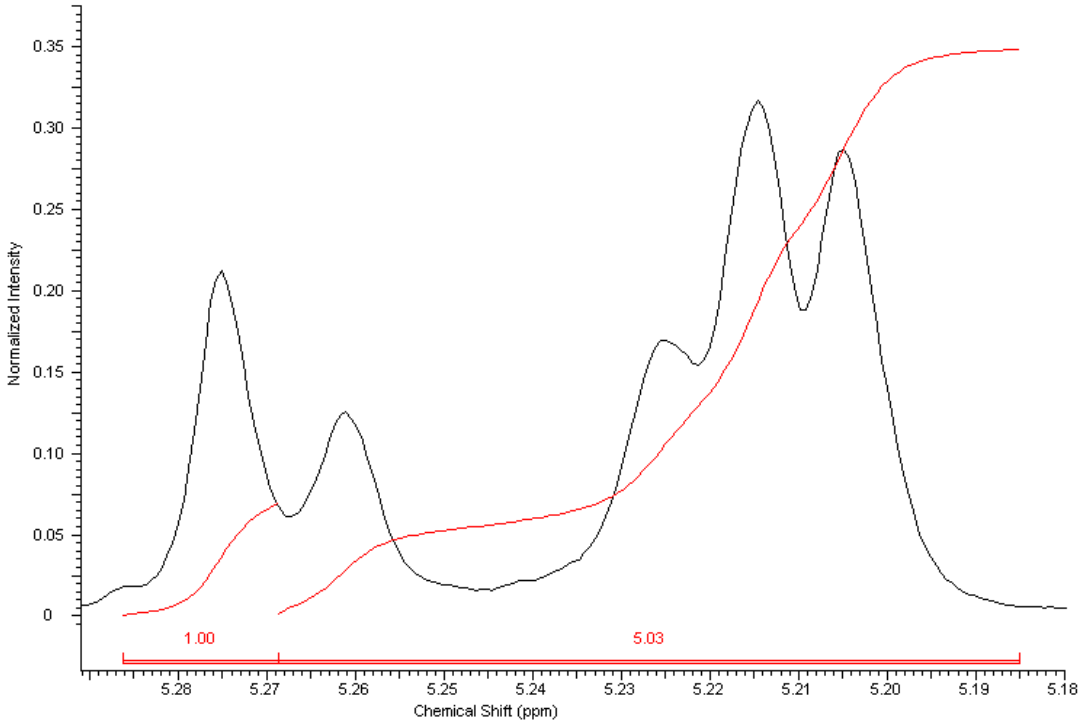

Figure 3.20 – Integrated methine region of the homonuclear decoupled ^{1}H NMR spectrum of polylactide produced by (PhMe PhO)Zn.

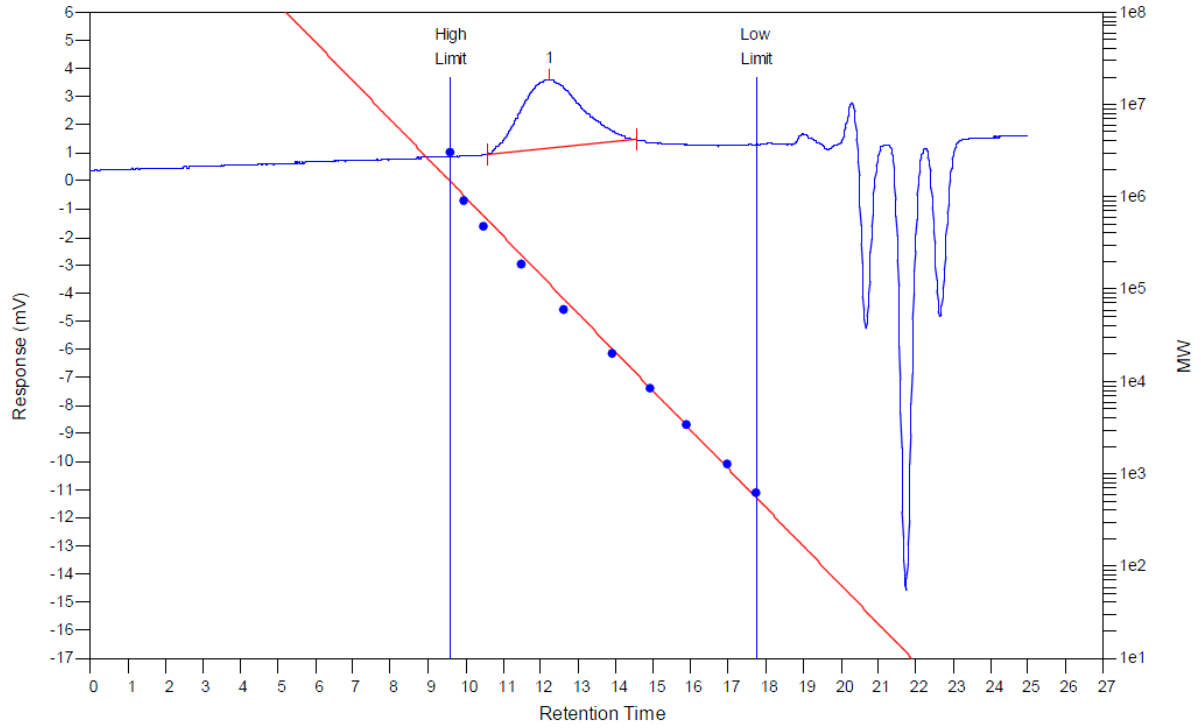

Figure 3.21 – GPC chromatograph of polylactide produced by Al(LHO)2Me.

The results of the solvent free polymerisations are presented in Table 3.5 and the solution polymerisations are presented in Table 3.6.

Catalyst	Time	Conv (%)	M_n	M_w (actual)	PDI	P_r	M_n (Theoretical)
(MeMe PhO)Zn	4 hrs	57	42100	73600	1.75	0.59	82080
(PhMe PhO)Zn	2 hrs	58	77100	126100	1.64	0.57	83520
(PhMe EtO)Zn	10 mins	88	102050	171850	1.68	0.53	126720
(PhMe PhDIP)$_2$Zn	10 mins	75	92850	156300	1.68	0.56	108000
(PhPh PhO)Zn	24 hrs	40	75550	138750	1.84	0.59	57600
(PhPh Ph^{tBu}O)Zn	24 hrs	50	71800	130750	1.82	0.58	72000

Table 3.5 – Solvent free ROP of *rac*-lactide using a range of novel zinc(II) complexes.

All initiators tested for solvent free polymerisations gave polymer of reasonable molecular weight relative to the ratio of monomer used. The theoretical molecular weights are in close agreement with the observed values and suggest the growth of a single chain per metal centre with the exception of (MeMe PhO)Zn. The (MeMe PhO)Zn complex is the least sterically hindered and produces a polymer with half the expected M_n value for a single chain per metal centre. The reactions showed a reasonable level of control over chain length with all PDI values being less than 2.0. The (PhMe EtO)Zn and (PhMe PhDIP)$_2$Zn polymerised the lactide into a visibly solid product within 10 minutes of the reaction being started. The initiators with a PhMe backbone appear to show the greatest activities followed by the MeMe complex and

the PhPh complexes. The reduced activity in the PhPh complexes could be due to excess steric hindrance at the active metal centre slowing the reaction rate. Unfortunately there is little to no stereo-control shown by these initiators. However they produce PLA with good control of molecular weight under solvent free conditions without the need for a co-initiator.

Catalyst	Time	Conv (%)	M_n	M_w (actual)	PDI	P_r	M_w (Theoretical)
MeMe Ph(DIP)ZnMe	24h	99+	11250	18750	1.66	0.43	14250
PhMe Ph(DIP)ZnMe	24h	99+	6250	9500	1.52	0.44	14250
MeMe Ph(DIP)ZnMe	1h	83	20500	26850	1.31	0.50	11950
PhMe Ph(DIP)ZnMe	1h	63	17425	24750	1.42	0.50	9070

Table 3.6 –ROP of *rac*-lactide in toluene using a range of novel zinc(II) complexes.

Due to the presence of the Zn-Me bond in the MeMe Ph(DIP)ZnMe and PhMe Ph(DIP)ZnMe complexes they were tested for activity using a benzyl alcohol co-iniator. Over a 24 hour period both complexes showed complete conversion of *rac*-lactide to PLA producing polymer of reasonable molecular weight distribution. As the polymer produced over 24 hours showed a slight isotactic bias the initiators were tested over a shorter time period to explore whether there would be increased stereocontrol with less conversion. Unfortunately, the initiators did not show any isotactic bias when tested over a 1 hour period but produced atactic polymer of reasonable molecular weight distribution. It is interesting to note that the M_w of the polymer at high conversion was significantly lower than after 1 hour and had a significantly higher PDI value. This is presumably due to transesterification side reactions occurring after the monomer is consumed.

The PhMe $(PhDIP)_2Zn$ had showed good activity under solvent free conditions and was selected for testing under conditions that more closely resemble those of an industrial scale. The complex was exposed to air for 7 days prior to testing. The initiator was then tested for the polymerisation of 35 g of recrystallised, but not resublimed, *rac*-lactide with a ratio of 1000:1 (monomer:initiator). The reaction was carried out at 150 °C and tracked over a five hour period by in situ infrared spectroscopy following a method described by *Messman et al.*[206] A plot showing the decreasing 1240 cm^{-1} (monomer C-O-C) peak compared to the increasing 1185 cm^{-1} (polymer (C-O-C) peak is shown in Figure 3.22. Based on the IR data a conversion of

80 % was observed over five hours. A sample of the polymer product was analysed by ^{1}H NMR spectroscopy and showed a conversion of approximately 87 %, which was consistent with the IR data. A sample was also analysed by GPC analysis and showed a M_n of 11,150 and PDI value of 1.67, this is considerably lower than the calculated value for a 1000:1 ratio at 87 % conversion (~119,000). The difference between the calculated and observed molecular weight could be due to transesterification reactions which are more pronounced at higher reaction temperatures and when using unpurified monomer. The IR data can also be used to determine a conversion as a function of time. The semi-logarithmic plot of this data is shown in Figure 3.23. The gradient of which is the first order rate constant, this is found to be 0.0054 mins $^{-1}$.

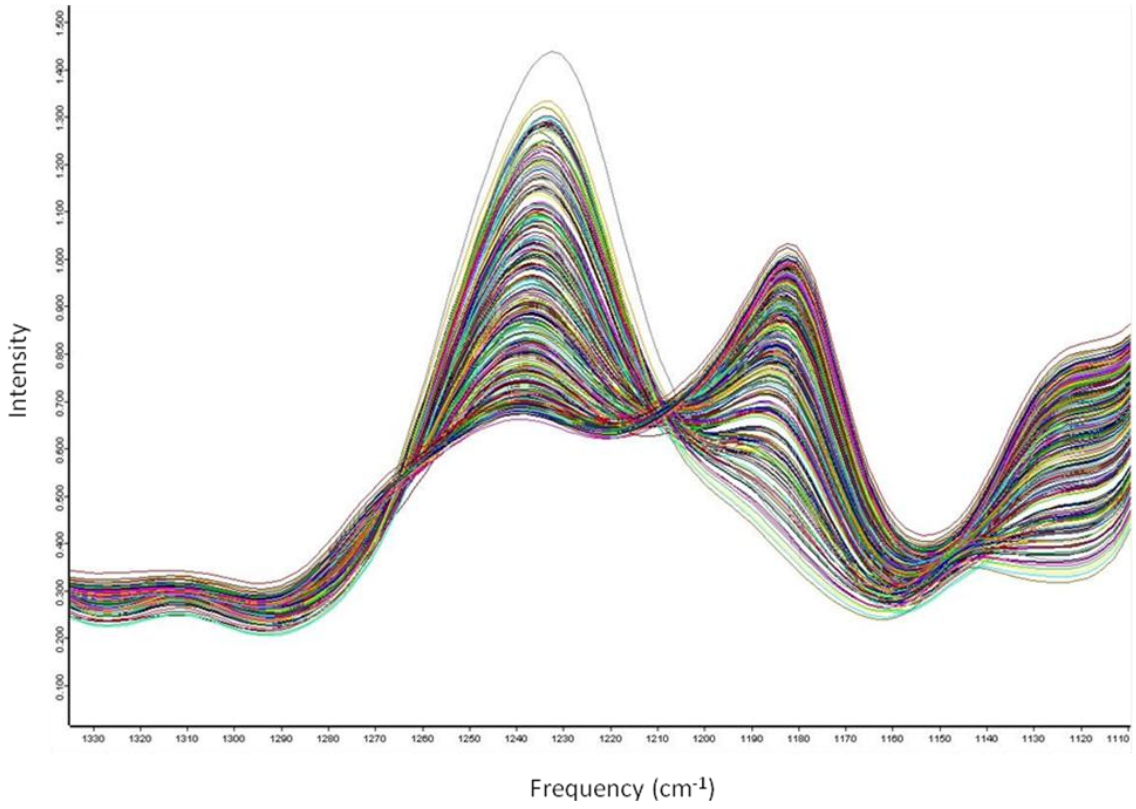

Figure 3.22 – In situ IR spectra of the polymerisation of *rac*-lactide using a PhMe (PhDIP)$_2$Zn initiator.

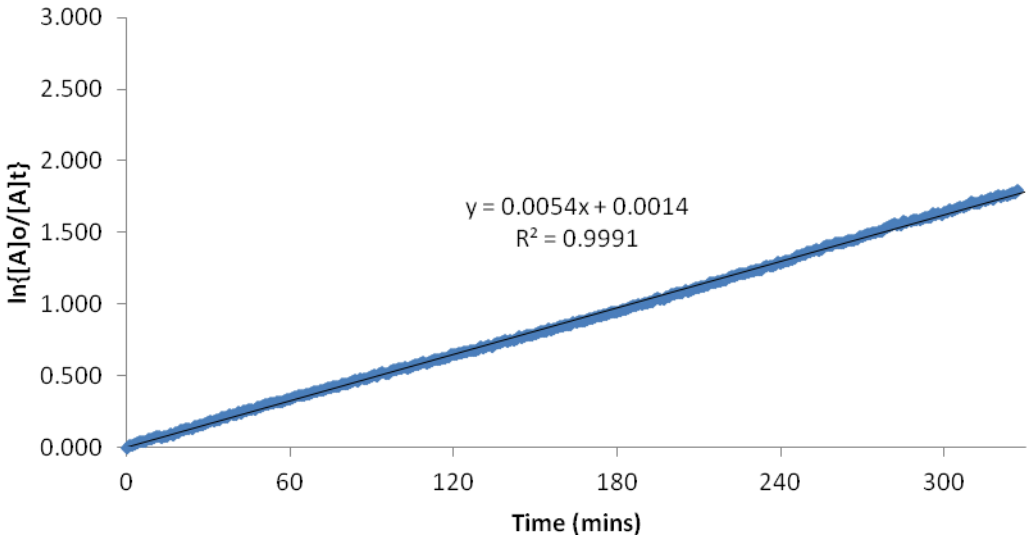

Figure 3.23 – Semi-log plot of the polymerisation reaction over time.

3.5. Future Work

All complexes described within this chapter were active for the ROP of *rac*-lactide, however, no stereospecificity was observed. The complexes were crystallised in the presence of DMSO to coordinate to the Zn(II) centre. It would be interesting to attempt the recystallisation in the presence of other coordinating systems, such as the monomer lactide or various esters. The ligands used and developed within this work were mainly focused on steric effects. It would also be interesting to test other substituted functional groups on the phenyl rings, for example incorporating electron withdrawing Cl or F groups could influence the activity of the zinc centre. Initial kinetic investigations have been presented under melt conditions. The molecular weight for the results was lower than expected, due to impurities in the monomer. Further experiments should focus on reduction of monomer-to-initiator ratios or purifying the monomer to increase the molecular weight of the polymer.

3.6. Summary

This work in this chapter describes a range of complexes based on a β-ketoiminate ligand system with varied steric properties. The ligands were complexed with Zn(II) to produce a range of novel complexes. Single crystal X-ray diffraction data was collected for seven novel complexes and two ligands.

The complexes were tested for the ROP of *rac*-lactide and all showed activity. The PhMe complexes were particularly active and the $(PhMe\ PhDIP)_2Zn$ complex was tested under industrial conditions in which the initiator was exposed to air before use and the *rac*-lactide monomer was not sublimed before use. The complex was active under these conditions and is a potential candidate for further testing.

Chapter Four

Lignin Processing

4. Lignin Processing

4.1. Introduction

As previously discussed in section 1.3, lignin describes a polymeric material which constitutes approximately 20-30% of plant biomass depending on species and growth conditions. Physiologically the role of lignin is to add rigidity and strength to the plant and to protect it from microbial and fungal attack. Lignin is a highly cross-linked 3-dimensional complex polymer with a large molecular mass (600-15000 kDa).[18,19]

Lignin is already a significant product stream of the paper industry and is currently mainly combusted to produce heat energy to fuel other processes.[29] Lignin describes a polyphenolic structure and it is widely accepted that significant value could be added if it could consistently be processed into small monomeric building blocks which could act as platform chemicals for a variety of applications.[21]

Many depolymerisation techniques have been reported but the processing of lignin remains an active area of research both academically and industrially.[26] Often these processes necessitate high temperature and pressure which requires the availability of capable reactor vessels.[36] In recent years there has been an increase in research into mild depolymerisation using oxidative catalysis.[65,66,73] The mild reaction conditions enable these methods to be evaluated without the need for specific reactor vessels.

Unlocking the economic potential of lignin could help to make bio-refining processes a commercial reality rather than a theoretical alternative to petrochemical processes. The aim of the work in this chapter was to gain an understanding of lignin chemistry and to develop novel catalytic depolymerisation processes.

4.2. Characterisation

In order to ascertain the success of any processing technique it is important to be able to characterise the lignin starting material and any products. Kraft lignin (Sigma-Aldrich) was characterised using ^{1}H NMR spectroscopy and gas chromatography.

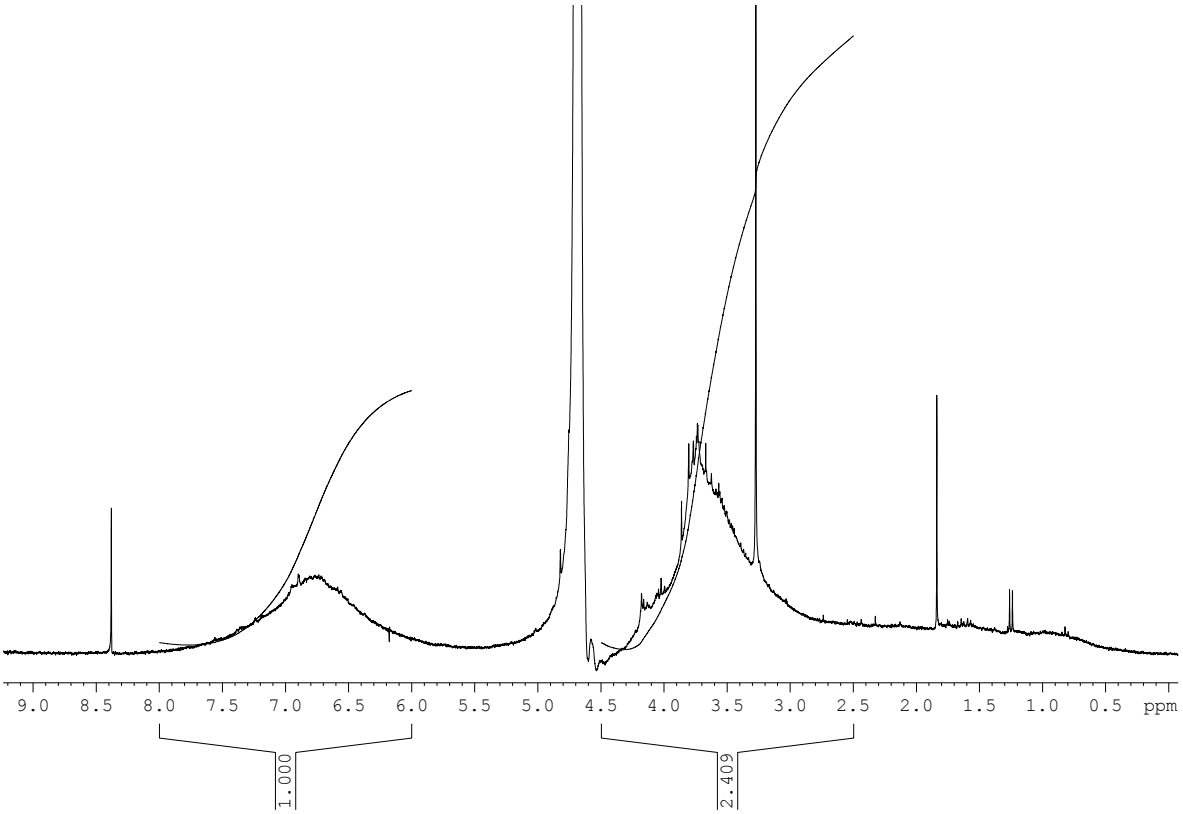

Figure 4.1 – ^{1}H NMR spectrum of Kraft lignin in D_2O, the spectra shows an approximate ratio of 1 aromatic proton to 2.4 aliphatic protons.

The NMR spectrum showed two broad resonances, one in the aromatic region and one in the aliphatic region in a ratio of (1 : 2.4) (Figure 4.1). A proposed theoretical structure of lignin is shown in Figure 1.2. The ^{1}H NMR spectrum is consistent with this structure, with the protons in the aromatic region of the spectrum appearing due to the phenyl protons in the structure and the broad aliphatic resonance consisting of protons from both linking and terminal alkyl, ether and alkoxy groups. Other characterisation methods gave little insight into the structure and product characterisation methods were focused on to assess the success of any potential experimental reaction.

4.2.1.1. Product Characterisation

In general it is easier to focus on product characterisation rather than characterising lignin itself. After a process or catalyst has been tested the depolymerised products can be analysed by various methods. Since the product will tend to be a mixture of a range of products chromatographic techniques tend to be favoured. Gas chromatography (GC) is a technique used to separate mixtures of volatile products, a basic schematic of GC is shown in Figure 4.2.

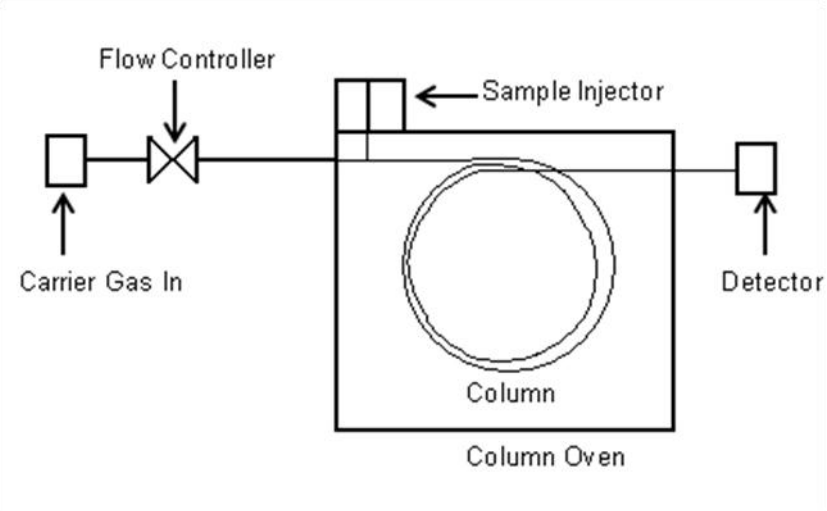

Figure 4.2- Schematic of gas chromatography.

In gas chromatography a volatised sample containing a mixture of products to be separated is injected onto a column which is held in an oven. A flow of carrier gas is controlled over the column to ensure consistent flow of the volatised analytes. Separation occurs by two main processes; the interaction of analytes with the solid phase of the column and separation by boiling point due to oven temperature. As analytes are eluted from the column they are detected by a detector, of which there are many different types, for example MS (Mass spectrometry), FID (Flame ionisation detection) and TCD (Thermal Conductivity Detection).

Gas chromatography is a powerful tool and is popular in lignin product characterisation as the desirable monophenolic products tend to be volatile and easy to separate by GC. GC processes vary by the detection technique employed. In GC-FID (Flame Ionisation Detection) a signal is given when products elute from the column and are combusted in H_2. This technique offers the potential to identify products based on a characteristic retention time. A variety of pure potential lignin products

(Figure 4.3) were analysed by GC-FID and their characteristic retention times measured. (Table 4.1).

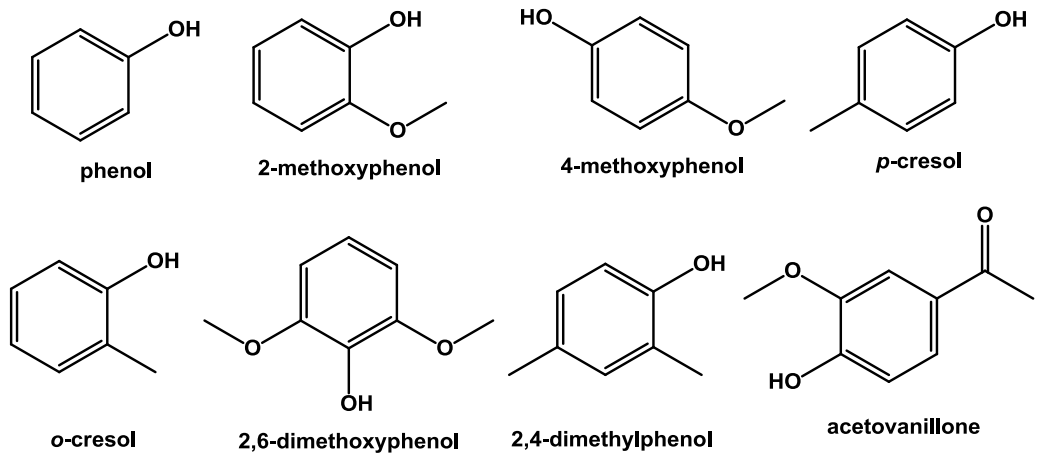

Figure 4.3- A range of potential lignin products which were analysed by GC-FID.

Compound	Retention Time
Phenol	9.96
o-cresol	11.80
p-cresol	12.30
Guaiacol	12.75
2,4-dimethylphenol	14.12
4-methoxyphenol	15.70
2,6-dimethoxyphenol	18.72
Acetovanillone	21.54

Table 4.1 – Characteristic retention times of a range of potential lignin products when analysed under controlled conditions on a GC-FID.

The potential products were then run as a mixture with a dodecane internal standard to demonstrate a potential lignin product mixture (Figure 4.4). This trace shows good separation between potential products. When working with depolymerised lignin product mixtures, previously characterised molecules can now be identified by their characteristic retention time, however the identification of unknown products is not trivial by GC-FID alone.

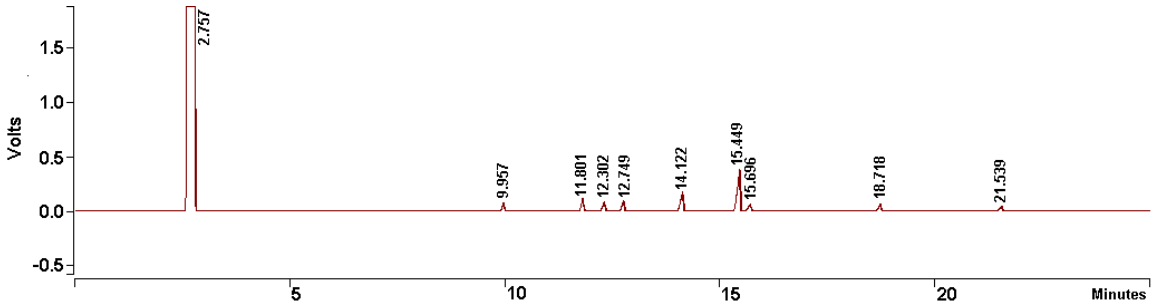

Figure 4.4- GC-FID spectrum of a range of potential lignin products run as a mixture along with a dodecane internal standard.

Gas chromatography mass spectrometry (GC-MS) offers a significant improvement on GC-FID processes as the eluted stream is analysed by a mass spectrometer. In this technique products can be analysed both by their retention time and their mass spectrum. The mass spectrum can be compared to databases of known spectra to identify previously unknown samples. An example GC-MS trace is shown (Figure 4.5), in this trace there are a variety of soxhlet extraction products (discussed later in section 4.4) which have been separated by GC.

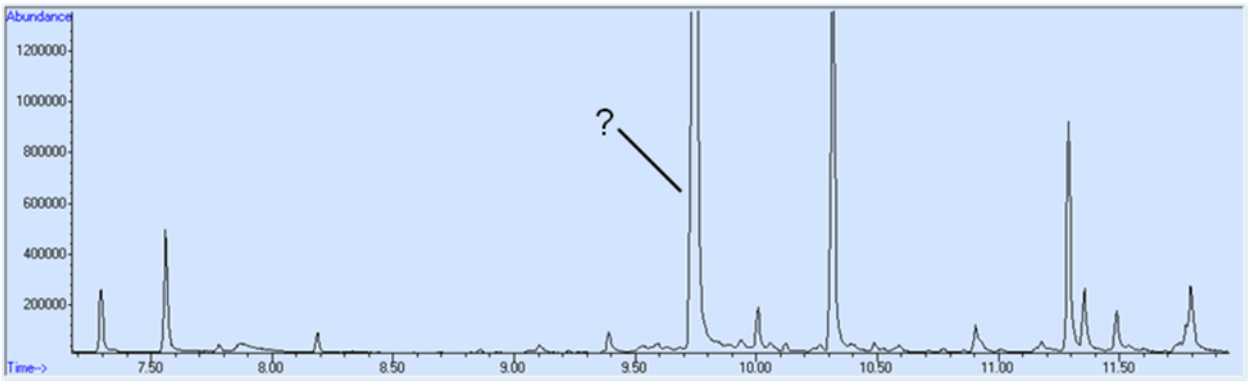

Figure 4.5 – Identification of the major peak from a mixture of unknown products of a soxhlet extraction.

The major peak of this spectrum was at a retention time of *ca.* 9.75 minutes and was previously unknown. From comparison of the mass spectrum of the product (Figure 4.6) to a known database it was identified with high probability to be the common lignin product vanillin.

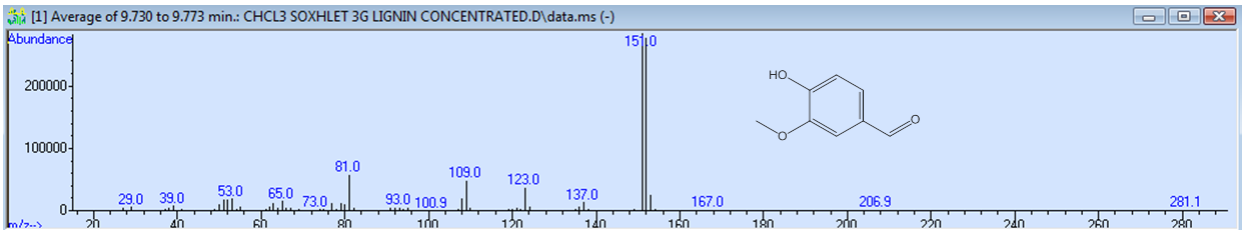

Figure 4.6 – The product eluted at 9.75 minutes was identified as vanillin by its mass spectrum.

If further confirmation is required then a pure sample can be analysed on the same column to confirm the retention time. GC-MS is a powerful tool in lignin product analysis as it offers rapid identification of unknown products.

4.3. Model Compounds

As discussed in section 1.3.2 model compounds are often used in lignin research to assess the reactivity of a catalyst or process. Many lignin compounds exist in the literature, for the work reported in this thesis, three main model compounds have been used (Figure 4.7).

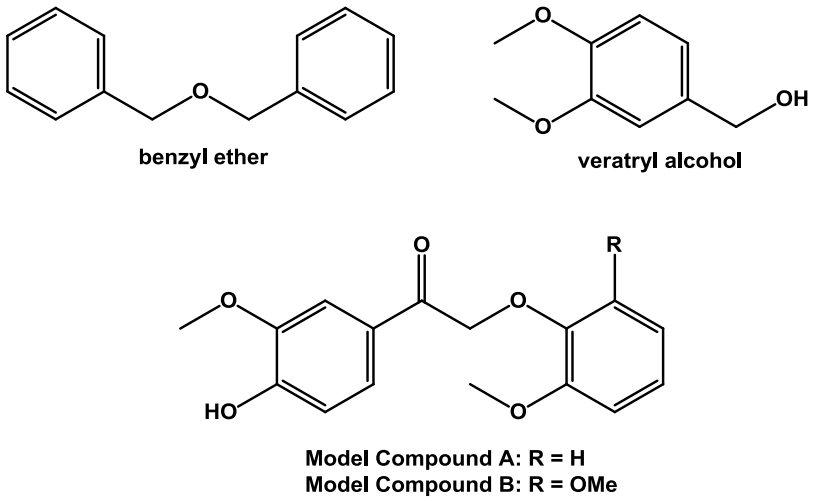

Figure 4.7 – Lignin Model Compounds

Veratryl alcohol was selected as it is commercially available and contains methyl ethers and primary alcohol functionality which are characteristic of lignin. Benzyl ether was used to assess the ability of a catalyst to break ether bonds specifically and is commercially available. Dimeric model compounds (**A, B**) were also synthesised using adapted methods from the literature (Scheme 4.1).[207] To synthesise model compound **A** acetovanillone was first reacted with ethyl iodide in the presence of potassium carbonate to yield the corresponding ethoxy product (int**1**) in 88 % yield.

The isolated product (int**1**) was then subjected to bromination conditions using $CuBr_2$ overnight to yield the brominated product (int**2**) in a 50 % yield. The bromide intermediate (int**2**) was then reacted with 2-methoxyphenol in the presence of potassium carbonate to give **A** in a 76 % yield. This synthesis was successfully performed on an 8 g scale. Model Compound B was synthesised by the same procedure but used 2,6-dimethoxyphenol in place of 2-methoxyphenol in the final step and has been conducted on a 3 g scale.

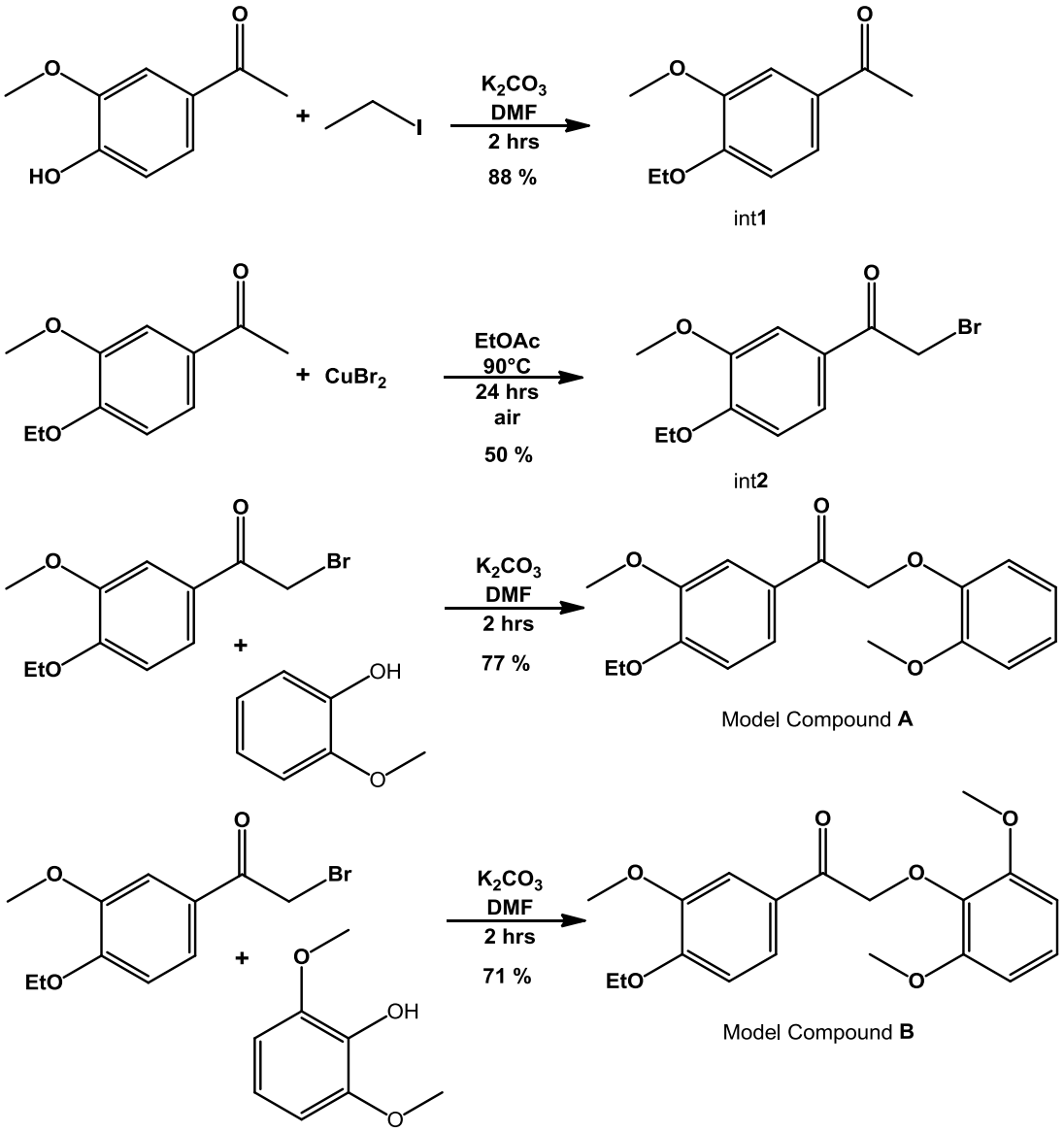

Scheme 4.1 - Synthesis of Model Compound A.

4.4. Soxhlet Extraction

A soxhlet extractor is used to extract partially soluble compounds from solid material in a solvent heated to reflux. The setup allows boiling solvent through the vapour arm causing it to build up in the chamber which contains a porous finger and the solid material to be extracted. When the chamber fills to a certain level the siphon arm releases the solvent back into the boiling flask and the process is repeated (Figure 4.8).

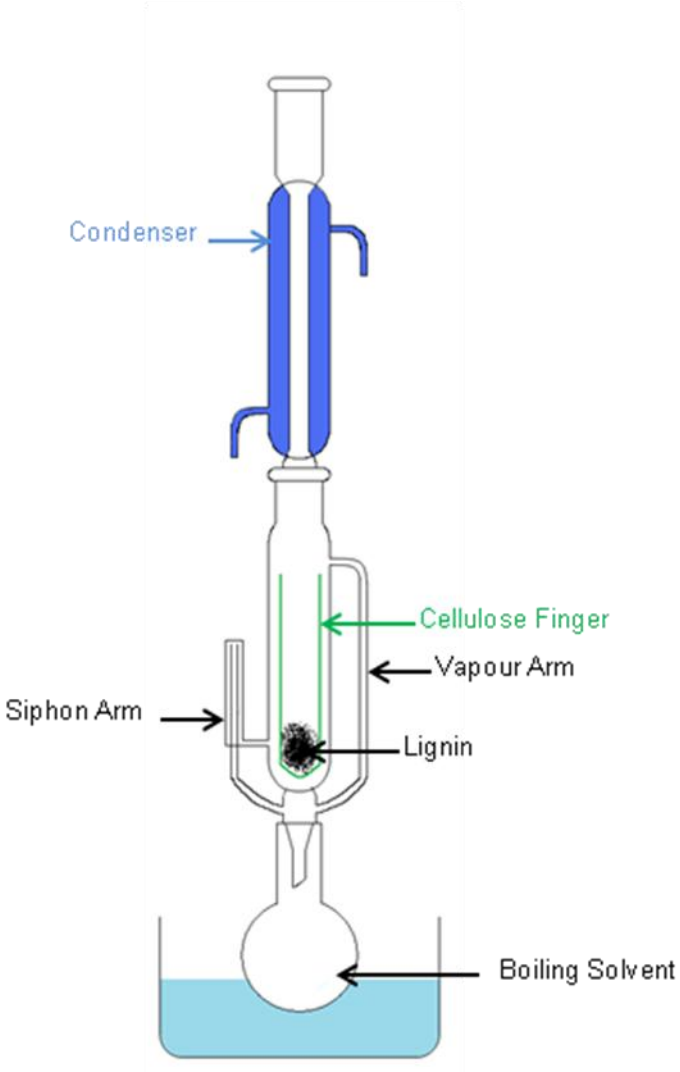

Figure 4.8 – Apparatus used for the Soxhlet extraction of kraft lignin.

Kraft Lignin (3 g) was subjected to a soxhlet extraction containing 150 ml of $CHCl_3$ for 24 hours (approximately 48 pumps). The entire process was repeated 3 times using the same lignin sample but a new cellulose finger and solvent each time and the results are presented in Table 4.2. The loss of lignin in each run not associated with extracted product was due to difficulty in recovering all of the unextracted lignin from the consumed cellulose finger between runs.

Amount of Lignin (g)	Amount of Extracted Product (mg)	Lignin Recovered (g)
3.00	100	2.90
2.90	85	2.78
2.78	70	2.61

Table 4.2 – Amount of product extracted during soxhlet extraction of Kraft lignin.

A total of 255 mg (8.5 wt%) of extracted products were recovered over the three runs and were analysed by GC-MS after each run. Figure 4.9 shows the spectrum and some identified peaks for the first run, the spectra from runs two and three showed similar profiles and peaks.

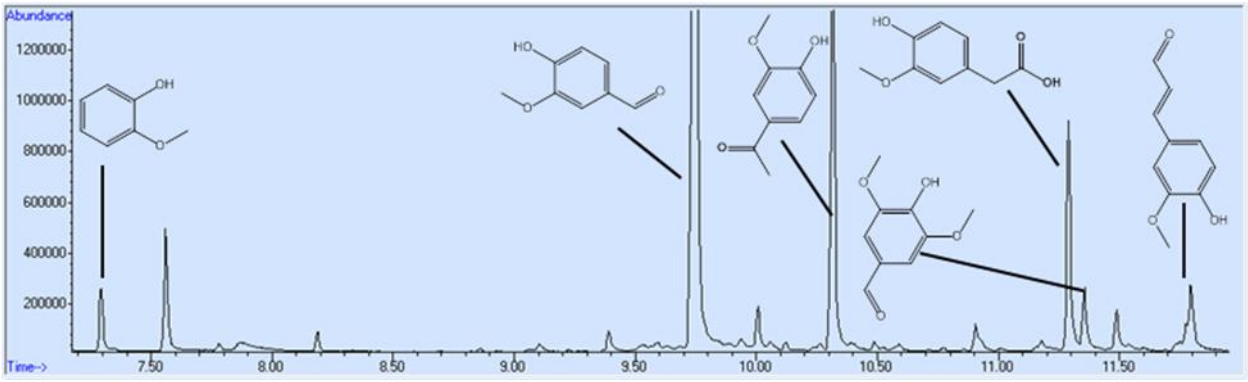

Figure 4.9 – Recorded GC chromatogram of the Soxhlet extracted products ($CHCl_3$) of Kraft lignin.

The spectrum shows a range of monophenol products the main products are vanillin, 1-(4-hydroxy-3-methoxyphenyl)ethanone and 2-(4-hydroxy-3-methoxyphenyl)acetic acid with relative abundances of 55 %, 18 % and 9 % respectively. These values are consistent with previously reported figures.[208,209] When a cold solvent extraction was performed on a similar lignin sample no products were successfully extracted. These results provide a benchmark which could be used to evaluate the success of a novel catalytic process. Lignin depolymerisation processes tend to be evaluated based on the products obtained in a cold extraction process from the solid products.

Novel techniques could be further evaluated by their ability to increase the yield of monophenolic products in the soxhlet extraction process.

4.5. Oxidative Catalysis

4.5.1. Methyltrioxorhenium

Crestini et al previously reported the depolymerisation of lignin and transformation of lignin model compounds by a homogeneous methyltrioxorhemium (MTO) catalyst (Figure 4.10).[65,66] In this work the transformation of veratryl alcohol was described with a high conversion (98 %) but poor mass balance (12 %) Oxidation of the primary alcohol to an aldehyde and carboxylic acid was reported along with the formation of a lactone (Scheme 4.2).

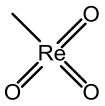

Figure 4.10 – Homogeneous methyltrioxorhenium (MTO) catalyst.

In the same work the group reported loading the MTO onto a variety of heterogeneous supports. Similar catalytic activity was reported in the heterogeneous catalysts as the soluble homogeneous catalyst. One support used was poly(4-vinylpyridine) and the reported heterogeneous catalyst is shown in Figure 4.11.

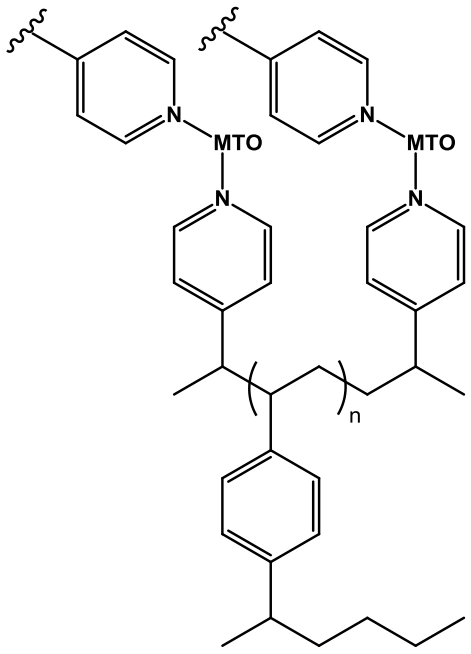

Figure 4.11 – Heterogeneous poly(4-vinylpyridine) methyltrioxorhenium (MTO) catalyst synthesised by *Crestini et al.* [65]

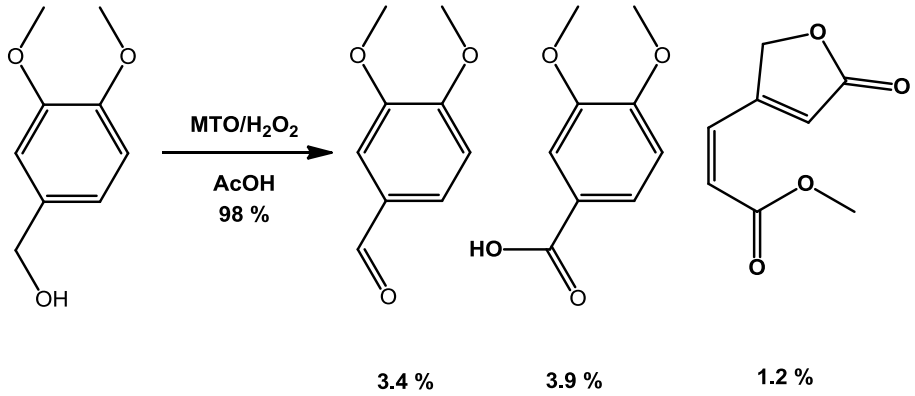

Scheme 4.2 - Transformation of veratryl alcohol reported by *Crestini et al.*

Attempts were made to repeat the catalytic experiments as well as to synthesise new heterogeneous MTO catalysts based on previously unreported silica supports. The synthesis of a novel silica loaded heterogeneous MTO catalyst by sequential tethering is shown in Scheme 4.3.

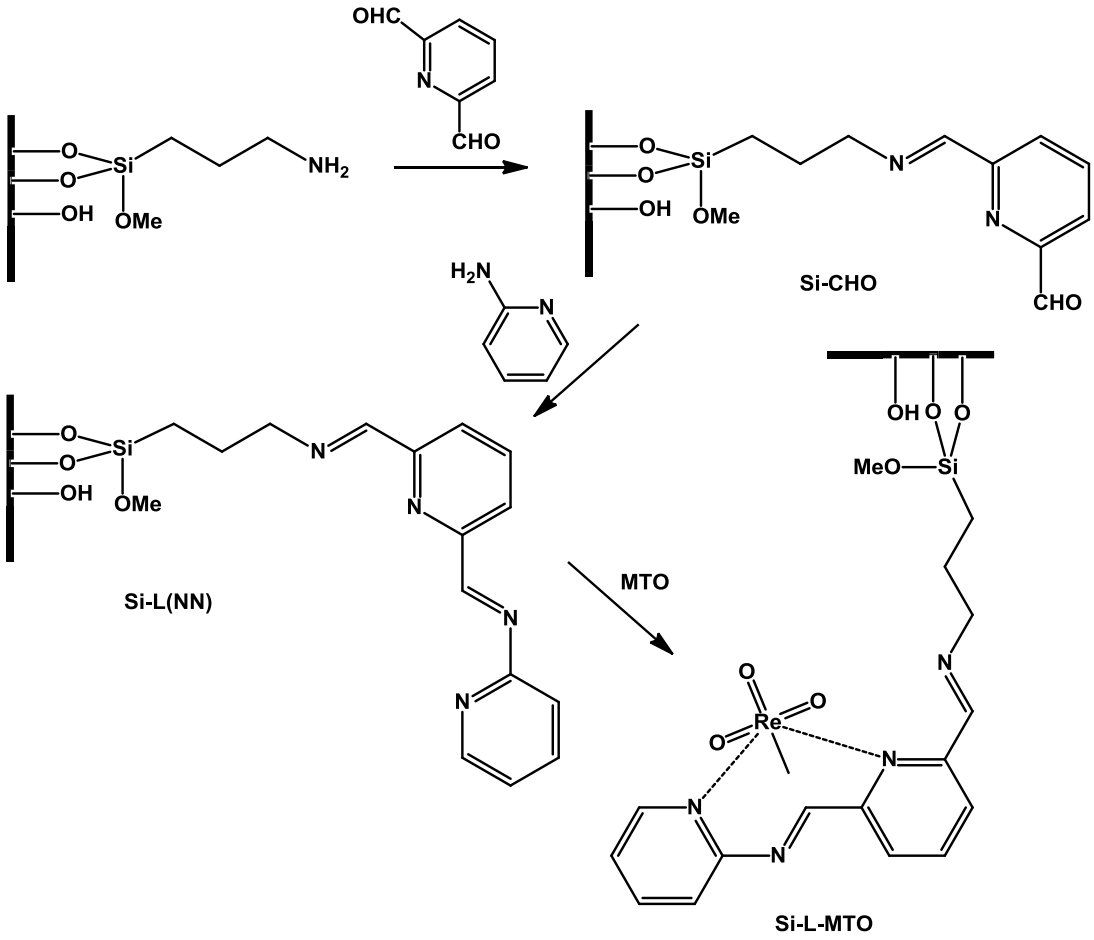

Scheme 4.3 – Synthesis and coordination of a sequentially tethered ligand to MTO.

The sequential tethering was achieved by reaction of the starting reagents together in methanol for 24 hours at room temperature. The reactions were monitored by solid state $^{13}C\{^{1}H\}$ NMR spectroscopy and observation of colour changes in the solid product. The solid state $^{13}C\{^{1}H\}$ NMR spectra for Si-CHO, Si-L(NN) and Si-L-MTO are presented in Figure 4.12. The spectra show resonances between 0-35 ppm relating to the alkyl carbons, between 45 and 70 ppm relating to the alkyl carbons adjacent to heteroatoms, between 115 and 200 ppm relating to aromatic and imine carbons and the Si-CHO spectrum shows a resonance at approximately 225 ppm relating to the aldehyde.

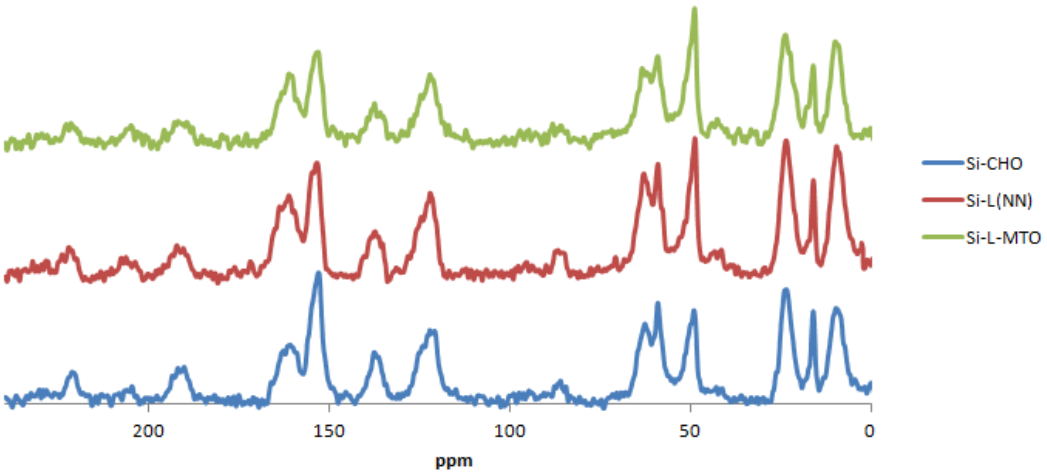

Figure 4.12 – Solid state $^{13}C\{^{1}H\}$ NMR spectra of Si-CHO, Si-L(NN) and Si-L-MTO.

4.5.1.1. Catalytic Testing

The novel heterogeneous and the homogeneous MTO catalyst were tested for activity in the oxidation of veratryl alcohol, as previously reported.[65] Despite extensive efforts to repeat these results none of the reported products were observed despite the use of conditions identical to those reported. The reactions were monitored by GC-MS analysis and only rapid esterification of the primary alcohol by acetic acid was observed (< 30 mins) despite the reaction being allowed to proceed for a period of 7 days. However, small amounts of veratraldehyde were observed as an impurity in the starting material (97 %, Sigma Aldrich). This leads to the conclusion that the reported products maybe an impurity of the starting materials used and not a product of the reaction.

The reaction of veratryl alcohol with the homogeneous MTO catalyst was further explored to assess the reactivity in the absence of esterification by acetic acid, to achieve this methanol was used as a solvent in place of the acetic acid. After a period of 7 days the reaction was sampled for GC-MS analysis and formation of a methylated product (prod**1**) was observed as well as a minor product caused by the coupling of two veratryl alcohols to form an ether (prod**2**) (Scheme 4.4).

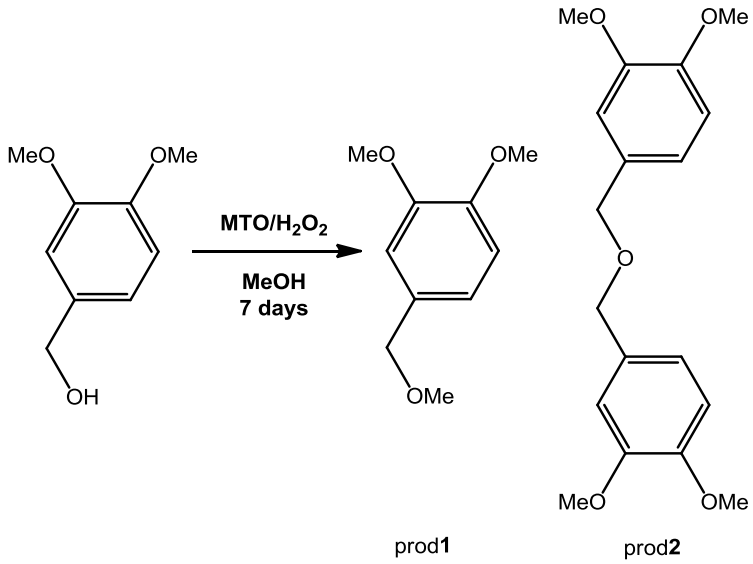

Scheme 4.4 - Transformation of veratryl alcohol in the presence of MeOH and a MTO catalyst.

The formation of the methylated product was presumed to occur from the reaction of veratryl alcohol with the methanol solvent. The reaction was repeated in the absence of H_2O_2 and MTO independently and both were shown to be required for the formation of prod**1** and prod**2**. The combination of MTO/H_2O_2 appeared to be catalytically coupling two primary alcohols together to form an ether. To the knowledge of the author this reactivity had not previously been described for this catalytic system and so warranted further investigation. The reaction was conducted using a stoichiometric amount of deuterated methanol (CD_3OD) and peaks in the mass spectrum were observed with increased m/z of 3 which confirms the reaction of methanol with veratryl alcohol (Figure 4.13).

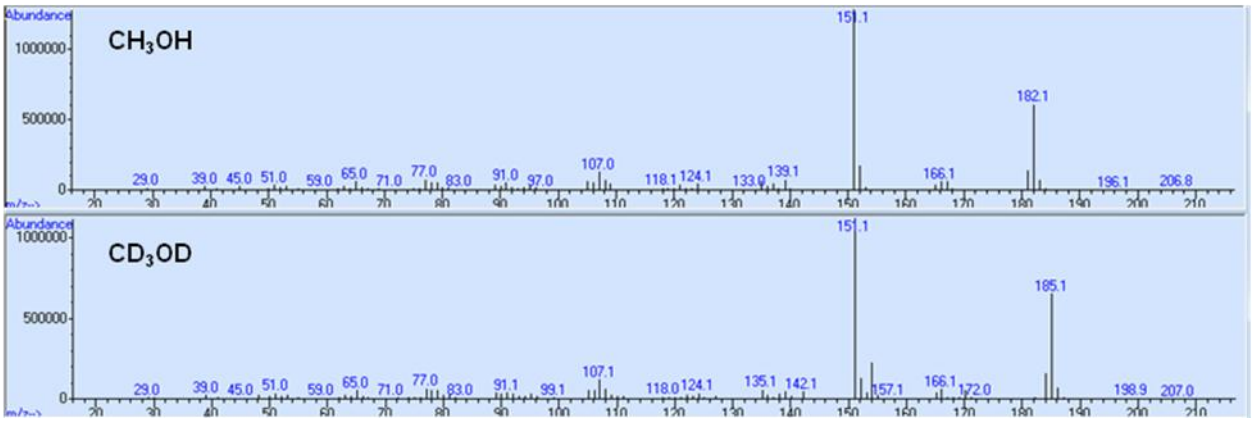

Figure 4.13 – 1,2-dimethoxy-4-(methoxymethyl)benzene product shows increased m/z of 3 in some peaks when reacted with CD_3OD in comparison to CH_3OH.

The reaction was repeated using a stoichiometric amount of MeOH and 1,4-dioxane as a solvent. Under these conditions a conversion in excess of 60 % with regards to veratryl alcohol (VA) was observed after 24 hours**.** After a period of 4 days the reaction had proceeded almost to completion with prod**1** having a relative abundance of 96 % (Table 4.3). The increase in reactivity when compared to using MeOH as a solvent could be due to the catalyst becoming saturated with MeOH when it is used as a solvent but not when it is used in stoichiometric amounts.

Time	Relative abundance % VA	Relative abundance % prod**1**	Relative abundance % prod**2**
24 h	38	61	1
96 h	1	96	3

Table 4.3 – Relative abundances of starting material and products when veratryl alcohol was reacted with a stoichiometric amount of MeOH in 1,4-dioxane.

At this point a GC calibration method was developed allowing quantitation with respect to veratryl alcohol by using an internal standard of dodecane. The dilutions used in a catalytic experiment were mimicked over a range of sample volumes to ensure that the response for both VA and the dodecane internal standard was linear over a range of potential sample volumes (Figure 4.14). GC-FID was used for quantification and an average response factor of 3.45 (VA:dodecane) was observed.

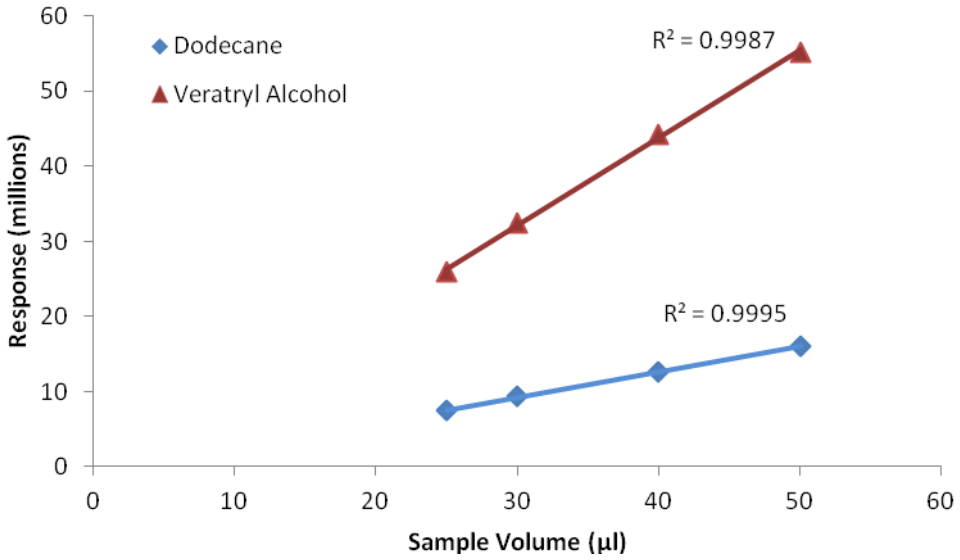

Figure 4.14 – Calibration of GC-FID instrument with respect to VA using dodecane as an internal standard.

The MTO system was then further assessed by reaction of 1 equivalent of veratryl alcohol with 2 equivalents of a variety of primary and secondary alcohols. The expected product in each reaction is veratryl alcohol coupled to the corresponding alcohol by an ether bond and was identified by the appropriate ion in the EI mass spectrum. Selectivity was calculated based on the assumption that the product had the same response factor as the VA starting material with respect to dodecane. (Table 4.4).

Alcohol	Time	Conversion of VA %	Selectivity % to expected product
Methanol	24 h	57	62
Ethanol	24 h	77	53
1-hexanol	24 h	53	10
Isopropyl alcohol	96 h	33	8
2,4-dimethyl-phenol	24 h	82	26

Table 4.4 – Results of the reaction of veratryl alcohol with 2 equivalents of a variety of alcohols.

In all cases the expected product was formed, however, differences were observed in reactivity and selectivity of each reaction depending on the alcohol starting material. It is important to note that these reactions were conducted with a relatively low loading of catalyst (0.1 mol %) and gave reasonable conversions over a 24 hour period. This catalytic system could offer a novel route to ether formation from alcohol

groups and might have uses as tool in organic synthesis. Similar results have previously been reported using a series of iridium complexes.[210]

4.5.2. Vanadium & Cobalt oxidation.

There is precedent in the literature for the ability of the oxidative breakdown of lignin model compounds by vanadium complexes.[73] A novel vanadium(IV) complex was synthesised by the reaction of a previously reported salalen ligand [211] with vanadium oxide triisopropoxide (Scheme 4.5). Single crystal X-ray diffraction data was obtained for the resulting complex V(L^{tBu}OO)O. The solid state structure is presented (Figure 4.15) along with selected bond lengths and angles (Table 4.5).

In the synthesis the vanadium centre has been reduced from vanadium(V) to vanadium(IV). Similar behaviour has previously been reported and the reduction was associated with the presence of pyridine.[73,212] Mechanistic studies showed that the reduction of V(V) to V(IV) proceeded by a radical mechanism and generated half an equivalent of alcohol and half an equivalent of aldehyde. [213] It is likely that the reduction of vanadium(V) in the reaction with $^{LtBu}(OH)_2$ proceeded by a similar mechanism generating 0.5 eq of acetone and 0.5 eq of isopropyl alcohol per vanadium centre reduced.

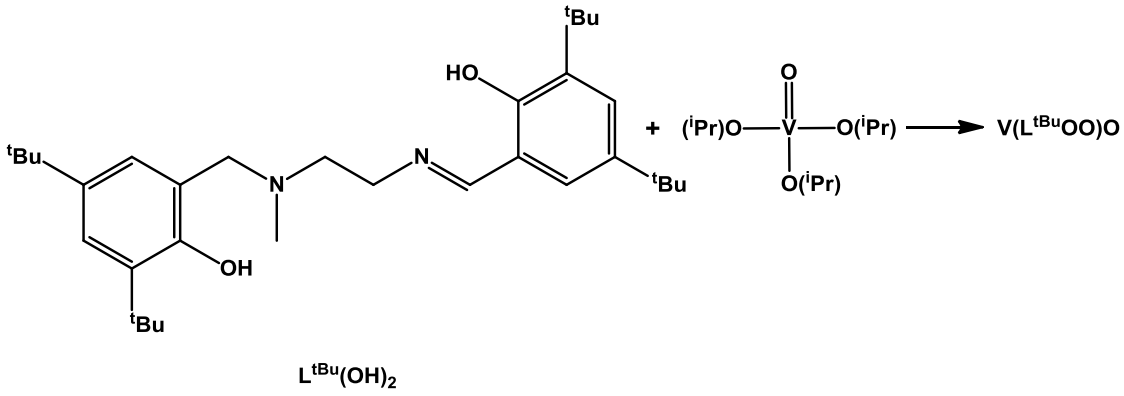

Scheme 4.5 – Synthesis of V(L^{tBu}OO)O

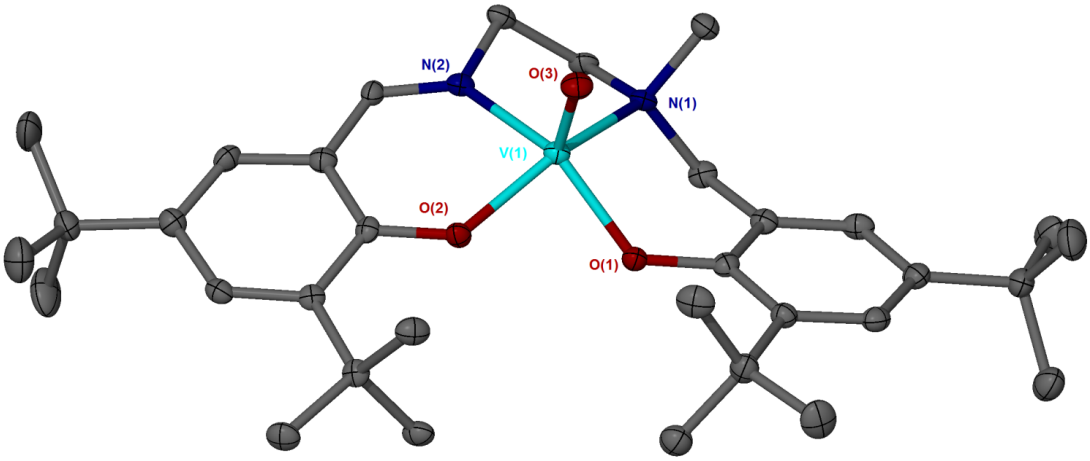

Figure 4.15 – Solid state structure of V(L^{tBu}OO)O, thermal ellipsoids are shown at the 30 % probability level.

Bond Lengths (Å)			Bond Angles (°)			
V(1)	N(1)	2.180(3)	O(3)	V(1)	O(2)	109.84(13)
V(1)	N(2)	2.066(3)	O(2)	V(1)	O(1)	86.02(11)
V(1)	O(1)	1.922(3)	O(2)	V(1)	N(1)	144.46(12)
V(1)	O(2)	1.927(3)				
V(1)	O(3)	1.592(3)				

Table 4.5 – Selected bond angles and lengths from the solid state structure of V(L^{tBu}OO)O.

The solid state structure shows the successful chelation of the ligand to the vanadium centre. The V(1) metal centre is in a pseudo-square based pyramidal environment with the O(3)-V(1)-O(2) bond angle being 109.84(13) °, the O(2)-V(1)-O(1) bond angle being 86.02(11) ° and the O(2)-V(1)-N(1) bond angle being 144.46(12) °. The V(1)-O(3) bond length is 1.592(3) Å which is comparable to the bond oxygen-vanadium double bond length of 1.588(2) Å previously reported by *Hanson et al.* [212] A search of the Cambridge Crystallographic Data Centre database of reported structures suggests that this is the first example of a vanadium salalen complex.

The complex was tested for the catalytic breakdown of Kraft lignin in methanol in both the presence and absence of H_2O_2. The reaction was conducted at 140°C with 1 wt% of vanadium added in a sealed reactor vessel (Parr Instruments model 4748) for 24 hours. After the reaction had been completed the MeOH was removed under vacuum and the product was dissolved in water and a CH_2Cl_2 fraction was extracted. When using this method the success of the reaction is determined by the mass of products contained in the $CHCl_3$ extract as well as its contents when analysed by GC-

MS. A control reaction was conducted under the same conditions but without a catalyst for comparison.

Catalyst	Kraft Lignin	H_2O_2 (30 % in H_2O)	Mass of $CHCl_3$ fraction (mg)	Notable Products Identified by GC-MS
None	0.5g	1 ml	0	None
V(L^{tBu}OO)O	0.5g	1 ml	50	Ligand breakdown products
V(L^{tBu}OO)O	0.5g	None	40	Ligand breakdown products

Table 4.6 – Attempts of catalytic breakdown of kraft lignin using V(L^{tBu}OO)O.

Table 4.6 shows that the V(L^{tBu}OO)O catalyst was unsuccessful in the depolymerisation of Kraft lignin as there were no lignin products in the $CHCl_3$ extract.

4.5.3. Cobalt Catalysis

Cobalt catalysts have previously been associated with the oxidative processing of lignin.[67-71] In an attempt to further this area of research a range of cobalt catalysts were synthesised based on a salophen ligand system. The salophen ligands are synthesised from the reaction of *o*-phenylenediamine with the corresponding salicylaldehyde (Scheme 4.6).

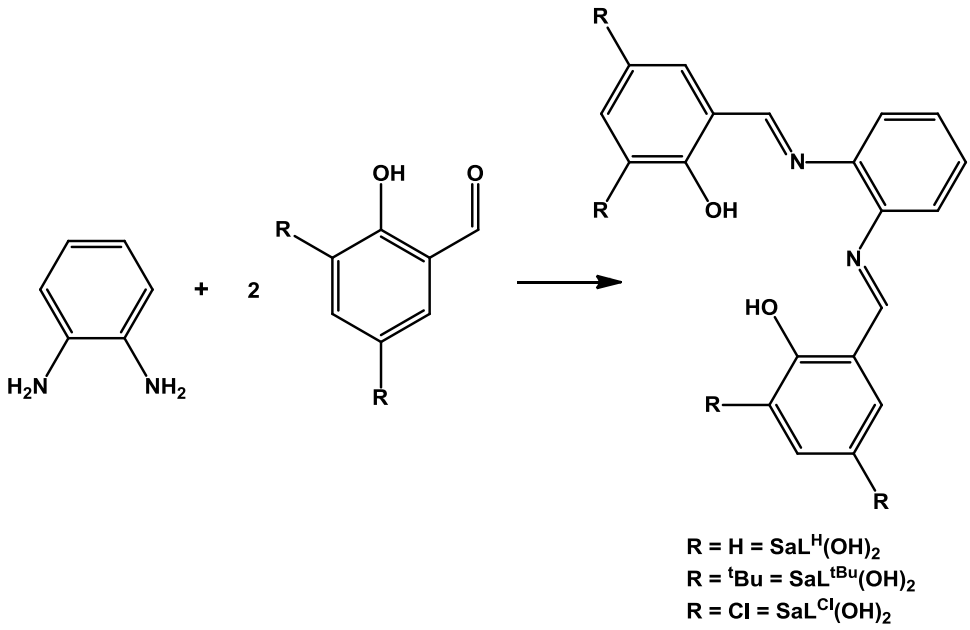

Scheme 4.6 – Synthesis $SaL^{H}(OH)_2$, $SaL^{tBu}(OH)_2$ and $SaL^{Cl}(OH)_2$

The ligands were reacted with Co(II) acetate over 16 hours at 80 °C in toluene to form the complexes CoSaL^{H}OO, CoSaL^{tBu}OO and CoSaL^{Cl}OO. Due to the paramagnetic

nature of the complexes characterisation by NMR spectroscopy was not possible. The complexes were characterised by high resolution mass spectrometry and magnetic moment analysis by the gouy method. Crystals of CoSaL^{tBu}OO suitable for analysis by X-ray crystallography were obtained and the solid state structure is presented in Figure 4.16.

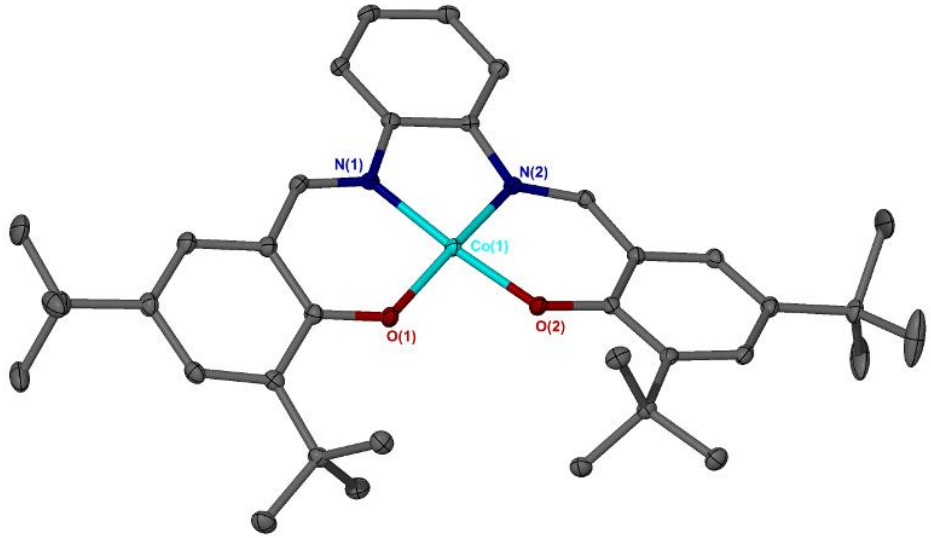

Figure 4.16 – Solid state structure of CoSaL^{tBu}OO, one set of methyl groups were disordered over two positions and so were modelled in a 70:30 ratio, thermal ellipsoids are shown at the 30 % probability level.

The cobalt(II) centre is in a pseudo-square planar molecular environment with a Co(1)-O(1)-O(2) bond angle of 87.50(5) ° and a Co(1)-O(2)-N(1) bond angle of 174.18(5) °. The Co(1)-O(1) and Co(1)-N(1) bond lengths were determined to be 1.8496(11) Å and 1.8626(13) Å respectively. The bond angles and lengths are consistent with similar previously reported cobalt(II) complexes.[214-216]

The complexes were tested for the depolymerisation of Kraft lignin under the same conditions as the vanadium complex in section 4.5.2. 10 wt % of cobalt was added to each reaction and the results are presented (Table 4.7).

Catalyst	Kraft Lignin	H_2O_2 (30 % in H_2O)	Mass of $CHCl_3$ fraction (mg)	Notable Products Identified by GC-MS
None	0.5g	1 ml	0	None
$CoSaL^{H}OO$	0.5g	1 ml	180	Ligand breakdown products
$CoSaL^{H}OO$	0.5g	None	205	Ligand breakdown products
$CoSaL^{tBu}OO$	0.5g	1 ml	240	Ligand breakdown products
$CoSaL^{tBu}OO$	0.5g	None	235	Ligand breakdown products
$CoSaL^{Cl}OO$	0.5g	1 ml	210	Ligand breakdown products
$CoSaL^{Cl}OO$	0.5g	None	201	Ligand breakdown products

Table 4.7 – Attempts of catalytic breakdown of Kraft lignin using a variety of cobalt complexes.

All attempts were essentially unsuccessful with only ligand breakdown products observed in the $CHCl_3$ fraction.

4.6. Other Methods Tested

4.6.1. Hydrolysis using noble metal catalysts

Literature methods have shown noble metal catalysts to be active in the depolymerisation of lignin at 250 °C when used under a hydrogen atmosphere in the presence of a strong acid. [36] Available reactors have operating limits of 200 °C in an air atmosphere or room temperature under 10 Bar of H_2. Experiments were carried out at the limits of what could be achieved in terms of heat and pressure and the results are shown (Table 4.8). Model compound A was used and the experiments were run for 12 hours.

At 200 °C in air only starting material was isolated for all three catalysts. When the reaction was run under a hydrogen atmosphere the carbonyl group was simply reduced to an alcohol. Conditions for hydrolysis were unobtainable with the available reactor vessels.

Conditions	Catalysts tested	Observed Products
Model Compound A 200 °C High Pressure (Air) Formic Acid	Pt/C Pd/C Ru/C	Starting Material 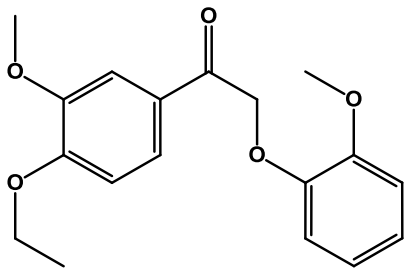 Reduced Starting Material
Model Compound A 25° C 10 Bar H_2	Pt/C Pd/C Ru/C	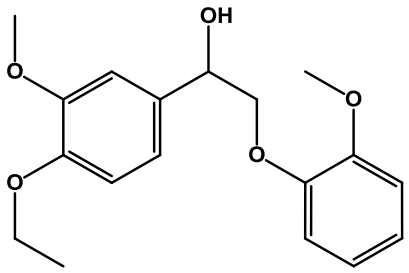

Table 4.8 – Results of hydrolysis experiments

4.7. Future Work

The large majority of work described in this chapter was focused on the development of suitable model compounds and analytical techniques to assess the success of any potential processes. The GC-MS analysis combined with appropriate model compound work allows the assessment of any potential catalysts. Further work could focus on the synthesis and catalytic screening of other oxidative catalysts for the depolymerisation reaction. Literature has shown that cobalt and vanadium complexes are active for the depolymerisation, hence the initial motivation for this study. Further work should focus on new ligated complexes and screening for activity as depolymerisation systems. Microwave or ultrasound conditions could also be tested to explore whether they enhance the depolymerisation.

4.8. Summary

This chapter describes significant efforts to enhance the field of lignin depolymerisation. Described within is a novel vanadium complex based on a recently reported ligand system which was unsuccessful in initial attempts to process lignin but warrants further investigation. Many attempts were made to depolymerise and characterise lignin but all were ultimately unsuccessful. The bulk of reactions reported in the literature for lignin depolymerisation require reactor vessels capable of high temperature and high pressure which simply weren't available.

The area of oxidative depolymerisation offers an interesting alternative and is the subject of several recent papers. Whilst attempts to depolymerise lignin have been unsuccessful a great wealth of knowledge was gained in this area. Understanding of lignin characterisation data, the use of model compounds and the relevance of tools such as GC-MS and NMR spectroscopy to lignin research was an area of research which had not previously been pursued at the university. The work described in this chapter describes significant efforts and could provide a platform for future work in this area.

Chapter Five

Experimental Methods

5. Experimental

5.1. General Experimental

All work involving metal complexes were carried out under an atmosphere of dry argon using standard Schlenk and glove-box techniques. Solvents were purified by a MBraun SPS solvent system. $Ti(O^iPr)_4$ (97 %, Aldrich) was purified by vacuum distillation prior to use, *rac*-LA (Aldrich) was recrystallised from toluene and sublimed twice prior to use. All other starting materials were used as received and purchased from Aldrich, Acros Organics, Alfa Aesar or Lancaster. Solution ^1H and $^{13}C(^1H)$ NMR experiments were performed at ambient temperature unless otherwise stated using a Bruker Advance-300, Bruker DRX400 or Bruker DRX500 MHz FT-NMR spectrometer. $CDCl_3$ and C_6D_6 for NMR analysis of metal complexes was distilled from calcium hydride prior to use. Coupling constants are given in Hertz. Wilmad 5 mm NMR tubes were used for ligand and polymer characterisation, while NMR tubes fitted with Young's taps were used for metal complexes and kinetic experiments. All chemical shifts are quoted as δ values in ppm relative to residual protio solvent resonances and all coupling constants are given in Hertz.

High resolution mass spectrometry was recorded on a micrOTOF electrospray time-of-flight (ESI-TOF) spectrometer. The samples were dissolved in methanol and the spectra recorded in positive mode. Metal complexes analysed by mass spectrometry were analysed using a micrOTOF electrospray quadrupole time-of-flight (ESI-QTOF) spectrometer in CH_2Cl_2 solution. MALDI-TOF Mass Spectra of polymeric products were recorded at the EPSRC National Mass Spectrometry Service Centre, Swansea, UK. The samples were solubilised in THF and analysed by positive MALDI in linear and reflectron modes using Dithranol matrix with LiCl as an additive to promote $[M^+Li]^+$ or NaOAc.

X-ray crystallographic analysis were carried out at 150 K on a Nonius Kappa or Nonius Helix X-ray diffractometer using Mo-Kα radiation (λ = 0.71073 Å) at the University of Bath. Structures were solved by direct methods and refined on all F^2 data using SHELXL-97 suite of programs, with hydrogen atoms included in idealized positions and refined using the riding model unless otherwise stated.[217]

Elemental analysis was performed by Mr. A. K. Carver at the Department of Chemistry, University of Bath, on an Exeter Analytical CE440 Elemental Analyzer.

Gas chromatography (GC) analysis was conducted using an Agilent 5975 gas chromatograph with triple detection (GC-FID, GC-TCD, GC-MS). The MS is electron impact and fragmentation patterns were analysed by reference to the NIST database of spectra. The FID and TCD were operated at 300 °C. Unless otherwise stated the samples were injected at 300 °C onto a HP-5 column which was held in the oven. The oven temperature was initially 50 °C and held for 2 minutes before heating to 270 °C at a rate of 15 °C min^{-1} and being held at 270 °C for 200 seconds.

For homogeneous polymerisations a monomer:initiator ratio of 100:1 was used unless otherwise stated. In all cases toluene (10 ml) was added to a Schlenk followed by the initiator and 1 eq of BnOH for each M-CH_3 unit in the complex unless otherwise stated, the lactide (1 g) was added and the flask heated at the desired temperature for the given length of time. For heterogeneous polymerisations a monomer:initiator ratio of 300:1 or 1000:1 was used. Unless otherwise stated toluene (10 ml) was added to a Schlenk followed by the appropriate amount of initiator and 2 eq of BnOH, the lactide (1 g) was added and the flask heated for the specified time at 80 °C. For simplicity a catalyst loading of 1 mmol g^{-1} Het-$AlMe_2$ was assumed. The reaction was quenched by the addition of methanol (2 ml). ^{1}H NMR spectroscopy ($CDCl_3$) and GPC (THF) were used to determine tacticity and molecular weights (M_n and M_w) of the polymers produced; P_r (the probability of heterotactic linkages) were determined by analysis of the methine region of the homonuclear decoupled ^{1}H NMR spectra.

GPC analyses were performed on a Polymer Laboratories PL-GPC 50 integrated system using a PLgel 5 μm MIXED-D 300 x 7.5 mm column at 35 °C, using THF as the solvent at a flow rate of 1.0 mL/min. The polydispersity index (PDI) was determined from M_w/M_n, where M_n is the number average molecular weight and M_w is the weight average molecular weight. The polymers were referenced to 10 narrow molecular weight polystyrene standards with a range of M_w 615 – 568,000 Da. The equations used to calculate P_r are given by Coates *et al*.[218]

5.2. Chapter 2 Experimental

5.2.1. Silsesquioxane Ligand Synthesis

5.2.1.1. L-NH_2

1,3,5,7,9,11,14-heptaisobutyltricyclo[7.3.3.15,11]-heptasiloxane-endo-3,7,14-triol (1.5 g, 1.90 mmol) was dissolved in THF (20 ml) to which (3-aminopropyl)trimethoxysilane (0.34 g, 0.33 ml, 1.90 mmol) was added. The reaction mixture was stirred for 48 hours at 20 °C and the solvent was removed *in-vacuo*. The white residue was washed with cold MeCN (3 × 20 ml) to yield 1.52 g of a pure white precipitate L-NH_2 in 92 % yield.

^{1}H NMR (C_6D_6) 0.84 (m, 2H, Si-CH_2 tether, 14H, Si-CH_2), 1.08 (42H, m, CH_3), 1.63 (2H, m, CH_2 tether), 2.07 (7H, m, CH), 2.57 (2H, t J = 7 Hz, -C$\underline{H_2}$$NH_2$ tether).

^{13}C(^{1}H) NMR (C_6D_6) 10.1 (Si-CH_2, tether), 23.4 (CH_2, ^{i}butyl) 24.8 (CH, ^{i}butyl), 26.3 (CH_3, ^{i}butyl) 28.0 (CH_2, tether), 45.5 (C$\underline{H_2}$-NH_2 tether).

^{29}Si(^{1}H) NMR (C_6D_6) -66.3, -67.3, -67.4.

ESI-QTOF MS for $C_{31}H_{71}N_1O_{12}Si_8$+H 874.3203 found 874.3209.

5.2.1.2. $L^{H}OH$

The amine functionalised silsesquioxane L-NH_2 (1 g, 1.14 mmol) was dissolved in CH_2Cl_2 (20ml) to which salicylaldehyde (0.12 ml, 1.13 mmol) was added. The solution turned yellow and was left to stir for 2 hours. The solvent was removed *in-vacuo* and the yellow residue was washed with MeOH (5 × 30 ml) to yield 0.85 g of a pure yellow precipitate $L^{H}OH$ in a 77 % yield.

^{1}H NMR (C_6D_6) 0.84 (m, 2H, Si-CH_2 tether, 14H, Si-CH_2), 1.08 (42H, m, CH_3), 1.88 (2H, m, CH_2 tether), 2.07 (7H, m, CH), 3.21 (2H, t J = 7 Hz, -C<u>H</u>$_2$N) 6.67 (1H, m, Ar-H), 6.89 (1H, m, Ar-H), 7.07 (2H, m Ar-H), 7.76 (1H, s, C<u>H</u>=N), 13.58 (1H, s, OH).
$^{13}C(^{1}H)$ NMR (C_6D_6) 10.1 (Si-CH_2, tether), 23.4 (CH_2, ^{i}butyl) 24.8 (CH, ^{i}butyl), 25.2 (CH_2, tether) 26.3 (CH_3, ^{i}butyl), 62.5 (C<u>H</u>$_2$-N), 117.9 (Ar), 118.8 (Ar), 119.7 (Ar), 131.8 (Ar), 132.7 (Ar), 162.5 (C, Ar-OH), 165.6 (CH, C=N).

$^{29}Si(^{1}H)$ NMR (C_6D_6) -67.4, -67.1, -67.0.

ESI-QTOF MS calculated for $C_{38}H_{75}N_1O_{13}Si_8$+H 978.3465 found 978.3445.

5.2.1.3. $L^{tBu}OH$

The amine functionalised silsesquioxane L-NH_2 (1 g, 1.14 mmol) was dissolved in CH_2Cl_2 (20 ml) to which 3,5-di-*tert*-butyl-2-hydroxybenzaldehyde (0.27 g, 1.15 mmol) was added. The solution turned yellow and was left to stir for 2 hours. The solvent was removed *in-vacuo* and the yellow residue was washed with MeOH (5 × 30ml) to yield 0.90 g of a pure yellow precipitate $L^{tBu}OH$ in a 72 % yield.

^{1}H NMR (C_6D_6) 0.84 (m, 2H, Si-CH_2 tether, 14H, Si-CH_2), 1.08 (42H, m, CH_3), 1.32 (9H, s, C(C$\underline{H}_3$)$_3$), 1.63 (9H, s, C(C$\underline{H}_3$)$_3$) 1.88 (2H, m, CH_2), 2.07 (7H, m, CH), 3.27 (2H, t J = 7 Hz, -C$\underline{H}_2$N) 6.95 (1H, d J = 3 Hz, Ar-H), 7.55 (1H, d J = 3 Hz, Ar-H), 7.84 (1H, s, CH=N), 14.20 (1H, s, OH).

$^{13}C(^{1}H)$ NMR (C_6D_6) 10.8 (Si-CH_2, tether), 23.7 (CH_2, ^{i}butyl) 25.0 (CH, ^{i}butyl), 25.7 (CH_2, tether), 26.5 (CH_3, ^{i}butyl), 30.4 (CH_3, *tert*-butyl), 32.4 (CH_3, *tert*-butyl), 34.8 (C, *tert*-butyl), 36.1 (C, *tert*-butyl), 62.7 (CH_2-N), 119.2 (Ar), 127.0 (Ar), 127.4 (Ar), 137.8 (Ar), 140.6 (Ar), 159.6 (C, Ar-OH), 167.0 (CH, C=N).

$^{29}Si(^{1}H)$ NMR (C_6D_6) -67.5, -67.2, -66.9

ESI-QTOF MS calculated for $C_{46}H_{91}N_1O_{13}Si_8$+H 1090.4717 found 1090.4697.

5.2.1.4. $L^{Cl}OH$

The amine functionalised silsesquioxane L-NH_2 (1 g, 1.14 mmol) was dissolved in CH_2Cl_2 (20 ml) to which 3,5-dichloro-2-hydroxybenzaldehyde (0.22 g, 1.15 mmol) was added. The solution turned yellow and was left to stir for 2 hours. The solvent was removed *in-vacuo* and the yellow residue was washed with MeOH (5 × 30 ml) to yield 0.86 g of a yellow precipitate $L^{Cl}OH$ in a 71 % yield.

^{1}H NMR ($CDCl_3$) 0.57-0.71 (m, 2H, Si-CH_2 tether, 14H, Si-CH_2), 0.95 (42H, m, CH_3), 1.76-1.93 (m 2H, CH_2-tether, 7H, CH), 3.62 (2H, t J = 7 Hz, -C$\underline{H_2}$N) 7.12 (1H, d J = 3 Hz, Ar-H), 7.40 (1H, d J = 3 Hz, Ar-H), 8.20 (1H, s, C=N), 14.71 (1H, s, OH).

$^{13}C(^{1}H)$ NMR (C_6D_6) 10.6 (Si-CH_2, tether), 23.5 (CH_2, ^{i}butyl) 25.0 (CH, ^{i}butyl), 26.5 (CH_2, tether), 26.5 (CH_3, ^{i}butyl), 61.9 (CH_2-N), 120.5 (Ar), 123.1 (Ar), 123.8 (Ar), 129.7 (Ar), 132.8 (Ar), 157.6 (C, Ar-OH), 164.1 (CH, C=N).

$29Si(^{1}H)$ NMR (C_6D_6) -67.4, -67.3, -67.1

ESI-QTOF MS calculated for $C_{38}H_{73}Cl_2N_1O_{13}Si_8$+H 1048.2660 found 1048.2670.

5.2.2. Zinc (II) Homogeneous Complex Preparation

5.2.2.1. $Zn_4(L^HO)_4(OMe)_2Me_2$

Ligand L^HOH (0.5 g, 0.51 mmol) was dissolved in THF (20 ml) to which a 1M solution of $Zn(Me)_2$ in heptane (0.51 ml, 0.51 mmol) was added. The solution turned from yellow to clear and effervescence was observed. The reaction was stirred for 10 minutes at 298 K and the solvent was removed *in-vacuo* to yield a white residue. The residue was dissolved in hexane and crystallised to form 150 mg of white crystals of $Zn_4(L^HO)_4(OMe)_2Me_2$ in a 28 % yield.

^{1}H NMR (C_6D_6) 0.14 (6H, s, Zn-Me), 0.84 (56H, m, Si-CH_2, 6H, m, Si-CH_2 tether) 1.08 (168H, m, CH_3), 1.83 (4H, m, CH_2 tether), 2.09 (m, 28H, CH, 4H, CH_2 tether), 3.30 (6H, s, Zn-OCH_3) 3.50 (4H, m, C$\underline{H}_2$-N) 3.73 (4H, m, -C$\underline{H}_2$-N) 6.56 (4H, m, Ar-H), 7.02 (4H, m, Ar-H), 7.21 (4H, m, Ar-H), 7.59 (4H, m, Ar-H), 8.05 (4H, s, C=N).

^{13}C(^{1}H) NMR (C_6D_6) -13.2 (Zn-Me), 10.8 (Si-CH_2, tether), 23.6 (CH_2, ^{i}butyl) 25.0 (CH, ^{i}butyl), 25.1 (CH_2, tether), 26.5 (CH_3, ^{i}butyl), 53.3 (O-CH_3), 63.8 (CH_2-N), 116.5 (Ar), 120.9 (Ar), 122.0 (Ar), 134.7 (Ar), 136.4 (Ar), 168.1 (C, Ar-OH), 169.9 (CH, C=N).

^{29}Si(^{1}H) NMR (C_6D_6) -67.5 (3), -67.5 (1), -67.4 (3), -67.3 (1)

Calculated C 43.9 %, H 7.22 %, N 1.31% Found C 42.6 %, H 6.92 %, N 1.21 %.

5.2.2.2. $Zn(L^{H}O)_2$

Ligand $L^{H}OH$ (0.5 g, 0.51 mmol) was dissolved in THF (20ml) to which a 1M solution of $Zn(Me)_2$ in heptane (0.26 ml, 0.5 eq, 0.26 mmol) was added. The solution remained yellow and effervescence was observed. The reaction was stirred for 10 minutes at 298 K and the solvent was removed *in-vacuo* to yield a yellow residue. The residue was dissolved in hexane and crystallised to form 75 mg of pale yellow crystals of $Zn(L^{H}O)_2$ in a 14 % yield.

^{1}H NMR (C_6D_6) 0.69 (4H, t, J = 8Hz, Si-CH_2 tether) 0.83 (28H, m, Si-CH_2), 1.08 (84H, m, CH_3), 1.89 (4H, m, CH_2), 2.07 (14H, m, CH), 3.29 (4H, t J = 7 Hz, C$\underline{H}_2$-N) 6.55 (2H, m, Ar-H), 6.88 (1H, d, J = 1.5 Hz, Ar-H), 6.91 (1H, d, J = 1.5 Hz, Ar-H) 7.26 (4H, m Ar-H), 7.78 (2H, s, CH=N)

$^{13}C(^{1}H)$ NMR (C_6D_6) 10.3 (Si-CH_2, tether), 23.5 (CH_2, ^{i}butyl), 23.6 (CH_2, tether) 25.0 (CH, ^{i}butyl), 26.5 (CH_3, ^{i}butyl), 64.0 (CH_2-N), 114.8 (Ar), 118.9 (Ar), 124.8 (Ar), 135.9 (Ar), 136.6 (Ar), 172.2 (C, Ar-OH), 172.8 (CH, C=N).

$^{29}Si(^{1}H)$ NMR (C_6D_6) -67.4, -67.4, -67.2.

CHN – Calculated C 45.13%, H 7.32%, N 1.39% Found C 44.6%, H 7.15%, N 1.32%.

ESI-QTOF MS calculated for $C_{76}H_{148}N_2O_{26}Si_{16}Zn_1$+H 2021.5984 found 2021.5692.

5.2.2.3. $Zn_4(L^{H}O)_4(OEt)_2Et_2$

Unfortunately this could not be obtained in sufficient yield to be fully characterised. Despite prolonged exposure to air and significant recrystallisation efforts only $Zn(L^{H}O)_2$ could be isolated.

5.2.2.4. $Zn(L^{tBu}O)_2$

Ligand $L^{tBu}OH$ (0.46 g, 0.42 mmol) was dissolved in THF (20 ml) to which a 1M solution of $Zn(Me)_2$ in heptane (0.21 ml, 0.5eq, 0.21 mmol) was added. The solution remained yellow and effervescence was observed. The reaction was stirred for 10 minutes at 298 K and the solvent was removed *in-vacuo* to yield a yellow residue. The residue was dissolved in hexane and crystallised to form 90 mg pale yellow crystals of $Zn(L^{tBu}O)_2$ in a 20 % yield.

^{1}H NMR (C_6D_6) 0.83 (m, 4H, Si-CH_2 tether, 28H, Si-CH_2), 1.08 (84H, m, CH_3), 1.39 (18H, s, C($C\underline{H}_3)_3$), 1.73 (18H, s, C($C\underline{H}_3)_3$), 1.93 (4H, m, CH_2) 2.08 (m, 14H, CH,), 3.44 (4H, m, $C\underline{H}_2$-N) 6.89 (2H, d, J = 3Hz, Ar-H), 7.66 (2H, d, J = 3Hz, Ar-H), 7.97 (2H, s, CH=N)

^{13}C(^{1}H) NMR (C_6D_6) 10.3 (Si-CH_2, tether), 23.5 (CH_2, ^{i}butyl), 23.6 (CH_2, tether) 25.0 (CH, ^{i}butyl), 26.5 (CH_3, ^{i}butyl), 64.0 (CH_2-N), 114.8 (Ar), 118.9 (Ar), 124.8 (Ar), 135.9 (Ar), 136.6 (Ar), 172.2 (C, Ar-OH), 172.8 (CH, C=N).

^{29}Si(^{1}H) NMR (C_6D_6) -67.5, -67.4, -67.2

Calculated C 49.22 %, H 8.08 %, N 1.24 % Found C 48.5 %, H 8.11 %, N 1.24 %

ESI-QTOF MS calculated for $C_{92}H_{180}N_2O_{26}Si_{16}Zn_1$+H calc. 2245.8495 found 2245.9005

5.2.2.5. $Zn(L^{Cl}O)_2$

Ligand $L^{Cl}OH$ (0.2 g, 0.19 mmol) was dissolved in THF (20 ml) to which a 1M solution of $Zn(Me)_2$ in heptane (0.10 ml, 0.5 eq, 0.10 mmol) was added. The solution remained yellow and effervescence was observed. The reaction was stirred for 10 minutes at 298 K and the solvent was removed *in-vacuo* to yield a yellow residue. The residue was dissolved in hexane and crystallised to form 70 mg of pale yellow crystals of $Zn(L^{Cl}O)_2$ in a 32 % yield.

^{1}H NMR (C_6D_6) 0.71 (4H, m, Si-CH_2 tether), 0.83 (28H, m, Si-CH_2), 1.08 (84H, m, CH_3), 1.83 (4H, m, CH_2), 2.07 (14H, m, CH), 3.22 (4H, t, J = 7 Hz, -C$\underline{H}_2$N) 6.61 (2H, d J = 3 Hz, Ar-H), 7.34 (2H, s, CH=N), 7.45 (2H, d, J = 3 Hz, Ar-H).

$^{13}C(^{1}H)$ NMR (C_6D_6) 10.5 (Si-CH_2, tether), 23.6 (CH_2, ^{i}butyl) 25.0 (CH, ^{i}butyl), 26.5 (CH_2, tether), 26.6 (CH_3, ibutyl), 64.2 (CH_2-N), 118.4 (CH, Ar), 119.2 (CH, Ar), 133.7 (CH, Ar), 135.1 (CH, Ar), 165.1 (CH, C=N), 171.1 (C, Ar-O-Zn). 1 Aryl Carbon under solvent peak.

$^{29}Si(^{1}H)$ NMR (C_6D_6) -67.9, -67.4, -67.2

ESI-QTOF MS calculated for $C_{76}H_{144}Cl_4N_2O_{26}Si_{16}Zn_1$+H 2159.4396 found 2159.4060

5.2.3. Aluminium (III) Homogeneous Complex Preparation

5.2.3.1. $Al(L^{H}O)_2Me$

Ligand $L^{H}OH$ (0.978 g, 1 mmol) was dissolved in THF (10 ml) to which a 2M solution of $Al(Me)_3$ in heptane (0.25 ml, 0.50 mmol) was added. The solution turned from yellow to clear and effervescence was observed. The reaction was stirred for 1 hour at 298 K, heated to reflux, and the solvent was removed *in-vacuo* to yield a pale yellow residue. The residue was dissolved in hexane and crystallised to form 320 mg of a pale yellow crystalline solid, $Al(L^{H}O)_2Me$, in a 32 % yield.

^{1}H NMR (C_6D_6) -0.42 (s, 3H, Al-CH_3), 0.84 (m, 4H, Si-CH_2 tether, 28H, Si-CH_2), 1.06 (84H, m, CH_3), 2.07 (14H, m, CH), 2.37 (m, 4H, CH_2 tether), 3.47 (m, 2H, CH_2 tether), 3.83 (m, 2H, CH_2 tether), 6.65 (m, 2H, Ar-H), 6.89 (m, 2H, Ar-H), 7.10 (m, 2H, Ar-H), 7.31 (m, 2H, Ar-H), 7.68 (m, 2H, CH=N)

$^{13}C(^{1}H)$ NMR (C_6D_6) 2.0 (Al-CH_3) 11.2 (Si-CH_2, tether), 23.6 (CH_2, ^{i}butyl), 25.0 (CH, ^{i}butyl), 25.0 (Si-CH_2, tether), 26.5 (CH_3, ^{i}butyl), 60.8 (CH_2-N), 68.4 (CH_2-N), 117.4 (Ar), 121.1 (Ar), 122.2 (Ar), 134.0 (Ar), 135.1 (Ar), 165.2 (C, Ar-O), 167.5 (CH, C=N).

$^{29}Si(^{1}H)$ NMR (C_6D_6) -67.4, -67.2, -67.1

Calculated C 46.3 %, H 7.62 %, N 1.40 % Found C 45.2 %, H 7.52 %, N 1.42 %

5.2.3.2. Al(L^{tBu}O)Me_2

Ligand L^{tBu}OH (0.26 g, 0.24 mmol) was dissolved in THF (10 ml) to which a 2M solution of $Al(Me)_3$ in heptane (0.12 ml, 0.24 mmol) was added. The solution turned from yellow to clear and effervescence was observed. The reaction was stirred for 1 hour at 298 K, heated to reflux, and the solvent was removed *in-vacuo*. The residue was dissolved in hexane and crystallised to form 130 mg of a white crystalline solid, Al(L^{tBu}O)Me, in a 47 % yield.

^{1}H NMR (C_6D_6) -0.25 (s, 6H, Al-CH_3), 0.85 (m, 2H, Si-CH_2 tether, 14H, Si-CH_2), 1.06 (42H, m, CH_3), 1.30 (9H, s, CH_3), 1.57 (9H, s, CH_3), 1.87 (m, 2H, CH_2 tether), 2.07 (7H, m, CH), 3.12 (m, 2H, CH_2 tether), 6.74 (m, 1H, Ar-H), 7.32 (m, 1H, Ar-H), 7.66 (m, 2H, CH=N).

^{13}C(^{1}H) NMR (C_6D_6) 2.0 (Al-CH_3) 10.7 (Si-CH_2, tether), 23.6 (CH_2, ^{i}butyl), 25.0 (Si-CH_2, tether), 25.0 (CH, ^{i}butyl), 26.5 (CH_3, ^{i}butyl), 30.2 (CH_3, *tert*-butyl), 32.1 (CH_3, *tert*-butyl), 34.7 (CH_3, *tert*-butyl), 36.2 (CH_3, *tert*-butyl), 60.5 (CH_2-N), 119.5 (Ar), 129.5 (Ar), 132.2 (Ar), 139.4 (Ar), 141.4 (Ar), 162.6 (Ar), 172.4 (CH, C=N).

^{29}Si(^{1}H) NMR (C_6D_6) -67.5, -67.4, -67.2, -67.1

CHN – calculated C 50.3 %, H 8.44 %, N 1.22 % found C 45.7 %, H 8.18 %, N 1.04 %

5.2.3.3. $Al(L^{Cl}O)_2Me$

Ligand $L^{Cl}OH$ (1.05 g, 1 mmol) was dissolved in THF (10 ml) to which a 2M solution of $Al(Me)_3$ in heptane (0.25 ml, 0.50 mmol) was added. The solution turned from yellow to clear and effervescence was observed. The reaction was stirred for 1 hour at 298 K, heated to reflux, and the solvent was removed *in-vacuo* to yield 350 mg of a pale yellow residue of $Al(L^{Cl}O)_2Me$ in a 33 % yield.

^{1}H NMR (C_6D_6) -0.44 (s, 3H, Al-CH_3), 0.85 (m, 4H, Si-CH_2 tether) (28H, m, Si-CH_2), 1.06 (84H, m, CH_3), 2.07 (14H, m, CH) (m, 4H, CH_2 tether), 3.72 (m, 2H, CH_2 tether), 4.15 (m, 2H, CH_2 tether), 6.49 (m, 2H, Ar-H), 6.89 (m, 2H, Ar-H), 7.30 (m, 2H, Ar-H), 7.32 (s, 2H, CH=N)

$^{13}C(^{1}H)$ NMR (C_6D_6) 1.8 (Al-CH_3) 10.9 (Si-CH_2, tether), 23.4 (CH_2, ^{i}butyl), 24.6 (Si-CH_2, tether), 24.8 (CH, ^{i}butyl), 26.3 (CH_3, ^{i}butyl), 60.1 (CH_2-N), 121.4 (Ar), 121.8 (Ar), 126.7 (Ar), 131.5 (Ar), 134.1 (Ar), 158.0 (Ar), 165.2 (CH, C=N).

$^{29}Si(^{1}H)$ NMR (C_6D_6) -67.5, -67.4, -67.1

Calculated C 43.3 %, H 6.94 %, N 1.31 % Found C 41.9%, H 6.77%, N 1.31 %

5.2.4. Preparation of Heterogeneous Systems

5.2.4.1. Si-NH_2

SiO_2 (pore diameter 60 Å, Davisil) was dried at 130 °C under vacuum for 5 h. The dried silica (5 g) was added to methanol (20 ml) to give a suspension to which (3-aminopropyl)trimethoxysilane (0.87 ml, 0.90 g, 5 mmol) was added and stirred vigorously for 24 h. The reaction mixture was filtered and washed with copious methanol and the solid dried under vacuum at 80 °C for 5 h to yield the amine functionalised silica.

Found C 4.45 %, H 1.30 %, N 1.56 %.

5.2.4.2. Si-$L^{H}OH$

The dry amine functionalised silica (1 g) was suspended in methanol (20 ml) to which salicylaldehyde was added (0.11 ml, 0.12 g, 1 mmol). The suspension was stirred vigorously for 24 h after which it was filtered and the solid washed with copious amounts of methanol. The resulting solid was dried under vacuum at 80 °C for 5 h.

5.2.4.3. Si-$L^{tBu}OH$

The dry amine functionalised silica was suspended in methanol (20 ml) to which 3,5-di-tert-butyl-2-hydroxybenzaldehyde was added (0.23 g, 1 mmol). The suspension was stirred vigorously for 24 h after which it was filtered and the solid washed with copious amounts of methanol. The resulting solid was dried under vacuum at 80 °C for 5 h. The material was characterised via solid state NMR spectroscopy.

5.2.4.4. Si-$L^{Cl}OH$

The dry amine functionalised silica was suspended in methanol (20 ml) to which 3,5-dichloro-2-hydroxybenzaldehyde was added (0.19 g, 1 mmol). The suspension was stirred vigorously for 24 h after which it was filtered and the solid washed with copious amounts of methanol. The resulting solid was dried under vacuum at 80 °C for 5 h to yield ligand. The material was characterised via solid state NMR spectroscopy.

5.2.4.5. Preparation of heterogeneous Zinc(II) complexes

In a typical procedure the silica ligand (0.50 g) was suspended in dry THF (10 ml) to which a 1M solution of $ZnMe_2$ in heptane (0.50 ml, 0.5 eq, 0.50 mmol) was added. The solid product was washed 3 times with dry THF (10 ml) to yield a zinc(II) complex.

5.2.4.6. Preparation of heterogeneous Aluminium(III) complexes

In a typical procedure the silica ligand (0.50 g) was suspended in dry THF (10 ml) to which a 2M solution of $AlMe_3$ in heptane (0.25 ml, 0.5 eq, 0.50 mmol) was added. The solid product was washed 3 times with dry THF (10 ml) to yield an aluminium(III) complex.

5.2.5. Chapter 2 Crystal Data

5.2.5.1. $Zn_4(L^HO)_4(OMe)_2Me_2$

Empirical formula	$C_{39}H_{77}N_1O_{13.50}Si_8Zn_1$
Formula weight	1066.11
Temperature	150(2) K
Wavelength	0.71073 Å
Crystal system, space group	Triclinic, *P*-1
Unit cell dimensions	a = 16.5280(8) Å α= 67.289(3) º
	b = 17.9250(6) Å β= 79.143(2) º
	c = 22.1100(11) Å γ= 78.634(3) º
Volume	5878.2(5) $Å^3$
Z, Calculated density	4, 1.205 Mg/m^3
Absorption coefficient	0.633 mm^{-1}
F(000)	2272
Crystal size	0.20 × 0.10 × 0.10 mm
Theta range for data collection	3.65 to 25.06 º
Limiting indices	-19<=h<=19, -21<=k<=21, -26<=l<=26
Reflections collected / unique	50834 / 20434 [R(int) = 0.0805]
Completeness to θ = 25.06	98.0 %
Absorption correction	multi-scan
Max. and min. transmission	0.9395 and 0.8839
Refinement method	Full-matrix least-squares on F^2
Data / restraints / parameters	20434 / 2 / 1324
Goodness-of-fit on F^2	1.069
Final R indices [I>2σ(I)]	R_1 = 0.0766, wR_2 = 0.1898
R indices (all data)	R_1 = 0.1408, wR_2 = 0.2315
Largest diff. peak and hole	1.196 and -0.624 e.$Å^{-3}$

Isobutyls showed significant disorder:
Si(2) – groups disordered in a 75:25 ratio; Si(3) - groups disordered in a 50:50 ratio; Si(4) - groups disordered in a 65:35 ratio; Si(6) - groups disordered in a 75:25 ratio.
Si(7) - groups disordered in a 60:40 ratio (in this case better convergence was observed in the CH_2 group was not modelled over two positions and has an occupancy

of 1). Si(10) - groups disordered in a 50:50 ratio; Si(13) - groups disordered in a 75:25 ratio.

Fractional disordered atoms with occupancies less than 50% were treated isotropically. Some C-C and Si…C restraints were included in some disordered groups to assist convergence. ADP restraints were also included for C58, C70 and C73.

5.2.5.2. $Zn_4(L^HO)_4(OEt)_2Et_2$

Empirical formula	$C_{40}H_{79}N_1O_{13.50}Si_8Zn_1$
Formula weight	1080.13
Temperature	150(2) K
Wavelength	0.71073 Å
Crystal system, space group	Triclinic, *P*-1
Unit cell dimensions	a = 16.4370(12) Å α= 67.732(3) º
	b = 18.3800(15) Å β= 79.022(3) º
	c = 21.8890(14) Å γ= 77.307(4) º
Volume	5928.0(8) $Å^3$
Z, Calculated density	4, 1.210 Mg/m^3
Absorption coefficient	0.628 mm^{-1}
F(000)	2304
Crystal size	0.20 × 0.10 × 0.10 mm
Theta range for data collection	3.64 to 25.06 º
Limiting indices	-19<=h<=19, -19<=k<=21, -26<=l<=26
Reflections collected / unique	67487 / 20747 [R(int) = 0.0756]
Completeness to θ = 25.06	98.7 %
Absorption correction	None
Max. and min. transmission	0.9399 and 0.8847
Refinement method	Full-matrix least-squares on F^2
Data / restraints / parameters	20747 / 6 / 1438
Goodness-of-fit on F^2	1.050
Final R indices [I>2σ(I)]	R_1 = 0.0828, wR_2 = 0.2220
R indices (all data)	R_1 = 0.1316, wR_2 = 0.2747
Largest diff. peak and hole	1.297 and -0.554 $e.Å^{-3}$

In this case one silsesquioxane cube {Si(9) to Si(23)} and associated isobutyl groups were modelled over two positions in a 50:50 ratio. However, for the isobutyl group adorning Si(14) and Si(15) better convergence was observed when the methyl carbon (C76) was shared. Also, for the isobutyl group adorning Si(18) and Si(19) better convergence was observed when the methyl carbon (C63) was shared.

Carbon atoms in disordered isobutyl groups were treated isotropically in this structure, as the electron density associated with these regions in the electron density map was quite smeared. A number of C-C, Si…C and C…C restraints were necessitated, in order to stabilize the refinement. Other fractional carbons atoms in the disordered isobutyl based C53' could not be located with any credibility, and hence were omitted from the refinement.

For the non-disordered silsesquioxane Si(1) to Si(8) carbon atoms of the isobutyl groups connected to the following silicon atoms were disordered:
Si(2) - groups disordered in a 50:50 ratio; Si(5) - groups disordered in a 60:40 ratio; Si(7) - groups disordered in a 60:40 ratio; Si(8) - groups disordered in a 60:40 ratio.

5.2.5.3. $Zn_4(L^HO)_2$

Empirical formula	$C_{38}H_{74}N_{0.5}O_{13}Si_8Zn_{0.50}$
Formula weight	1010.39
Temperature	150(2) K
Wavelength	0.71073 Å
Crystal system, space group	Triclinic, *P*-1
Unit cell dimensions	a = 10.8690(1) Å α= 107.998(1) º
	b = 19.6260(3) Å β= 98.256(1) º
	c = 28.1330(4) Å γ= 92.026(1) º
Volume	5628.09(13) $Å^3$
Z, Calculated density	4, 1.192 Mg/m^3
Absorption coefficient	0.450 mm^{-1}
F(000)	2160
Crystal size	0.20 × 0.15 × 0.10 mm
Theta range for data collection	3.53 to 27.49 º
Limiting indices	-14<=h<=14, -25<=k<=24, -36<=l<=36
Reflections collected / unique	85665 / 25433 [R(int) = 0.0547]
Completeness to θ = 27.49	98.4 %
Absorption correction	multi-scan
Max. and min. transmission	0.9564 and 0.9153
Refinement method	Full-matrix least-squares on F^2
Data / restraints / parameters	25433 / 4 / 1415
Goodness-of-fit on F^2	1.025
Final R indices [I>2σ(I)]	R_1 = 0.0709, wR_2 = 0.1952
R indices (all data)	R_1 = 0.1279, wR_2 = 0.2409
Largest diff. peak and hole	1.224 and -0.924 $e.Å^{-3}$

In this structure one silsesquioxane cube {Si(9) to Si(24)} and associated isobutyl groups were modelled over two positions in a 55:45 ratio. However, for the isobutyl group attached to partial silicon Si(23) and Si(24), optimal convergence was observed when the isobutyl group was modelled in one position with the alpha-carbon of said functionality equidistant from both Si(23) and Si(24). In contrast, for the isobutyl group attached to partial silicon Si(19) and Si(20), the best model invoked splitting of

the C(65) over 2 sites, and an absence of disorder for C(66)-C(68). This approach precluded the inclusion of a hydrogen at a calculated position on C(66). For the non-disordered silsesquioxane Si(1) to Si(8) carbon atoms of the isobutyl groups connected to the following silicon atoms were disordered:

Si(5) - groups disordered in a 80:20 ratio; Si(8) - groups disordered in a 50:50 ratio.

All atoms with occupancy greater than 20% were treated anisotropically. ADP restraints, as well as Si…C and C…C distance restraints were included as appropriate to assist convergence.

There was some evidence of a very small amount of diffuse solvent in a locus surrounding 0.39, 1.00, 0.44 in the asymmetric unit. However, the level of residual electron density was similar to spurious maxima at non-chemically significant distances from atoms in the silsesquioxane containing molecule. Thus, on balance, it was felt that SQUEEZE would not be appropriate in this case.

5.2.5.4. $Zn_4(L^{tBu}O)_2$

Empirical formula	$C_{47}H_{92.50}N_1O_{13.25}Si_8Zn_{0.50}$
Formula weight	1141.13
Temperature	100(2) K
Wavelength	1.54180 Å
Crystal system, space group	Triclinic, *P*-1
Unit cell dimensions	a = 16.9827(6) Å α= 103.387(3) º
	b = 18.6099(5) Å β= 94.555(3) º
	c = 21.6637(8) Å γ= 99.867(3) º
Volume	6511.3(4) $Å^3$
Z, Calculated density	4, 1.164 Mg/m^3
Absorption coefficient	2.174 mm^{-1}
F(000)	2458
Crystal size	0.20 × 0.10 × 0.10 mm
Theta range for data collection	3.19 to 62.27 º
Limiting indices	-19<=h<=19, -21<=k<=21, -24<=l<=24
Reflections collected / unique	34549 / 19675 [R(int) = 0.0558]
Completeness to θ = 62.27	95.2 %
Absorption correction	Semi-empirical from equivalents
Max. and min. transmission	1.00000 and 0.40734
Refinement method	Full-matrix least-squares on F^2
Data / restraints / parameters	19675 / 186 / 1583
Goodness-of-fit on F^2	1.360
Final R indices [I>2σ(I)]	R_1 = 0.1140, wR_2 = 0.3320
R indices (all data)	R_1 = 0.1530, wR_2 = 0.3718
Largest diff. peak and hole	1.058 and -0.756 $e.Å^{-3}$

One silsesquioxane {Si(1) – Si(8)} cube is disordered over two positions in a 75:25 ratio. Si(1) and Si(2) are common to both cubes and were hence refined with full site occupancies. The isobutyl groups are modelled over two positions for Si(6)/(6') and Si(7)/(7') in the same 75:25 ratio. The isobutyl groups bonded to the remaining silicon centres (each one listed below) were treated on individual merit – as follows:

Si(2): best convergence was observed when one full occupancy isobutyl group was modelled.
Si(3) and Si(3'): the electron density of the isobutyl was so smeared that no credible model could be constructed. Only C(40) and its disordered counterpart C(40') could be reliably included in the model.
Si(4) and Si(4'); best convergence was observed when one fully occupancy isobutyl group was modelled
Si(8) and Si(8'): optimal convergence was observed when the isobutyl group was refined at one site. This resulted in asymmetry between the Si(8)-C(60), and Si(8)'-C(60) distances. However, efforts to model the functionality based on C(60) over 2 sites were not successful.

The second silsesquioxane cube {Si(9) – Si(26)} was disordered over two positions in a 50:50 ratio. The isobutyl groups were – once again - poorly defined and consequently were treated on individual merit – as follows:

Si(10), Si(20) - CH_2 (C64/64') was modelled over 2 positions and $CH(CH_3)_2$ over one position. Si(11), Si(21) - CH_2 (C60) was modelled at 1 positions and $CH(CH_3)_2$ over two positions. Si(12), Si(22) - isobutyl group modelled over one position. Si(13), Si(23) – isobutyl group modelled over one position
Si(14), Si(24) - the electron density of the isobutyl was so smeared that no credible model could be constructed. Only C(80)-(82) and their disordered counterparts C(80)' and C(81') could be reliably included in the model.
Si(15), Si(25) - isobutyl group modelled over one position
Si(16), Si(26) - CH_2 (C88) was modelled over one position and $CH(CH_3)_2$ over two regions.

A considerable number of ADP and distance restraints were needed to assist convergence in this structure. Non-silicon atoms with occupancy of 25% were treated isotropically, as was a small fraction of solvent (modelled as ½ of a diethyl ether moiety) proximate to the inversion centre at 1, 0, 1.

C35 was also split over 2 sites – and modelled as such.

5.3. Chapter 3 Experimental

5.3.1. Ligand Synthesis

5.3.1.1. MeMe PhOH

To a solution of 2,4-pentanedione (2.0 g, 20 mmol) in absolute ethanol (30 ml) was added 2-aminophenol (2.18 g, 20 mmol). The reaction was heated to reflux, stirred for 2 hrs, then cooled to 20 °C after which pale yellow crystals formed. The precipitate was washed with EtOH (3 x 25 ml) to yield 2.66 g of a pale yellow crystalline solid, MeMe PhOH, in a 70 % yield.

^{1}H NMR ($CDCl_3$): δ 11.71 (1H, s, NH), 7.21 (1H, m, Ar-H), 6.95 (2H, m, Ar-H), 6.80 (1H, m, Ar-H), 5.12 (1H, s, C=CH), 2.00 (3H, s, CH_3), 1.75 (3H, s, CH_3)

$^{13}C\{^{1}H\}$ ($CDCl_3$): δ 196.2 (C=O), 163.5 (C=C-N), 152.5 (Ar C-OH), 128.8 (CH, Ar), 128.0 (CH, Ar), 125.3 (CH, Ar), 120.2 (CH, Ar), 117.3 (CH, Ar), 97.3 (C=CH), 28.6 (CH_3), 19.6 (CH_3).

ESI-TOF MS calculated for $C_{11}H_{14}N_1O_2+H^+$ 192.1019 found 192.1093

5.3.1.2. MeMe PhDIP

To a solution of 2,4-pentanedione (2.0 g, 20 mmol) in toluene was added 2,6-diisopropylaniline (3.54 g, 20 mmol) and a catalytic amount of *p*-toluenesulfonic acid. The solution was heated to reflux for 24 hours. The reaction was concentrated until an orange precipitate was formed which was collected, washed with cold ethanol (3 x 25 ml) and dried to yield 4.15 g of a white solid, MeMe PhDIP, in a 80 % yield. Analytical data was consistent with previously observed values.[203]

5.3.1.3. PhMe PhOH

To a solution of 1-Phenyl-1,3-butanedione (3.24 g, 20 mmol) in methanol (30 ml) was added 2-aminophenol (2.18 g, 20 mmol). The reaction was stirred for 24 hrs after which a yellow precipitate had formed. The product was filtered and washed with *n*-hexane (5 x 30 ml) to yield 2.61 g of a pure yellow solid, PhMe PhOH, in a 52 % yield.

^{1}H NMR ($CDCl_3$): δ 12.39 (1H, s, NH), 7.89 (2H, m, ArH), 7.45 (3H, m, Ar-H), 7.18 (1H, m, Ar-H), 7.03 (2H, m, Ar-H), 6.85 (1H, m, Ar-H), 5.67 (1H, s, C=CH), 1.63 (3H, s, CH_3).

^{13}C{^{1}H} NMR ($CDCl_3$): δ 188.3 (C=O), 165.4 (C=C-N), 152.3 (C-OH, Ar), 139.8 (CH, Ar), 130.8 (CH, Ar), 128.5 (CH, Ar), 128.2 (CH, Ar), 127.3 (CH, Ar), 127.2 (CH, Ar), 126.9 (CH, Ar), 125.1 (CH, Ar), 119.7 (CH, Ar), 117.3 (CH, Ar), 94.5 (C=CH), 19.7 (CH_3).

ESI-TOF MS calculated for $C_{16}H_{15}N_1O_2+H^+$ 254.1181 found 254.1192.

5.3.1.4. PhMe PhDIP

To a solution of 1-Phenyl-1,3-butanedione (3.24 g, 20 mmol) in methanol (30 ml) was added 2,6-diisopropylaniline (3.55 g, 3.78 ml, 20 mmol) and a catalytic amount of HCl. The reaction mixture was heated to reflux and stirred for 16 hrs after which the solvent was removed *in vacuo*. The solid product was dissolved in hot *n*-hexane and upon cooling white crystals formed. The product was filtered and washed with cold *n*-hexane (3 x 30 ml) to yield 3.83 g of a pure white crystalline solid, PhMe PhDIP, in a 60 % yield.

^{1}H NMR ($CDCl_3$): δ 12.57 (1H, s, NH), 7.89 (2H, m, Ar-H), 7.37 (3H, m, Ar-H), 7.24 (1H, m, Ar-H), 7.13 (2H, m, Ar-H), 5.86 (1H, s, C=CH), 3.01 (2H, m, CH-$(CH_3)_2$), 1.71 (3H, s, CH_3), 1.13 (12H, m, CH-$(CH_3)_2$).

^{13}C{^{1}H} NMR ($CDCl_3$): δ 188.5 (C=O), 165.2 (C=C-N), 146.3 (CH, Ar), 140.3 (CH, Ar), 140.1 (CH, Ar), 133.6 (CH, Ar), 132.5 (CH, Ar), 130.8 (CH, Ar), 128.5 (CH, Ar), 128.3 (CH, Ar), 127.2 (CH, Ar), 123.7 (CH, Ar), 122.8 (CH, Ar), 118.6 (CH, Ar), 92.3 (C=CH), 28.6 (CH-CH_3), 28.0 (CH-CH_3), 24.7 (CH-CH_3), 22.8 (CH-CH_3), 22.5 (CH-CH_3), 19.8 (CH_3).

ESI-TOF MS calculated for $C_{22}H_{27}N_1O_1$+H^+ 344.1990 found 344.1991.

5.3.1.5. PhMe EtOH

To a solution of 1-Phenyl-1,3-butanedione (3.24 g, 20 mmol) in methanol (30 ml) was added 2-aminoethanol (1.22 g, 1.20 ml, 20 mmol). The reaction was stirred for 24 hrs and the solvent was removed *in vacuo* to yield a white solid. The crude product was washed with *n*-hexane (5 x 30 ml) to yield 3.65 g of a pure yellow solid, PhMe EtOH, in a 68 % yield.

^{1}H NMR ($CDCl_3$): δ 11.48 (1H, s, OH), 7.84 (2H, m, Ar-H), 7.41 (3H, m, Ar-H), 5.64 (1H, s, C=CH), 3.80 (2H, m, CH_2OH), 3.65 (1H, m, NH), 3.46 (2H, q, J = 5.5 Hz, CH_2), 2.00 (3H, s, CH_3).

$^{13}C\{^{1}H\}$ NMR ($CDCl_3$): δ 187.6 (C=O), 165.8 (C=**C**-N), 140.4 (CH, Ar), 130.5 (CH, Ar), 128.2 (CH, Ar), 126.9 (CH, Ar) 92.6 (C=**C**H), 61.5 (CH_2-OH), 45.7 (N-CH_2), 19.5 (CH_3).

ESI-TOF MS calculated for $C_{12}H_{15}N_1O_2+H^+$ 206.1181 found 206.1209

5.3.1.6. PhPh PhOH

To a solution of 1,3-Diphenyl-1,3-propanedione (2.24 g, 10 mmol) in absolute ethanol (20 ml) was added 2-aminophenol (1.09 g, 10 mmol). The reaction was heated to reflux and stirred for 72 hrs. The solvent was removed *in vacuo* and the product was recrystallised from methanol to yield 0.40 g of crystalline yellow solid, PhPh PhOH, in a 13 % yield.

^{1}H NMR ($(CD_3)_2SO$): δ 12.65 (1H, s, NH) 10.09 (1H, s, Ar-OH), 7.99 (2H, m, ArH), 7.38-7.57 (8H, m, Ar-H), 6.87 (2H, m, ArH), 6.44 (1H, m, ArH), 6.28 (1H, m, ArH), 6.12 (1H, s, C=CH)

$^{13}C\{^{1}H\}$ NMR ($CDCl_3$) 189.9 (C=O), 163.0 (C=C-N), 149.6 (Ar C-OH), 140.0 (CH, Ar), 131.4 (CH, Ar), 129.8 (CH, Ar), 128.5 (CH, Ar), 128.4 (CH, Ar), 128.0 (CH, Ar), 127.4 (CH, Ar), 126.1 (CH, Ar), 125.2 (CH, Ar), 121.5 (CH, Ar), 119.9 (CH, Ar), 116.0 (CH, Ar), 97.3 (C=CH).

ESI-TOF MS calculated for $C_{21}H_{17}N_1O_2+H^+$ 316.1337 found 316.1316.

5.3.1.7. PhPh Ph^{tBu}OH

To a solution of 1,3-Diphenyl-1,3-propanedione (2.24 g, 10 mmol) in absolute ethanol (20 ml) was added 2-amino-4-tert-butylphenol (0.825 g, 5 mmol). The reaction was heated to reflux and stirred for 72 hrs. The solvent was removed *in vacuo* and the crude product was washed with hexane (5x 30 ml) and purified by column chromatography using DCM / MeOH (0-5%) as an eluent. The fractions were combined and the solvent removed *in vacuo* to 0.64 g of a yellow solid, PhPh Ph^{tBu}OH, in a 35 % yield.

^{1}H NMR ($CDCl_3$): δ 12.78 (1H, s, NH), 8.14 (1H, s, Ar-H), 7.90 (2H, m, Ar-H), 7.39 (3H, m, Ar-H), 7.21 (3H, m, Ar-H), 6.75 (2H, m, Ar-H), 6.30 (1H, d, J = 2.0 Hz, Ar-H), 6.02 (1H, s, Ar-H), 5.21 (1H, s, C=CH), 0.82 (9H, s, C_3H_9)

^{13}C{^{1}H} NMR ($CDCl_3$): δ 189.4 (C=O), 162.6 (C=C-N), 147.0 (Ar C-OH), 142.2 (CH, Ar), 140.2 (CH, Ar), 136.0 (CH, Ar), 131.2 (CH, Ar), 129.5 (CH, Ar), 128.5 (CH, Ar), 128.4 (CH, Ar), 128.4 (CH, Ar), 128.1 (CH, Ar), 127.4 (CH, Ar), 126.2 (CH, Ar), 122.1 (CH, Ar), 122.0 (CH, Ar), 115.3 (CH, Ar), 97.0 (C=CH), 33.7 (C-C_3H_9), 31.0 (C-C_3H_9).

ESI-TOF MS calculated for $C_{25}H_{25}N_1O_2$+H^+ 372.1963 found 372.1987.

5.3.2. Zinc Complex Preparation

5.3.2.1. (MeMe PhO)$_2$Zn

To a solution of MeMe PhOH (0.38 g, 2 mmol) in toluene (15 ml) dimethylzinc (1.0 ml, 1M in heptane, 1.0 mmol) was added dropwise. The reaction was heated to 100°C and stirred for 4 hours after which a yellow precipitate formed. The solvent was removed by cannula filtration at 100 °C to yield 0.15g of a pure yellow solid, MeMe PhOH, in a 53 % yield.

^{1}H NMR ((CD$_3$)$_2$SO): δ 6.97 (2H, m, Ar-H), 6.80 (1H, m, Ar-H), 6.47 (1H, m, Ar-H), 4.90 (1H, s, C=CH), 2.13 (3H, s, CH$_3$), 1.93 (3H, s, CH$_3$)

^{13}C{^{1}H} NMR ((CD$_3$)$_2$SO): 182.2 (C=O) 167.3 (C=**C**-N), 156.7 (C-O, Ar), 136.6 (CH, Ar), 124.1 (CH, Ar), 121.6 (CH, Ar), 117.7 (CH, Ar), 110.4 (CH, Ar), 98.5 (CH, Ar), 28.3 (CH$_3$), 23.3 (CH$_3$).

5.3.2.2. (MeMe PhDIP)ZnMe

To a solution of MeMe PhDIP (0.26 g, 1 mmol) in toluene (15 ml) dimethylzinc (1.0 ml, 1M in heptane, 1.0 mmol) was added dropwise. The reaction was stirred for 1 hour, heated to reflux and allowed to cool after which a white precipitate formed. The solvent was removed by cannula filtration to yield 0.26 g of a pure yellow solid, (MeMe PhDIP)ZnMe, in a 77 % yield.

^{1}H NMR (C$_6$D$_6$): δ **7**.20 (3H, m, Ar-H), 5.13 (1H, s, C=C-H,), 3.23 (2H, m, C<u>H</u>-CH$_3$), 1.99 (3H, s, CH$_3$), 1.60 (3H, s, CH$_3$), 1.37 (3H, s, CH$_3$), 1.35 (3H, s, CH$_3$), 1.23 (3H, s, CH$_3$), 1.21 (3H, s, CH$_3$), -0.20 (3H, s, Zn-CH$_3$),

^{13}C{^{1}H} NMR (C$_6$D$_6$): 183.32 (C=O), 173.61 (C=<u>C</u>-N), 143.5 (CH, Ar), 141.8 (CH, Ar), 126.8 (CH, Ar), 124.5 (CH, Ar), 99.5 (C=CH), 28.6 (CH), 27.9 (CH), 24.7 (CH$_3$), 24.4 (CH$_3$), 23.5 (CH$_3$), -16.5 (Zn-CH3)

5.3.2.3. (PhMe PhO)Zn

To a solution of 3-((2-hydroxyphenyl)amino)-1-phenylbut-2-en-1-one (0.72 g, 3 mmol) in toluene (10 ml) dimethylzinc (3 ml, 1M in heptane, 3 mmol) was added dropwise. The reaction was stirred at 20 °C for 1 hour after which time it was heated to reflux and allowed to cool. A yellow precipitate formed which was separated by cannula filtration and dried in vacuo to yield 0.75 g of a yellow solid, (PhMe PhO) Zn, in a 66 % yield.

^{1}H NMR ($(CD_3)_2SO$): δ 7.92 (2H, m, Ar-H), 7.41 (3H, m, Ar-H), 7.20 (1H, m, Ar-H), 7.06 (1H, m, Ar-H), 6.84 (1H, m, Ar-H), 6.50 (1H, m, Ar-H), 5.68 (1H, s, C=CH), 2.33 (3H, s, CH3).

^{13}C{^{1}H} NMR ($(CD_3)_2SO$) 353 K : δ 175.0 (C=O), 167.5 (C=C-N), 157.2 (C-O, Ar), 141.5 (CH, Ar), 136.2 (CH, Ar), 128.6 (CH, Ar), 128.5 (CH, Ar), 127.7 (CH, Ar), 127.5 (CH, Ar), 126.0 (CH, Ar), 124.1 (CH, Ar), 121.2 (CH, Ar), 117.4 (CH, Ar), 113.7 (CH, Ar), 96.2 (C=CH), 23.4 (CH3).

CHN – Calculated C 60.5 %, H 4.44 %, N 4.41 % Found C 60.3 %, H 4.20 %, N 4.20 %.

5.3.2.4. (PhMe EtO)Zn

To a solution of 3-((2-hydroxyethyl)amino)-1-phenylbut-2-en-1-one (0.57 g, 3 mmol) in toluene (10 ml) dimethylzinc (3 ml, 1M in heptane, 3 mmol) was added dropwise. The reaction was stirred at 20 °C for 1 hour after which time it was heated to reflux and allowed to cool. A white precipitate formed which was separated by cannula filtration and dried in vacuo to yield 0.60g of a white solid, PhMe EtOH Zn, in a 59% yield.

^{1}H NMR ($CDCl_3$): δ 7.84 (2H, m, Ar-H), 7.36 (3H, m, Ar-H), 5.52 (1H, s, C=CH), 4.16 (1H, m, CH_2), 3.96 (1H, m, CH_2), 3.66 (1H, m, CH_2), 3.32 (1H, m, CH_2), 2.12(3H, s, CH_3).

^{13}C{^{1}H} NMR ($CDCl_3$): δ 178.1 (C=O), 172.8 (C=C-N), 142.0 (CH, Ar), 129.1 (CH, Ar), 129.0 (CH, Ar), 128.2 (CH, Ar), 127.9 (CH, Ar), 125.3 (CH, Ar), 94.6 (C=CH), 63.7 (CH_2-O), 52.4 (CH_2), 23.3 (CH_3).

CHN – Calculated C 53.5 %, H 5.23 %, N 5.19 % Found C 53.3 %, H 4.82 %, N 5.11 %.

5.3.2.5. (PhMe PhDIP)ZnMe

To a solution of PhPh PhDIP (0.97 g, 3 mmol) in toluene (10 ml) dimethylzinc (3.0 ml, 1M in heptane, 3.0 mmol) was added dropwise. The reaction stirred for 1 hour, heated to reflux and allowed to cool after which a yellow precipitate formed. The solvent was removed by cannula filtration to yield 0.65 g of a pure yellow solid, (PhMe PhDIP)ZnMe, in a 54 % yield.

^{1}H NMR (C_6D_6): δ 7.95 (2H, m, Ar-H), 7.17 (6H, m, Ar-H), 5.94 (1H, s, C=CH), 2.33 (3H, s, CH_3), 3.14 (2H, m, C**H**-$(CH_3)_2$), 1.62 (3H, s, CH_3), 1.16 (12H, m, CH-(C**H$_3$**)$_2$), -0.25 (3H, s, Zn-CH_3).

^{13}C{^{1}H} NMR (C_6D_6): δ 177.8 (C=O), 174.2 (C=**C**-N), 143.3 (CH, Ar), 141.4 (CH, Ar), 140.2 (CH, Ar), 130.3 (CH, Ar), 127.5 (CH, Ar), 126.6 (CH, Ar), 124.4 (CH, Ar), 96.6 (C=**C**H), 28.4 (**C**H-CH_3), 24.3 (**C**H-CH_3), 23.7 (CH-**C**H_3), 23.7 (CH-**C**H_3), -16.3 (Zn-CH_3)

CHN – Calculated C 68.9 %, H 7.29 %, N 3.49 % Found C 68.3 %, H 7.25 %, N 3.43 %.

5.3.2.6. (PhMe PhDIP)$_2$Zn

To a solution of PhPh PhDIP (0.97 g, 3 mmol) in toluene (10 ml) dimethylzinc (1.5 ml, 1M in heptane, 1.5 mmol) was added dropwise. The reaction stirred for 1 hour and heated to reflux. The solvent was removed *in vacuo* and the product dissolved in hot hexane. Upon cooling white crystals were formed and filtered to yield 0.34 g of a pure white solid, (PhMe PhDIP)$_2$Zn, in a 32 % yield.

^{1}H NMR ($CDCl_3$): δ 7.89 (2H, m, Ar-H), 7.00 (3H, m, Ar-H), 6.93 (3H, m, Ar-H), 5.61 (1H, s, C=CH), 1.51 (3H, s, CH_3), 1.06 (broad, 12H, m, CH-(C**H$_3$**)$_2$). A broad resonance is observed between 3.05 and 3.41 relating to C**H**-(CH_3)$_2$.

^{13}C{^{1}H} ($CDCl_3$): δ 179.5 (C=O), 175.1 (C=**C**-N), 165.0 (CH, Ar), 143.1 (CH, Ar), 140.8 (CH, Ar), 139.9 (CH, Ar), 128.5 (CH, Ar), 124.9 (CH, Ar), 122.9 (CH, Ar), 93.4 (C=**C**H), 26.8 (CH_3), 22.8 (CH), 22.5 (CH_3).

CHN – Calculated C 74.6 %, H 7.68 %, N 3.96 % Found C 75.0 %, H 7.74 %, N 3.93 %.

5.3.2.7. (PhPh PhO)Zn

To a solution of 3-((2-hydroxyphenyl)amino)-1,3-diphenylprop-2-en-1-one (0.20 g, 0.6 mmol) in toluene (5 ml) dimethylzinc (0.6 ml, 1M in heptane, 0.6 mmol) was added dropwise. The reaction turned deep red and was stirred at 20 °C for 1 hour. The solvent was removed *in vacuo* to yield 0.20g of a yellow solid, (PhPh PhO)Zn, in a 88% yield.

^{1}H NMR ($(CD_3)_2SO$): δ 7.77 (2H, m, ArH), 7.20 (8H, m, ArH), 7.00 (3H, m, ArH), 6.53 (1H, m, ArH), 5.85 (2H, m, ArH), 5.55 (1H, s, C=CH)

$^{13}C\{^{1}H\}$ NMR ($(CD_3)_2SO$): δ 178.1 (C=O) 168.5 (C=**C**-N), 157.2 (C-O, Ar), 141.6 (CH, Ar), 136.7 (CH, Ar), 130.1 (CH, Ar), 129.0 (CH, Ar), 128.8 (CH, Ar), 128.6 (CH, Ar), 127.7 (CH, Ar), 126.7 (CH, Ar), 124.3 (CH, Ar), 121.9 (CH, Ar), 118.5 (CH, Ar), 115.0 (CH, Ar), 97.6 (**C**=CH).

CHN – Calculated C 72.7 %, H 4.65 %, N 4.04 % Found C 72.3 %, H 5.08 %, N 4.49 %.

5.3.2.8. (PhPh Ph^{tBu}O)Zn

To a solution of 3-((5-(tert-butyl)-2-hydroxyphenyl)amino)-1,3-diphenylprop-2-en-1-one (0.37 g, 1 mmol) in THF (5 ml) dimethylzinc (1 ml, 1M in heptane, 1 mmol) was added dropwise. The solution turned deep red and was stirred at 20 °C for 1 hour after which time a red precipitate had formed. The solid product was filtered and dried *in vacuo* to yield 0.11g of a red solid, (PhPh Ph^{tBu}O)Zn, in a 25% yield.

^{1}H NMR ($(CD_3)_2SO$): δ 8.00 (2H, m, ArH), 7.45 (8H, m, ArH), 7.16 (1H, m, ArH), 6.79 (1H, m, ArH), 6.22 (1H, s, ArH), 5.79 (1H, s, C=CH), 0.89 (9H, s, C-CH_3).

^{13}C{^{1}H} NMR ($(CD_3)_2SO$): δ 177.6 (C=O) 167.8 (C=**C**-N), 154.5 (C-O, Ar), 141.5 (CH, Ar), 141.4 (CH, Ar), 136.4 (CH, Ar), 135.2 (CH, Ar), 129.6 (CH, Ar), 128.7 (CH, Ar), 128.2 (CH, Ar), 127.3 (CH, Ar), 126.5 (CH, Ar), 120.4 (CH, Ar), 110.4 (CH, Ar), 117.3 (CH, Ar), 97.1 (**C**=CH), 33.2 (**C**-CH_3) 31.1 (C-**C**H_3)

CHN – Calculated C 75.9 %, H 7.02 %, N 3.05 % Found C 74.6 %, H 6.67 %, N 3.21 %.

5.3.3. Chapter 3 Crystal Data

5.3.3.1. PhMe PhDIP

Empirical formula	$C_{22}H_{27}NO$
Formula weight	321.45
Temperature	150(2) K
Wavelength	0.71073 Å
Crystal system, space group	Monoclinic, $P2_1/c$
Unit cell dimensions	a = 6.452(1) Å α = 90 º
	b = 11.421(2) Å β = 95.834(1) º
	c = 25.2090(4) Å γ = 90 º
Volume	1847.99(5) $Å^3$
Z, Calculated density	4, 1.155 Mg/m^3
Absorption coefficient	0.070 mm^{-1}
F(000)	696
Crystal size	0.30 × 0.30 × 0.30 mm
Theta range for data collection	3.64 to 27.48 º
Limiting indices	-8<=h<=8, -14<=k<=14, -32<=l<=32
Reflections collected / unique	26205 / 4226 [R(int) = 0.0533]
Completeness to θ = 27.48	99.7 %
Absorption correction	None
Max. and min. transmission	0.9794 and 0.9794
Refinement method	Full-matrix least-squares on F^2
Data / restraints / parameters	4226 / 0 / 226
Goodness-of-fit on F^2	1.024
Final R indices [I>2σ(I)]	R_1 = 0.0459, wR_2 = 0.1093
R indices (all data)	R_1 = 0.0649, wR_2 = 0.1215
Largest diff. peak and hole	0.220 and -0.214 $e.Å^{-3}$

5.3.3.2. PhPh PhOH

Empirical formula	$C_{21}H_{17}NO_2$
Formula weight	315.36
Temperature	150(2) K
Wavelength	0.71073 Å
Crystal system, space group	Triclinic, *P-1*
Unit cell dimensions	a = 9.0120(2) Å α = 70.6470(10) º
	b = 10.1330(2) Å β = 81.7780(10) º
	c = 10.9010(2) Å γ = 63.7160(10)º
Volume	842.10(3) $Å^3$
Z, Calculated density	2, 1.244 Mg/m^3
Absorption coefficient	0.080 mm^{-1}
F(000)	332
Crystal size	0.10 × 0.10 × 0.10 mm
Theta range for data collection	3.68 to 27.49 º
Limiting indices	-11<=h<=11, -13<=k<=13, -14<=l<=14
Reflections collected / unique	18096 / 3833 [R(int) = 0.0349]
Completeness to θ = 27.49	99.2 %
Absorption correction	None
Max. and min. transmission	0.9920 and 0.9920
Refinement method	Full-matrix least-squares on F^2
Data / restraints / parameters	3833 / 0 / 219
Goodness-of-fit on F^2	1.005
Final R indices [I>2σ(I)]	R_1 = 0.0397, wR_2 = 0.1039
R indices (all data)	R_1 = 0.0474, wR_2 = 0.1106
Largest diff. peak and hole	0.204 and -0.242 $e.Å^{-3}$

5.3.3.3. PhPh Ph^{tBu}OH

Empirical formula	$C_{25.50}H_{25.50}Cl_{1.50}NO_2$
Formula weight	431.14
Temperature	150(2) K
Wavelength	0.71073 Å
Crystal system, space group	Orthorhombic, $P2_12_12_1$
Unit cell dimensions	a = 12.39500(10) Å α = 90 º
	b = 18.3440(2) Å β = 90 º
	c = 20.1330(3) Å γ = 90 º
Volume	4577.72(9) Å^3
Z, Calculated density	8, 1.251 Mg/m^3
Absorption coefficient	0.247 mm^{-1}
F(000)	1816
Crystal size	0.10 × 0.10 × 0.10 mm
Theta range for data collection	3.61 to 27.48 º
Limiting indices	-16<=h<=16, -23<=k<=23, -26<=l<=26
Reflections collected / unique	81673 / 10442 [R(int) = 0.0729]
Completeness to θ = 27.48	99.5 %
Absorption correction	None
Max. and min. transmission	0.9758 and 0.9758
Refinement method	Full-matrix least-squares on F^2
Data / restraints / parameters	10442 / 0 / 563
Goodness-of-fit on F^2	1.047
Final R indices [I>2σ(I)]	R_1 = 0.0677, wR_2 = 0.1771
R indices (all data)	R_1 = 0.0852, wR_2 = 0.1962
Largest diff. peak and hole	0.825 and -0.727 e.Å^{-3}

5.3.3.4. (MeMe PhDIP)ZnMe

Empirical formula	$C_{18}H_{27}NOZn$
Formula weight	338.78
Temperature	150(2) K
Wavelength	0.71073 Å
Crystal system, space group	Monoclinic, $P2_1/n$
Unit cell dimensions	a = 11.4270(2) Å α = 90 º
	b = 10.3060(2) Å β = 104.4910(10) º
	c = 15.6740(3) Å γ = 90 º
Volume	1787.15(6) $Å^3$
Z, Calculated density	4, 1.259 Mg/m^3
Absorption coefficient	1.373 mm^{-1}
F(000)	720
Crystal size	0.43 × 0.30 × 0.25 mm
Theta range for data collection	3.22 to 27.53 º
Limiting indices	-14<=h<=14, -13<=k<=13, -20<=l<=20
Reflections collected / unique	19054 / 4082 [R(int) = 0.0426]
Completeness to θ = 27.53	99.3 %
Absorption correction	None
Max. and min. transmission	0.7252 and 0.5897
Refinement method	Full-matrix least-squares on F^2
Data / restraints / parameters	4082 / 0 / 198
Goodness-of-fit on F^2	1.056
Final R indices [I>2σ(I)]	R_1 = 0.0247, wR_2 = 0.0610
R indices (all data)	R_1 = 0.0294, wR_2 = 0.0637
Largest diff. peak and hole	0.337 and -0.330 $e.Å^{-3}$

5.3.3.5. (PhMe PhO)Zn-DMSO

Empirical formula	$C_{43}H_{46}N_2O_6S_2Zn_2$
Formula weight	881.68
Temperature	150(2) K
Wavelength	0.71073 Å
Crystal system, space group	Monoclinic, $P2_1/c$
Unit cell dimensions	a = 14.3560(7) Å α = 90 º
	b = 7.4210(5) Å β = 95.344(5) º
	c = 37.413(3) Å γ = 90 º
Volume	3968.6(4) $Å^3$
Z, Calculated density	4, 1.476 Mg/m^3
Absorption coefficient	1.365 mm^{-1}
F(000)	1832
Crystal size	0.20 × 0.10 × 0.05 mm
Theta range for data collection	3.71 to 25.03 º
Limiting indices	-17<=h<=17, -8<=k<=8, -44<=l<=44
Reflections collected / unique	31344 / 6784 [R(int) = 0.0763]
Completeness to θ = 25.03	96.7 %
Absorption correction	multi-scan
Max. and min. transmission	0.9349 and 0.7719
Refinement method	Full-matrix least-squares on F^2
Data / restraints / parameters	6784 / 0 / 530
Goodness-of-fit on F^2	1.042
Final R indices [I>2σ(I)]	R_1 = 0.0465, wR_2 = 0.1215
R indices (all data)	R_1 = 0.0810, wR_2 = 0.1377
Largest diff. peak and hole	1.545 and -0.713 $e.Å^{-3}$

5.3.3.6. (PhMe EtO)Zn

Empirical formula	$C_{48}H_{58}N_4O_8Zn_4$
Formula weight	1074.42
Temperature	150(2) K
Wavelength	0.71073 Å
Crystal system, space group	Tetragonal, *I*-4
Unit cell dimensions	a = 18.2570(2) Å α = 90 º
	b = 18.2570(2)Å β = 90 º
	c = 7.80800(10) Å γ = 90 º
Volume	2602.55(5) $Å^3$
Z, Calculated density	2, 1.371 Mg/m^3
Absorption coefficient	1.872 mm^{-1}
F(000)	1104
Crystal size	0.12 × 0.06 × 0.06 mm
Theta range for data collection	3.61 to 27.47 º
Limiting indices	-23<=h<=23, -23<=k<=23 -10<=l<=10
Reflections collected / unique	19506 / 2975 [R(int) = 0.0406]
Completeness to θ = 27.47	99.1 %
Max. and min. transmission	0.8960 and 0.8065
Refinement method	Full-matrix least-squares on F^2
Data / restraints / parameters	2975 / 0 / 146
Goodness-of-fit on F^2	1.062
Final R indices [I>2σ(I)]	R_1 = 0.0268, wR_2 = 0.0822
R indices (all data)	R_1 = 0.0309, wR_2 = 0.0842
Largest diff. peak and hole	0.608 and -0.821 $e.Å^{-3}$

5.3.3.7. (PhMe PhDIP)ZnMe

Empirical formula	$C_{26.50}H_{33}NOZn$
Formula weight	446.91
Temperature	150(2) K
Wavelength	0.71073 Å
Crystal system, space group	Triclinic, *P*-1
Unit cell dimensions	a = 10.76200(10) Å α = 107.1920(10) °
	b = 10.87800(10) Å β = 101.4740(10) °
	c = 11.8240(2) Å γ = 110.1030(10) °
Volume	1170.07(3) $Å^3$
Z, Calculated density	2, 1.268 Mg/m^3
Absorption coefficient	1.066 mm^{-1}
F(000)	474
Crystal size	0.20 × 0.20 × 0.17 mm
Theta range for data collection	3.31 to 27.43 º
Limiting indices	-13<=h<=13, -14<=k<=14, -15<=l<=15
Reflections collected / unique	22204 / 5276 [R(int) = 0.0364]
Completeness to θ = 27.43	98.9 %
Absorption correction	None
Max. and min. transmission	0.8395 and 0.8150
Refinement method	Full-matrix least-squares on F^2
Data / restraints / parameters	5276 / 0 / 292
Goodness-of-fit on F^2	1.054
Final R indices [I>2σ(I)]	R_1 = 0.0260, wR_2 = 0.0666
R indices (all data)	R_1 = 0.0283, wR_2 = 0.0679
Largest diff. peak and hole	0.325 and -0.420 $e.Å^{-3}$

5.3.3.8. (PhMe PhDIP)$_2$Zn

Empirical formula	$C_{44}H_{51}N_2O_2Zn$
Formula weight	705.24
Temperature	150(2) K
Wavelength	0.71073 Å
Crystal system, space group	Monoclinic, $P2_1/n$
Unit cell dimensions	a = 11.95000(10) Å α = 90 °
	b = 23.4250(10) Å β = 96.84 °
	c = 16.33200(2) Å γ = 90 °
Volume	4539.29(6) Å^3
Z, Calculated density	4, 1.032 Mg/m^3
Absorption coefficient	0.573 mm^{-1}
F(000)	1500
Crystal size	0.20 × 0.13 × 0.08 mm
Theta range for data collection	7.86 to 25.04 º
Limiting indices	-14<=h<=14, -27<=k<=27, -19<=l<=19
Reflections collected / unique	58583 / 7761 [R(int) = 0.0498]
Completeness to θ = 25.04	96.6 %
Absorption correction	None
Max. and min. transmission	0.9583 and 0.8940
Refinement method	Full-matrix least-squares on F^2
Data / restraints / parameters	7761 / 0 / 452
Goodness-of-fit on F^2	1.039
Final R indices [I>2σ(I)]	R_1 = 0.0533, wR_2 = 0.1539
R indices (all data)	R_1 = 0.0603, wR_2 = 0.1601
Largest diff. peak and hole	1.711 and -0.431 e.Å^{-3}

5.3.3.9. (PhPh PhO)Zn

Empirical formula	$C_{25}H_{27}NO_4S_2Zn$
Formula weight	534.97
Temperature	150(2) K
Wavelength	0.71073 Å
Crystal system, space group	Triclinic, *P*-1
Unit cell dimensions	a = 7.5750(12) Å α = 79.276(/) °
	b = 13.846(3) Å β = 82.123(10) °
	c = 24.444(4) Å γ = 82.717(14) °
Volume	2481.7(7) $Å^3$
Z, Calculated density	4, 1.432 Mg/m^3
Absorption coefficient	1.189 mm^{-1}
F(000)	1112
Crystal size	0.10 × 0.05 × 0.10 mm
Theta range for data collection	3.51 to 25.00 º
Limiting indices	-8<=h<=9, -16<=k<=16, -28<=l<=29
Reflections collected / unique	15963 / 7854 [R(int) = 0.1039]
Completeness to θ = 25.00	90.0 %
Absorption correction	none
Refinement method	Full-matrix least-squares on F^2
Data / restraints / parameters	7854 / 0 / 605
Goodness-of-fit on F^2	1.018
Final R indices [I>2σ(I)]	R_1 = 0.0715, wR_2 = 0.1425
R indices (all data)	R_1 = 0.1526, wR_2 = 0.1841
Largest diff. peak and hole	0.488 and -0.644 $e.Å^{-3}$

5.3.3.10. (PhPh Ph^{tBu}O)Zn

Empirical formula	$C_{27}H_{29}NO_3SZn$
Formula weight	512.94
Temperature	150(2) K
Wavelength	0.71073 Å
Crystal system, space group	Triclinic, *P*-1
Unit cell dimensions	a = 6.8090(2) Å α = 103.911(2) °
	b = 13.5120(4) Å β = 95.761(2) °
	c = 14.4480(6) Å γ = 103.607(2) °
Volume	1236.59(7) Å^3
Z, Calculated density	2, 1.378 Mg/m^3
Absorption coefficient	1.106 mm^{-1}
F(000)	536
Crystal size	0.20 × 0.15 × 0.10 mm
Theta range for data collection	3.67 to 27.66 º
Limiting indices	-8<=h<=8, -17<=k<=17, -18<=l<=18
Reflections collected / unique	22511 / 22519 [R(int) = 0.000]
Completeness to θ = 27.66	97.7 %
Absorption correction	multi-scan
Max. and min. transmission	0.8975 and 0.8091
Refinement method	Full-matrix least-squares on F^2
Data / restraints / parameters	22519 / 0 / 304
Goodness-of-fit on F^2	1.073
Final R indices [I>2σ(I)]	R_1 = 0.0616, wR_2 = 0.1545
R indices (all data)	R_1 = 0.0768, wR_2 = 0.1651
Largest diff. peak and hole	0.753 and -0.926 e.Å^{-3}

5.4. Chapter 4 Experimental

5.4.1. Model Compound Synthesis

5.4.1.1. 1-(4-ethoxy-3-methoxyphenyl)ethanone (int**1**)

1-(4-ethoxy-3-methoxyphenyl)ethanone - To a solution of acetovanillone (9.96 g, 60 mmol, 1 eq.) in DMF (100 ml), K_2CO_3 (9.5 g, 69 mmol, 1.15 eq.) and ethyl iodide (7.25 ml, 90 mmol, 1.5 eq.) were added at 25 °C under magnetic stirring. After 2 h the reaction mixture was poured into hot water (250 ml). After cooling the precipitate was filtered and washed three times with n-hexane to give 1-(4-ethoxy-3-methoxyphenyl)ethanone in 88 % yield.

^{1}H NMR ($CDCl_3$) δ: 7.40-7.50 (m, 2H, Ar), 6.80 (d, 1H, J = 8Hz, Ar), 4.10 (q, 2 H, J = 7Hz, OCH_2), 3.83 (s, 3H, OCH_3), 2.46 (s, 3H, CH_3) and 1.40 (t, 3H, J = 7Hz, CH_3)

5.4.1.2. 2-bromo-1-(4-ethoxy-3-methoxyphenyl)ethanone (int**2**)

2-bromo-1-(4-ethoxy-3-methoxyphenyl)ethanone (int**2**) - To a stirred solution of 1-(4-ethoxy-3-methoxyphenyl)ethanone (11.65 g, 60 mmol, 1 eq.) in ethyl acetate (150 ml), $CuBr_2$ (120 mmol, 26.8 g, 2 eq.) was added and the reaction was left for 16 hours at 80 °C. The reaction mixture was poured into water (250 ml) and extracted with ethyl acetate (3x150 ml). The combined organic layers were dried over $MgSO_4$, filtered, and the solvent was removed under vacuum. The crude was dissolved in a minimal amount of ethyl acetate and recrystallised by addition of n-hexane to give 2-bromo-1-(4-ethoxy-3-methoxyphenyl)ethanone in a 50.3 % yield.

^{1}H NMR ($CDCl_3$) δ: 7.40-7.50 (m, 2H, Ar), 6.80 (d, 1H, J = 8Hz, Ar), 4.37 (s, 2H, CH_2Br), 4.12 (q, 2 H, J = 7Hz, OCH_2), 3.83 (s, 3H, OCH_3), and 1.40 (t, 3H, J = 7Hz, CH_3).

5.4.1.3. 1-(4-ethoxy-3-methoxyphenyl)-2-(2-methoxyphenoxy)ethanone (Model Compound A)

1-(4-ethoxy-3-methoxyphenyl)-2-(2-methoxyphenoxy)ethanone (**Model Compound A**) - To a solution of 2-bromo-1-(4-ethoxy-3-methoxyphenyl)ethanone (8.4 g, 31 mmol, 1 eq.) and 2-methoxyphenol (3.45 ml, 31 mmol, 1 eq.) in DMF (80 ml) K_2CO_3 (4.98 g, 36 mmol, 1.15 eq.) was added under magnetic stirring at 25°C. After 2 h the reaction mixture was poured into 250 ml of hot water and allowed to recrystallise. The solution was cooled and the precipitate was filtered and washed with n-hexane to give 1-(4-ethoxy-3-methoxyphenyl)-2-(2-methoxyphenoxy)ethanone in 76 % yield.

^{1}H NMR ($CDCl_3$) δ: 7.50-7.60 (m, 2H, Ar), 6.70-7.00 (m, 5H, Ar), 5.21 (s, 2H, CH_2CO), 4.12 (q, 2 H, J = 7Hz, OCH_2), 3.87 (s, 3H, OCH_3), 3.83 (s, 3H, OCH_3), and 1.40 (t, 3H, J = 7Hz, CH_3).

5.4.1.4. 1-(4-ethoxy-3-methoxyphenyl)-2-(2,6-dimethoxyphenoxy)ethanone (Model Compound B)

1-(4-ethoxy-3-methoxyphenyl)-2-(2,6-dimethoxyphenoxy)ethanone (**Model Compound B**) - To a solution of 2-bromo-1-(4-ethoxy-3-methoxyphenyl)ethanone (2.73 g, 10 mmol, 1 eq.) and 2-6-dimethoxyphenol (1.54 g, 10 mmol, 1 eq.) in DMF (40 ml) K_2CO_3 (1.59 g, 11.5 mmol, 1.15 eq.) was added under magnetic stirring at 25 °C. After 2 h the reaction mixture was poured into 150 ml of hot water and allowed to recrystallise. The solution was cooled and the precipitate was filtered and washed with n-hexane to give 1-(4-ethoxy-3-methoxyphenyl)-2-(2-methoxyphenoxy)ethanone in 71 % yield.

^{1}H NMR ($CDCl_3$): 7.65-7.70 (m, 2H, Ar), 7.02 (t, H, J = 7Hz, Ar), 6.83 (d, H, J = 7Hz, Ar), 6.50 (d, 2H, J = 8Hz, Ar), 5.21 (s, 2H, CH_2CO), 4.12 (q, 2 H, J = 7Hz, OCH_2), 3.9 (s, 3H, OCH_3), 3.78 (s, 6H, OCH_3), and 1.50 (t, 3H, J = 7Hz, CH_3).

5.4.2. Soxhlet Extraction

Soxhlet extraction was carried out using 150 ml of chloroform with an oil bath temperature of 90 °C. 3 g of kraft lignin was added to the cellulose finger and the system was heated for approximately 24 hours after which time the $CHCl_3$ was removed *in vacuo* and the extracted products analysed by GC-MS. The remaining lignin was dried and weighed to analyse the mass balance of the extraction.

5.4.3. Catalytic Transformation of Model Compounds by MTO

In a typical procedure 20 mmol of model compound was used with 0.10 ml of 30:70 % mixture of H_2O_2:H_2O and 20 µmol of methyltrioxorhenium catalyst. The reactions were generally sampled at 0, 1, 2, 24, 48 and 168 hours for GC-MS analysis.

5.4.4. Vanadium and Cobalt Complex Synthesis

5.4.4.1. $L^{tBu}(OH)_2$

To a solution of 3,5-di-*tert*-butyl-2-hydroxybenzaldehyde (3.228 g, 0.014 mol) in methanol (20 ml) methylethylene diamine (1.02 g, 1.2 ml, 0.014 mol) was added. The solution was stirred until a clear solution was observed, and left to stand for 24 hours to yield a yellow oil which was collected and dried (2.68 g, 65.9 %).
^{1}H NMR ($CDCl_3$) 1.31 (9H, s, $C(CH_3)_3$), 1.45 (9H, s, $C(CH_3)_3$), 2.47 (3H, s, CH_3), 2.92 (2H, t J = 6 Hz, CH_2), 3.73 (2H, t J = 6 Hz, CH_2), 7.09 (1H, d J = 2.5 Hz, Ar-H), 7.39 (1H, d J = 2.5 Hz, Ar-H), 8.40 (1H, s, CH).

$^{13}C(^1H)$ NMR ($CDCl_3$) 29.8, 31.8 ($C(CH_3)_3$), 34.4, 35.3 ($C(CH_3)_3$), 36.6 (CH_3), 52.2, 59.8 (CH_2), 118.1, (Ar-C), 126.3, 127.3 (Ar-CH), 137.0, 140.5 (Ar-C), 158.3 (Ar-O), 167.5 (CH).

ESI-TOF MS calculated for $C_{18}H_{31}N_2O$ = 291.2437, found 291.2267.

The yellow oil (1 g, 3.44 mmol) was dissolved in THF (20 ml), to which a solution of 3,5-di-tert-2-hydroxybenzyl bromide (1.029 g, 3.44 mmol) in THF (20 ml) was added. Triethylamine (0.35 g, 0.48 ml, 3.44 mmol) was added and the reaction mixture stirred at 80 ^oC for three hours. The white precipitate was filtered and the solvent removed under reduced pressure. The product was isolated *via* flash chromatography to obtain the product (1.33 g, 76.2 %).
^{1}H NMR ($CDCl_3$) 1.29 (9H, s, $C(CH_3)_3$), 1.32 (9H, s, $C(CH_3)_3$), 1.39 (9H, s, $C(CH_3)_3$), 1.46 (9H, s, $C(CH_3)_3$), 2.40 (3H, s, CH_3), 2.85 (2H, t J = 6.5 Hz, CH_2), 3.76 (2H, s, CH_2), 3.78 (2H, t J = 6.5 Hz, CH_2), 6.84 (1H, d J = 2.5 Hz, Ar-H), 7.09 (1H, d J = 2.5 Hz, Ar-H), 7.22 (1H, d J = 2.5 Hz, Ar-H), 7.40 (1H, d J = 2.5 Hz, Ar-H), 8.39 (1H, s, CH).

$^{13}C(^1H)$ NMR ($CDCl_3$) 29.4, 29.4, 31.5, 31.7 ($C(CH_3)_3$), 34.1, 35.0 ($C(CH_3)_3$), 41.9 (CH_3), 57.1, 57.3, 62.2 (CH_2), 117.8, 120.9, (Ar-C), 122.9, 123.2, 125.9, 127.0 (Ar-CH), 135.6, 136.6, 140.1, 140.4 (Ar-C), 154.3, 158.0 (Ar-O), 167.3 (CH).

ESI-TOF MS calculated for $C_{33}H_{53}N_2O_2$ = 509.4107, found 509.4145.

5.4.4.2. V(L^{tBu}OO)O

To a solution of $L^{tBu}(OH)_2$ (0.508 g, 1mmol) in THF (10 ml) was added 1 mmol (0.244 g, 0.236 ml) of $VO(O^iPr)_3$. The reaction mixture was allowed to stir for 1 hour and a precipitate was observed. The precipitate was redissolved by heating to reflux and crystals of V(L^{tBu}OO)O formed in a 62 % yield.

Unfortunately NMR spectroscopic data could not be collected for V(L^{tBu}OO)O due to the paramagnetic nature of the complex.

5.4.4.3. $SaL^H(OH)_2$

To a solution of *o*-phenylenediamine (10 mmol, 1.08 g) in MeOH (30 ml) was added 20 mmol (2 eq, 2.44 g) of salicylaldehyde and a catalytic amount of acetic acid (5 drops). The reaction mixture was allowed to stir at room temperature and an orange precipitate was observed. The precipitate was filtered and washed with MeOH (3x 50 ml) to yield 2.71 g of $SaL^H(OH)_2$ in an 86 % yield.

^{1}H NMR ($CDCl_3$) 6.81 (2H, m, Ar-H), 6.95 (2H, m, Ar-H), 7.12 (2H, m, Ar-H), 7.21 (2H, m, Ar-H), 8.51 (2H, s, N=C-H)

ESI-TOF MS calculated for $C_{20}H_{17}N_2O_2$ = 317.1285, found 317.1254

5.4.4.4. $SaL^{tBu}(OH)_2$

To a solution of *o*-phenylenediamine (10 mmol, 1.08 g) in MeOH (30 ml) was added 20 mmol (2 eq, 4.69 g) of 3,5-di-*tert*-butyl-2-hydroxybenzaldehyde and a catalytic amount of acetic acid (5 drops). The reaction mixture was allowed to stir at room temperature and a pale yellow precipitate was observed. The precipitate was filtered and washed with MeOH (3x 50 ml) to yield 4.25 g of $SaL^{tBu}(OH)_2$ in an 79 % yield.

^{1}H NMR ($CDCl_3$) 1.39 (9H, s, {C-CH_3}$_3$), 1.48 (9H, s, {C-CH_3}$_3$), 7.21 (2H, m, Ar-H), 7.35 (2H, m, Ar-H), 8.80 (2H, s, N=C-H)

ESI-TOF MS calculated for $C_{36}H_{49}N_2O_2$ = 541.3789, found 541.3818

5.4.4.5. $SaL^{Cl}(OH)_2$

To a solution of *o*-phenylenediamine (10 mmol, 1.08 g) in MeOH (30 ml) was added 20 mmol (2 eq, 3.82 g) of 3,5-dichloro-2-hydroxybenzaldehyde and a catalytic amount of acetic acid (5 drops). The reaction mixture was allowed to stir at room temperature and a bright red precipitate was observed. The precipitate was filtered and washed with MeOH (3x 50 ml) to yield 3.25 g of $SaL^{tBu}(OH)_2$ in an 72 % yield.

^{1}H NMR (d_8-THF) 7.30 (2H, s, Ar-H), 7.48 (2H, s, Ar-H), 8.70 (2H, s, N=C-H)

5.4.4.6. $Co(SaL^{H}OO)$

To a solution of $SaL^{H}(OH)_2$ (1 mmol, 0.32 g) in toluene (10 ml) was added 1 mmol (0.18 g) of cobalt(II) acetate. The reaction mixture was heated to reflux and stirred for 16 hours and a brown precipitate was observed. The mixture was cooled and the precipitate filtered and washed with toluene (3x 30 ml) to yield 0.285 g of $Co(SaL^{H}OO)$ in a 76 % yield.

ESI-TOF MS calculated for $C_{20}H_{14}N_2O_2Co$ = 373.0387, found 373.0394
Gouy analysis: µeff calculated for Co^{2+} = 1.73, observed 1.50

5.4.4.7. Co(SaL^{tBu}OO)

To a solution of SaL^{tBu}(OH)$_2$ (1 mmol, 0.54 g) in toluene (10 ml) was added 1 mmol (0.18 g) of cobalt(II) acetate. The reaction mixture was heated to reflux and stirred for 16 hours and a brown precipitate was observed. The mixture was cooled and the precipitate filtered and washed with toluene (3x 30 ml) to yield 0.397 g of Co(SaL^{tBu}OO) in a 66 % yield.

ESI-TOF MS calculated for $C_{36}H_{46}N_2O_2Co$ = 597.2891, found 597.2984
CHN calculated C 73.3 %; H 7.76 %; N 4.69 %, found C 73.1 %; H 8.07 %; N 4.08 %.
Gouy analysis: µeff calculated for Co^{2+} = 1.73, observed 1.28

5.4.4.8. Co(SaL^{Cl}OO)

To a solution of SaL^{Cl}(OH)$_2$ (1 mmol, 0.45 g) in toluene (10 ml) was added 1 mmol (0.18 g) of cobalt(II) acetate. The reaction mixture was heated to reflux and stirred for 16 hours and a brown precipitate was observed. The mixture was cooled and the precipitate filtered and washed with toluene (3x 30 ml) to yield 0.367 g of Co(SaL^{tBu}OO) in a 72 % yield.

ESI-TOF MS calculated for $C_{20}H_{10}N_2O_2Cl_4Co$ = 510.8799, found 510.8890
CHN calculated C 47.0 %; H 1.97 %; N 5.48 %, found C 46.4 %; H 2.25 %; N 5.28 %.
Gouy analysis: µeff calculated for Co^{2+} = 1.73, observed 1.54.

5.4.5. Oxidative Depolymerisation of Lignin

In a typical procedure the reactor vessel was charged with solvent (MeOH, 10 ml), kraft lignin (0.5 g) and a specified amount of catalyst (1-10 wt %). H_2O_2 (1 ml, 30 % in H_2O) was added and the reactor was immediately sealed. The reactor vessel was placed in an oven at the specified temperature for 24 hours then removed and allowed to cool. Upon opening the reactor vessel a sample of the reaction mixture was taken for GC-MS analysis. The reaction mixture was transferred to a round bottom flask and the MeOH removed *in vacuo*. 10 ml of H2O was added and extracted 3 times with $CHCl_3$ (3x 10 ml). A sample was taken for GC-MS analysis before the $CHCl_3$ fractions were combined and the solvent removed *in vacuo* before the solid product was weighed.

5.4.6. Hydrolysis of model compounds

5.4.6.1. Parr series 4748

The appropriate model compound (10 mmol) was dissolved in 10 ml of formic acid and loaded into a non-stirred reactor (Parr Instruments model 4748). The carbon supported catalyst {Rh, Pd, Pt (Johnson Matthey Catalysts)} was added (1 % w/w of active catalyst) and the reactor was sealed. The vessel was heated to 200 °C in an oven for 24 hours.

5.4.6.2. Parr series 4560

The appropriate model compound (10 mmol) was dissolved in 10 ml of formic acid and loaded into a stirred reactor (Parr Instruments model 4560). The carbon supported catalyst (Rh, Pd, Pt (Johnson Matthey Catalysts)) was added (1 % w/w of active catalyst) and the reactor was sealed. The vessel was purged and raised to a pressure of 10 Bar of H_2. The reaction was allowed to proceed at room temperature for 24 hours and then vented.

5.4.7. Chapter 4 Crystal Data

5.4.7.1. V(L^{tBu}OO)O

Empirical formula	$C_{37}H_{58}N_2O_4V$
Formula weight	645.79
Temperature	150(2) K
Wavelength	0.71073 Å
Crystal system, space group	Orthorhombic, $P2_12_12_1$
Unit cell dimensions	a = 10.0400(5) Å α = 90 °.
	b = 11.6740(6) Å β = 90 °.
	c = 30.8460(15) Å γ = 90 °.
Volume	3615.4(3) $Å^3$
Z, Calculated density	4, 1.186 Mg/m^3
Absorption coefficient	0.313 mm^{-1}
F(000)	1396
Crystal size	0.10 × 0.10 × 0.10 mm
Theta range for data collection	3.88 to 25.01 º
Limiting indices	-11<=h<=11, -12<=k<=13, -36<=l<=36
Reflections collected / unique	25456 / 5898 [R(int) = 0.0808]
Completeness to θ = 25.01	96.3 %
Absorption correction	None
Max. and min. transmission	0.9694 and 0.9694
Refinement method	Full-matrix least-squares on F^2
Data / restraints / parameters	5898 / 0 / 411
Goodness-of-fit on F^2	1.009
Final R indices [I>2σ(I)]	R_1 = 0.0578, wR_2 = 0.1221
R indices (all data)	R_1 = 0.0991, wR_2 = 0.1397
Largest diff. peak and hole	0.551 and -0.353 e.$Å^{-3}$

5.4.7.2. CoSaL^{tBu}OO

Empirical formula	$C_{36}H_{46}N_2O_2Co$
Formula weight	597.68
Temperature	150(2) K
Wavelength	0.71073 Å
Crystal system, space group	Triclinic, *P*-1
Unit cell dimensions	a = 9.2330(2) Å α = 107.5770(10) °. b = 12.9700(3) Å β = 93.6090(10) °. c = 14.4030(3) Å γ = 95.9210(10) °.
Volume	1627.42(6) Å^3
Z, Calculated density	2, 1.220 Mg/m^3
Absorption coefficient	0.560 mm^{-1}
F(000)	638
Crystal size	0.20 × 0.20 × 0.15 mm
Theta range for data collection	3.54 to 27.49 º
Limiting indices	-11<=h<=11, -16<=k<=16, -18<=l<=18
Reflections collected / unique	32974 / 7436 [R(int) = 0.0515]
Completeness to θ = 27.49	99.7 %
Absorption correction	None
Max. and min. transmission	0.9207 and 0.8962
Refinement method	Full-matrix least-squares on F^2
Data / restraints / parameters	7436 / 0 / 413
Goodness-of-fit on F^2	1.042
Final R indices [I>2σ(I)]	R_1 = 0.0368, wR_2 = 0.0847
R indices (all data)	R_1 = 0.0550, wR_2 = 0.0928
Largest diff. peak and hole	0.323 and -0.507 e.Å^{-3}

6. References

(1) "State Of World Population," United Nations Population Fund, 2011.
(2) "International Energy Outlook," U.S. Energy Information Administration, 2011.
(3) http://www.eia.gov/dnav/pet/hist/LeafHandler.ashx?n=PET&s=RBRTE&f=D 26 March 2012
(4) Goldemberg, J. *Science* **2007**, *315*, 808.
(5) Jones, M. D.; Keir, C. G.; Di Iulio, C.; Robertson, R. A. M.; Williams, C. V.; Apperley, D. C. *Catal. Sci. Tech.* **2011**, *1*, 267.
(6) Amen-Chen, C.; Pakdel, H.; Roy, C. *Bioresour. Tech.* **2001**, *79*, 277.
(7) Bobleter, O. *Prog. Polym. Sci.* **1994**, *19*, 797.
(8) Dorrestijn, E.; Laarhoven, L. J. J.; Arends, I. W. C. E.; Mulder, P. *J. Anal. Appl. Pyrolysis* **2000**, *54*, 153.
(9) Galbe, M.; Zacchi, G. *Appl. Microbiol. Biotechnol.* **2002**, *59*, 618.
(10) Petrus, L.; Noordermeer, M. A. *Green Chemistry* **2006**, *8*, 861.
(11) Kumar, R.; Singh, S.; Singh, O. V. *J. Ind. Microbiol. Biotechnol.* **2008**, *35*, 377.
(12) Rude, M. A.; Schirmer, A. *Curr. Opin. Microbiol.* **2009**, *12*, 274.
(13) Voet, D.; Voet, J. G. *Biochemistry*; 3rd ed.; John Wiley: Hoboken, N.J., 2004.
(14) Lin, Y. C.; Huber, G. W. *Energy Environ. Sci.* **2009**, *2*, 68.
(15) Ghatak, H. R. *Renew. Sust. Energ. Rev.* **2011**, *15*, 4042.
(16) Demirbas, A. *Energ. Convers. Manage.* **2009**, *50*, 2782.
(17) Lynd, L. R.; Wyman, C. E.; Gerngross, T. U. *Biotechnol. Prog.* **1999**, *15*, 777.
(18) Kleinert, M.; Barth, T. *Chem. Eng. Technol.* **2008**, *31*, 736.
(19) Chakar, F. S.; Ragauskas, A. J. *Ind. Crop. Prod.* **2004**, *20*, 131.
(20) Boerjan, W.; Ralph, J.; Baucher, M. *Annu. Rev. Plant Biol.* **2003**, *54*, 519.
(21) Weng, J. K.; Li, X.; Bonawitz, N. D.; Chapple, C. *Curr. Opin. Biotechnol.* **2008**, *19*, 166.
(22) Mohan, D.; Pittman, C. U.; Steele, P. H. *Energ. Fuel.* **2006**, *20*, 848.
(23) Onnerud, H.; Zhang, L. M.; Gellerstedt, G.; Henriksson, G. *Plant Cell* **2002**, *14*, 1953.
(24) Vanholme, R.; Morreel, K.; Ralph, J.; Boerjan, W. *Curr. Opin. Plant Biol.* **2008**, *11*, 278.
(25) Achyuthan, K. E.; Achyuthan, A. M.; Adams, P. D.; Dirk, S. M.; Harper, J. C.; Simmons, B. A.; Singh, A. K. *Molecules* **2010**, *15*, 8641.
(26) Zakzeski, J.; Bruijnincx, P. C. A.; Jongerius, A. L.; Weckhuysen, B. M. *Chem. Rev.* **2010**, *110*, 3552.
(27) Mialon, L.; Pemba, A. G.; Miller, S. A. *Green Chemistry* **2010**, *12*, 1704.
(28) Sixta, H. *Handbook of Pulp*; John Wiley & Sons, 2006.
(29) Doherty, W. O. S.; Mousavioun, P.; Fellows, C. M. *Ind. Crop. Prod.* **2011**, *33*, 259.
(30) Harris, E. E.; D'Ianni, J.; Adkins, H. *J. Am. Chem. Soc.* **1938**, *60*, 1467.
(31) Brewer, C. P.; Cooke, L. M.; Hibbert, H. *J. Am. Chem. Soc.* **1948**, *70*, 57.
(32) Pepper, J. M.; Hibbert, H. *J. Am. Chem. Soc.* **1948**, *70*, 67.
(33) Pepper, J. M.; Lee, Y. W. *Can. J. Chem.* **1969**, *47*, 723.
(34) Pepper, J. M.; Supathna, P. *Can. J. Chem.* **1978**, *56*, 899.
(35) Meier, D.; Ante, R.; Faix, O. *Bioresour. Tech.* **1992**, *40*, 171.
(36) Yan, N.; Zhao, C.; Dyson, P. J.; Wang, C.; Liu, L. T.; Kou, Y. *Chemsuschem* **2008**, *1*, 626.
(37) LaVopa, V.; Satterfield, C. N. *Energ. Fuel.* **1987**, *1*, 323.
(38) Rollmann, L. D. *J. Catal.* **1977**, *46*, 243.
(39) Romero, Y.; Richard, F.; Renème, Y.; Brunet, S. *Appl. Catal., A* **2009**, *353*, 46.
(40) Bunch, A. Y.; Wang, X.; Ozkan, U. S. *Appl. Catal., A* **2008**, *346*, 96.
(41) Bunch, A. Y.; Ozkan, U. S. *J. Catal.* **2002**, *206*, 177.
(42) Lee, C.-L.; Ollis, D. F. *J. Catal.* **1984**, *87*, 325.
(43) Edelman, M. C.; Maholland, M. K.; Baldwin, R. M.; Cowley, S. W. *J. Catal.* **1988**, *111*, 243.
(44) Viljava, T. R.; Komulainen, R. S.; Krause, A. O. I. *Catal. Today* **2000**, *60*, 83.
(45) Laurent, E.; Delmon, B. *Ind. Eng. Chem. Res.* **1993**, *32*, 2516.
(46) Şenol, O. İ.; Ryymin, E. M.; Viljava, T. R.; Krause, A. O. I. *J. Mol. Catal. A: Chem.* **2007**, *277*, 107.
(47) Ratcliff, M.; Johnson, D.; Posey, F.; Chum, H. *App. Biochem. Biotech.* **1988**, *17*, 151.
(48) Koyama, M. *Bioresour. Tech.* **1993**, *44*, 209.
(49) Odebunmi, E. O.; Ollis, D. F. *J. Catal.* **1983**, *80*, 56.
(50) Yang, Y.; Gilbert, A.; Xu, C. *Appl. Catal., A* **2009**, *360*, 242.
(51) Huuska, M.; Rintala, J. *J. Catal.* **1985**, *94*, 230.
(52) Ferrari, M.; Delmon, B.; Grange, P. *Carbon* **2002**, *40*, 497.
(53) de la Puente, G.; Gil, A.; Pis, J. J.; Grange, P. *Langmuir* **1999**, *15*, 5800.

(54) Centeno, A.; Laurent, E.; Delmon, B. *J. Catal.* **1995**, *154*, 288.
(55) Laurent, E.; Delmon, B. *Appl. Catal., A* **1994**, *109*, 77.
(56) Kallury, R. K. M. R.; Restivo, W. M.; Tidwell, T. T.; Boocock, D. G. B.; Crimi, A.; Douglas, J. *J. Catal.* **1985**, *96*, 535.
(57) Hurff, S. J.; Klein, M. T. *Ind. Eng. Chem. Fund.* **1983**, *22*, 426.
(58) Bredenberg, J. B. s.; Huuska, M.; Toropainen, P. *J. Catal.* **1989**, *120*, 401.
(59) Petrocelli, F. P.; Klein, M. T. *Ind. Eng. Chem. Prod. R.D.* **1985**, *24*, 635.
(60) Meier, D.; Berns, J.; Faix, O.; Balfanz, U.; Baldauf, W. *Biomass Bioenergy* **1994**, *7*, 99.
(61) Shabtai, J. S., Patent, 1999, US5959167
(62) Zmierczak, W. W.; Miller, J. D., Patent, 2011, US 2011/0237838 A1
(63) Herrmann, W. A.; Weskamp, T.; Zoller, J. P.; Fischer, R. W. *J. Mol. Catal. A: Chem.* **2000**, *153*, 49.
(64) Herrmann, W. A.; Kuchler, J. G.; Felixberger, J. K.; Herdtweck, E.; Wagner, W. *Angew. Chem., Int. Ed. Engl.* **1988**, *27*, 394.
(65) Crestini, C.; Caponi, M. C.; Argyropoulos, D. S.; Saladino, R. *Bioorg. Med. Chem.* **2006**, *14*, 5292.
(66) Crestini, C.; Pro, P.; Neri, V.; Saladino, R. *Bioorg. Med. Chem.* **2005**, *13*, 2569.
(67) Bozell, J. J.; Hames, B. R.; Dimmel, D. R. *J. Org. Chem.* **1995**, *60*, 2398.
(68) Drago, R. S.; Corden, B. B.; Barnes, C. W. *J. Am. Chem. Soc.* **1986**, *108*, 2453.
(69) Kervinen, K.; Korpi, H.; Gerbrand Mesu, J.; Soulimani, F.; Repo, T.; Rieger, B.; Leskelä, M.; Weckhuysen, B. M. *Eur. J. Inorg. Chem.* **2005**, *2005*, 2591.
(70) Sippola, V.; Krause, O.; Vuorinen, T. *J. Wood Chem. Technol.* **2004**, *24*, 323.
(71) Kervinen, K.; Allmendinger, M.; Leskela, M.; Repo, T.; Rieger, B. *Phys. Chem. Chem. Phys.* **2003**, *5*, 4450.
(72) Badamali, S. K.; Luque, R.; Clark, J. H.; Breeden, S. W. *Catal. Commun.* **2009**, *10*, 1010.
(73) Hanson, S. K.; Baker, R. T.; Gordon, J. C.; Scott, B. L.; Thorn, D. L. *Inorg. Chem.* **2010**, *49*, 5611.
(74) Thorn, D. L.; Harlow, R. L.; Herron, N. *Inorg. Chem.* **1996**, *35*, 547.
(75) Dry, M. E. *Appl. Catal., A* **1996**, *138*, 319.
(76) Bridgwater, A. V.; Double, J. M. *Res. Therm. Biomass Conv.* **1988**, 98.
(77) Bridgwater, A. V.; Beenackers, A. A. C. M. *Biomass Energ. Ind. Vols. 1 & 2* **1990**, B827.
(78) Bridgwater, A. V. *Chem. Eng. J.* **2003**, *91*, 87.
(79) Hanping, C.; Bin, L.; Haiping, Y.; Guolai, Y.; Shihong, Z. *Energ. Fuel.* **2008**, *22*, 3493.
(80) Subramani, V.; Gangwal, S. K. *Energ. Fuel.* **2008**, *22*, 814.
(81) Mohan, D.; Pittman, C. U.; Steele, P. H. *Energ. Fuel.* **2006**, *20*, 848.
(82) Britt, P. F.; Buchanan, A. C.; Cooney, M. J.; Martineau, D. R. *J. Org. Chem.* **2000**, *65*, 1376.
(83) Gellerstedt, G. r.; Li, J.; Eide, I.; Kleinert, M.; Barth, T. *Energ. Fuel.* **2008**, *22*, 4240.
(84) Kleinert, M.; Barth, T. *Energ. Fuel.* **2008**, *22*, 1371.
(85) Li, J. B.; Henriksson, G.; Gellerstedt, G. *Bioresour. Tech.* **2007**, *98*, 3061.
(86) Furusawa, T.; Sato, T.; Saito, M.; Ishiyama, Y.; Sato, M.; Itoh, N.; Suzuki, N. *Appl. Catal., A* **2007**, *327*, 300.
(87) Kronholm, J.; Kuosmanen, T.; Hartonen, K.; Riekkola, M. L. *Waste Manage.* **2003**, *23*, 253.
(88) Matsumura, Y.; Sasaki, M.; Okuda, K.; Takami, S.; Ohara, S.; Umetsu, M.; Adschiri, T. *Combust. Sci. Technol.* **2006**, *178*, 509.
(89) Fang, Z.; Sato, T.; Smith, R. L.; Inomata, H.; Arai, K.; Kozinski, J. A. *Bioresour. Tech.* **2008**, *99*, 3424.
(90) Okuda, K.; Umetsu, M.; Takami, S.; Adschiri, T. *Fuel Process. Technol.* **2004**, *85*, 803.
(91) Saisu, M.; Sato, T.; Watanabe, M.; Adschiri, T.; Arai, K. *Energ. Fuel.* **2003**, *17*, 922.
(92) http://www.natureworksllc.com/ 27 March 2012
(93) http://www.purac.com 27 March 2012
(94) Auras, R.; Harte, B.; Selke, S. *Macromol. Biosci.* **2004**, *4*, 835.
(95) Drumright, R. E.; Gruber, P. R.; Henton, D. E. *Adv. Mater.* **2000**, *12*, 1841.
(96) Lunt, J. *Polym. Degrad. Stab.* **1998**, *59*, 145.
(97) Williams, C. K.; Hillmyer, M. A. *Polym. Rev.* **2008**, *48*, 1.
(98) Dechy-Cabaret, O.; Martin-Vaca, B.; Bourissou, D. *Chem. Rev.* **2004**, *104*, 6147.
(99) Dittrich, W.; Schulz, R. C. *Angew. Makromol. Chem.* **1971**, *15*, 109.
(100) Whitelaw, E. L., University of Bath, 2011.
(101) Albertsson, A. C.; Varma, I. K. *Biomacromolecules* **2003**, *4*, 1466.
(102) Platel, R. H.; Hodgson, L. M.; Williams, C. K. *Polym. Rev.* **2008**, *48*, 11.
(103) Kricheldorf, H. R. *Macromol. Symp.* **2000**, *153*, 55.

(104) Kricheldorf, H. R.; Kreiser-Saunders, I.; Stricker, A. *Macromolecules* **2000**, *33*, 702.
(105) Nijenhuis, A. J.; Grijpma, D. W.; Pennings, A. J. *Macromolecules* **1992**, *25*, 6419.
(106) Schwach, G.; Coudane, J.; Engel, R.; Vert, M. *J. Polym. Sci. Pol. Chem.* **1997**, *35*, 3431.
(107) Kowalski, A.; Duda, A.; Penczek, S. *Macromolecules* **2000**, *33*, 7359.
(108) Wisniewski, M.; Borgne, A. L.; Spassky, N. *Macromol. Chem. Phys.* **1997**, *198*, 1227.
(109) Spassky, N.; Wisniewski, M.; Pluta, C.; Le Borgne, A. *Macromol. Chem. Phys.* **1996**, *197*, 2627.
(110) Ovitt, T. M.; Coates, G. W. *J. Am. Chem. Soc.* **1999**, *121*, 4072.
(111) Ovitt, T. M.; Coates, G. W. *J. Am. Chem. Soc.* **2002**, *124*, 1316.
(112) Ovitt, T. M.; Coates, G. W. *J. Polym. Sci. Pol. Chem.* **2000**, *38*, 4686.
(113) Radano, C. P.; Baker, G. L.; Smith, M. R. *J. Am. Chem. Soc.* **2000**, *122*, 1552.
(114) Zhong, Z.; Dijkstra, P. J.; Feijen, J. *J. Am. Chem. Soc.* **2003**, *125*, 11291.
(115) Zhong, Z.; Dijkstra, P. J.; Feijen, J. *Angew. Chem., Int. Ed.* **2002**, *41*, 4510.
(116) Nomura, N.; Ishii, R.; Akakura, M.; Aoi, K. *J. Am. Chem. Soc.* **2002**, *124*, 5938.
(117) Nomura, N.; Ishii, R.; Yamamoto, Y.; Kondo, T. *Chem. Eur. J.* **2007**, *13*, 4433.
(118) Hormnirun, P.; Marshall, E. L.; Gibson, V. C.; White, A. J. P.; Williams, D. J. *J. Am. Chem. Soc.* **2004**, *126*, 2688.
(119) Qian, F.; Liu, K.; Ma, H. *Dalton Trans.* **2010**, *39*, 8071.
(120) Kreiser-Saunders, I.; Kricheldorf, H. R. *Macromol. Chem. Phys.* **1998**, *199*, 1081.
(121) Kricheldorf, H. R.; Damrau, D.-O. *Macromol. Chem. Phys.* **1997**, *198*, 1753.
(122) Kricheldorf, H. R.; Damrau, D.-O. *Macromol. Chem. Phys.* **1998**, *199*, 1747.
(123) Kricheldorf, H. R.; Kreiser-Saunders, I.; Damrau, D.-O. *Macromol. Symp.* **1999**, *144*, 269.
(124) Chamberlain, B. M.; Cheng, M.; Moore, D. R.; Ovitt, T. M.; Lobkovsky, E. B.; Coates, G. W. *J. Am. Chem. Soc.* **2001**, *123*, 3229.
(125) Cheng, M.; Attygalle, A. B.; Lobkovsky, E. B.; Coates, G. W. *J. Am. Chem. Soc.* **1999**, *121*, 11583.
(126) Chisholm, M. H.; Gallucci, J.; Phomphrai, K. *Inorg. Chem.* **2002**, *41*, 2785.
(127) Chisholm, M. H.; Huffman, J. C.; Phomphrai, K. *Dalton Trans.* **2001**, 222.
(128) Chisholm, M. H.; Gallucci, J.; Phomphrai, K. *Chem. Commun.* **2003**, 48.
(129) Chisholm, M. H.; Eilerts, N. W. *Chem. Commun.* **1996**, 853.
(130) Chisholm, M. H.; Eilerts, N. W.; Huffman, J. C.; Iyer, S. S.; Pacold, M.; Phomphrai, K. *J. Am. Chem. Soc.* **2000**, *122*, 11845.
(131) Chisholm, M. H.; Gallucci, J. C.; Phomphrai, K. *Inorg. Chem.* **2004**, *43*, 6717.
(132) Chisholm, M. H.; Gallucci, J. C.; Zhen, H.; Huffman, J. C. *Inorg. Chem.* **2001**, *40*, 5051.
(133) Williams, C. K.; Breyfogle, L. E.; Choi, S. K.; Nam, W.; Young, V. G.; Hillmyer, M. A.; Tolman, W. B. *J. Am. Chem. Soc.* **2003**, *125*, 11350.
(134) Chmura, A. J.; Davidson, M. G.; Frankis, C. J.; Jones, M. D.; Lunn, M. D. *Chem. Commun.* **2008**, 1293.
(135) Kol, M.; Shamis, M.; Goldberg, I.; Goldschmidt, Z.; Alfi, S.; Hayut-Salant, E. *Inorg. Chem. Commun.* **2001**, *4*, 177.
(136) Frankis, C. J., University of Bath, 2010.
(137) Karimi, B.; Zamani, A.; Abedia, S.; Clark, J. H. *Green Chemistry* **2009**, *11*, 109.
(138) Macquarrie, D. J. *Green Chemistry* **1999**, *1*, 195.
(139) Pescarmona, P. P.; Masters, A. F.; van der Waal, J. C.; Maschmeyer, T. *J. Mol. Catal. A: Chem.* **2004**, *220*, 37.
(140) Yokoi, T.; Yoshitake, H.; Tatsumi, T. *J. Mater. Chem.* **2004**, *14*, 951.
(141) Yu, K. Q.; Sommer, W.; Weck, M.; Jones, C. W. *J. Catal.* **2004**, *226*, 101.
(142) Duchateau, R. *Chem. Rev.* **2002**, *102*, 3525.
(143) Cordes, D. B.; Lickiss, P. D.; Rataboul, F. *Chem. Rev.* **2010**, *110*, 2081.
(144) Brown, J. F.; Vogt, L. H. *J. Am. Chem. Soc.* **1965**, *87*, 4313.
(145) Feher, F. J.; Newman, D. A.; Walzer, J. F. *J. Am. Chem. Soc.* **1989**, *111*, 1741.
(146) Lichtenhen, J. D., Patent, 2005, US6972312
(147) Coperet, C.; Chabanas, M.; Saint-Arroman, R. P.; Basset, J. M. *Angew. Chem., Int. Ed.* **2003**, *42*, 156.
(148) Feher, F. J. *J. Am. Chem. Soc.* **1986**, *108*, 3850.
(149) Feher, F. J.; Weller, K. J. *Organometallics* **1990**, *9*, 2638.
(150) Feher, F. J.; Blanski, R. L. *Chem. Commun.* **1990**, 1614.
(151) Feher, F. J.; Walzer, J. F. *Inorg. Chem.* **1991**, *30*, 1689.
(152) Feher, F. J.; Walzer, J. F.; Blanski, R. L. *J. Am. Chem. Soc.* **1991**, *113*, 3618.

(153) Budzichowski, T. A.; Chacon, S. T.; Chisholm, M. H.; Feher, F. J.; Streib, W. *J. Am. Chem. Soc.* **1991**, *113*, 689.
(154) Feher, F. J.; Budzichowski, T. A.; Rahimian, K.; Ziller, J. W. *J. Am. Chem. Soc.* **1992**, *114*, 3859.
(155) Feher, F. J.; Budzichowski, T. A.; Ziller, J. W. *Inorg. Chem.* **1992**, *31*, 5100.
(156) Feher, F. J.; Weller, K. J.; Ziller, J. W. *J. Am. Chem. Soc.* **1992**, *114*, 9686.
(157) Das, N.; Eckert, H.; Hu, H. C.; Wachs, I. E.; Walzer, J. F.; Feher, F. J. *J. Phys. Chem.* **1993**, *97*, 8240.
(158) Feher, F. J.; Tajima, T. L. *J. Am. Chem. Soc.* **1994**, *116*, 2145.
(159) Feher, F. J.; Budzichowski, T. A. *Polyhedron* **1995**, *14*, 3239.
(160) Feher, F. J.; Budzichowski, T. A.; Ziller, J. W. *Inorg. Chem.* **1997**, *36*, 4082.
(161) Duchateau, R.; van Meerendonkt, W. J.; Huijser, S.; Staal, B. B. P.; van Schilt, M. A.; Gerritsen, G.; Meetsma, A.; Koning, C. E.; Kemmere, M. F.; Keurentjes, J. T. F. *Organometallics* **2007**, *26*, 4204.
(162) Severn, J. R.; Duchateau, R.; van Santen, R. A.; Ellis, D. D.; Spek, A. L. *Organometallics* **2002**, *21*, 4.
(163) Severn, J. R.; Duchateau, R.; van Santen, R. A.; Ellis, D. D.; Spek, A. L.; Yap, G. P. A. *Dalton Trans.* **2003**, 2293.
(164) Gerritsen, G.; Duchateau, R.; van Santen, R. A.; Yap, G. P. A. *Organometallics* **2003**, *22*, 100.
(165) Duchateau, R.; Dijkstra, T. W.; van Santen, R. A.; Yap, G. P. A. *Chem. Eur. J.* **2004**, *10*, 3979.
(166) Dijkstra, T. W.; Duchateau, R.; van Santen, R. A.; Meetsma, A.; Yap, G. P. A. *J. Am. Chem. Soc.* **2002**, *124*, 9856.
(167) Duchateau, R.; Dijkstra, T. W.; Severn, J. R.; van Santen, R. A.; Korobkov, I. V. *Dalton Trans.* **2004**, 2677.
(168) Abbenhuis, H. C. L.; Krijnen, S.; vanSanten, R. A. *Chem. Commun.* **1997**, 331.
(169) Crocker, M.; Herold, R. H. M.; Orpen, A. G. *Chem. Commun.* **1997**, 2411.
(170) Maschmeyer, T.; Klunduk, M. C.; Martin, C. M.; Shephard, D. S.; Thomas, J. M.; Johnson, B. F. G. *Chem. Commun.* **1997**, 1847.
(171) Klunduk, M. C.; Maschmeyer, T.; Thomas, J. M.; Johnson, B. F. G. *Chem. Eur. J.* **1999**, *5*, 1481.
(172) Thomas, J. M.; Sankar, G.; Klunduk, M. C.; Attfield, M. P.; Maschmeyer, T.; Johnson, B. F. G.; Bell, R. G. *J. Phys. Chem. B* **1999**, *103*, 8809.
(173) Skowronska-Ptasinska, M. D.; Vorstenbosch, M. L. W.; van Santen, R. A.; Abbenhuis, H. C. L. *Angew. Chem., Int. Ed.* **2002**, *41*, 637.
(174) Jones, M. D.; Davidson, M. G.; Keir, C. G.; Wooles, A. J.; Mahon, M. F.; Apperley, D. C. *Dalton Trans.* **2008**, 3655.
(175) Jones, M. D.; Keir, C. G.; Johnson, A. L.; Mahon, M. F. *Polyhedron* **2010**, *29*, 312.
(176) Jones, M. D.; Davidson, M. G.; Keir, C. G.; Hughes, L. M.; Mahon, M. F.; Apperley, D. C. *Eur. J. Inorg. Chem.* **2009**, 635.
(177) Nowotny, M.; Maschmeyer, T.; Johnson, B. F. G.; Lahuerta, P.; Thomas, J. M.; Davies, J. E. *Angew. Chem., Int. Ed.* **2001**, *40*, 955.
(178) Di Iulio, C.; Jones, M. D.; Mahon, M. F.; Apperley, D. C. *Inorg. Chem.* **2010**, *49*, 10232.
(179) Chisholm, M. H.; Gallucci, J. C.; Zhen, H. H.; Huffman, J. C. *Inorg. Chem.* **2001**, *40*, 5051.
(180) Darensbourg, D. J.; Rainey, P.; Yarbrough, J. *Inorg. Chem.* **2001**, *40*, 986.
(181) Benisvy, L.; Bill, E.; Blake, A. J.; Collison, D.; Davies, E. S.; Garner, C. D.; McArdle, G.; McInnes, E. J. L.; McMaster, J.; Ross, S. H. K.; Wilson, C. *Dalton Trans.* **2006**, 258.
(182) Paital, A. R.; Wu, A. Q.; Guo, G. C.; Aromi, G.; Ribas-Arino, J.; Ray, D. *Inorg. Chem.* **2007**, *46*, 2947.
(183) Wiznycia, A. V.; Desper, J.; Levy, C. J. *Chem. Commun.* **2005**, 4693.
(184) Lewinski, J.; Marciniak, W.; Lipkowski, J.; Justyniak, I. *J. Am. Chem. Soc.* **2003**, *125*, 12698.
(185) Lewinski, J.; Dranka, M.; Bury, W.; Sliwinski, W.; Justyniak, I.; Lipkowski, J. *J. Am. Chem. Soc.* **2007**, *129*, 3096.
(186) Lewinski, J.; Dranka, M.; Kraszewska, I.; Sliwinski, W.; Justyniak, I. *Chem. Commun.* **2005**, 4935.
(187) Lewinski, J.; Sliwinski, W.; Dranka, M.; Justyniak, I.; Lipkowski, J. *Angew. Chem., Int. Ed.* **2006**, *45*, 4826.
(188) Lewinski, J.; Bury, W.; Dutkiewicz, M.; Maurin, M.; Justyniak, I.; Lipkowski, J. *Angew. Chem., Int. Ed.* **2008**, *47*, 573.
(189) Lewinski, J.; Koscielski, M.; Suwala, K.; Justyniak, I. *Angew. Chem., Int. Ed.* **2009**, *48*, 7017.

(190) Lewinski, J.; Suwala, K.; Kaczorowski, T.; Galezowski, M.; Gryko, D. T.; Justyniak, I.; Lipkowski, J. *Chem. Commun.* **2009**, 215.
(191) Hollingsworth, N.; Johnson, A. L.; Kingsley, A.; Kociok-Kohn, G.; Molloy, K. C. *Organometallics* **2010**, *29*, 3318.
(192) AbdelFattah, T. M.; Pinnavaia, T. J. *Chem. Commun.* **1996**, 665.
(193) Deshayes, G.; Poelmans, K.; Verbruggen, I.; Camacho-Camacho, C.; Degee, P.; Pinoie, V.; Martins, J. C.; Piotto, M.; Biesemans, M.; Willem, R.; Dubois, P. *Chem. Eur. J.* **2005**, *11*, 4552.
(194) Yu, K. Q.; Jones, C. W. *J. Catal.* **2004**, *222*, 558.
(195) Kim, E.; Shin, E. W.; Yoo, I. K.; Chung, J. S. *J. Mol. Catal. A: Chem.* **2009**, *298*, 36.
(196) Kageyama, K.; Ogino, S.; Aida, T.; Tatsumi, T. *Macromolecules* **1998**, *31*, 4069.
(197) Kageyama, K.; Tatsumi, T.; Aida, T. *Polym. J.* **1999**, *31*, 1005.
(198) Tortosa, K.; Hamaide, T.; Boisson, C.; Spitz, R. *Macromol. Chem. Phys.* **2001**, *202*, 1156.
(199) Pollet, E.; Hamaide, T.; Tayakout-Fayolle, M.; Jallut, C. *Polym. Int.* **2004**, *53*, 550.
(200) Yu, K. Q.; Jones, C. W. *Organometallics* **2003**, *22*, 2571.
(201) Deshayes, G.; Mercier, F. A. G.; Degee, P.; Verbruggen, I.; Biesemans, M.; Willem, R.; Dubois, P. *Chem. Eur. J.* **2003**, *9*, 4346.
(202) Dagorne, S.; Lavanant, L.; Welter, R.; Chassenieux, C.; Haquette, P.; Jaouen, G. *Organometallics* **2003**, *22*, 3732.
(203) Granum, D. M.; Riedel, P. J.; Crawford, J. A.; Mahle, T. K.; Wyss, C. M.; Begej, A. K.; Arulsamy, N.; Pierce, B. S.; Mehn, M. P. *Dalton Trans.* **2011**, *40*, 5881.
(204) Grunova, E.; Roisnel, T.; Carpentier, J. F. *Dalton Trans.* **2009**, 9010.
(205) Lesikar, L. A.; Gushwa, A. F.; Richards, A. F. *J. Organomet. Chem.* **2008**, *693*, 3245.
(206) Messman, J. M.; Storey, R. F. *J. Polym. Sci. Pol. Chem.* **2004**, *42*, 6238.
(207) Crestini, C.; DAuria, M. *Tetrahedron* **1997**, *53*, 7877.
(208) McDaniel, L. H.; Ashraf-Khorassani, M.; Taylor, L. T. *The Journal of Supercritical Fluids* **2001**, *19*, 275.
(209) Thurbide, K. B.; Hughes, D. M. *Ind. Eng. Chem. Res.* **2000**, *39*, 3112.
(210) Fujita, K.-i.; Li, Z.; Ozeki, N.; Yamaguchi, R. *Tetrahedron Lett.* **2003**, *44*, 2687.
(211) Whitelaw, E. L.; Loraine, G.; Mahon, M. F.; Jones, M. D. *Dalton Trans.* **2011**, *40*, 11469.
(212) Hanson, S. K.; Baker, R. T.; Gordon, J. C.; Scott, B. L.; Sutton, A. D.; Thorn, D. L. *J. Am. Chem. Soc.* **2008**, *131*, 428.
(213) Hanson, S. K.; Baker, R. T.; Gordon, J. C.; Scott, B. L.; Silks, L. A. P.; Thorn, D. L. *J. Am. Chem. Soc.* **2010**, *132*, 17804.
(214) Belokon, Y. N.; Fuentes, J.; North, M.; Steed, J. W. *Tetrahedron* **2004**, *60*, 3191.
(215) Dey, S.; Powell, D. R.; Hu, C.; Berkowitz, D. B. *Angew. Chem., Int. Ed.* **2007**, *46*, 7010.
(216) Yuan, W.-B.; Wang, H.-Y.; Du, J.-F.; Chen, S.-W.; Zhang, Q. *Acta Cryst. Sec. E* **2006**, *62*, m3504.
(217) Sheldrick, G. M. *University of Gottingen, Germany* **1997**.
(218) Chamberlain, B. M.; Cheng, M.; Moore, D. R.; Ovitt, T. M.; Lobkovsky, E. B.; Coates, G. W. *J. Am. Chem. Soc.* **2001**, *123*, 3229.